Design and Synthetic Use of Heterobimetallic Catalysts with *N*-Heterocyclic Carbene Ligands

(含窒素複素環カルベン配位子を有する異種２核金属錯体触媒の設計と反応開発)

Miyu Sato

2025

Contents

General Introduction

Overview

Transition metal complexes are widely used as catalysts for modern synthetic chemistry because the reactivity of the metal center can be controlled easily by tuning the electronic and/or steric properties of the ligands. As for homogeneous catalysts, dinuclear systems are rarely used compared with mononuclear ones because of the lack of preparation methods. Although there has been an impressive progress with mono-metal catalysis, which often activates a single substrate, a challenge in this field is that it is usually difficult to simultaneously activate two inert substrates on a single metal center. Bimetallic catalysis represents an alternative paradigm that complements the more traditional mono-metal catalysis approach in the reaction involving activation of two inert substrates.

It has been known that a number of enzymes have active sites containing two metal ions, showing unique catalytic activities based on their cooperative nature. This inspired the author to design synthetic heterobimetallic system. Heterobimetallic catalysts show the characteristic reactivity, but guidelines for design of ligands for synthetic dinuclear species have not yet been established. *N*-Heterocyclic carbenes (NHCs) are indispensable ligands for transition metals and have found multiple applications in numerous significant catalytic transformations. In addition, Sawamura group already has the enough knowledge about NHC-metal complexes and their reactivity. The author aimed at design and synthetic applications of heterobimetallic complexes using a stable, rigid, and well-defined *N*-heterocyclic carbene ligand.

In general introduction, the previously reported heterobimetallic systems that show cooperativity of two metal centers are summarized. Besides, *N*-heterocyclic carbene ligands, especially imidazo[1,5-*a*]pyridine ligands, for cooperative catalysis are reviewed and discussed. In the end of this introduction, the main contents of this thesis are introduced.

1.1. Dinuclear Metalloenzymes

Nature harnesses the power of bimetallic system.[1] Naturally occurring metalloenzymes can catalyze reactions with high chemoselectivity due to the cooperative action of multiple metal centers. For instance, a dinuclear copper active site of hemocyanin can capture dioxygen (Figure 1.1a).[2a] The related metalloenzyme, tyrosinase activates dioxygen and hydroxylates monophenols to form catechols and oxidize these catechols to *ortho*-quinones (Figure 1.1 b).[2b] Such dinuclear active sites show cooperativity of two metal centers.

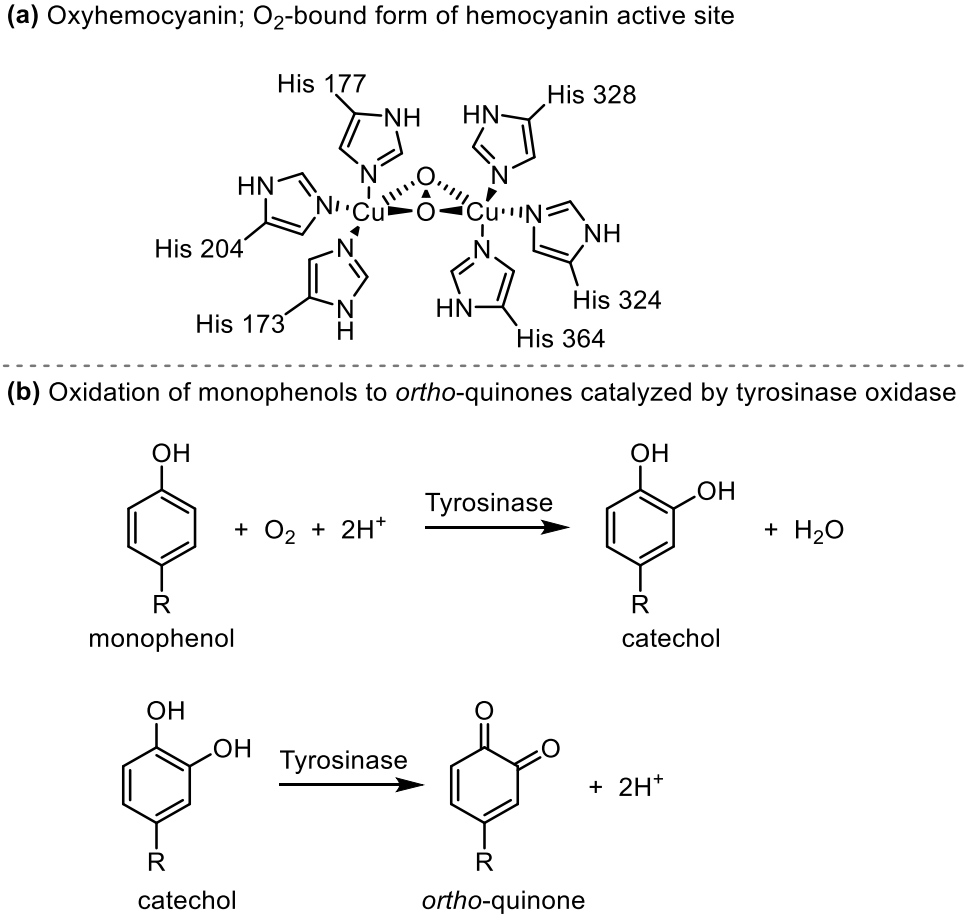

Figure 1.1. Examples of dinuclear metalloenzymes.

In addition, there are various types of dinuclear enzymes with Cu–Zn (SOD: *superoxide dismutase*),[3a] Fe–Fe (Hemerythrin)[3b], Fe–Cu (cytochrome c oxidase)[3c], Zn–Zn (Metallo-β-Lactamase)[3d] etc. Whereas metalloenzymes and conventional biomimetic systems, it would be better if we could tune the metal complex applicable to a broad range of substrates.

1.2 Synthetic Bimetallic Catalysts

1.2.1. Homometallic System

Bimetallic system exhibits enhanced catalytic activity and higher levels of stereoselectivity not found in mononuclear transition metal complexes,[1,4] but the design of such catalysts (particularly the ligands) remains a difficult challenge. There are only a few limited examples of its use in developing new reactions.

So far, dinuclear metal complexes commonly used in the field of organic chemistry are limited to complexes containing the same metals, because such homometallic catalysts are readily preparable or commercially available. For example, it has been reported that reactions of diazo compounds **2** via metal carbenoids can be catalyzed by rhodium (II) carboxylates having a dinuclear structure (Figure 1.2a),[5] and that Pawson-Khand reactions usually employed dinuclear cobalt carbonyl compounds **5** to give cyclopentenone **12** (Figure 1.2b)[6] etc. Pauson-Khand reaction mechanism is elucidated by Magnus in 1985[7] and Nakamura in 2001 by computational studies.[8] Binding of an alkene **4** with dicobalt octacarbonyl complex **5** while expelling CO molecule gives a metallacyclopentene complex **6**. And then ligand dissociates to form a 16-electron complex and immediately alkene coordinated complex **8** is formed. Subsequent alkene insertion followed by migratory insertion of CO affords **10**. Finally reductive elimination gives the cyclopentenone product **12** and regenerates the cobalt catalyst **5** by associating two CO molecules.

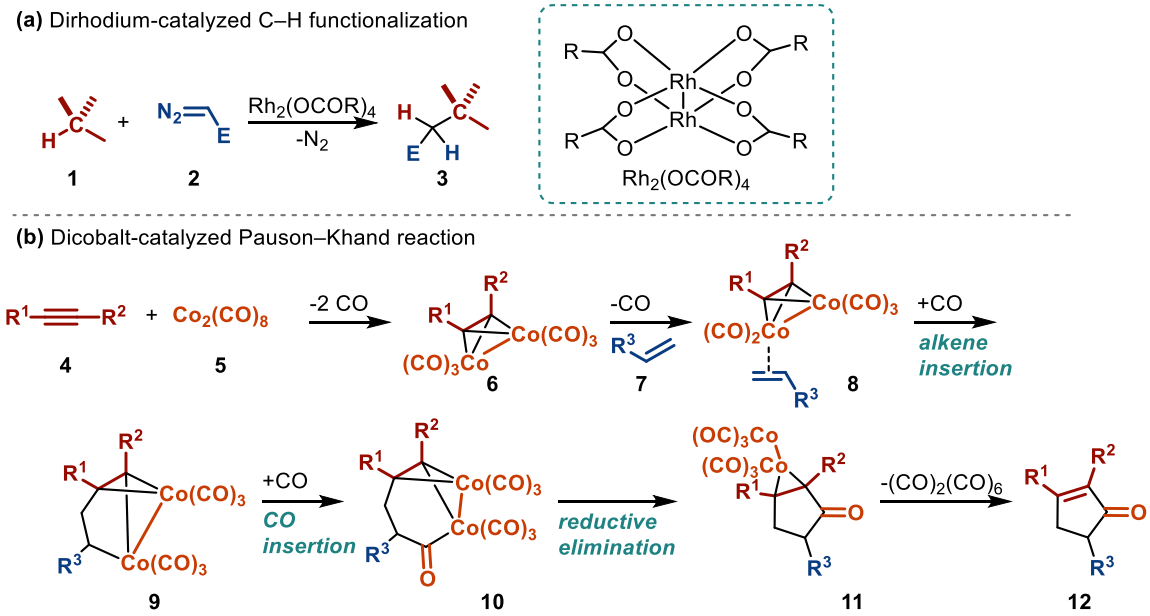

Figure 1.2. Examples of reactions catalyzed by homodinuclear metal complexes.

1.2.2 Heterobimetallic System

Heterobimetallic catalytic system which activates two inert substrates has emerged as a powerful approach to achieve new reaction development that were impossible with previous strategy using conventional mononuclear systems. Here, the author summarizes representative examples of the heterobimetallic systems which show cooperativity towards two substrates and their application especially for catalytic enantioselective reactions. Heterobimetallic system can be divided into two classes (Figure 1.3). (1) Two-component system: cooperative dual metal catalysis. (2) Single-component system: cooperative intramolecular dinuclear catalysis. By following these categories, the author describes some representative reported examples of heterobimetallic systems.

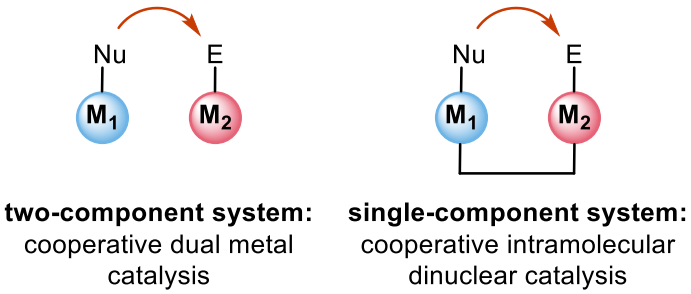

Figure 1.3. Approaches to the heterobimetallic catalytic reactions between nucleophile (Nu) and electrophile (E).

1.2.2.1 Two-component Heterobimetallic System

Sawamura and co-workers reported the two-component rhodium/palladium catalyst for allylic alkylation of activated nitriles as a pioneering example of heterobimetallic system.[9] By applying the *trans*-chelating chiral phosphine ligand, TRAP,[10] which originally developed in combination with $Rh(acac)(CO)_2$,[11] they achieved highly enantioselective reaction of allyl carbonates **13** and 2-cyanopropionates **14**.

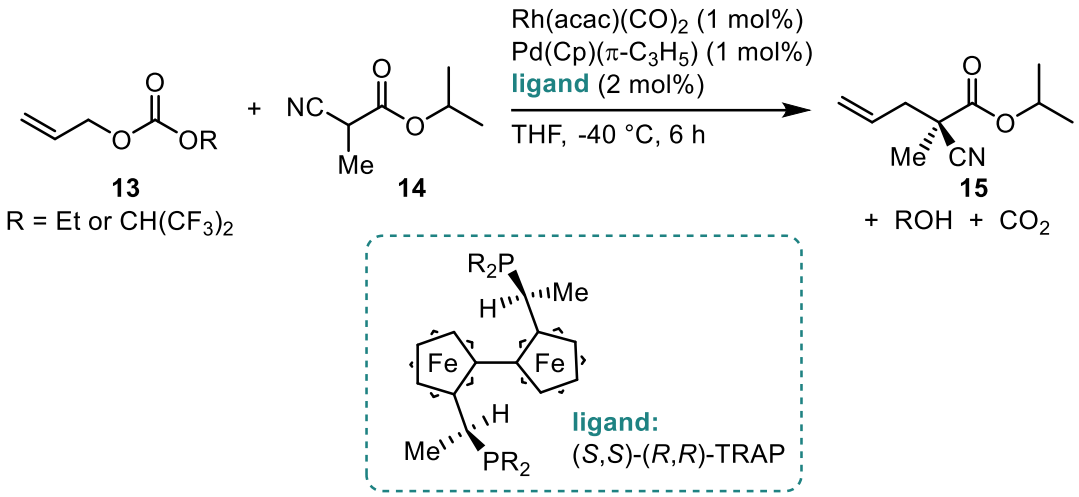

Scheme 1.1. Allylic alkylation of activated nitriles.

Proposed mechanism is shown below (Figure 1.4). While π-allylpalladium(II) complex **18** is formed by the decarboxylative oxidative addition of allyl carbonate **13** to palladium(0) complex **19**, rhodium(I)-coordinated enolate complex **16** is initially formed from Rh(acac)(CO)$_2$, TRAP, and cyanoester **14**. Enolate (**16**) attacks to the π-allylpalladium(II) complex (**18**) enantioselectively (TS **20**) to produce optically active product **15**. In this step, the palladium(0) is reproduced, and alkoxide anion (RO^-) becomes a ligand of the rhodium to form alkoxy rhodium(I) complex **17**. The catalytic cycle is completed by the proton exchange between **17** and **14**, which forms the enolate complex (**16**) and alcohol (ROH).

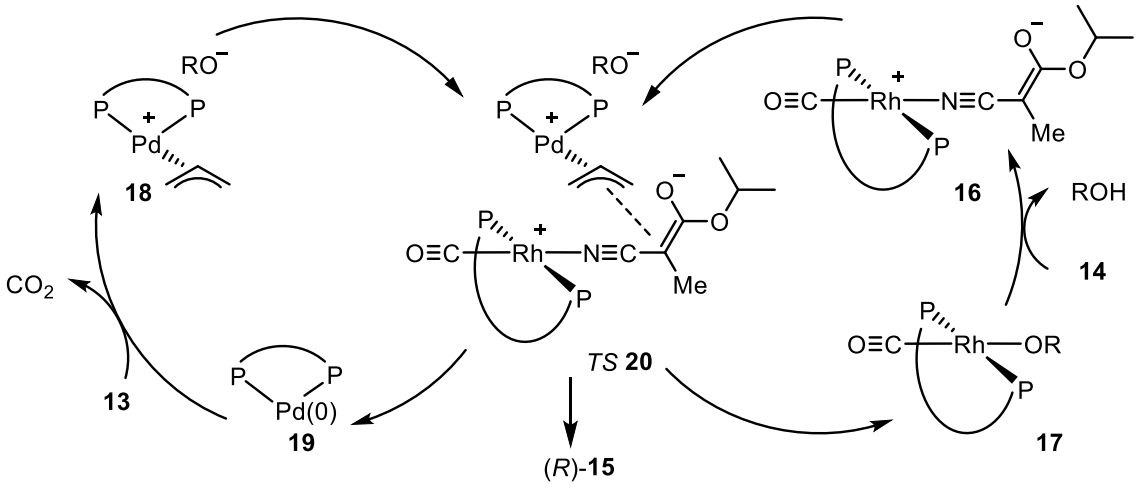

Figure 1.4. Proposed mechanism.

In 2004, Jacobsen and co-workers reported a highly enantioselective conjugate

cyanation of unsaturated imides **21**.[12] Control experiments revealed that both chiral (salen)Al complex[13] and chiral (pybox)$ErCl_3$[14] complex are indispensable for improving the reactivity (Table 1.1).

Table 1.1. Control experiments for cyanide conjugate addition.[a]

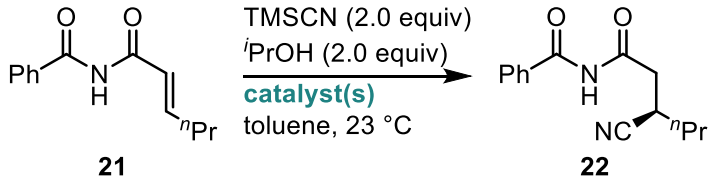

entry	Al complex	Er complex	conversiton (%)[b]	ee (%)[c]
1	+	-	<3	-
2	-	+	<3	-
3	+	+	99	96

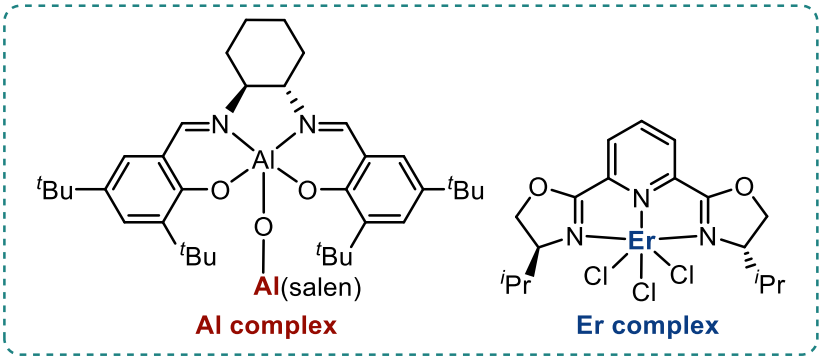

[a] Al complex (2 mol%), Eu complex (3 mol%). [b] Determined by ^1H NMR. [c] Determined by HPLC using a Pirkle L-Leucine column.

Nishibayashi and co-workers reported ruthenium- and copper-catalyzed enantioselective alkylation of propargylic alcohols **23** with β-ketoesters **24** which affords the corresponding propargylic alkylated products **25** in 2012.[15] In their system, ruthenium and copper complexes activate propargylic alcohols **23** and β-ketoesters **24** respectively, thereby cooperatively promoting the propargylic alkylation enantioselectively via ruthenium-allenylidene complex and β-ketoesters activated by the copper complex as a key reactive intermediate (Figure 1.5).

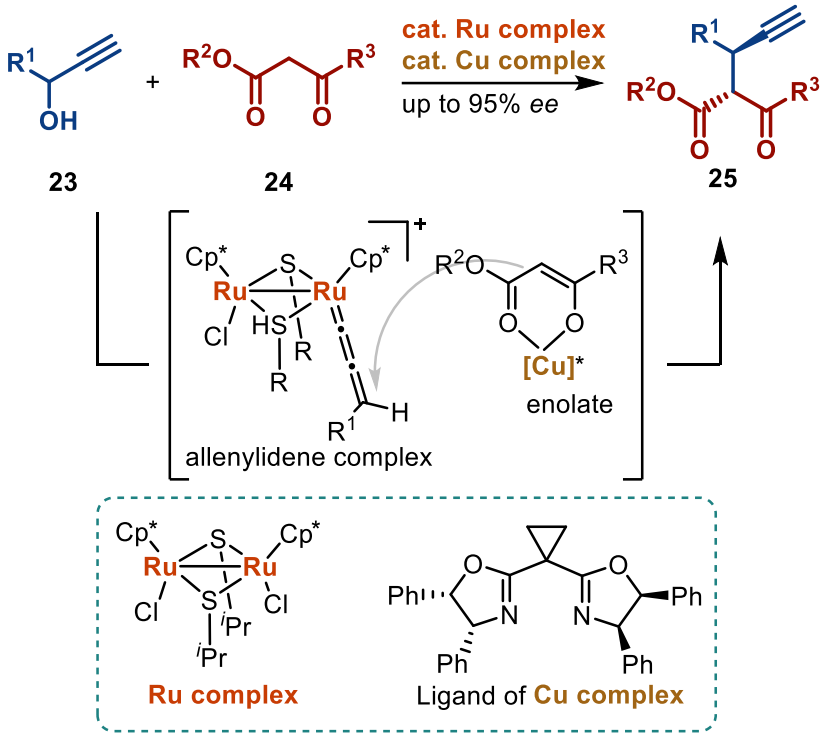

Figure 1.5. Cooperative catalytic propargylic alkylation reaction.

1.2.2.2 Single-component Heterobimetallic Systems

Various two-component systems have been developed as mentioned before. The author introduces single-component system: cooperative intramolecular dinuclear catalysis. In this case, precise ligand design should be required to control the two metals.

Shibasaki, Kanai, Matsunaga and Kumagai developed a series of asymmetric bifunctional catalysts and reported their practical application for enantioselective transformations (Figure 1.6).[16] Specifically, they utilized heterobimetallic rare earth–alkali metal–binol (abbreviated as REMB; RE = rare earth metal, M = alkali metal, B = BINOL) complexes for various highly enantioselective reactions; for examples, nitro aldol, Michael reaction, nitro Mannich reaction and so on. However, these systems were limited to use of bimetallic catalysts as Lewis acid and base catalysts in combination with lanthanides and alkali metals.

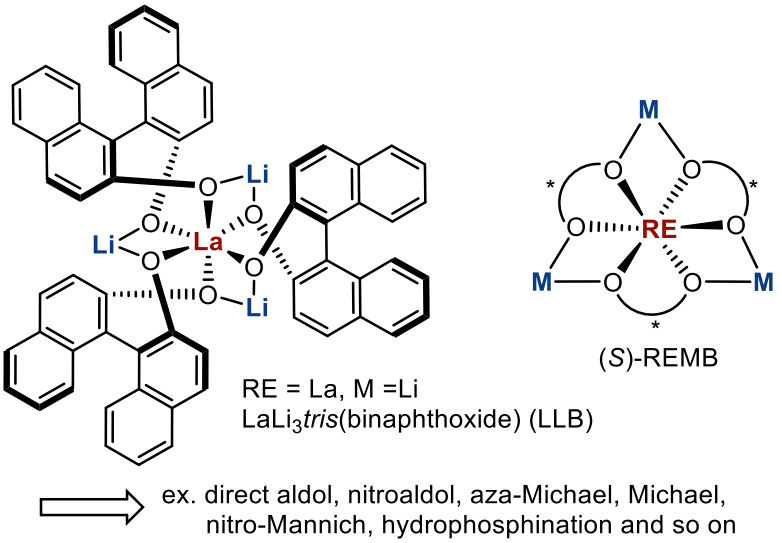

Figure 1.6. Structures of heterobimetallic RE-M_3-*tris*(binaphthoxide) (REMB) catalyst (*S*)-LLB and representative asymmetric reactions catalyzed by REMB complexes.

Sawamura and co-workers reported that allylic alkylation using (*Z*)-allylic phosphate **27** with alkyne **26** in the presence of CuCl (10 mol %), tetrafluoroboric acid salt of ligand **28** (12 mol%) and LiO^{t}Bu (2.6 equiv).[17] While investigating various chiral NHC ligands, they found that the ligand **28** with phenolic hydroxy group and mesityl group resulted in the highest enantioselectivity.

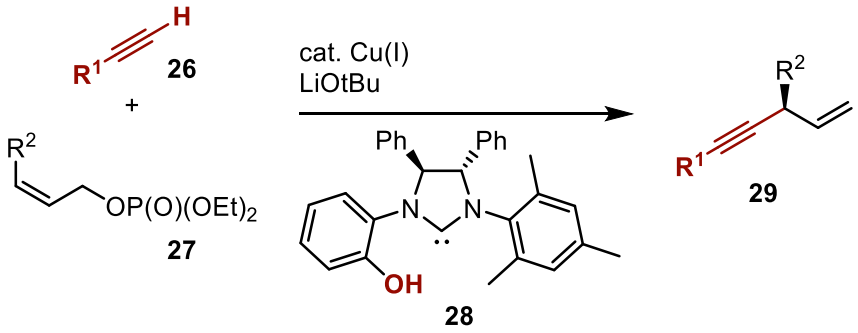

Scheme 1.2. Allylic alkylation of terminal alkyne.

A proposed reaction pathway giving the major enantiomer of the skipped enyne **29** is shown in Figure 1.7. In this reaction pathway, the diastereoselective π-coordination of the alkene moiety with the lithium (alkynyl)(aryloxo)cuprate **32** forms **37**. Li+-assisted allylic oxidative addition generates a (π-en-σ-yl)copper(III) complex (**36**) featuring a secondary sp^3 carbon atom bound to Cu. Due to steric repulsion between the γ-substituent (R′) and the chiral NHC ligand **28**, this intermediate is relatively unstable and isomerizes

to the more stable isomer **35**, with retention of the configuration at the secondary sp^3 carbon atom. This intermediate (**35**) is also common to the reaction pathway with **27′**. The isomerization is achieved through a flip of the allyl ligand, accompanied by dissociation of the π-coordination of the alkene moiety, likely via some isomeric intermediates. The 1,3-allylic strain in the allyl ligand may further contribute to the lability of the π-en-σ-yl coordination. Finally, reductive elimination of **35** affords the major enantiomer of the skipped enyne **29** with a tertiary stereogenic center at the allylic/propargylic position.

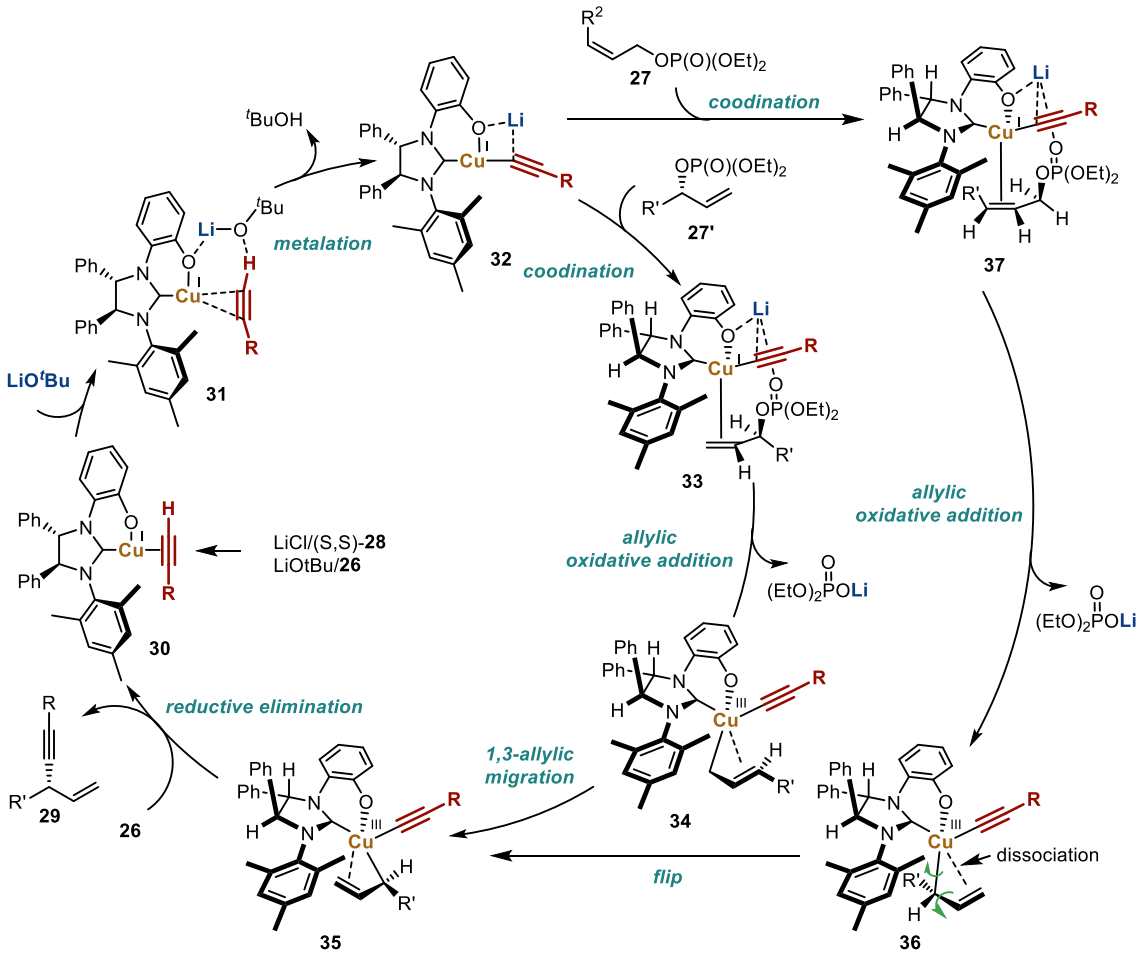

Figure 1.7. Proposed mechanism.

Sawamura and co-workers expand the application of the phenol/*N*-Heterocyclic carbene chiral ligand to allyl-allyl coupling between allylic boronates and phospahtes (Scheme 1.3).[18]

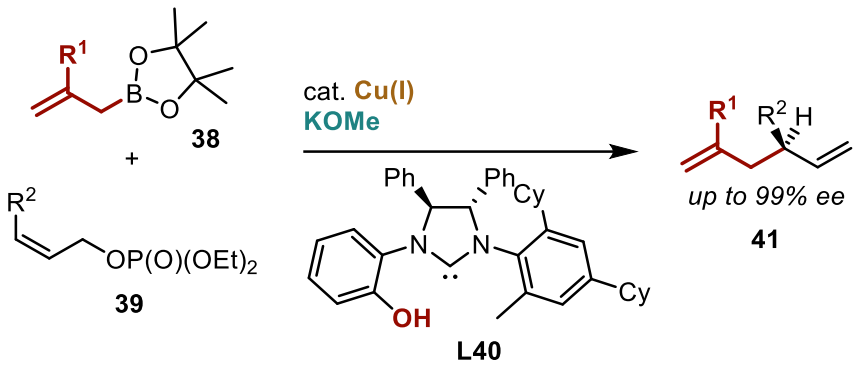

Scheme 1.3. Copper-catalyzed enantioselective allyl-allyl coupling between allylic boronate and phosphate.

They postulated a catalytic reaction pathway for the enantioselective allyl–allyl coupling catalyzed by Cu/(*S*,*S*)-**L40**, as shown in Figure 1.8. The reaction of CuCl, (*S,S*)-**L40**, and KOMe generates an alkoxycopper(I) complex (**42**), wherein the chiral NHC ligand coordinates to Cu as an anionic C,O-bidentate ligand. Subsequent transmetalation between **42** and an allylborate (**43**) affords a potassium phenoxo(allyl)cuprate (**44**). Complex **44** engages with the allylic phosphate **39** to form a π-complex (**45**), in which Cu is positioned *anti* to the phosphate leaving group, potentially activated by the participation of Lewis acidic MeOBpin. Oxidative addition then yields the (π-en-σ-yl)copper(III) complex **46**, featuring a secondary sp^3-carbon atom coordinated to Cu. Reductive elimination of **46**, which proceeds more rapidly than allylic 1,3-Cu migration to form **47**, delivers the enantioenriched chiral 1,5-dienes with a tertiary carbon stereogenic center at the allyic/homoallylic position **41** and regenerates **42**, thereby completing the catalytic cycle. The observed regioselectivity dependence on the *E/Z* geometry of the allylic substrate (**39**) can be rationalized by the higher instability of **47** relative to the corresponding Cu(III) species derived from the *E* substrate, attributed to increased steric repulsion within the allyl moiety of the *Z*-derived substrate. Accordingly, complex **46** may be more accurately described as an (η^1-allyl)copper(III) complex, lacking alkene coordination. Although it is not clear whether the potassium cation coordinates to NHC as in the mechanism shown below and whether this work have to be classified as single-component heterobimetallic system, the author described this work here as a Sawamura's further application of phenol/*N*-Heterocyclic carbene chiral ligand.

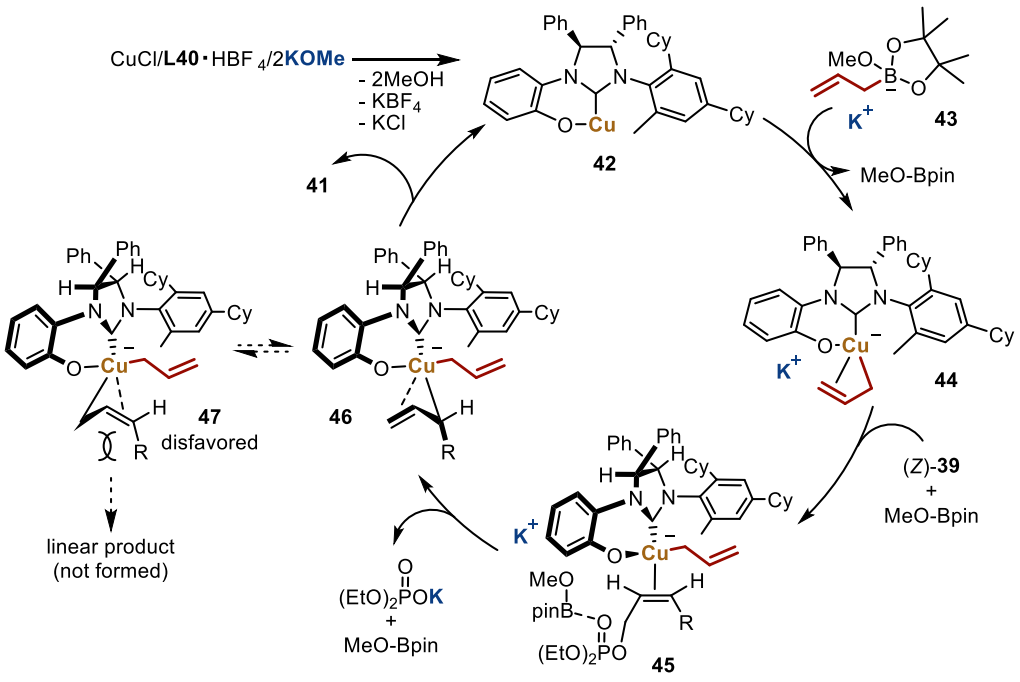

Figure 1.8. Proposed mechanism.

1.2.3 Discussion of the Current Design of Heterobimetallic Catalyst

The strategies for new reaction development using heterobimetallic catalyst have been well-developed during the last few decades. Despite the progress of heterobimetal complex-catalyzed high-chemoselective reactions, guidelines for ligand design for construction dinuclear species have not so much been established. Sawamura's reports about catalytic allylic substitution reaction with the phenoxy-NHC ligand indicate that functionalized *N*-heterocyclic carbenes would be a potential candidate of ligands for other heterobimetallic catalysts. Especially, Imidazo[1,5-a]pyridine structures would be the versatile heterobimetallic platform because of their ease of fine-tuning and a rigid character of their pyridine backbone.

In the next section, the history of *N*-heterocyclic carbene ligand is briefly described. And then, imidazo[1,5-a]pyridine structure NHCs will be introduced.

1.3 *N*-heterocyclic carbene (NHC) Ligands

1.3.1 *N*-Heterocyclic Carbenes (NHCs)

N-Heterocyclic carbenes (NHCs) chemistry was started by Öfele and Wanzlick in

1968.[19] Since free carbenes had been available through the important work of Arudengo et al. in 1991,[20] numerous NHC-metal compounds were synthesized and characterized. Arduengo's "original" imidazol-2-ylidenes **48** in Figure 1.9 are the most widely exploited as organocatalysts and ligands for transition metal complexes.[21] They are considered as neutral, two-electron donor ligands and generally form stable complexes with various metals. Moreover, the geometry of NHC is different from other ligands, allowing the design of new ligand geometries.

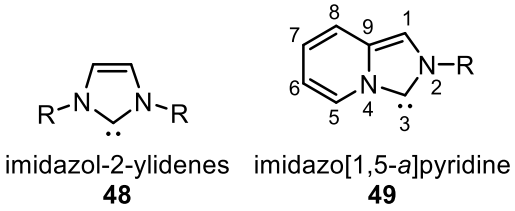

imidazol-2-ylidenes **48** imidazo[1,5-*a*]pyridine **49**

Figure 1.9. Structure of NHC.

1.3.2 Imidazo[1,5-*a*]pyridine

Imidazo[1,5-*a*]pyridine skeletons **49** in Figure 1.9 are important class of nitrogen ring-junction heterocyclic compounds. In 2005, Glorious and Lassaletta independently and pioneeringly reported on the development of this rigid bicyclic framework.[22] It was found that the pyrido-annulation significantly influences the σ-donor and π-acceptor properties of carbenes.

Efficient synthetic procedure of imidazo[1,5-*a*]pyridinium salts was reported by Aron in 2011 (Scheme 1.4).[23] In their synthetic methodology, reaction proceeds in high yields under mild conditions just combining 3 components.

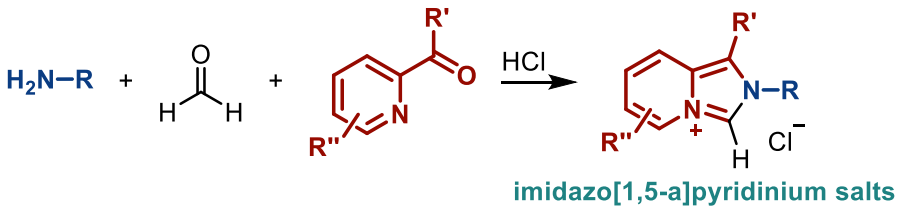

Scheme 1.4. Single-step synthesis of imidazo[1,5-*a*]pyridinium.

Unsymmetrical NHCs provide tunable control of metal ligand sphere geometry. Especially Imidazo[1,5-*a*]pyridinium salts must be unsymmetrical NHC precursors in a single transformation by introducing diverse functionality and chiral substituents. In fact, imidazo[1,5-*a*]pyridin-3-ylidene ligands have been modified at the C5 position with

sterically bulky aromatic rings,[24] coordinative substituents,[25] chiral auxiliaries,[26] and other substituents.[27]

Sawamura, Higashida and Rawat developed imidazo[1,5-a]pyridin-3-ylidene type cooperative catalyst for cyclization for alkyne-tethered carboxylic acids in 2021.[28] They anticipated that modifying the ligand at the C5 position would significantly influence the catalyst's properties, as this position is proximal to the NHC-bound metal center (Figure 1.10a). They proposed that imidazo[1,5-a]pyridin-3-ylidene could serve as a robust template for designing acid-base cooperative catalysts, by positioning a Lewis acidic transition metal center at the C3 carbene carbon and a basic functional group, such as imidazole, at the C5 position (Figure 1.10b).

Specifically, they selected the 4-(*tert*-butyl)-1H-imidazol-1-yl group as a rigid basic substituent at the C5 position to spatially separate the Lewis acidic and basic centers within the catalytic region. The study reports the synthesis of protonated precursors for imidazo[1,5-a]pyridin-3-ylidene ligands, their conversion into the corresponding silver(I) complexes, and their application in silver-catalyzed cyclization reactions of alkyne-tethered carboxylic acids (Figure 1.10c).[29,30]

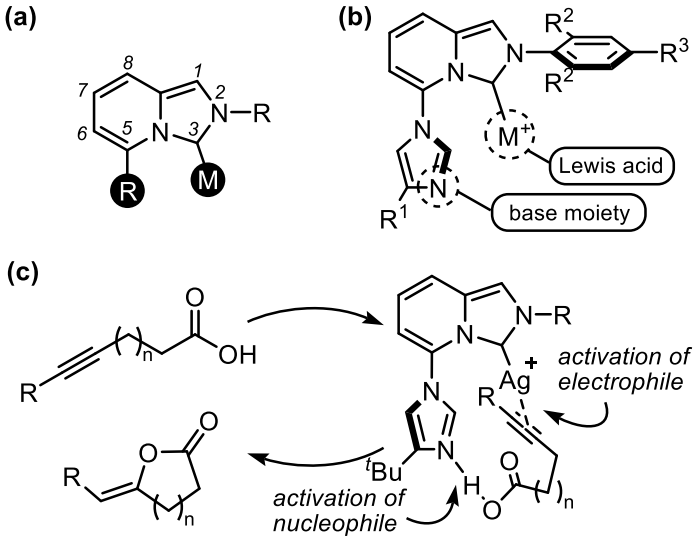

Figure 1.10. General chemical diagrams for (a) imidazo[1,5-*a*] pyridin-3-ylidene metal complexes and (b) Lewis acid-base cooperative catalysts with an imidazo[1,5-*a*]pyridin-3-ylidene platform. (c) Cyclization of alkyne-tethered carboxylic acids through Lewis acid-base cooperative catalysis.

Based on the above mentioned design of functionalized NHC-Ag complex, they successfully synthesized the gold-zinc cooperative catalysts. The reason why they chose

cationic gold(I) center is, that is well-known as effective catalysts for nucleophilic additions toward alkynes with excellent turnover efficiency due to their strong Lewis acidic character and high affinity for alkyne π-systems.

Sawamura, Higashida and Rawat envisioned that heterobimetallic complexes would be effective catalyst candidates for *O*-nucleophilic addition toward nonactivated internal alkynes, expecting cooperative action of the two metal sites for dual activation of electrophiles and nucleophiles as in enzymatic reactions.[31] As a platform for heterobimetallic cooperative catalysis, they synthesized a rigid imidazo[1,5-a]pyridin-3-ylidene ligand featuring a 2,2'-bipyridine moiety at the C5 position and employed it to prepare a gold(I) carbene complex. The resulting gold complex was further transformed into heterobimetallic catalysts through in situ coordination of various hard metals to the bipyridine moiety. These heterobimetallic catalysts were evaluated for their catalytic activity in the intermolecular addition of weak *O*-nucleophiles, such as carboxylic acids and phenols, to nonactivated internal alkynes.

The catalytic performance of gold complexes **50** was investigated in the hydrocarboxylation of nonactivated alkynes (Scheme 1.5). Bimetallic catalysts were generated in situ by combining **50**, a hard metal salt, and an anion source. When benzoic acid (**52**) was used as the nucleophile in the addition reaction with diphenylacetylene (**51**), catalysis with **50** and $Zn(acac)_2$ in 1,2-dichloroethane (DCE) at 80 °C for 16 hours produced enol ether **53** in 98% isolated yield.

The choice of hard metal salt had a substantial impact on the catalytic activity of **50**, with $Zn(acac)_2$ providing optimal results. Furthermore, the use of sodium tetrakis[3,5-bis(trifluoromethyl)phenyl]borate ($NaBAr^F$)[32] as a noncoordinating anion source significantly enhanced the yield.

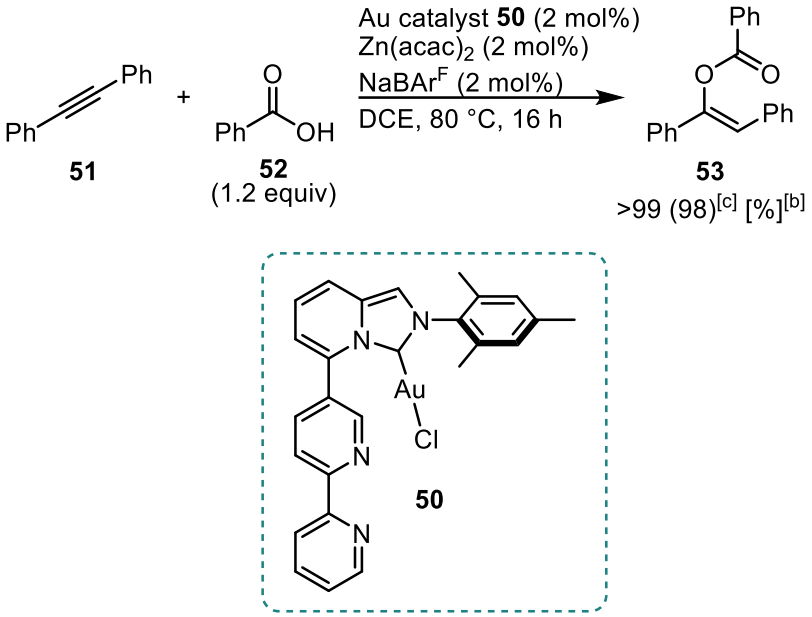

Scheme 1.5. Intermolecular hydrocarboxylation of nonactivated internal alkyne by gold-zinc cooperative catalyst.[a] [a] Au catalyst (2 mol %), metal salt (2 mol %), anion source (2 mol %), **51** (0.10 mmol) and **52** (0.12 mmol) in DCE (0.1 mL, 12 M). [b] Determined by ^{1}H NMR analysis using 1,3,5-trimethoxybenzene as an internal standard. [c] Isolated yield.

To obtain the mechanistic insights to the gold–zinc cooperative catalytic system, DFT calculations were performed at the M06/SDD,6-311+G(d,p)/SMD(DCE)//M06/SDD,6-31G(d) level of theory with the Gaussian 16 package (Figure 1.11).[33] Energy calculations revealed that nucleophilic attack could occur through either **TS$_{3-4}$** or **TS$_{1-2}$**.

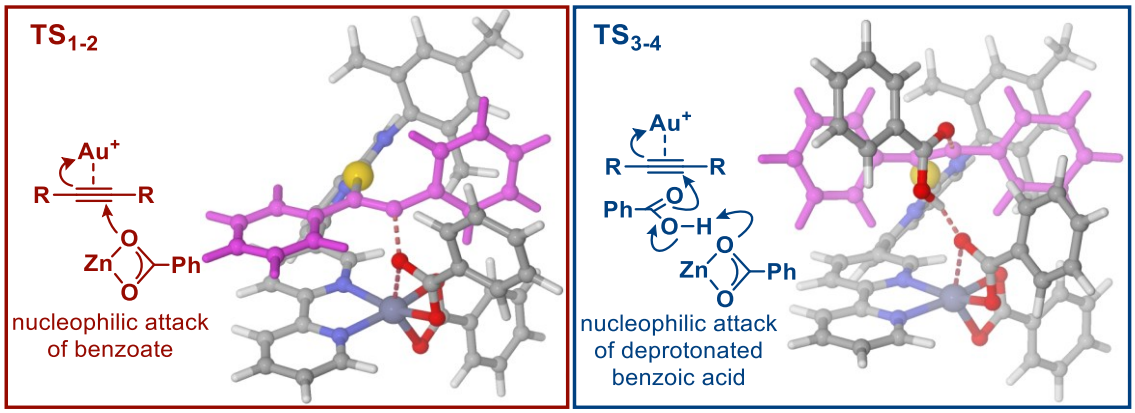

Figure 1.11. Transition States for nucleophilic addition of **52** toward **51**. DFT calculations were conducted at the M06/SDD,6-311+G(d,p)/SMD(DCE)//M06/SDD,6-31G(d) level of theory.

The nucleophilic *anti*-attack of the zinc benzoate toward the alkyne moiety activated by the gold atom proceeds through $\mathbf{TS_{1–2}}$. Alternatively, the benzoate can act as a base to deprotonate benzoic acid. The bound benzoic acid undergoes deprotonation coupled with nucleophilic *anti*-attack toward the alkyne moiety through $\mathbf{TS_{3–4}}$.

DFT calculations supported the proposed cooperative action of the Au–Zn bimetallic catalyst system. As for the further application of this bimetallic system, the author achieved alkynoate hydrocarboxylation with *N*-Protected amino acids for preparation of storable acylating reagents as described in Chapter 1.

1.4 Overview of This Thesis

The author has developed a series of bimetallic system based on *N*-heterocyclic carbene. Chapter 1 illustrates the preparation of storable acylating reagents and racemization-free peptide synthesis using gold-zinc cooperative catalyst. In chapter 2, gold-zinc cooperative catalysis for seven-*exo-dig* hydrocarboxylation of internal alkynes is described.

1.4.1 Chapter 1: Gold-Zinc Co-Catalyzed Alkynoate Hydrocarboxylation with *N*-Protected Amino Acids for Preparation of Storable Acylating Reagents and Racemization-Free Peptide Synthesis

General peptide synthetic method is the formation of amide bonds between α-amino acids via active intermediates using condensing reagents (Figure 1.12a). To date, various coupling reagents have been developed. Dicyclohexylcarbodiimide developed in 1955 by Sheehan is the most widely used for peptide bond formation (Figure 1.12b).[34] In 1958, a diphenylketenimine coupling reagent was reported by Stevens.[35] However, racemization is induced via the oxazolone pathway (Figure 1.12b; *Path A*) or via an intramolecular α-proton abstraction (Figure 1.12b; *Path B*). The former occurs easily due to the increased acidity of α-proton by the existence of mesomeric forms via tautomeric enol.[36] The latter is caused by the action of a basic sites derived from those kind of condensation reagents. Although peptide synthesis seems to have reached a level of maturity in the field of science, there is still a continuing demand for the development of racemization-free coupling reagents.

The common feature among the developed various condensing reagents so far is that the addition reaction of a carbonyl group to a vicinal double bond with electrophilic sp carbon occurs. Zhao revealed that allenone derivatives with electrophilic sp carbon can be used as a condensing reagent without suffering from racemization since such reagents don't have basic center (Figure 1.12c).[37]

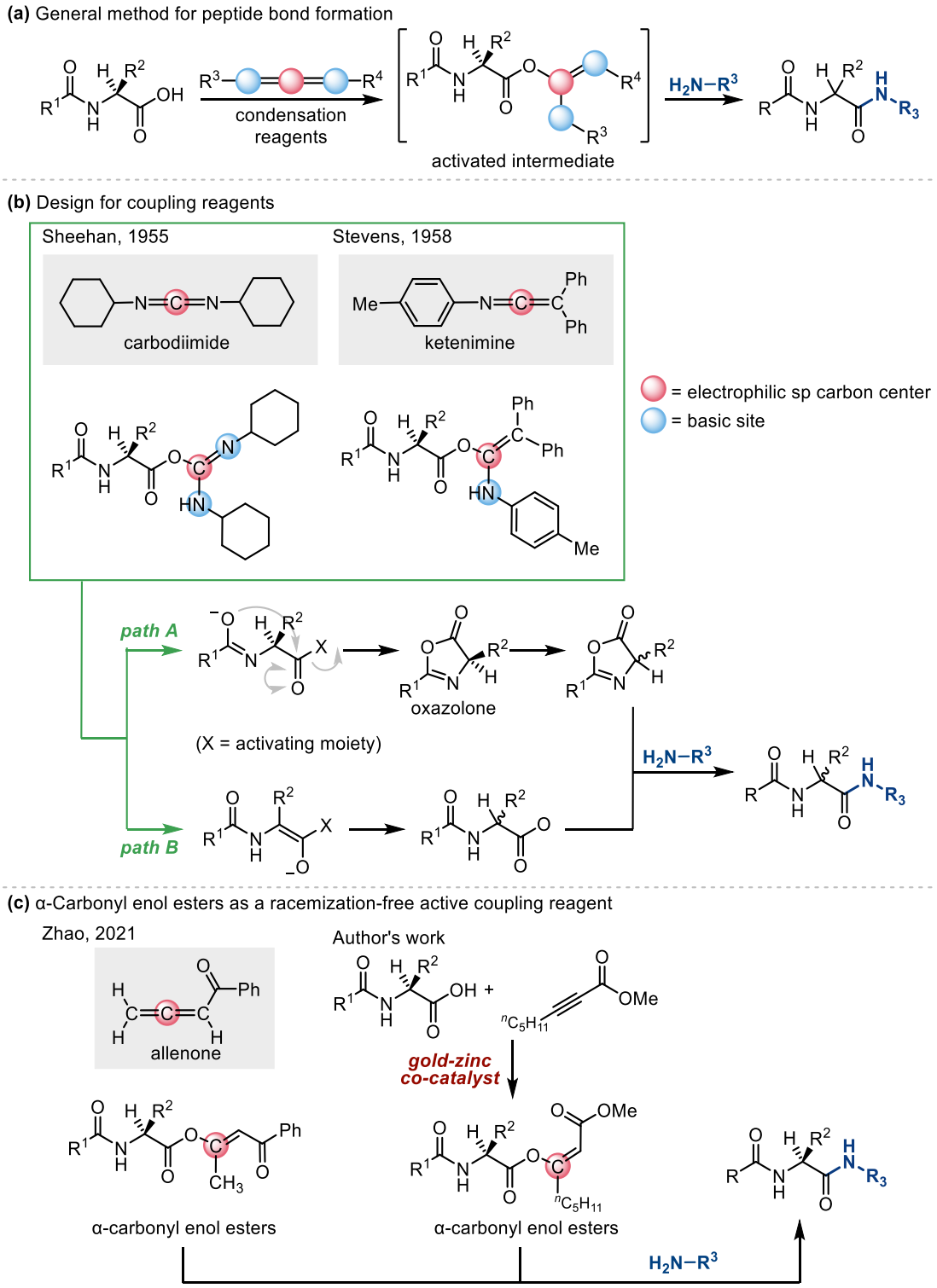

Figure 1.12. Peptide synthesis with coupling reagents.

Based on the knowledge got through the work of intermolecular reaction between non-activated internal alkyne and carboxylic acid developed by Sawamura and co-workers, the author aimed to use this bimetallic system for hydrocarboxylation of alkynes with

amino acids to synthesize α-methoxycarbonyl enol esters (Figure 1.13). The α-methoxycarbonyl enol esters were isolable through silica-gel column chromatography and storable without precautions regarding moisture. Acylation of free amines with the α-methoxycarbonyl enol esters proceeded without epimerization of the stereogenic center derived from the enol esters, affording analytically pure dipeptide compounds through filtration and hexane-washing.

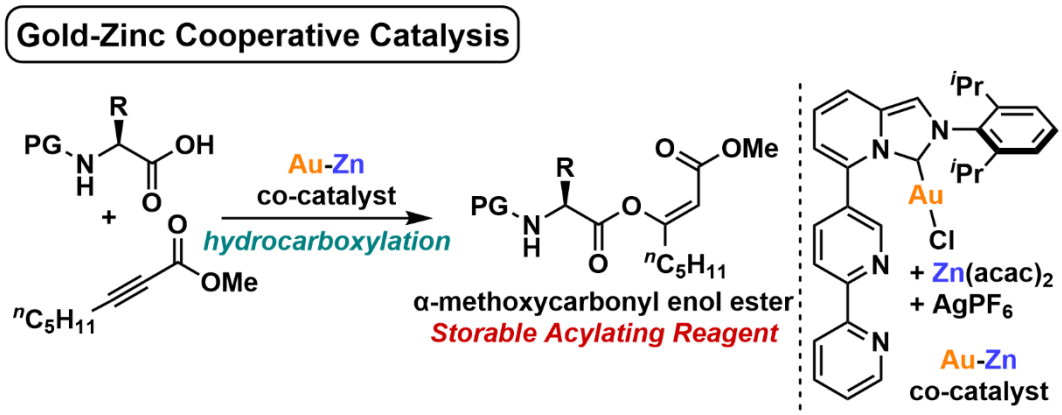

Figure 1.13. Gold-zinc Co-catalyzed alkynoate hydrocarboxylation with *N*-protected amino acids.

1.4.2 Chapter 2: Gold-Zinc Cooperative Catalysis for Seven-*exo-dig* Hydrocarboxylation of Internal Alkynes

Development of construction method of medium-sized carbocycles (7–11-membered ring structures) is a major objective in organic chemistry.[38] There are multiple factors that affect reactivity in cyclization reaction. Utilization of Thorpe–Ingold effect or proximity effect (an enthalpic effect) might help to construct such challenging products and transannular strain prevalent in particularly in medium-sized rings have to be overcome.

1.4.2.1 Thorpe–Ingold Effect

Thorpe–Ingold effect is proposed by Thorpe and Ingold in 1915.[39] This effect was originally based on the concept that the replacement of methylene hydrogens with more sterically demanding alkyl groups on acyclic chain starting materials increases bond angle β between the *geminal*-dialkyl groups and simultaneously compress the internal bond angle α (Figure 1.14). This would make the reactive termini be located more proximal, thereby substantially increasing the rate of intramolecular cyclization.

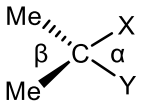

Figure 1.14. Thorpe–Ingold effect.

In 1961, Schleyer pointed out that rate enhancement cannot be caused by Thorpe–Ingold effect solely because the change in bond angle is too small to enhance the cyclization rate dramatically.[40] Instead, they proposed that alkyl substitution affects the distribution of rotational conformation due to the noncovalent interactions within the chain. Bruice and Pandit named it "reactive rotamer effect" as the different theory which is explained by the decrease in inappropriate rotamer distribution at the ground state.[41] These two hypotheses are still an object to debate because both effects are difficult to distinguish rigorously. For example, Parrill demonstrated that the concentrations of reactive rotamer and relative reaction rates doesn't exhibit a linear correlation and this result suggest a "facilitated transition" hypothesis alternatively which states that activation energy is reduced due to a facilitation rotation through the transition state.[42]

In any case, Thorpe–Ingold effect is reviewed[43] and it is indisputable that this kind of chemical phenomena contribute in the synthesis of medium or large size ring architectures [44] and natural products[45]

1.4.2.2 Proximity Effect (Enthalpic Effect)

Generally, intramolecular reactions proceed more rapidly than intermolecular counterparts by virtue of their more favorable entropy change on the transition state.[46] Gronert and co-workers mentioned that this trend is obviously opposition to the Hammond postulate which is a hypothesis that the geometric structure of the transition state would resemble the structure of the nearest stable species (reactant, intermediate or product).[47] However, Gronert's computational work indicated that enthalpic effect is likely to contribute the formation of the ring system.[48] Such proximity effect (an enthalpic effect) augments the entropic factor. Furthermore, proximity effect correlates with the size of the nucleophiles. When bulky or delocalized nucleophiles (i.e. carbanions) are involved in the reaction, the proximity effect is enhanced. In the case of the formation of the medium-sized ring, this doesn't seem feasible without the assistance of catalytic pocket to put two reaction sites in the vicinity for increasing enthalpic factor like Sawamura's work as the author mentions below because the further away two reaction sites are located, the less likely they are to meet.[9]

1.4.2.3 Transannular Strain

Although enthalpic effect is significant as mentioned above, ring strain existing in the product or in the transition state is another factor in determining the ease of cyclization. Regarding lactones that the author wants to synthesize, Wiberg and others calculated their strain energy (Table 1.2).[50] One of the major obstacles in cyclization is transannular interactions within a ring which cause repulsive interactions. It also makes more difficult to construct medium size ring lactones.

Table 1.2. Strain energies of lactones.

Ring size *n*	strain enegies of lactones [kcal/mol]
3	40.4
4	23.3
5	7.7
6	9.5
7	10.7
8	12.4
9	11.6
10	8.2
11	7.3
12	7.1
13	6.7
14	4.5

1.4.2.4 Medium Size Ring Constructions Promoted by Designed Ligand

Sawamura and co-workers designed unique semihorrow triethynylphosphine ligands (C-dtbm and Si-dtbm in Scheme 1.6).[51] and used them for the gold(I)-catalyzed cyclization to form medium-sized ring compounds. Gold catalysts with C-type triethynylphosphine ligands were suitable for the 8-*exo-dig* annulation of silyl enol ethers **54, 56**[52] and enyne [2+2] cycloaddition of **58**.[53] Thorpe–Ingold effect may work efficiently for these substrates. Deep cavity in the ligand places the nucleophilic center (enol or alkene) close to the gold-activated terminal-alkyne, bending flexible starting materials to get exomethylene products.

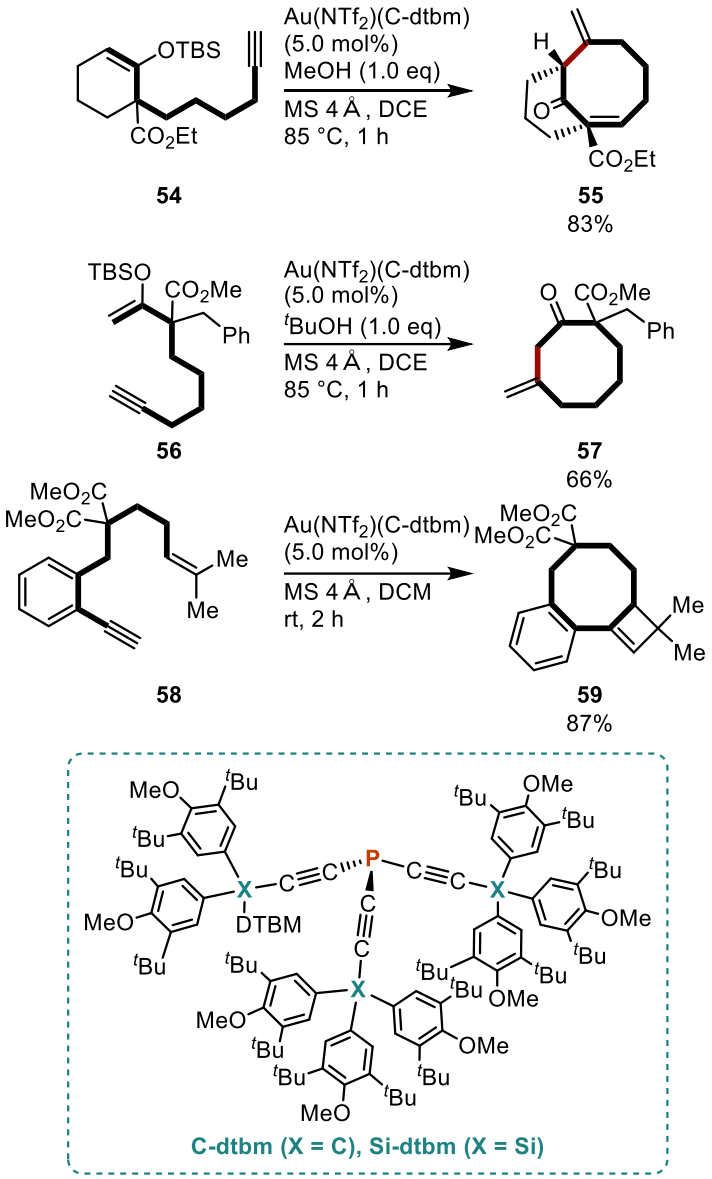

Scheme 1.6. Semihorrow triethynylphosphines and their use for medium-sized ring construction.

Inspired by this pioneering work of designing the catalytic pocket for medium-sized ring formation, the author envisioned that appropriate design of NHC ligands would enable a gold-zinc bimetallic catalyzed medium ring formation reaction (Figure 1.15). Seven-membered ring lactone formation by intramolecular hydrocarboxylation of alkyne-tethered carboxylic acids by gold-zinc cooperative catalyst was achieved. Design of catalytic pocket for bending flexible chain of starting materials realize challenging ring construction. DFT calculation explained the substituent on the nitrogen atom of NHC makes the concave reaction sites.

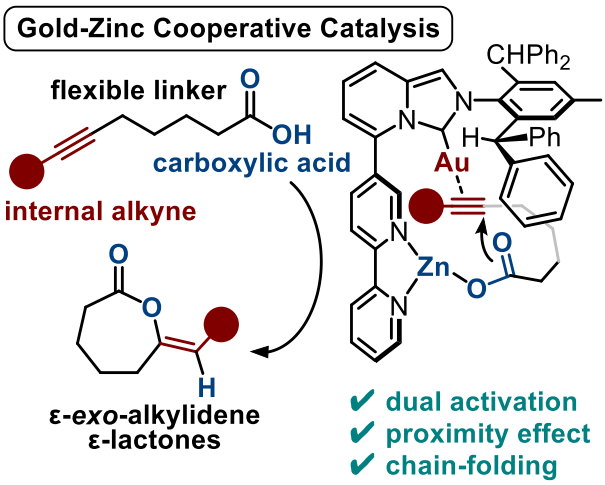

Figure 1.5. 7-membered ring lactone formation by intramolecular hydrocarboxylation of alkyne-tethered carboxylic acids by gold-zinc cooperative catalyst.

1.5 References

[1] E. K. van den Beuken, B. L. Feringa, *Tetrahedron* **1998***, 54,* 12985–13011.

[2] a) K. A. Magnus, H. Ton-That, J. E. Carpenter, *Chem. Rev.* **1994**, *94,* 727–735; b) E. I. Solomon, U. M. Sundaram, T. E. Machonkin, *Chem. Rev.* **1996**, *96*, 2563–2606.

[3] a) R. H. Holm, P. Kennepohl, E. I. Solomon, *Chem. Rev.* **1996,** *96*, 2239–2314; b) R. E. Stenkamp, *Chem. Rev.* **1994**, *94,* 715–726; c) G. T Babcock, M. Wikström, *Nature* **1992**, *356*, 301–309; d) J. Morán-Barrio, M.-N. Lisa, N. Larrieux, S. I. Drusin, A. M. Viale, D. M. Moreno, A. Buschiazzo, A. J. Vila, *Antimicrob. Agents Chemother.* **2016**, *60*, 6013–6022.

[4] a) J. Park, S. Hong, *Chem. Soc. Rev.* **2012**, *41*, 6931–6943; b) D. R. Pye, N. P. Mankad, *Chem. Sci.* **2017**, *8*, 1705–1718; c) X. Huo, G. Li, X. Wang, W. Zhang, *Angew. Chem. Int. Ed.* **2022**, *61*, e202210086.

[5] A. G. H. Wee, *Curr. Org. Synth.*, **2006**, *3*, 499–555.

[6] a) I. U. Khand, G. R. Knox, P. L. Pauson, W. E. Watts *J. Chem. Soc., Perkin. Trans. 1* **1973**, 977−981. For recent related review see; b) T. Shibata, *Adv. Synth. Catal.*, **2006**, *348*, 2328–2336.

[7] P. Magnus, L. M. Principe, ***T****etrahedron Lett*. **1985**, *26*, 4851–4854

[8] M. Yamanaka, E. Nakamura, *J. Am. Chem. Soc*. **2001**, *123*, 1703–1708.

[9] M. Sawamura, M. Sudoh, Y. Ito, *J. Am. Chem. Soc.* **1996**, *118*, 3309–3310.

[10] a) M. Sawamura, H. Hamashima, Y. Ito, *Tetrahedron: Asymmetry* **1991**, *2*, 593–596; b) M. Sawamura, H. Hamashima, M. Sugawara, R. Kuwano, Y. Ito, *Organometallics* **1995**, *14*, 4549–4558.

[11] a) M. Sawamura, H. Hamashima, Y. Ito, *J. Am. Chem. Soc.* **1992**, *114*, 8295–8296; b) M. Sawamura, H. Hamashima, Y. Ito, *Tetrahedron* **1994**, *50*, 4439–4454; c) M. Sawamura, H. Hamashima, H. Shinoto, Y. Ito, *Tetrahedron Lett.* **1995**, *36*, 6479–6482.

[12] G. M. Sammis, H. Danjo, E. N. Jacobsen, *J. Am. Chem. Soc.* **2004***, 126,* 9928–9929.

[13] G. M. Sammis, E. N. Jacobsen, *J. Am. Chem. Soc*. **2003**, *125*, 4442–4443.

[14] S. E. Schaus, E. N. Jacobsen, *Org. Lett.* **2000**, *2*, 1001–1004.

[15] M. Ikeda, Y. Miyake, Y. Nishibayashi, *Chem. Eur. J*. **2012**, *18*, 3321–3328.

[16] Reviews: a) M. Shibasaki, H. Sasai, T. Arai, *Angew. Chem., Int. Ed. Engl.* **1997**, *36*, 1236–1256; b) M. Shibasaki, N. Yoshikawa, *Chem. Rev.* **2002**, *102*, 2187–2210; c) S. Matsunaga, M. Shibasaki, *Bull. Chem. Soc. Jpn.* **2008**, *81*, 60–75; d) M. Shibasaki, M. Kanai, S. Matsunaga, N. Kumagai, *Acc. Chem. Res.* **2009**, *42*, 1117–1127.

[17] A. Harada, Y. Makida, T. Sato, H. Ohmiya, M. Sawamura, *J. Am. Chem. Soc.* **2014**,

136, 13932–13939.

[18] Y. Yasuda, H. Ohmiya, M. Sawamura, *Angew. Chem. Int. Ed.* **2016**, *55*, 10816–10820.

[19] a) K. Öfele, *J. Organomet. Chem.* **1968**, *12*, 42–43; b) H.-W. Wanzlick, H.-J. Schönherr, *Angew. Chem*. **1968**, *80*, 154–154.

[20] A. J. Arduengo III, R. L. Harlow, M. Kline, *J. Am. Chem. Soc.* **1991**, *113*, 361–363.

[21] a) S. Díez-González, N. Marion, S. P. Nolan, *Chem. Rev.* **2009**, *109*, 3612–3676; b) D. Zhang, G. Zi, *Chem. Soc. Rev.* **2015**, *44*, 1898–1921.

[22] a) C. Burstein, C. W. Lehmann, F. Glorius, *Tetrahedron* **2005**, *61*, 6207–6217; b) M. Alcarazo, S. J. Roseblade, A. R. Cowley, R. Fernández, J. M. Brown, and J. M. Lassaletta, *J. Am. Chem. Soc.* **2005**, *127*, 3290–3291.

[23] J. T. Hutt, Z. D. Aron, *Org. Lett.* **2011**, *13*, 5256–5259.

[24] a) M. Espina, I. Rivilla, A. Conde, M. M. Díaz-Requejo, P. J. Pérez, E. Álvarez, R. Fernández, J. M. Lassaletta, *Organometallics* **2015**, *34*, 1328–1338; b) Y. Kim, Y. Kim, M. Y. Hur, E. Lee, *J. Organomet. Chem.* **2016**, *820*, 1–7; c) D.-A. Park, J. Y. Ryu, J. Lee, S. Hong, *RSC Adv.* **2017**, *7*, 52496–52502; d) M. Kashihara, R.-L. Zhong, K. Semba, S. Sakaki, Y. Nakao, *Chem. Commun*. **2019**, *55*, 9291–9294; e) X. Yi, K. Chen, J. Guo, W. Chen, W. Chen, *Adv. Synth. Catal.* **2020**, *362*, 4373–4377 f) R. Pedrazzani, A. Pintus, R. D. Ventura, M. Marchini, P. Ceroni, C. S. López, M. Monari, M. Bandini, *ACS Org. Inorg. Au* **2022**, *2*, 229–235; g) W. Han, H. Ryu, C. Kang, S. Hong, *Org. Lett.* **2024**, *26*, 9891–9896.

[25] a) C. Grohmann, T. Hashimoto, R. Fröhlich, Y. Ohki, K. Tatsumi, F. Glorius, *Organometallics* **2012**, *31*, 8047–8050; b) E. Y. Tsui, T. Agapie, *Polyhedron* **2014**, *84*, 103–110; c) R. Nakao, K. Nozaki, *J. Am. Chem. Soc.* **2015**, *137*, 10934–10937; d) W. Tao, R. Nakano, S. Ito, K. Nozaki, *Angew. Chem. Int. Ed.* **2016**, *55*, 2835–2839; *Angew. Chem.* **2016**, *128*, 2885–2889; e) W. Tao, S. Akita, S. Ito, Y. Hoshimoto, S. Ogoshi, K. Nozaki, *Chem. Commun.* **2017**, *53*, 2630–2633; f) G. Liu, C. Liu, F. Han, Z. Wang, J. Wang, *Tetrahedron Lett.* **2017**, *58*, 726–731; g) K. Azouzi, C. Duhayon, I. Benaissa, N. Lugan, Y. Canac, S. Bastin, V. César, *Organometallics* **2018**, 37, 4726–4735; h) I. Benaissa, K. Gajda, L. Vendier, N. Lugan, A. Kajetanowicz, K. Grela, V. Michelet, V. César, S. Bastin, O*rganometallics* **2021**, *40*, 3223–3234; i) S. Kuriyama, W. Zhao, Y. Nishibayashi, *Z. Anorg. Allg. Chem.* **2021**, *647*, 1408–1414; j) P. Krzesiński, K. Gajda, L. Vendier, A. Kajetanowicz, K. Grela, Stéphanie Bastin, V. César, *Z. Anorg. Allg. Chem.* **2024**, *650*, e202400199; k) M. Konwar, A. Das, *Org. Lett.* **2024**, *26*, 10235–10240; l) C. Kang, S. Kim, W. Han, H. Ryu, W. Seong, J. Kim, D.-A. Park, S. Park, K. Park, H. M. Park, H. T. Kim, C. H. Lee, S. Hong, *J. CO_2 Util.* **2025**, *91*, 103004.

[26] a) F. Grande-Carmona, J. Iglesias-Sigüenza, E. Álvarez, E. Díez, R. Fernández, J. M. Lassaletta, *Organometallics* **2015**, *34*, 5073–5080; b) C. T. Check, K. P. Jang, C. B. Schwamb, A. S. Wang, M. H. Wang, K. A. Scheidt, *Angew. Chem. Int. Ed.* **2015**, *54*, 4264–4268; *Angew. Chem.* **2015**, *127*, 4338–4342; c) J. Iglesias-Sigüenza, C. Izquierdo, E. Díez, R. Fernández, J. M. Lassaletta, *Dalton Trans.* **2016**, *45*, 10113–10117; d) J.-Q. Zhang, Y. Liu, X.-W. Wang, L. Zhang, *Organometallics* **2019**, *38*, 3931–3938; e) C. A. Swamy P, A. Varenikov, G. de Ruiter, *Chem. Eur. J.* **2020**, *26*, 2333–2337; f) L. Pallova, L. Abella, M. Jean, N. Vanthuyne, C. Barthes, L. Vendier, J. Autschbach, J. Crassous, S. Bastin, V. César, *Chem. Eur. J.* **2022**, *28*, e202200166.

[27] a) A. Fürstner, M. Alcarazo, H. Krause, C. W. Lehmann, *J. Am. Chem. Soc.* **2007**, *129*, 12676–12677; b) S. J. Roseblade, A. Ros, D. Monge, M. Alcarazo, E. Álvarez, J. M. Lassaletta, R. Fernández, *Organometallics* **2007**, *26*, 2570–2578; c) M. Alcarazo, T. Stoke, A. Anoop, W. Thiel, A. Fürstner, *Angew. Chem. Int. Ed.* **2010**, *49*, 2542–2546; *Angew. Chem.* **2010**, *122*, 2596–2600; d) Y. Tang, I. Benaissa, M. Huynh, L. Vendier, N. Lugan, S. Bastin, P. Belmont, V. César, V. Michelet, *Angew. Chem. Int. Ed.* **2019**, *58*, 7977–7981; e) S. Byun, H. Seo, J.-H. Choi, J. Y. Ryu, J. Lee, W. Chung, S. Hong, *Organometallics* **2019**, *38*, 4121–4132; f) L. Borislavov, I. Z. Koleva, V. Lozanova, M. Ivanova, R. Lyapchev, *Molbank* **2024**, *2024*, M1868.

[28] V. K. Rawat, K. Higashida, M. Sawamura, *Adv. Synth. Catal*. **2021**, *363*, 1631–1637.

[29] Silver-catalyzed cyclization of alkynoic acids, see: a) K. Schötz, T. Clark, H. Schaller, P. von R. Schleyer, *J. Org. Chem.* **1984**, *49*, 735–736; b) P. Pale, J. Chuche, *Tetrahedron Lett.* **1987**, *28*, 6447–6448; c) V. Dalla, P. Pale, *Tetrahedron Lett.* **1994**, *35*, 3525–3528; d) J. A. Marshall, M. A. Wolf, E. M. Wallace, *J. Org. Chem.* **1997**, *62*, 367–371; e) R. Rossi, F. Bellina, C. Bechini, L. Mannina, P. Vergamini, *Tetrahedron* **1998**, *54*, 135–156; f) V. Dalla, P. Pale, *New J. Chem.* **1999**, *23*, 803–805; g) F. Bellina, D. Ciucci, P. Vergamini, R. Rossi, *Tetrahedron* **2000**, *56*, 2533–2545; h) T. Yoshikawa, M. Shindo, *Org. Lett.* **2009**, *11*, 5378–5381; i) R. Nolla-Saltiel, E. Robles-Marín, S. Porcel, *Tetrahedron Lett.* **2014**, *55*, 4484–4488; j) I. J. Barve, T. U. Thikekar, C.-M. Sun, *Org. Lett.* **2017**, *19*, 2370–2373.

[30] For cyclization of alkynoic acids catalyzed by acid-base cooperative catalysts, see: a) N. Á. Espinosa-Jalapa, D. Ke, N. Nebra, L. L. Goanvic, S. Mallet-Ladeira, J. Monot, B. Martin-Vaca, D. Bourissou, *ACS Catal.* **2014**, *4*, 3605–3611; b) J. Monot, P. Brunel, C. E. Kefalidis, N. Á. Espinosa-Jalapa, L. Maron, B. Martin-Vaca, D. Bourissou, *Chem. Sci.* **2016**, *7*, 2179–2187.

[31] V. K. Rawat, K. Higashida, M. Sawamura, *ACS Catal.* **2022**, *12*, 8325–8330.

[32] N. A. Yakelis, R. G. Bergman, *Organometallics* **2005**, *24*, 3579–3581.

[33] Frisch, M. J.; Trucks, G. W.; Schlegel, H. B.; Scuseria, G. E.; Robb, M. A.; Cheeseman, J. R.; Scalmani, G.; Barone, V.; Petersson, G. A.; Nakatsuji, H.; Li, X.; Caricato, M.; Marenich, A. V.; Bloino, J.; Janesko, B. G.; Gomperts, R.; Mennucci, B.; Hratchian, H. P.; Ortiz, J. V.; Izmaylov, A. F.; Sonnenberg, J. L.; Williams-Young, D.; Ding, F.; Lipparini, F.; Egidi, F.; Goings, J.; Peng, B.; Petrone, A.; Henderson, T.; Ranasinghe, D.; Zakrzewski, V. G.; Gao, J.; Rega, N.; Zheng, G.; Liang, W.; Hada, M.; Ehara, M.; Toyota, K.; Fukuda, R.; Hasegawa, J.; Ishida, M.; Nakajima, T.; Honda, Y.; Kitao, O.; Nakai, H.; Vreven, T.; Throssell, K.; Montgomery, J. A., Jr., Peralta, J. E.; Ogliaro, F.; Bearpark, M. J.; Heyd, J. J.; Brothers, E. N.; Kudin, K. N.; Staroverov, V. N.; Keith, T. A.; Kobayashi, R.; Normand, J.; Raghavachari, K.; Rendell, A. P.; Burant, J. C.; Iyengar, S. S.; Tomasi, J.; Cossi, M.; Millam, J. M.; Klene, M.; Adamo, C.; Cammi, R.; Ochterski, J. W.; Martin, R. L.; Morokuma, K.; Farkas, O.; Foresman, J. B.; Fox, D. J. Gaussian 16, Revision C.01; Gaussian, Inc.: Wallingford, CT, 2019.

[34] J. C. Sheehan, G. P. Hess, *J. Am. Chem. Soc.* **1955**, *77*, 1067–1068.

[35] C. L. Stevens, M. E. Munk, *J. Am. Chem. Soc.* **1958**, *80*, 4069–4071.

[36] M. Goodman, L. Levine, *J. Am. Chem. Soc.* **1964**, *86*, 2918–2922.

[37] Z. Wang, X. Wang, P. Wang, J. Zhao, *J. Am. Chem. Soc.* **2021**, *143*, 10374–10381.

[38] a) M. A. Winnik, *Chem. Rev.* **1981**, *81*, 491–524; b) G. A. Molander, *Acc. Chem. Res.* **1998**, *31*, 603–609; c) G. Mehta, V. Singh, *Chem. Rev.* **1999**, *99*, 881–930; d) A. Hussain, S. K. Yousuf, D. Mukherjee, *RSC Adv.* **2014**, *4*, 43241–43257; e) R. L. Reyes, T. Iwai, M. Sawamura, *Chem. Rev.* **2021**, *121*, 8926–8947; f) T. Yao, J. Li, C. Jiang, C. Zhao, *Chem Catal.* **2022**, *2*, 2929–2964.

[39] R. M. Beesley, C. K. Ingold, J. F. Thorpe, *J. Chem. Soc., Trans.* **1915**, *107*, 1080–1106.

[40] P. von Ragué Schleyer, *J. Am. Chem. Soc.* **1961**, *83*, 1368–1373.

[41] a) T. C. Bruice, U. K. Pandit, *J. Am. Chem. Soc.* **1960**, *82*, 5858–5865; b) T. C. Bruice, U. K. Pandit, *Proc. Natl. Acad. Sci. USA* **1960**, *46*, 402–404.

[42] A. L. Parrill, D. P. Dolata, *Tetrahedron Lett.* **1994**, 35, 7319–7322.

[43] Reviews for Thorpe–Ingold effect: a) P. G. Sammes, D. J. Weller, *Synthesis*, **1995**, 1205; b) C. Galli, L. Mandolini, *Eur. J. Org. Chem.*, **2000**, 3117–3125; c) M. E. Jung, G. Piizzi, *Chem. Rev.* **2005**, *105*, 1735–1766.

[44] C. Galli, G. Giovannelli, G. Illuminati, L. Mandolini, *J. Org. Chem.* **1979**, *44*, 1258–1261.

[45] a) C. H. Kim, K. P. Jang, S. Y. Choi, Y. K. Chung, E. Lee, *Angew. Chem. Int. Ed.*

2008, *47*, 4009–4011; b) H. Kim , Y. Park, J. Hong, *Angew. Chem. Int. Ed.* **2009**, *48*, 7577–7581.

[46] M. I. Page, W. P. Jencks, *Proc. Natl. Acad. Sci. U.S.A.* **1971**, 68, 1678–1683.

[47] G. S. Hammond, *J. Am. Chem. Soc.* **1955**, *77*, 334–338.

[48] a) S. Gronert, J. M. Lee, *J. Org. Chem.* **1995**, *60*, 6731–6736. b) S. Gronert, K. Azizian, M. A. Friedman, *J. Am. Chem. Soc.* **1998**, *120*, 3220–3226.

[49] L. Ruzicka. W. Brugger, M. Pfeiffer, H. Schinz, M. *Stoll, Helv. Chim. Acta* **1926**, *9*, 499–520.

[50] a) K. B Wiberg, R. F. Waldron, *J. Am. Chem. Soc.* **1991**, *113*, 7697–7705; b) J. M. Brown, A. D. Conn, G. Pilcher, M. L. P. Leitão, Y. Meng-Yan, *J. Chem. Soc., Chem. Commun.* **1989**, 1817–1819; c) H. J. Rodriguez, J.-C. Chang, T. F. Thomas, *J. Am. Chem. Soc*. **1976**, 98, 2027–2034; d) C. F. Rodriquez, I. H. Williams, *J. Chem. Soc., Perkin Trans. 2* 1997, 953–957.

[51] A. Ochida, H. Ito, and M. Sawamura, *J. Am. Chem. Soc.* **2006**, *128*, 16486–16487.

[52] T. Iwai, H. Okochi, H. Ito, M. Sawamura, *Angew. Chem. Int. Ed*. **2013**, *52*, 4239–4242.

[53] T. Iwai, M. Ueno, H. Okochi, M. Sawamura, *Adv. Synth. Catal*. **2018**, *360*, 670–675.

Chapter 1

Gold-Zinc Co-Catalyzed Alkynoate Hydrocarboxylation with *N*-Protected Amino Acids for Preparation of Storable Acylating Reagents and Racemization-Free Peptide Synthesis

2.1 Introduction

Peptide synthesis is a vast research field in organic chemistry due to the importance of peptides in drug discovery[1] and materials science.[2] Peptide coupling methodology has made great advances with the development of new coupling reagents[3] that convert carboxylic acid termini of amino acids or peptides into activated ester intermediates. While reactivity of the activated esters is the key for peptide synthesis, epimerization of the activated esters through oxazolone formation is an issue to be considered. In this context, α-carbonyl enol esters can be ideal forms of activated esters since they readily react with amines under mild conditions but are stable enough in most cases to be isolated without racemization (Scheme 2.1a).[4] In 1961, peptide synthesis *via* α-carbonyl enol ester intermediates was reported for the first time, using isoxazolium salt **A** as a peptide coupling reagent.[5] Later, 4-(dimethylamino)but-3-yn-2-one (**B**) was introduced as a reagent to form α-carbonyl enol esters.[6] More recently, a racemization-free peptide synthesis protocol, which utilizes the 1,4-addition/isomerization cascade reaction of carboxylic acids with allenone **C**, was reported.[4] However, the use of hazardous and expensive chemicals is required for the preparation of the allenone reagent (**C**). Although a more simple protocol to generate α-carbonyl enol ester intermediates by using a combination of commercially available reagents, ethyl propiolate (**D**) and a tertiary amine catalyst, also exists in the literature,[7] unavoidable partial epimerization during the preparation of the α-carbonyl enol ester caused by the basic amine catalyst remains problematic. Hence, a novel epimerization-free protocol for α-carbonyl enol esters with readily available reagents is demanded.

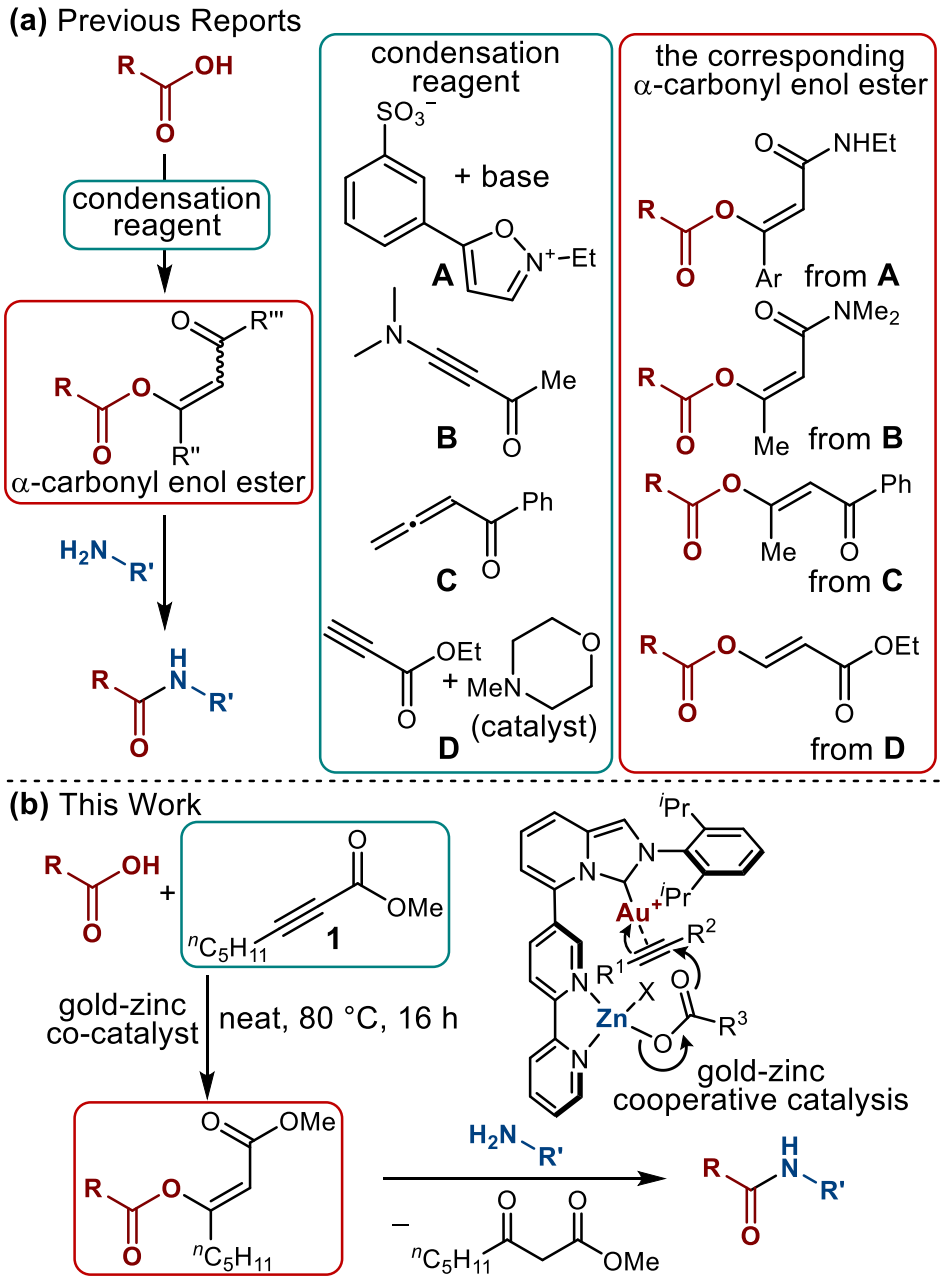

Scheme 2.1. (a) Reported synthesis of α-carbonyl enol esters as methods to activate carboxylic acids for peptide bond formation. (b) This work: Gold-zinc co-catalyzed hydrocarboxylation of methyl 2-octynoate (**1**).

Hydrocarboxylation of alkynes is one of the most straightforward methods for preparing enol ester derivatives.[8] Earlier, Sawamura and co-workers developed gold-zinc cooperative catalysis systems involving 5-[(2,2′-bipyridin)-5-yl]imidazo[1,5-*a*]pyridin-3-ylidene ligands for use in hydrocarboxylations of alkynes, in which the carboxylic acid was activated by deprotonation, with the basic zinc site for attacking the

alkyne partner activated by π-Lewis acidic coordination of the cationic gold(I) center.[9] Here, the author reports an application of gold-zinc cooperative catalysis for transformation of *N*-protected amino acids to α-alkoxycarbonyl enol esters, which simply utilizes methyl 2-octynoate (**1**) as a condensation reagent (Scheme 2.1b).[10, 11] The author selected this specific alkynoate since it is commercially available at a particularly low cost[12, 13] as a fragrance in cosmetics and as a food additive.[14] The α-methoxycarbonyl enol esters can be isolated and stored without racemization for use in *N*-acylative direct peptide synthesis.

2.2 Results and Discussion

Hydrocarboxylation of methyl 2-octynoate (**1**, 0.55 mmol) with *N*-Boc-glycine (Boc−Gly−OH, **2 a**, 0.50 mmol) catalyzed by the gold-zinc system (**3 a**/$AgPF_6$/$Zn(acac)_2$ 1:1:1, 0.4 mol%) occurred efficiently with exclusive regio- and *anti*-stereoselectivity by heating at 80 °C for 16 h under neat conditions, affording α-methoxycarbonyl enol ester **4 a** in >99% yield based on *N*-protected amino acid **2 a** as determined by ^{1}H NMR spectroscopy (Table 2.1, entry 1; Figure 2.1). The reaction also proceeded efficiently using 1,2-dichloroethane as a solvent, albeit with a slightly lower product yield (94% yield) (entry 2).[15] Only 1% of **4 a** was produced in the absence of $AgPF_6$, indicating that the cationic nature of the gold(I) center is crucial (entry 5). When $Zn(acac)_2$ was omitted, the yield of **4 a** dropped to 52%, in accordance with the assumed role of the zinc-acac moiety to activate the carboxylic acid through deprotonation (entry 6).

The hydrocarboxylation also occurred even when gold complex **3a** was omitted, albeit with much reduced product yield (22%), suggesting that the cationic silver(I) complex ($AgPF_6$) is also capable of activating the alkynoate (**1**) as a π-Lewis acid, although its efficiency is markedly lower than that of the gold(I) center (Table 2.1, entry 7).[16] The catalytic activity of $AgPF_6$ was still observed even in the absence of $Zn(acac)_2$, giving **4 a** in 14% yield (entry 8). Based on these observations, the author tested the feasibility of the silver-catalyzed reaction as a practical synthetic method by increasing the amount of $AgPF_6$ to 5 mol%; however, the silver-catalyzed reaction was not clean, forming **4 a** in only 26% yield together with a significant amount of unidentified byproducts (entry 9).

Using gold complexes **3 b**–**d** instead of **3 a** reduced the yields of **4 a** to 70–98%, showing the influence of the *N*-substituent (−**R**) of the *N*-heterocyclic carbene moiety

(Table 2.1, entries 10–12; Figure 2.1). The use of a commercially available phosphine-gold(I) complex, (Johnphos)AuCl (**5**), resulted in moderate yields of **4 a** regardless of the presence or absence of $Zn(acac)_2$ and an external bipyridine ligand (63–80%) (entries 13–15; Figure 1).[17] Another commercially available NHC-gold(I) catalyst, (IPr)AuCl (**6**), was also tested, revealing that the combination of **6**, $Zn(acac)_2$, $AgPF_6$, and bipyridine as an external ligand showed high catalytic performance both under solventless conditions (93% yield) and under diluted conditions with 1,2-dichloroethane (92% yield) (entry 17 and 18; Figure 2.1). The necessity for both $Zn(acac)_2$ and the bipyridine ligand for the high activity of **6** also supported the assumed cooperative action between the NHC-gold(I) complex and the basic zinc(II) complex in the nucleophilic addition (vs. entries 16 and 19).

When all manipulations for the hydrocarboxylation with **3 a** and $Zn(acac)_2$ were conducted under air with AgOTf instead of deliquescent $AgPF_6$, the reaction efficiency was nearly maintained to give **4 a** in 91% yield (Table 2.1, entry 3). Reducing the loading (0.1 mol%) of the **3 a**/$Zn(acac)_2$/$AgPF_6$ catalyst system to 0.1 mol% caused a drop in the yield of **4 a** (64%) (entry 4). Hence, the conditions in entry 1 [0.4 mol% loading of the **3 a**/$Zn(acac)_2$/$AgPF_6$ (1:1:1) catalyst system, 80 °C, 16 h, neat] were determined to be optimal.

Table 2.1. Screening of reaction conditions for hydrocarboxylation.

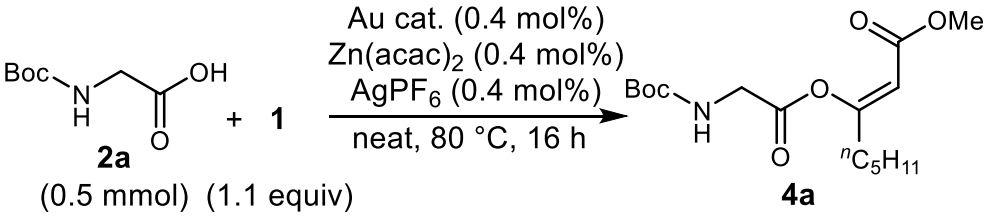

entry	Au cat.	$Zn(acac)_2$	$AgPF_6$	yield [%][a]
1	**3a**	+	+	>99
2[b]	**3a**	+	+	94
3[c]	**3a**	+	+	91
4[d]	**3a**	+	+	64
5	**3a**	+	−	1
6	**3a**	−	+	52
7	−	+	+	22
8	−	−	+	14
9[e]	−	−	+	26
10	**3b**	+	+	89
11	**3c**	+	+	70
12	**4d**	+	+	98
13	**5**	+	+	80
14[f]	**5**	+	+	79
15	**5**	−	+	63
16	**6**	+	+	76
17[f]	**6**	+	+	93
18[b,f]	**6**	+	+	92
19	**6**	−	+	69

[a] Yield was determined by ^{1}H NMR analysis using phenanthrene as an internal standard. [b] In 1,2-dichloroethane (2 M). [c] Under benchtop conditions with a simple screw-cap vial using AgOTf instead of $AgPF_6$. [d] 0.1 mol% of catalyst loading with **2a** (2.0 mmol) and 1 (2.2 mmol). [e] 5.0 mol% of $AgPF_6$ was used. [f] Addition of 2,2'-bipyridine (0.4 mol%).

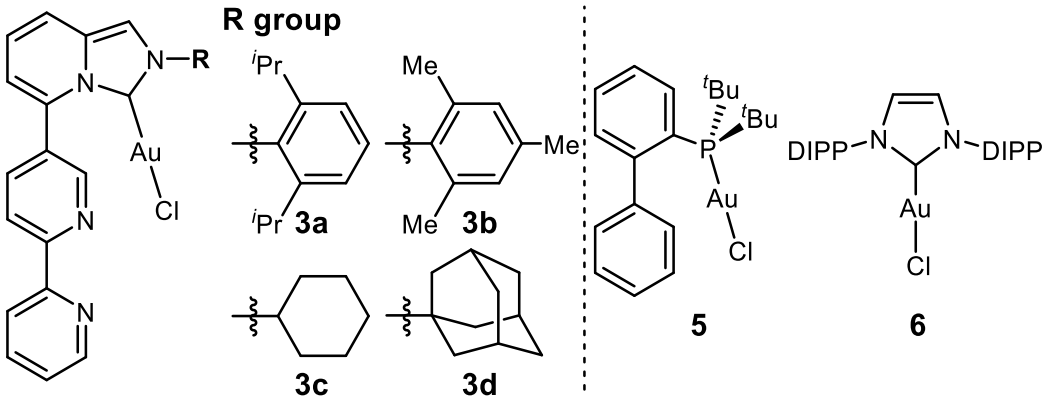

Figure 2.1. Structures of gold(I) complexes.

With the optimal conditions in hand, the author examined the substrate scope of *N*-protected amino acids (Scheme 2.2). The α-methoxycarbonyl enol ester (**4a**) produced by the reaction between **1** and **2 a** was isolated in analytically pure form in 96% yield by silica-gel column chromatography. The purified activated *N*-protected amino acid (**4a**) was stable enough to be handled under air at ambient temperature. When the gold-zinc catalyzed hydrocarboxylation was performed with enantiopure chiral *N*-protected amino acids such as Boc−L−Val−OH, Boc−L−Phe−OH, Boc−L−Pro−OH, and Boc−L−Phg−OH, the corresponding α-methoxycarbonyl enol esters **4b**–**e** were obtained in high yields (84–98%) without loss of their enantiopurities (>99% ee). *O*-Benzyl-protected Boc−L−Ser−OH was also converted into activated ester **4f** in 97% yield. The reaction conditions tolerated unprotected phenol and indole moieties of Boc−L−Tyr−OH and Boc−L−Trp−OH to give the corresponding α-methoxycarbonyl enol esters **4g** and **4h** in 89% and 78% yields, respectively, although 3 equivalents of **1** were required for the reaction of Boc−L−Try−OH due to its low solubility. An α,α-disubstituted amino acid, 2-(*tert*-butoxycarbonylamino)isobutyric acid, was also a suitable substrate, giving **4i** in 82% yield. An azetidine skeleton of 1-(*tert*-butoxycarbonyl)azetidine-3-carboxylic acid was tolerated under the reaction conditions to afford **4j** in 95% yield. Thus, the gold-zinc cooperative hydrocarboxylation is broadly applicable to natural and unnatural *N*-Boc-protected amino acids. However, Boc−L−Met−OH and Boc−L−His−OH showed low or no reactivity for this reaction, suggesting unfavorable effects of metal-coordination of the sulfide moiety and imidazole ring. An *N*-Fmoc-protected amino acid, Fmoc−L−Phe−OH, which showed a low solubility, reacted with **1** (3 equiv.), giving the corresponding α-methoxycarbonyl enol ester **4k** in 90% yield.

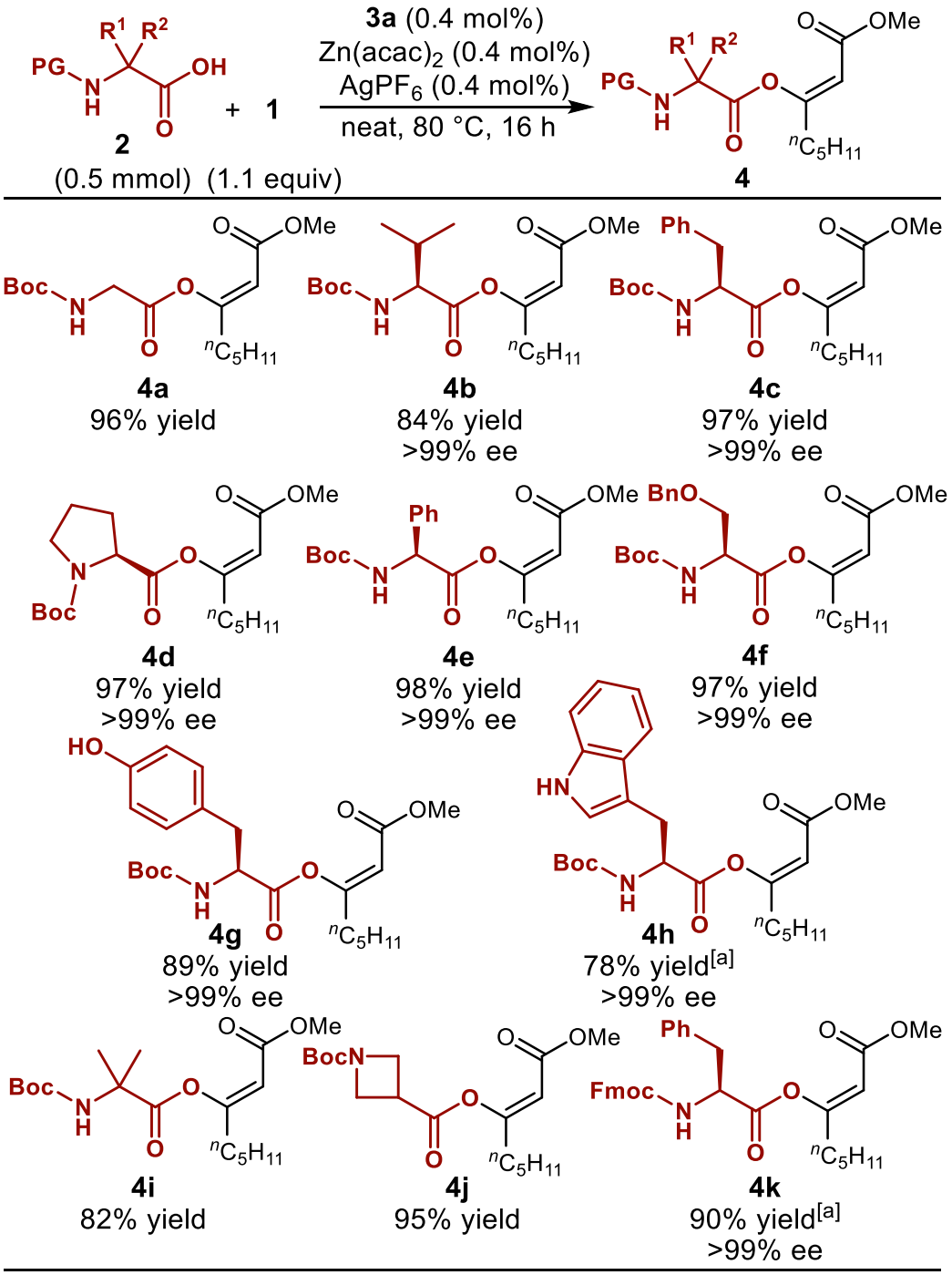

Scheme 2.2. Scope of *N*-Boc α-amino acids for transformation to α-methoxycarbonyl enol esters (**4**). Reactions were performed with **2** (0.50 mmol), **1** (0.55 mmol), **3a** (0.4 mol%), $Zn(acac)_2$ (0.4 mol%), and $AgPF_6$ (0.4 mol%) at 80 °C for 16 h. The yields were reported as isolated yield. [a]3.0 equiv. of **1** (1.5 mmol) was used

Next, the reaction conditions for amide bond formation were investigated with α-methoxycarbonyl enol ester **4c** and L-phenylalanine methyl ester (**7a**) as a substrate couple (Table 2.2). The author selected EtOAc as a solvent for the dipeptide synthesis, considering its preferred use in pharmaceutical industry.[18] Treatment of **4c** and **7a** in EtOAc at room temperature for 1 h afforded dipeptide **8a** in 78% yield (entry 1). Increasing the reaction time (4 h) had only a slight effect on the yield of **8a** (85%) (entry 2). Amide bond formation required 12 h at room temperature to reach completion (entry 3). A higher reaction temperature (70 °C) facilitated the reaction, giving **8a** in 95% yield after 1 h and in quantitative yield after 2 h (entries 4 and 5). Notably, these reactions can be performed under benchtop conditions without the need for dehydrated EtOAc and dry inert gas. Since unreacted **4c** and methyl 3-oxooctanoate (**9**) were highly soluble in hexane, dipeptide **8a** could be isolated as a solid in analytically pure form in 93% yield simply by washing with hexane and drying (entry 5). HPLC analysis of the dipeptide (**8a**) confirmed that no epimerization of the stereogenic center derived from the activated ester (**4c**) occurred in this protocol (entry 5).

Table 2.2. Screening of reaction conditions for amide bond formation.

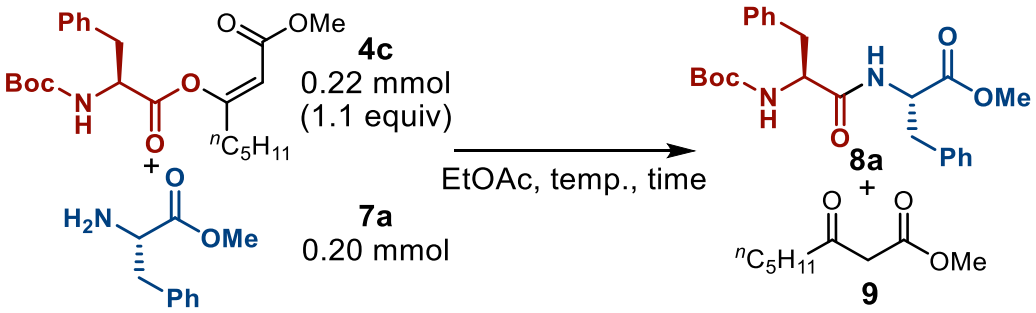

entry	temp.	time [h]	yield of **8a** [%][a]
1	r.t.	1	78
2	r.t.	4	85
3	r.t	12	97
4	70 °C	1	95
5	70 °C	2	>99 (93)[b,c]

[a] Determined by ^{1}H NMR analysis using phenanthrene as an internal standard. [b] Isolated yield after hexane-washing purification. [c] The area ratio for L,L-isomer and D,L-isomer of **8 a** from HPLC analysis is >99.5:<0.5.

The other α-methoxycarbonyl enol esters (**4**) shown in Scheme 2.2 were also successfully used for peptide synthesis with L-phenylalanine methyl ester (**7a**) with

complete retention of the configurations of the stereogenic centers. The results are summarized in Scheme 2.3. The hexane-washing purification protocol was effective for the dipeptides (**8c**,**e**–**i**,**k**), but an oily compound **8b** and soluble compounds **8d** and **8j** required purification by silica-gel column chromatography.

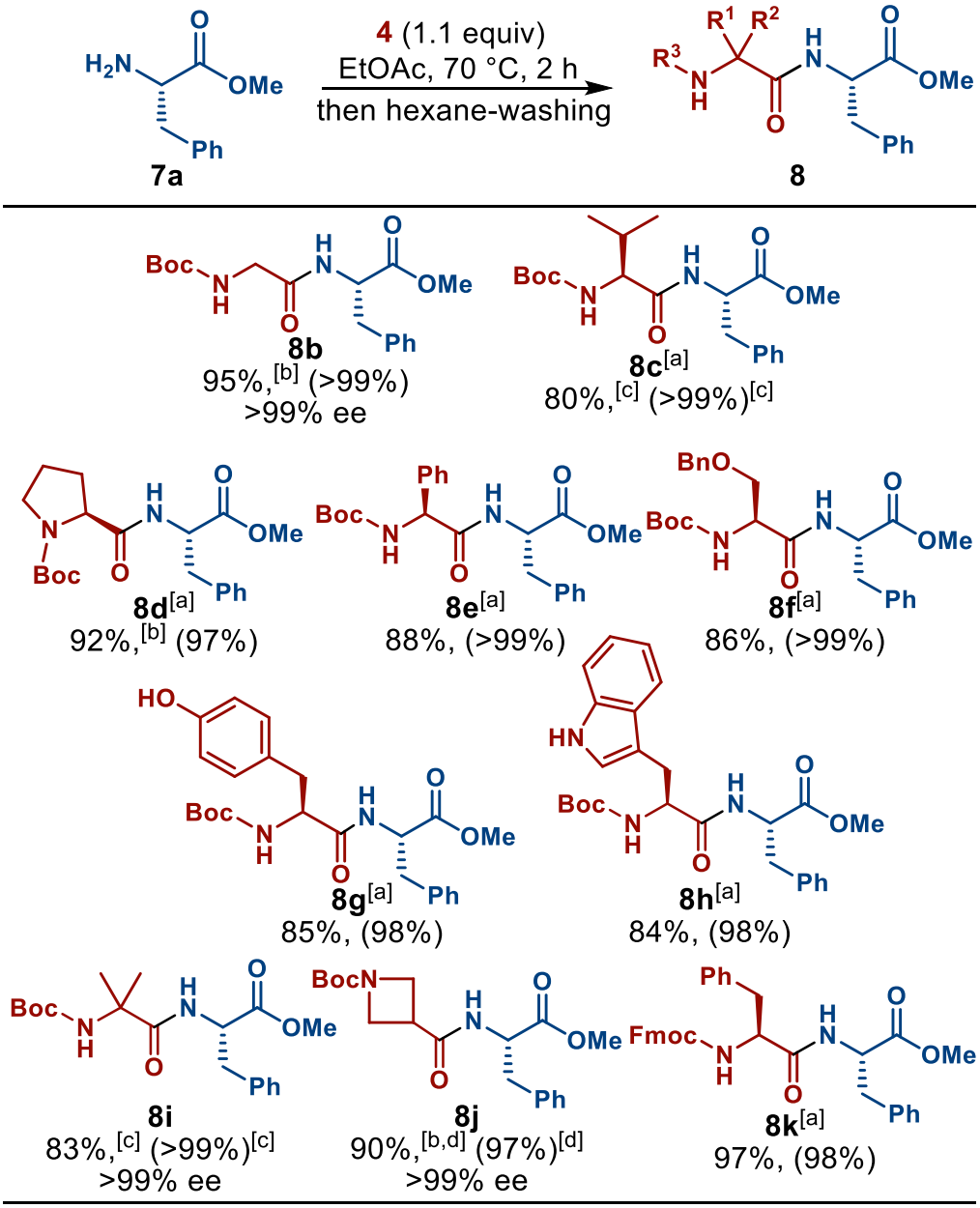

Scheme 2.3. Dipeptide synthesis with **4** (0.22 mmol) and **7a** (0.20 mmol) in EtOAc (1.0 mL) at 70 °C for 2 h. Dipeptides **8** were isolated with the hexane-washing protocol unless otherwise noted, and the yields were reported as isolated yield. ^{1}H NMR yields are given

in parentheses. [a]The area ratio for L,L-isomer and D,L-isomer from HPLC analysis is >99.5:<0.5. [b] Isolated by silica-gel column chromatography. [c] For 12 h. [d] For 4 h.

To demonstrate scalability of the protocol, gold-zinc co-catalyzed hydrocarboxylation of methyl 2-octynoate (**1**) was conducted with 10 mmol of Boc−L−Phe−OH (**2c**) (Scheme 2.4(a)). The catalytic hydrocarboxylation proceeded cleanly at 80 °C to afford α-methoxycarbonyl enol ester **4c** in 98% yield. The isolated **4 c** was shelf-stable, remaining unchanged after storage for six months under ambient conditions in a screw-cap vial. The activated *N*-Boc α-amino acid (**4c**) could be used as a reagent for *N*-acylation of the primary amino group of oseltamivir (**7 b**), an antiviral flu drug,[19] and the secondary amino group of amoxapine (**7c**), an antidepressant,[20] giving the corresponding amides **8l** and **8m** in 95% and >99% yields, respectively, in analytically pure forms (Scheme 2.4(b)). The protocol was also applicable to the synthesis of Boc−L−Val−L−Val−OBn (**8n**), a dipeptide with contiguous bulky amino acid residues (Scheme 2.4(c)).

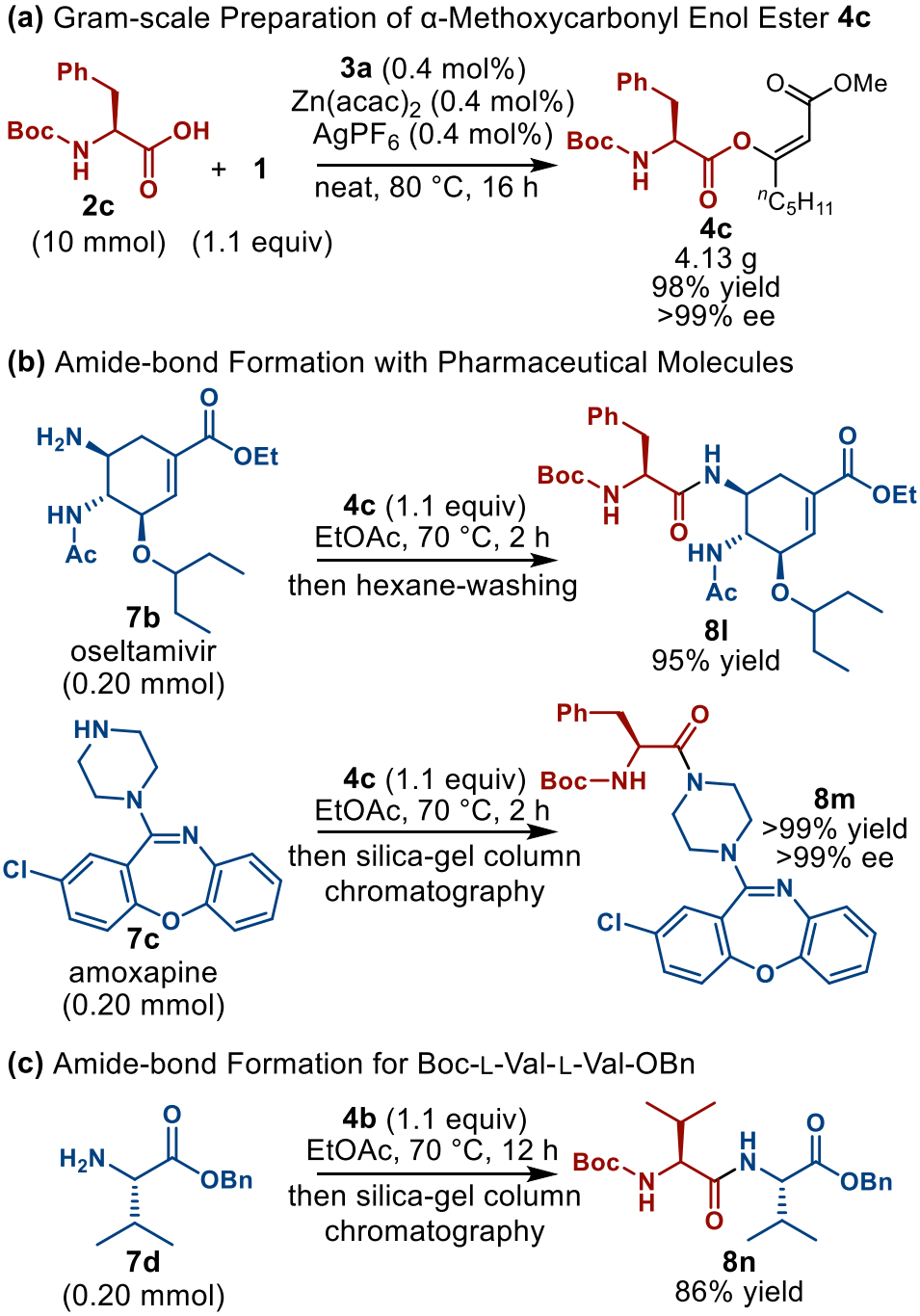

Scheme 2.4. Synthetic applications.

To gain insights into the high reactivity of enol esters **4** toward amide bond formation, the nucleophilic substitution of an α-methoxycarbonyl enol ester (**SM**) with glycine methyl ester was assessed by DFT calculations at the ωB97X−D/6–311G(d,p)/SMD(EtOAc) level of theory (Figure 2.2).[21] The amino group of the glycine methyl ester attacks the enol ester carbonyl group of **SM** with mutual protonative leaving

group activation through N−H···O hydrogen-bonding, forming an amide bond with concomitant release of methyl 3-hydroxybut-2-enoate through an eight-membered ring transition state (**TS$_{amine}$**) with a reasonable energy barrier (21.0 kcal/mol). This amide-bond formation is a 22.2 kcal/mol exergonic process.

To understand the reason for the high moisture tolerance of the α-methoxycarbonyl enol esters in the amide-bond formation, the pathway for hydrolysis of **SM** was also assessed by calculations. It was revealed that hydrolysis can also proceed through a similar eight-membered ring transition state (**TS$_{water}$**), but it requires a much higher activation energy (32.7 kcal/mol) given that amide-bond formation with α-carbonyl enol esters **4** occurs more readily than hydrolysis.

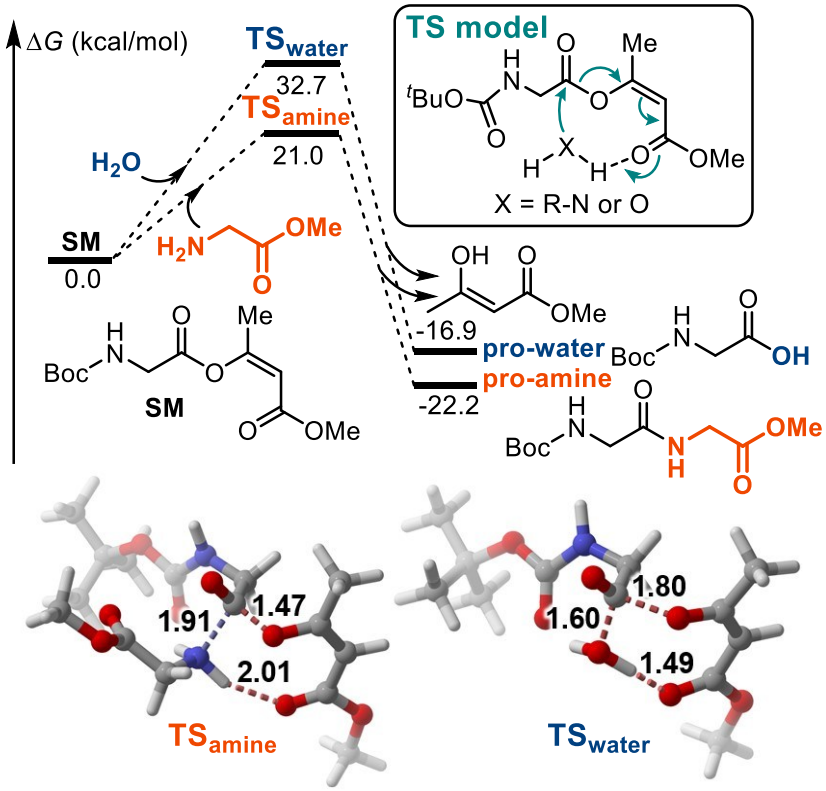

Figure 2.2. Energy diagram for amide-bond formation and hydrolysis of α-carbonyl enol ester. Selected bond distances [Å] are given in 3D-structures for transition states.

2.3 Conclusions

In summary, the author developed a gold-zinc co-catalyzed hydrocarboxylation process for methyl 2-octynoate with *N*-protected amino acids as a method for preparing α-

methoxycarbonyl enol esters as isolable intermediates for amide-bond formation. The gold-zinc cooperative catalyst system tethered with a 5-[(2,2′-bipyridin)-5-yl]imidazo[1,5-*a*]pyridin-3-ylidene was the most efficient, but an untethered system with bipyridine and a simple NHC ligand (IPr) was also practical. The enol esters are stable enough to be handled and stored without precautions to exclude air. Amide-bond formation between the enol esters and amines smoothly proceeded in EtOAc as a solvent without loss of enantiopurity. DFT calculations suggested that amide-bond formation proceeds with mutual protonative leaving group activation through amine-to-methoxycarbonyl group N−H···O hydrogen bonding.

2.4 Experimental Section

2.4.1 General Remarks

All air and moisture-sensitive reactions were operated using the standard Schlenk techniques and an argon- or nitrogen-filled glove box. Dehydrated 1,2-dichloroethane was purchased from Sigma-Aldrich Co. LLC. (Aldrich). Methyl 2-octynoate (CAS: 111-12-6) and $Zn(acac)_2$ (CAS: 14024-63-6) were used as received from Tokyo Chemical Industry Co., Ltd. (TCI). $AgPF_6$ (CAS: 26042-63-7) was purchased from TCI and Aldrich and handled in a glove box due to its hygroscopic property. Oseltamivir phosphate (CAS: 204255-11-8) was purchased from Thermo Fisher Scientific Inc.. Amoxapine (CAS: 14028-44-5) was purchased from TCI. Commercially available gold(I) complexes (Johnphos)AuCl (**5**) and (IPr)AuCl (**6**) were purchased from Aldrich. NHC-gold complexes (**3a**-**d**) bearing a bipyridine coordination site were prepared through the reported method.[9] Amino acid derivatives were purchased from TCI. Ethyl acetate (Wako 1st Grade, 99.0+%, FUJIFILM Wako Pure Chemical Corporation) was used for amide-bond formation as received. ^{1}H NMR (400 MHz) and ^{13}C{^{1}H} NMR (100 MHz) spectra were measured on JEOL ECZ-400S spectrometer. All ^{1}H NMR chemical shifts were reported in ppm (δ) relative to the chemical shifts of residual solvent resonances ($CDCl_3$ at δ 7.26). All ^{13}C{^{1}H} NMR chemical shifts were reported in ppm (δ) relative to carbon resonances of $CDCl_3$ at δ 77.0. High-resolution mass spectra were obtained with Thermo Fisher Scientific Exactive, JEOL JMS-T100LP, or JEOL JMS-700TZ at the Instrumental Analysis Division, Equipment Management Center, Creative Research Institution, Hokkaido University. Enantiomeric excess of the products was determined by HPLC analysis using JASCO EXTREMA. Optical rotations were obtained on JASCO P-2200. IR spectra were obtained on JASCO FT-IR-4600 spectrometer. Flash column

chromatography was performed using silica-gel (Wakogel FC-40, 0.020-0.040 nm >70%). The gold-zinc catalyzed reactions were conducted using EYELA RCH-1000 of TOKYO RIKAKIKAI CO, LTD as a heating reactor with a screw-cap vial (NN-13, φ13 mm) of Maruemu Corporation.

2.4.2. Experimental Section

General Procedure for Preparing α-Carbonyl Enol Esters 4

In an argon-filled glove box, *N*-protected amino acid (0.50 mmol), gold(I) complex **3a** (1.3 mg, 0.002 mmol, 0.4 mol%), $Zn(acac)_2$ (0.53 mg, 0.002 mmol, 0.4 mol%), and $AgPF_6$ (0.5 mg, 0.002 mmol, 0.4 mol%) were placed in a screw-cap vial containing a magnetic stirring bar. After addition of methyl 2-octynoate (91.2 μL, 0.55 mmol, 1.1 equiv.), the reaction vial was sealed with a screw-cap and removed from the glove box. The mixture was stirred at 80 °C for 16 h. The crude product was purified by silica-gel column chromatography to give the corresponding enol esters.

General Procedure for Amide-Bond Formation

4 (0.22 mmol, 1.1 equiv.) in EtOAc (1.0 mL) was added to **7** (0.20 mmol) in a screw-cap vial containing a stir bar. After stirring the mixture at 70 °C for 2 h, the resulting solution was transferred to a small screw-cap vial. Volatiles were removed by rotary evaporation. The residual solid was triturated and sonicated in hexane, and the white precipitate was collected by suction filtration washing with hexane. The resulting solid was dried under reduced pressure to afford the corresponding amide compounds.

Screening of the Reaction Conditions

In the initial study, reaction conditions for nucleophilic addition of Boc-Gly-OH toward methyl 2-octynoate were conducted in 1,2-dichloroethane (2.0 M) as a solvent, as shown in Table **2.3**. In these results, using $Zn(acac)_2$ and $AgPF_6$ gave enol ester in the highest yield (entry 8, 94% yield). Further optimization as well as control experiments were carried out under solvent-free conditions with gold-complexes, $Zn(acac)_2$, and $AgPF_6$.

Experimental Procedure for Table 2.3

In a nitrogen-filled glove box, Au catalyst (0.002 mmol, 0.4 mol%) and anion source (0.002 mmol, 0.4 mol%) were placed in a screw vial containing a magnetic stirring bar. After addition of dry DCE (0.25 mL), the reaction mixture was stirred for 10 minutes.

The resulting solution was filtered through a glass-fiber pad packed into a pipette, and the filtrate was added to metal salt (0.002 mmol, 0.4 mol%) in a screw vial containing a magnetic stirring bar. Boc-Gly-OH (87.6 mg, 0.50 mmol, 1.0 equiv) and methyl 2-octynoate (91.2 μL, 0.55 mmol, 1.1 equiv) were added to the mixture, and the reaction vial was sealed with a screw-cap and removed from the glove box. After stirring at 80 °C for 16 hours, the resulting mixture was quenched through short silica-gel column with EtOAc as an eluent. Yield was determined by ^{1}H NMR analysis using phenanthrene as an internal standard.

Table 2.3. Screening of Reaction Conditions.

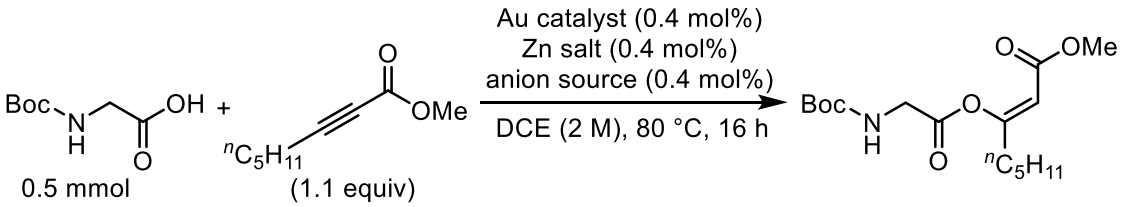

entry	Au catalyst	Zn salt	anion source	NMR yield [%][a]
1	**3a**	$Zn(acac)_2$	$NaBAr^F$	77
2	**3b**	$Zn(acac)_2$	$NaBAr^F$	40
3	**3c**	$Zn(acac)_2$	$NaBAr^F$	17
4	**3d**	$Zn(acac)_2$	$NaBAr^F$	18
5	**3a**	$Zn(hfac)_2{\cdot}2H_2O$	$NaBAr^F$	55
6	**3a**	$Zn(tmhd)_2$	$NaBAr^F$	47
7	**3a**	$Zn(acac)_2$	$AgBF_4$	70
8	**3a**	**$Zn(acac)_2$**	**$AgPF_6$**	**94**
9	**3a**	$Zn(acac)_2$	$AgSbF_6$	36
10	**3a**	$Zn(acac)_2$	AgOTf	92
11	**3a**	$Zn(acac)_2$	$AgNTf_2$	90
12	**3a**	$Zn(acac)_2$	$NaBPh_4$	9
13[b]	**3a**	$Zn(acac)_2$	$NaBAr^F$	69
14[c]	**6**	$Zn(acac)_2$	$AgPF_6$	92

acac = acetylacetonate, hfac = hexafluoroacetylacetonate, tmhd = tetramethyl heptanedioate
[a]Yield was determined by ^{1}H NMR analysis using phenanthrene as an internal standard.
[b]0.8 mol% of $NaBAr^F$ was used. [c]With 2,2'-bipyridine (0.4 mol%).

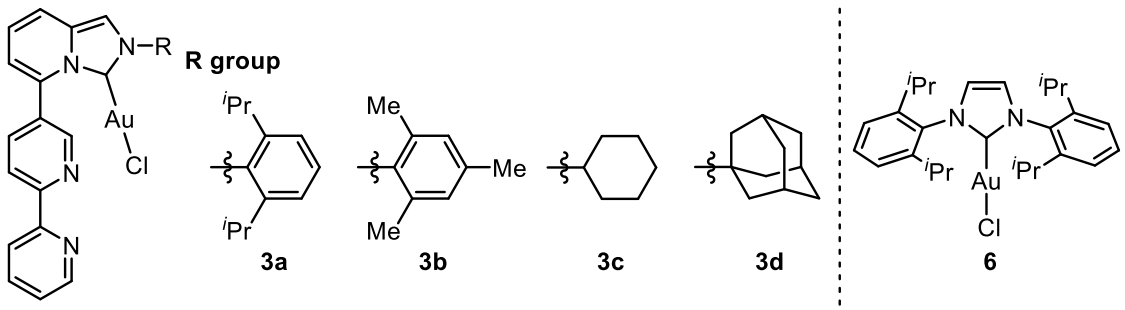

Catalytic Activity of IPr-AuCl toward Hydrocarboxylation with Boc-L-Phe-OH

The hydrocarboxylation of enantiopure *N*-protected amino acid, Boc-L-Phe-OH, was tested with commercially available (IPr)AuCl (**6**), $Zn(acac)_2$, $AgPF_6$, and 2,2'-bipyridine. As the result, the corresponding α-methoxycarbonyl enol ester was obtained in 85% yield lower than that of **3a**, $Zn(acac)_2$, and $AgPF_6$ system without loss of enantiopurity (>99% ee).

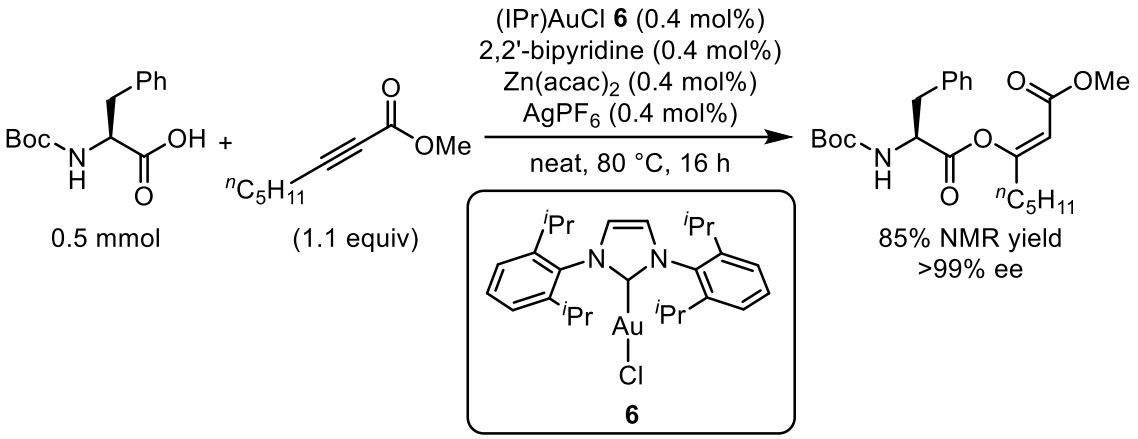

Hydrocarboxylation with *N*-Fmoc Protected Amino Acid

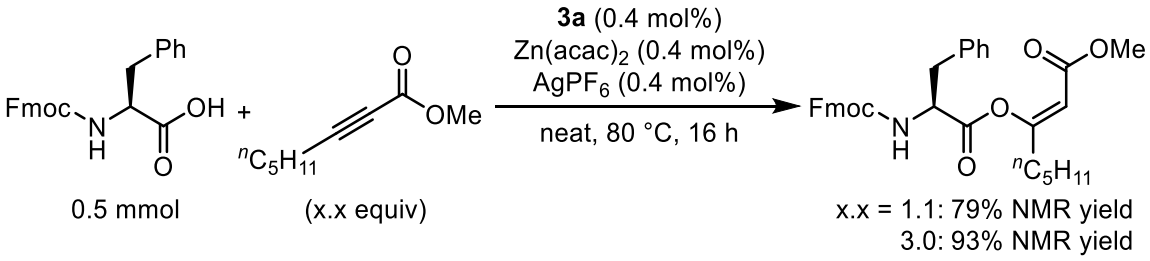

Hydrocarboxylation with Alkynyl Ketones and an Alkynyl Amide

Hydrocarboxylation with alkynyl ketones and an alkynyl amide was also tried under the optimized conditions; however, these reactions were not effective for preparing α-carbonyl enol esters.

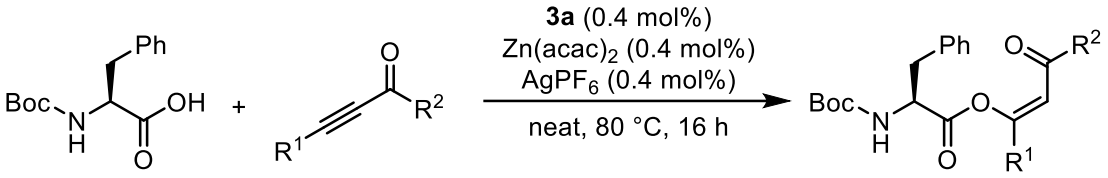

0.5 mmol (1.1 equiv)

entry	R^1	R^2	NMR yield [%][a]
1	$^nC_2H_5$	Me	complex mixture
2	Ph	Me	complex mixture
3	Ph	CF_3	n.d.
4	$^nC_5H_{11}$	NMe_2	n.d.

[a]Yield was determined by ^{1}H NMR analysis using phenanthrene as an internal standard.

Screening of Solvents for Amide Formation

The effects of solvents for amide formation were investigated by using methyl (*Z*)-3-(((*tert*-butoxycarbonyl)glycyl)oxy)oct-2-enoate (**4a**) and 2-phenylethylamine as free amine, as shown in Table 2.4. The results indicated that amide bond formation smoothly proceeded in any types of solvents.

Experimental Procedure for Table 2.4

In a screw vial containing a stirrer bar, methyl (*Z*)-3-(((*tert*-butoxycarbonyl)glycyl)oxy)oct-2-enoate (**4a**) (32.9 mg, 0.10 mmol) was dissolved in solvent (0.50 mL). After addition of 2-phenylethylamine (13.9 μL, 0.11 mmol, 1.1 equiv), the reaction mixture was stirred for 10 minutes. After addition of phenanthrene as an internal standard, the mixture was diluted with deionized water and EtOAc. The organic layer was separated, washed with brine, and dried over Na_2SO_4. In the case of the reaction in DCM, DCM was used for the extraction process instead of EtOAc. All volatiles were removed under reduced pressure, and yield was determined by ^{1}H NMR analysis.

Table 2.4. Screening of Solvents.

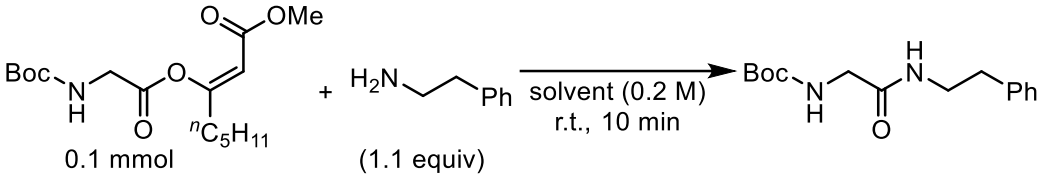

entry	solvent	NMR yield [%]
1	DMSO	>99
2	DMF	>99
3	NMP	>99
4	CH_3CN	>99
5	EtOAc	>99
6	DCM	>99

***tert*-Butyl (2-Oxo-2-(phenethylamino)ethyl)carbamate[22]**

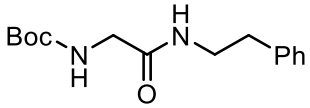

Isolated from the reaction using (*Z*)-3-(((*tert*-butoxycarbonyl)glycyl)oxy)oct-2-enoate (**4a**) (65.9 mg, 0.20 mmol) and 2-phenylethylamine (27.8 µL, 0.22 mmol, 1.1 equiv) in DMF (1.0 mL, 0.2 M). Colorless oil, 54.6 mg, 98% yield. ^{1}H NMR (400 MHz, $CDCl_3$, 25 °C): δ 7.31 (t, J = 7.8 Hz, 2H), 7.25-7.21 (m, 1H), 7.19 (d, J = 7.3 Hz, 2H), 6.05 (brs, 1H), 5.03 (brs, 1H), 3.74 (d, J = 4.6 Hz, 2H), 3.54 (q, J = 6.4 Hz, 2H), 2.82 (t, J = 6.9 Hz, 2H), 1.44 (s, 9H). ^{13}C{^{1}H} NMR (100 MHz, $CDCl_3$, 25 °C): δ 169.3, 156.0, 138.6, 128.70, 128.65, 126.6, 80.2, 44.4, 40.5, 35.6, 28.3.

Preparation of Free Amine 7a, 7b, and 7d

7a , **7b**, and **7d** were prepared through neutralization of the corresponding commercially available salts. These salts were suspended in DCM, and saturated $NaHCO_3$ was poured into the DCM suspension. After stirring for 10 minutes at room temperature, the aqueous layer was extracted with DCM. The organic layer was dried over Na_2SO_4, filtrated, and evaporated to give free amines.

Experimental Procedure for Table 2.5

Methyl (*Z*)-3-(((*tert*-butoxycarbonyl)-L-phenylalanyl)oxy)oct-2-enoate (**4c**) (92.3 mg, 0.22 mmol, 1.1 equiv) in EtOAc (1.0 mL in total) was added to L-phenylalanine methyl ester (35.8 mg, 0.20 mmol) in a screw vial containing a stirrer bar. After stirring at room temperature or 70 °C, volatiles were removed under reduced pressure. After addition of phenanthrene as an internal standard, yield was determined by ^{1}H NMR analysis.

Table 2.5. Screening of Reaction Conditions

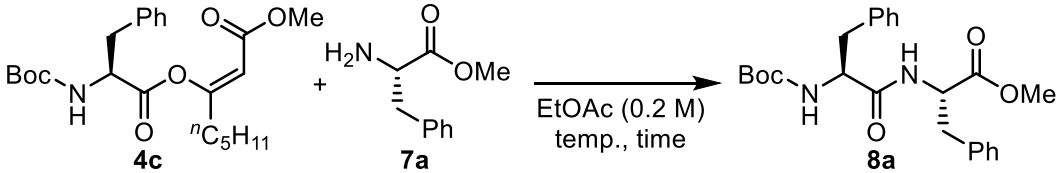

entry	temp.	time	recovered **4c**[a]	yield of **8a** [%][a]	*dr*[a]
1	r.t.	1 h	0.060 mmol	78	>20 : 1[b]
2	r.t.	4 h	0.050 mmol	85	>20 : 1[b]
3	r.t.	12 h	0.026 mmol	97	>20 : 1[b]
4	70 °C	1 h	0.028 mmol	95	>20 : 1[b]
5	70 °C	2 h	0.020 mmol	>99	>20 : 1[b]

[a]Determined by ^{1}H NMR analysis using phenanthrene as an internal standard.
[b]The minor diastereomer was not detected.

Experimental Procedure for Synthesizing 8a

Methyl (*Z*)-3-(((*tert*-butoxycarbonyl)-L-phenylalanyl)oxy)oct-2-enoate (**4c**) (92.3 mg, 0.22 mmol, 1.1 equiv) in EtOAc (1.0 mL in total) was added to L-phenylalanine methyl ester (**7a**) (35.8 mg, 0.20 mmol) in a screw-cap vial containing a stir bar. After stirring at 70 °C for 2 hours, the resulting solution was transferred to a small screw-cap vial. Volatiles were removed by rotary evaporation. The resulting solid was triturated and sonicated in hexane, and the white precipitate was collected by suction filtration washing with hexane. The white solid was dried under reduced pressure to afford dipeptide compound **8a** in 93% yield (79.0 mg, 0.185 mmol).

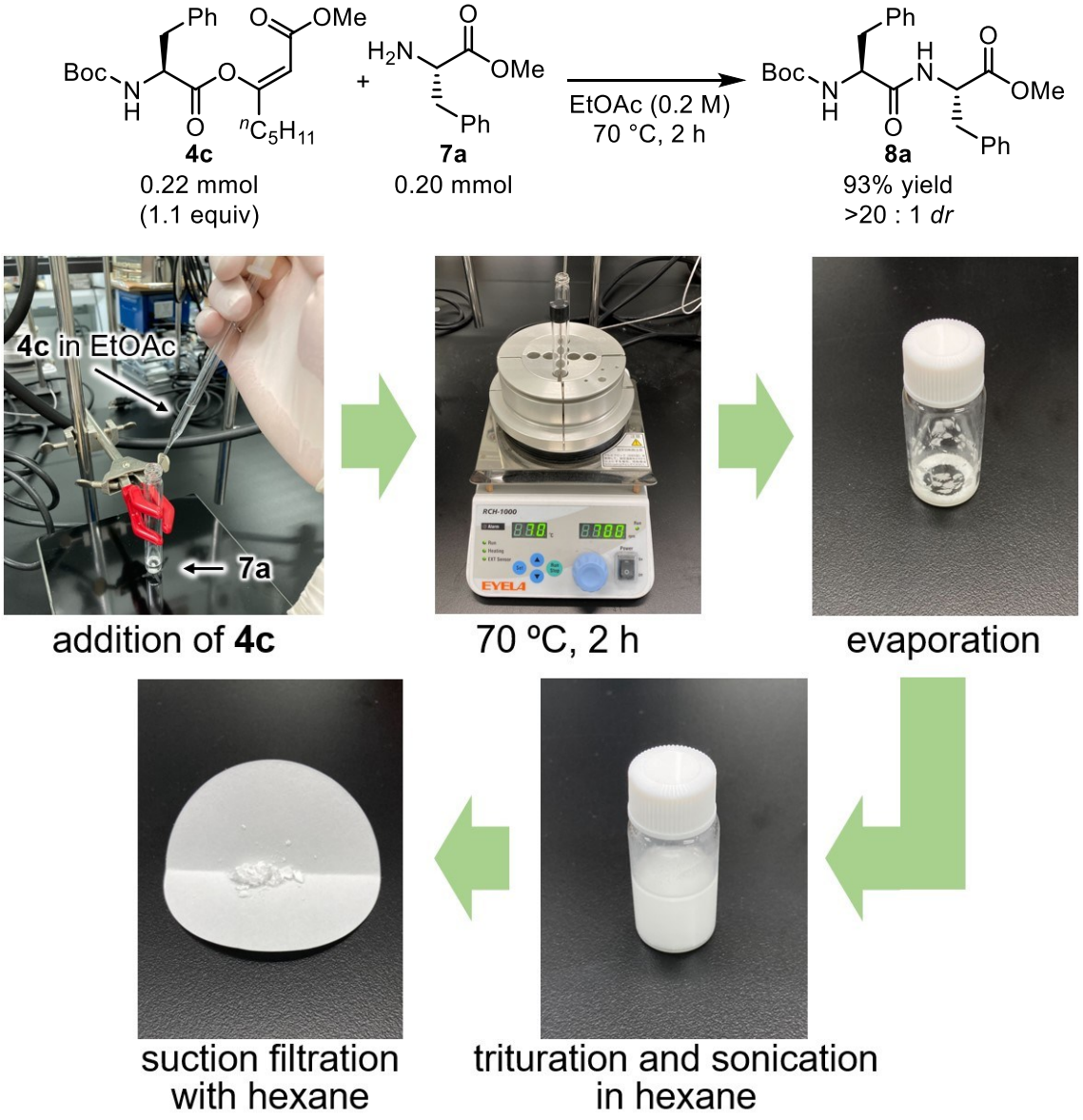

Figure 2.3. Photographic images illustrating the synthetic protocol for **8a**.

Investigation of Reaction Time for 8c, 8i, 8j, and 8n

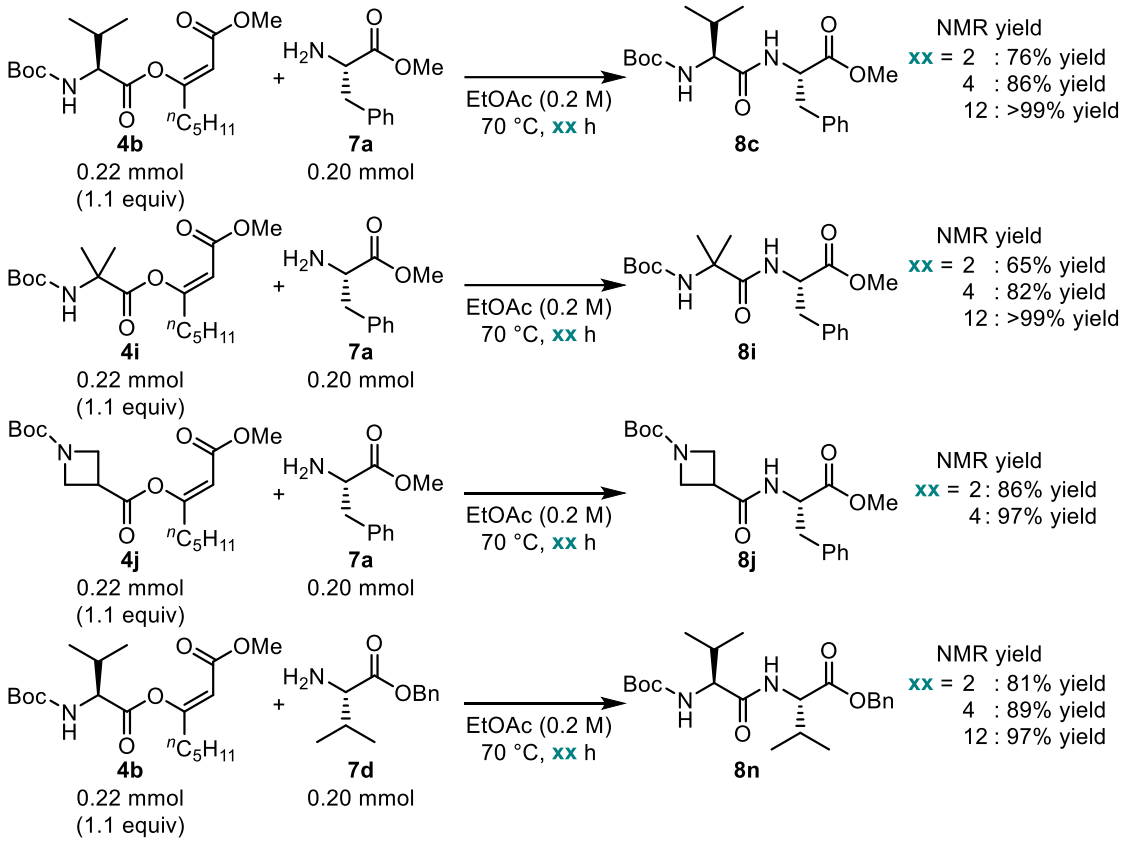

Preparation of Racemic and Epimeric Samples

Racemic authentic samples for α-methoxycarbonyl enol esters **4** were prepared through gold-zinc catalyzed nucleophilic addition with 1:1 mixture of commercially available L-amino acid derivatives and D-amino acid derivatives. The authentic samples were utilized for the HPLC analysis to determine the enantiomeric excess of the enol esters **4**.

Epimeric or racemic authentic samples for dipeptides **8** were prepared through a condensation reaction. EDC·HCl (288 mg, 1.5 mmol, 1.5 equiv) and DIPEA (523 μL, 3.0 mmol, 3.0 equiv) were added to a solution of H-L-Phe-OMe·HCl (1.1 mmol, 1.1 equiv), HOBt·H_2O (168 mg, 1.1 mmol, 1.1 equiv), and 1:1 mixture of *N*-protected L-amino acid and D-amino acid (1.0 mmol) in dry DCM (5.0 mL) at 0 °C. In the case of enol esters **4** not containing chiral center, 1:1 mixture of H-L-Phe-OMe·HCl and H-D-Phe-OMe·HCl (1.1 mmol, 1.1 equiv) was used. The mixture was stirred at room temperature, and the reaction progress was monitored by TLC. After consumption of the starting material, the reaction mixture was quenched with 1N HCl aq. The aqueous layer was extracted with EtOAc, and the organic layer was washed with saturated $NaHCO_3$ aq and brine, dried over Na_2SO_4, and filtrated. The crude mixture was purified by silica-gel column chromatography to give the corresponding products as a L,L-isomer and D,L-isomer mixture or a racemic compound. For discussing racemization of chiral center from activated esters **4**, the diastereomeric excess of the products **8** was assessed by comparison with L,L-isomer and D,L-isomer mixture in ^1H NMR and HPLC analysis.

General Procedure for Preparing α-Carbonyl Enol Esters

In an argon-filled glove box, *N*-protected amino acid **2** (0.50 mmol), gold(I) complex **3a** (1.3 mg, 0.002 mmol, 0.4 mol%), $Zn(acac)_2$ (0.53 mg, 0.002 mmol, 0.4 mol%), and $AgPF_6$ (0.5 mg, 0.002 mmol, 0.4 mol%) were placed in a screw-cap vial containing a magnetic stirring bar. After addition of methyl 2-octynoate (**1**) (91.2 μL, 0.55 mmol, 1.1 equiv), the reaction vial was sealed with a screw-cap and removed from the glove box. The mixture was stirred at 80 °C for 16 hours. The crude product was purified by silica-gel column chromatography to give the corresponding enol esters.

Methyl (*Z*)-3-(((*tert*-Butoxycarbonyl)glycyl)oxy)oct-2-enoate (4a)

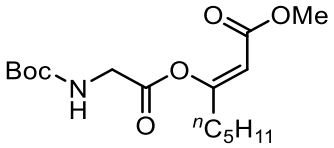

Colorless oil, 157.3 mg, 96% yield. IR (ATR, ν/cm^{-1}): 3384 br, 2955 w, 2932 w, 2871 w, 1778 m, 1713 s, 1666 m, 1508 m, 1455 w, 1435 w, 1366 m, 1123 s, 1052 m, 1027 m, 950 m, 862 m. ^{1}H NMR (400 MHz, $CDCl_3$, 55 °C): δ 5.60 (s, 1H), 5.03 (brs, 1H), 4.11 (d, *J* = 5.7Hz, 2H), 3.66 (s, 3H), 2.28 (t, *J* = 7.3 Hz, 2H), 1.55-1.50 (m, 2H), 1.47 (s, 9H), 1.36-1.28 (m, 4H), 0.90 (t, *J* = 7.1 Hz, 3H). ^{13}C{^{1}H} NMR (100 MHz, $CDCl_3$, 55 °C): δ 167.7, 164.3, 163.7, 155.7, 106.8, 80.1, 51.2, 42.7, 35.3, 31.1, 28.3, 25.4, 22.3, 13.8. HRMS (ESI$^+$) m/z calc. for $C_{16}H_{27}O_6NNa$ 352.17306 found 352.17251.

Methyl (*Z*)-3-(((*tert*-Butoxycarbonyl)-L-valyl)oxy)oct-2-enoate (4b)

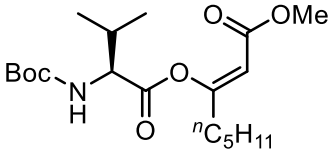

Colorless oil, 155.2 mg, 84% yield. IR (ATR, ν/cm^{-1}): 3384 br, 2960 w, 2932 w, 2873 w, 1764 m, 1715 s, 1671 m, 1498 m, 1458 w, 1436 w, 1391 w, 1366 m, 1306 w, 1277 w, 1237 m, 1217 m, 1170 s, 1139 s, 1087 s, 1026 m, 973 w, 943 w, 920 w, 871 w, 850 w. ^{1}H NMR (400 MHz, $CDCl_3$, 55 °C): δ 5.58 (s, 1H), 5.05 (brs, 1H), 4.40 (dd, *J* = 8.4, 4.4 Hz, 1H), 3.66 (s, 3H), 2.40-2.31 (m, 1H), 2.28 (t, *J* = 7.8 Hz, 2H), 1.56-1.49 (m, 2H), 1.45 (s, 9H), 1.35-1.27 (m, 4H), 1.05 (d, *J* = 6.9 Hz, 3H), 0.98 (d, *J* = 6.9 Hz, 3H), 0.90 (t, *J* = 6.9 Hz, 3H). ^{13}C{^{1}H} NMR (100 MHz, $CDCl_3$, 55 °C): δ 169.2, 164.0, 162.8, 155.7, 107.7, 79.8, 58.9, 51.2, 35.0, 31.1, 30.7, 28.4, 25.7, 22.3, 19.4, 17.3, 13.8. HPLC (Daicel CHIRALPAK ID-3, temperature: 30 °C, hexane : ^{i}PrOH = 95 : 5, detector : 230 nm, flow

rate 1.0 mL/min, t_1(D) = 13.1 min, t_2(L) = 17.5 min). $[\alpha]^{28}_D$ = -4.65 (c = 1.04, $CHCl_3$) (for an ee of >99%). HRMS (ESI^+) m/z calc. for $C_{19}H_{33}O_6NNa$ 394.22001 found 394.21926.

Methyl (*Z*)-3-(((*tert*-Butoxycarbonyl)-L-phenylalanyl)oxy)oct-2-enoate (4c)

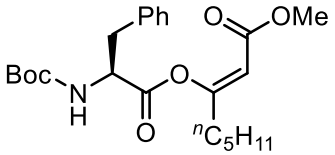

White solid, 204.2 mg, 97% yield. IR (ATR, ν/cm^{-1}): 3381 br, 2955 w, 2932 w, 2871 w, 1767 m, 1716 s, 1670 m, 1498 m, 1455 w, 1436 w, 1366 m, 1140 s, 1051 m, 1025 m, 923 m, 857 m. ^{1}H NMR (400 MHz, $CDCl_3$, 55 °C): δ 7.33-7.21 (m, 5H), 5.60 (s, 1H), 5.02 (brs, 1H), 4.73 (dd, *J* = 11.6, 6.0 Hz, 1H), 3.67 (s, 3H), 3.35 (dd, *J* = 14.2, 5.5 Hz, 1H), 3.09 (dd, *J* = 14.0, 7.8 Hz, 1H), 2.24 (t, *J* = 7.3 Hz, 2H), 1.51-1.45 (m, 2H), 1.41 (s, 9H), 1.34-1.26 (m, 4H), 0.90 (t, *J* = 6.9 Hz, 3H). ^{13}C{^{1}H} NMR (100 MHz, $CDCl_3$, 55 °C): δ 168.9, 164.1, 163.4, 155.1, 136.7, 129.5, 128.5, 126.8, 107.3, 79.9, 54.9, 51.2, 38.0, 35.1, 31.1, 28.3, 25.6, 22.3, 13.8. HPLC (Daicel CHIRALPAK IB N-3, temperature: 30 °C, hexane : ^{i}PrOH = 95 : 5, detector : 230 nm, flow rate 0.5 mL/min, t_1(L) = 13.0 min, t_2(D) = 16.3 min). $[\alpha]^{26}_D$ = -19.3 (c = 1.05, $CHCl_3$) (for an ee of >99%). HRMS (ESI^+) m/z calc. for $C_{23}H_{33}O_6NNa$ 442.22001 found 442.21942.

(*Z*)-1-(*tert*-Butyl) 2-(4-Methoxy-4-oxooct-2-en-2-yl) (*S*)-Pyrrolidine-1,2-dicarboxylate (4d)

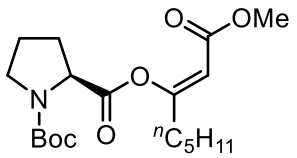

Colorless oil, 179.9 mg, 97% yield. IR (ATR, ν/cm^{-1}): 2955 w, 2932 w, 2873 w, 1769 m, 1727 m, 1696 s, 1671 m, 1391 s, 1365 m, 1216 m, 1120 s, 1081 s, 1029 m, 921 m, 772 m. ^{1}H NMR (400 MHz, $CDCl_3$, 25 °C): δ 5.61 (s, 0.55 H), 5.60 (s, 0.45 H), 4.46-4.38 (m, 1H), 3.65 (s, 3H), 3.63-3.35 (m, 2H), 2.58-2.50 (m, 0.55 H), 2.50-2.42 (m, 0.45 H), 2.30-2.16 (m, 3H), 2.15-2.00 (m, 1H), 1.95-1.86 (m, 1H), 1.57-1.48 (m, 2H), 1.46 (s, 4H), 1.45 (s, 5H), 1.35-1.27 (m, 4H), 0.92-0.86 (m, 3H) as a rotamer mixture. ^{13}C{^{1}H} NMR (100 MHz, $CDCl_3$, 25 °C): δ 169.4, 169.3, 164.2, 164.0, 163.7, 163.0, 154.3, 153.8, 107.4, 107.3, 80.0, 79.7, 59.1, 51.2, 46.6, 46.4, 35.2, 35.1, 31.0, 30.1, 29.2, 28.4, 25.6, 25.4, 24.4, 23.4, 22.3, 13.9 as a rotamer mixture. HPLC (Daicel CHIRALPAK IC-3, temperature: 30 °C, hexane : ^{i}PrOH = 90 : 10, detector : 215 nm, flow rate 1.0 mL/min, t_1(L) = 9.2 min,

t_2(D) = 11.1 min). $[\alpha]^{24}_D$ = -105.3 (c = 1.07, $CHCl_3$) (for an ee of >99%). HRMS (ESI^+) m/z calc. for $C_{19}H_{31}O_6NNa$ 392.20436 found 392.20349.

Methyl (*Z*)-3-(((*tert*-Butoxycarbonyl)-L-phenylglycyl)oxy)oct-2-enoate (4e)

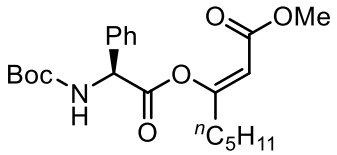

Colorless oil, 198.6 mg, 98% yield. IR (ATR, ν/cm^{-1}): 3384 br, 2954 w, 2931 w, 2871 w, 1766 m, 1712 s, 1495 m, 1456 m, 1436 m, 1366 m, 1130 s, 1050 m, 1025 m, 849 m, 755 m, 697 m. ^{1}H NMR (400 MHz, $CDCl_3$, 55 °C): δ 7.44 (d, *J* = 7.3 Hz, 2H), 7.40-7.29 (m, 3H), 5.66 (d, *J* = 5.5 Hz, 1H), 5.56 (s, 1H), 5.50 (d, *J* = 4.6 Hz, 1H), 3.58 (s, 3H), 2.22-2.10 (m, 2H), 1.43 (s, 9H), 1.32-1.15 (m, 6H), 0.83 (t, *J* = 6.9 Hz, 3H). ^{13}C{^{1}H} NMR (100 MHz, $CDCl_3$, 55 °C): δ 167.9, 164.1, 162.5, 154.7, 137.0, 128.8, 128.4, 127.4, 107.9, 80.2, 58.2, 51.2, 34.7, 30.9, 28.3, 25.3, 22.2, 13.7. HPLC (Daicel CHIRALPAK IA-3, temperature: 30 °C, hexane : ^{i}PrOH = 90 : 10, detector : 215 nm, flow rate 1.0 mL/min, t_1(D) = 8.3 min, t_2(L) = 10.6 min). $[\alpha]^{23}_D$ = +110.1 (c = 0.88, $CHCl_3$) (for an ee of >99%). HRMS (ESI^+) m/z calc. for $C_{22}H_{31}O_6NNa$ 428.20436 found 428.20355.

Methyl (*Z*)-3-((*O*-Benzyl-*N*-(*tert*-butoxycarbonyl)-L-seryl)oxy)oct-2-enoate (4f)

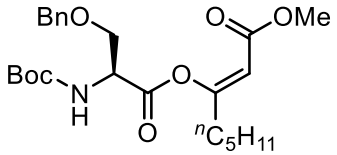

Pale yellow oil, 219.0 mg, 97% yield. IR (ATR, ν/cm^{-1}): 3444 br, 2954 w, 2931 w, 2871 w, 1771 m, 1714 s, 1670 m, 1497 m, 1365 m, 1131 s, 1025 s, 736 m, 697 m. ^{1}H NMR (400 MHz, $CDCl_3$, 55 °C): δ 7.35-7.25 (m, 5H), 5.59 (s, 1H), 5.38 (brs, 1H), 4.66 (brs, 1H), 4.58 (s, 2H), 4.01 (dd, *J* = 9.6, 4.4 Hz, 1H), 3.85 (dd, *J* = 9.6, 3.7 Hz, 1H), 3.65 (s, 3H), 2.26 (t, *J* = 7.8 Hz, 2H), 1.54-1.46 (m, 2H), 1.46 (s, 9H), 1.34-1.25 (m, 4H), 0.88 (t, *J* = 6.9 Hz, 3H). ^{13}C{^{1}H} NMR (100 MHz, $CDCl_3$, 55 °C): δ 167.7, 164.0, 163.1, 155.3, 137.8, 128.4, 127.7, 127.6, 107.6, 80.0, 73.5, 69.9, 54.4, 51.2, 35.0, 31.1, 28.4, 25.5, 22.3, 13.8. HPLC (Daicel CHIRALPAK ID-3, temperature: 30 °C, hexane : ^{i}PrOH = 85 : 15, detector : 215 nm, flow rate 1.0 mL/min, t_1(D) = 11.5 min, t_2(L) = 24.0 min). $[\alpha]^{22}_D$ = +21.50 (c = 0.88, $CHCl_3$) (for an ee of >99%). HRMS (ESI^+) m/z calc. for $C_{24}H_{35}O_7NNa$ 472.23057 found 472.22975.

Methyl (*Z*)-3-(((*tert*-Butoxycarbonyl)-L-tyrosyl)oxy)oct-2-enoate (4g)

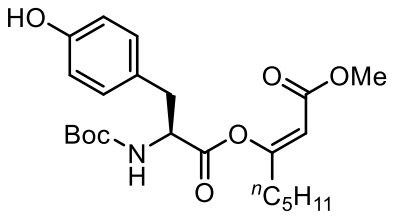

Colorless viscous oil, 193.3 mg, 89% yield. IR (ATR, ν/cm^{-1}): 3372 br, 2955 w, 2932 w, 2871 w, 1766 m, 1713 s, 1689 s, 1615 w, 1516 s, 1366 m, 1222 m, 1131 s, 1048 m, 1024 m, 837 m. ^{1}H NMR (400 MHz, $CDCl_3$, 55 °C): δ 7.10 (d, *J* = 8.5 Hz, 2H), 6.75 (d, *J* = 8.5 Hz, 2H), 5.59 (s, 1H), 5.03 (brs, 1H), 4.91 (brs, 1H), 4.70-4.62 (m, 1H), 3.67 (s, 3H), 3.27 (dd, *J* = 14.3, 5.5 Hz, 1H), 3.02 (dd, *J* = 14.2, 8.0 Hz, 1H), 2.25 (t, *J* = 7.1 Hz, 2H), 1.54-1.46 (m, 2H), 1.41 (s, 9H), 1.35-1.28 (m, 4H), 0.90 (t, *J* = 6.6 Hz, 3H). ^{13}C{^{1}H} NMR (100 MHz, $CDCl_3$, 55 °C): δ 169.0, 164.2, 163.4, 155.3, 154.9, 130.6, 128.6, 115.5, 107.3, 80.0, 55.1, 51.2, 37.1, 35.1, 31.1, 28.3, 25.6, 22.3, 13.8. HPLC (Daicel CHIRALPAK IA-3, temperature: 30 °C, hexane : ^{i}PrOH = 90 : 10, detector : 215 nm, flow rate 1.0 mL/min, t_1(D) = 18.5 min, t_2(L) = 28.8 min). $[\alpha]^{26}_{D}$ = -18.3 (c = 1.24, $CHCl_3$) (for an ee of >99%). HRMS (ESI^{+}) m/z calc. for $C_{23}H_{33}O_7NNa$ 458.21492 found 458.21404.

Methyl (*Z*)-3-(((*tert*-Butoxycarbonyl)-L-tryptophyl)oxy)oct-2-enoate (4h)

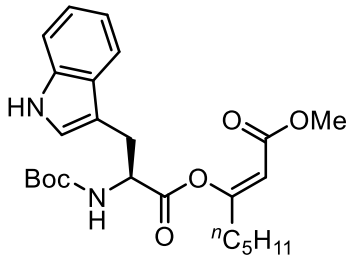

3.0 equivalents of methyl 2-octynoate were used. Pale yellow gum, 179.2 mg, 78% yield. IR (ATR, ν/cm^{-1}): 3372 br, 2954 w, 2931 w, 2870 w, 1764 m, 1699 s, 1500 m, 1435 m, 1245 m, 1135 s, 1048 m, 1025 m, 854 m, 740 s. ^{1}H NMR (400 MHz, $CDCl_3$, 55 °C): δ 8.05 (brs, 1H), 7.66 (d, *J* = 7.8 Hz, 1H), 7.34 (d, *J* = 8.0 Hz, 1H), 7.19 (t, *J* = 7.1 Hz, 1H), 7.15-7.08 (m, 2H), 5.59 (s, 1H), 5.11 (brs, 1H), 4.85-4.75 (m, 1H), 3.66 (s, 3H), 3.51 (dd, *J* = 15.1, 5.5 Hz, 1H), 3.35-3.26 (m, 1H), 2.19 (t, *J* = 7.3 Hz, 2H), 1.45-1.32 (m, 11H), 1.32-1.21 (m, 4H), 0.88 (t, *J* = 6.2 Hz, 3H). ^{13}C{^{1}H} NMR (100 MHz, $CDCl_3$, 55 °C): δ 169.3, 164.1, 163.4, 155.2, 136.3, 127.9, 122.9, 122.2, 119.7, 118.9, 111.1, 111.0, 107.3, 79.8, 54.6, 51.2, 35.0, 31.0, 28.3, 27.7, 25.5, 22.2, 13.8. HPLC (Daicel CHIRALPAK IA-3, temperature: 30 °C, hexane : ^{i}PrOH = 90 : 10, detector : 215 nm, flow rate 1.0 mL/min,

t_1(D) = 15.2 min, t_2(L) = 19.3 min). $[\alpha]^{22}_D$ = -31.8 (c = 0.73, $CHCl_3$) (for an ee of >99%). HRMS (ESI^+) m/z calc. for $C_{25}H_{34}O_6N_2Na$ 481.23091 found 481.23030.

Methyl (*Z*)-3-((2-((*tert*-Butoxycarbonyl)amino)-2-methylpropanoyl)oxy)oct-2-enoate (4i)

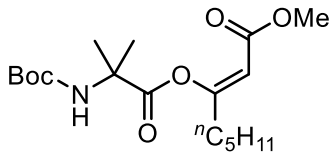

Colorless oil, 147.2 mg, 82% yield. IR (ATR, ν/cm^{-1}): 3383 br, 2955 w, 2932 w, 2872 w, 1762 m, 1713 s, 1669 m, 1504 m, 1365 m, 1206 m, 1165 s, 1110 s, 1077 s, 1029 m, 849 w. ^{1}H NMR (400 MHz, $CDCl_3$, 25 °C): δ 5.60 (s, 1H), 5.09 (s, 1H), 3.65 (s, 3H), 2.28 (t, *J* = 7.8 Hz, 2H), 1.63 (s, 6H), 1.58-1.48 (m, 2H), 1.44 (s, 9H), 1.35-1.25 (m, 4H), 0.88 (t, *J* = 6.9 Hz, 3H). ^{13}C{^{1}H} NMR (100 MHz, $CDCl_3$, 25 °C): δ 171.3, 164.1, 163.9, 154.4, 107.4, 79.6, 56.3, 51.2, 34.8, 31.0, 28.3, 25.6, 25.2, 22.3, 13.9. HRMS (ESI^+) m/z calc. for $C_{18}H_{31}O_6NNa$ 380.20436 found 380.20384.

(*Z*)-1-(*tert*-Butyl) 3-(4-Methoxy-4-oxooct-2-en-2-yl) Azetidine-1,3-dicarboxylate (4j)

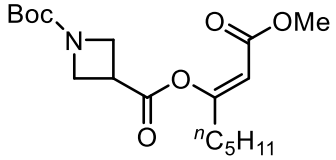

Pale yellow oil, 169.6 mg, 95% yield. IR (ATR, ν/cm^{-1}): 2956 w, 2932 w, 2871 w, 1764 m, 1702 s, 1667 m, 1393 m, 1365 m, 1123 s, 1032 m, 860 w, 773 w. ^{1}H NMR (400 MHz, $CDCl_3$, 25 °C): δ 5.62 (t, *J* = 0.9 Hz, 1H), 4.25 (dd, *J* = 8.9, 6.2 Hz, 2H), 4.15 (t, *J* = 8.9 Hz, 2H), 3.65 (s, 3H), 3.57-3.49 (m, 1H), 2.26 (td, *J* = 7.3, 0.7 Hz, 2H), 1.55-1.45 (m, 2H), 1.44 (s, 9H), 1.35-1.27 (m, 4H), 0.89 (t, *J* = 7.1 Hz, 3H). ^{13}C{^{1}H} NMR (100 MHz, $CDCl_3$, 25 °C): δ 169.4, 164.2, 163.3, 156.1, 107.0, 79.8, 51.6, 51.2, 35.1, 32.3, 31.0, 28.3, 25.4, 22.3, 13.8. HRMS (ESI^+) m/z calc. for $C_{18}H_{29}O_6NNa$ 378.18871 found 378.18804.

Methyl (*Z*)-3-(((((9*H*-Fluoren-9-yl)methoxy)carbonyl)-L-phenylalanyl)oxy)oct-2-enoate (4k)

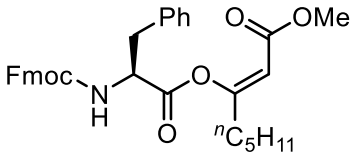

3.0 equivalents of methyl 2-octynoate were used. White solid, 243.8 mg, 90% yield. IR (ATR, ν/cm^{-1}): 3342 br, 3064 w, 3028 w, 2952 w, 2930 w, 2861 w, 1766 m, 1716 s, 1668 m, 1514 m, 1449 m, 1248 m, 1137 s, 1046 m, 755 s, 740 s, 700m. ^{1}H NMR (400 MHz, $CDCl_3$, 55 °C): δ 7.74 (d, *J* = 7.6 Hz, 2H), 7.56-7.50 (m, 2H), 7.37 (t, *J* = 7.3 Hz, 2H), 7.31-7.19 (m, 7H), 5.59 (s, 1H), 5.40 (brs, 1H), 4.82 (brs, 1H), 4.40-4.30 (m, 2H), 4.19 (t, *J* = 7.1 Hz, 1H), 3.64 (s, 3H), 3.35 (brs, 1H), 3.15 (brs, 1H), 2.22 (t, *J* = 7.1 Hz, 2H), 1.50-1.38 (m, 2H), 1.34-1.22 (m, 4H), 0.87 (t, *J* = 7.1 Hz, 3H). ^{13}C{^{1}H} NMR (100 MHz, $CDCl_3$, 55 °C): δ 168.5, 164.2, 163.5, 155.7, 144.01, 143.96, 141.4, 136.4, 129.5, 128.6, 127.7, 127.0, 125.1, 120.0, 107.2, 67.2, 55.3, 51.2, 47.3, 37.9, 35.1, 31.1, 25.6, 22.3, 13.8. HPLC (Daicel CHIRALPAK IC-3, temperature: 30 °C, hexane : ^{i}PrOH = 90 : 10, detector : 254 nm, flow rate 1.0 mL/min, t_1(L) = 20.3 min, t_2(D) = 23.5 min). $[\alpha]^{15}_{D}$ = -24.1 (c = 1.03, $CHCl_3$) (for an ee of >99%). HRMS (ESI^{+}) m/z calc. for $C_{33}H_{35}O_6NNa$ 564.23566 found 564.23451.

General Procedure for Amide-bond Formation

α-Methoxycarbonyl enol esters **4** (0.22 mmol, 1.1 equiv) in EtOAc (1.0 mL in total) was added to amine **7** (0.20 mmol) in a screw-cap vial containing a stir bar. After stirring the mixture at 70 °C for 2 hours, the resulting solution was transferred to a small screw-cap vial. Volatiles were removed by rotary evaporation. The residual solid was triturated and sonicated in hexane, and the white precipitate was collected by suction filtration washing with hexane. The resulting solid was dried under reduced pressure to afford dipeptide compound **8**.

Methyl (*tert*-Butoxycarbonyl)-L-phenylalanyl-L-phenylalaninate (8a)[23]

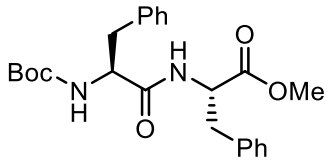

White solid, 79.0 mg, 93% yield. ^{1}H NMR (400 MHz, $CDCl_3$, 25 °C): δ 7.31-7.16 (m, 8H), 6.98 (dd, *J* = 7.6, 2.5 Hz, 2H), 6.29 (d, *J* = 7.1 Hz, 1H), 4.94 (brs, 1H), 4.78 (dd, *J* = 12.8, 6.0 Hz, 1H), 4.38-4.25 (m, 1H), 3.66 (s, 3H), 3.10-2.97 (m, 4H), 1.40 (s, 9H). ^{13}C{^{1}H} NMR (100 MHz, $CDCl_3$, 25 °C): δ171.3, 170.7, 155.2, 136.5, 135.6, 129.3, 129.2, 128.6, 128.5, 127.1, 126.9, 80.2, 55.7, 53.2, 52.2, 38.2, 37.9, 28.2. HPLC (Daicel CHIRALPAK IC-3, temperature: 30 °C, hexane : ^{i}PrOH = 90 : 10, detector : 215 nm, flow rate 1.0 mL/min, t_1(L,L) = 12.0 min, t_2(D,L) = 14.6 min). $[\alpha]^{28}_{D}$ = +31.8 (c = 2.40, $CHCl_3$).

Methyl (*tert*-Butoxycarbonyl)glycyl-L-phenylalaninate (8b)[24]

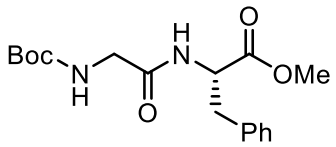

8b was isolated by silica-gel column chromatography (hexane/EtOAc = 4/1 to 1/1). Colorless oil, 63.9 mg, 95% yield. ^{1}H NMR (400 MHz, $CDCl_3$, 25 °C): δ 7.31-7.21 (m, 3H), 7.11-7.07 (m, 2H), 6.51 (d, *J* = 7.8 Hz, 1H), 5.07 (brs, 1H), 4.88 (dt, *J* = 7.8, 6.0 Hz, 1H), 3.87-3.72 (m, 2H), 3.71 (s, 3H), 3.14 (dd, *J* = 13.7, 5.5 Hz, 1H), 3.09 (dd, *J* = 14.2, 6.0 Hz, 1H), 1.44 (s, 9H). ^{13}C{^{1}H} NMR (100 MHz, $CDCl_3$, 25 °C): δ 171.6, 169.0, 155.9, 135.6, 129.2, 128.6, 127.2, 80.3, 53.0, 52.3, 44.2, 37.9, 28.3. HPLC (Daicel CHIRALPAK IC-3, temperature: 30 °C, hexane : ^{i}PrOH = 80 : 20, detector : 215 nm, flow rate 1.0

mL/min, t_1(L) = 17.2 min, t_2(D) = 35.0 min). $[\alpha]^{23}_D$ = +53.6 (c = 1.01, $CHCl_3$) (for an ee of >99%).

Methyl (*tert*-Butoxycarbonyl)-L-valyl-L-phenylalaninate (8c)[25]

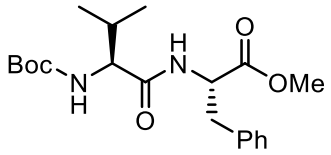

Reaction time was extended to 12 hours. White solid, 60.6 mg, 80% yield. ^{1}H NMR (400 MHz, $CDCl_3$, 25 °C): δ 7.31-7.21 (m, 3H), 7.13-7.08 (m, 2H), 6.28 (brd, *J* = 6.0 Hz, 1H), 5.00 (brd, *J* = 7.1 Hz, 1H), 4.87 (dt, *J* = 7.8, 6.0 Hz, 1H), 3.89 (t, *J* = 6.9 Hz, 1H), 3.71 (s, 3H), 3.15-3.05 (m, 2H), 2.14-2.03 (m, 1H), 1.44 (s, 9H), 0.92 (d, *J* = 6.9 Hz, 3H), 0.86 (d, *J* = 6.4 Hz, 3H). ^{13}C{^{1}H} NMR (100 MHz, $CDCl_3$, 25 °C): δ 171.6, 171.2, 155.7, 135.6, 129.2, 128.6, 127.2, 79.9, 59.9, 53.1, 52.3, 38.0, 30.8, 28.3, 19.1, 17.6. HPLC (Daicel CHIRALPAK IA-3, temperature: 30 °C, hexane : ^{i}PrOH = 90 : 10, detector : 215 nm, flow rate 1.0 mL/min, t_1(L,L) = 8.1 min, t_2(D,L) = 24.4 min). $[\alpha]^{23}_D$ = +37.4 (c = 0.97, $CHCl_3$).

Methyl (*tert*-Butoxycarbonyl)-L-prolyl-L-phenylalaninate (8d)[26]

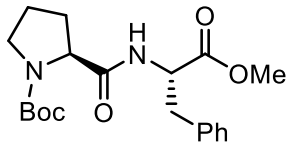

8d was isolated by silica-gel column chromatography (hexane/EtOAc = 4/1 to 1/1), since **8d** was soluble in hexane. White solid, 69.0 mg, 92% yield. ^{1}H NMR (400 MHz, $CDCl_3$, 25 °C): δ 7.32-7.18 (m, 3H), 7.09 (d, *J* = 7.1 Hz, 2H), 6.44 (brs, 0.5H), 4.85 (brs, 1H), 4.26 and 4.19 (brs, 1H in total), 3.71 (s, 3H), 3.38 (brs, 0.5H), 3.32-3.22 (m, 1.5H), 3.18 (dd, *J* = 14.0, 5.5 Hz, 1H), 2.99 (dd, *J* = 14.0, 6.9 Hz, 1H), 2.35-1.68 (m, 4H), 1.42 (s, 9H) as a rotamer mixture. ^{13}C{^{1}H} NMR (100 MHz, $CDCl_3$, 25 °C): δ 172.1, 171.6, 155.7, 154.5, 136.0, 135.8, 129.1, 128.5, 127.1, 80.7, 80.4, 60.9, 59.9, 53.2, 52.6, 52.2, 46.9, 38.1, 30.6, 28.2, 24.4, 23.4 as a rotamer mixture. HPLC (Daicel CHIRALPAK IA-3, temperature: 30 °C, hexane : ^{i}PrOH = 90 : 10, detector : 215 nm, flow rate 1.0 mL/min, t_1(D,L) = 9.6 min, t_2(L,L) = 12.2 min). $[\alpha]^{27}_D$ = -50.0 (c = 1.01, $CHCl_3$).

Methyl (*tert*-Butoxycarbonyl)-L-phenylglycyl-L-phenylalaninate (8e)[27]

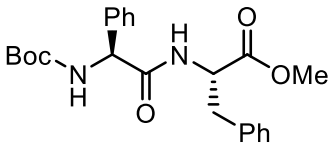

White solid, 72.2 mg, 88% yield. ^{1}H NMR (400 MHz, $CDCl_3$, 25 °C): δ 7.35-7.23 (m, 8H), 7.05 (dd, *J* = 7.3, 2.1 Hz, 2H), 6.26 (d, *J* = 7.3 Hz, 1H), 5.66 (brs, 1H), 5.11 (brs, 1H), 4.81 (dt, *J* = 7.6, 6.0 Hz, 1H), 3.64 (s, 3H), 3.16 (dd, *J* = 13.8, 5.7 Hz, 1H), 3.06 (dd, *J* = 14.0, 6.0 Hz, 1H), 1.42 (s, 9H). ^{13}C{^{1}H} NMR (100 MHz, $CDCl_3$, 25 °C): δ 171.3, 169.7, 155.0, 137.7, 135.5, 129.2, 128.9, 128.6, 128.4, 127.2, 127.1, 80.1, 58.8, 53.4, 52.3, 37.7, 28.2. HPLC (Daicel CHIRALPAK IC-3, temperature: 30 °C, hexane : ^{i}PrOH = 90 : 10, detector : 215 nm, flow rate 1.0 mL/min, t_1(D,L) = 21.1 min, t_2(L,L) = 26.6 min). $[\alpha]^{25}_{D}$ = +135.4 (c = 0.96, $CHCl_3$).

Methyl *O*-Benzyl-*N*-(*tert*-butoxycarbonyl)-L-seryl-L-phenylalaninate (8f)

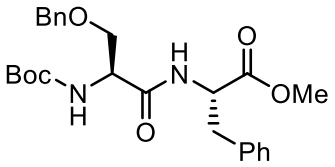

White solid, 78.6 mg, 86% yield. IR (ATR, ν/cm^{-1}): 3414 w, 3318 br, 3087 w, 3064 w, 3028 w, 3008 w, 2976 w, 2928 w, 2866 w, 1743 m, 1714 s, 1670 s, 1496 s, 1365 m, 1217 m, 1168 s, 757 s. ^{1}H NMR (400 MHz, $CDCl_3$, 25 °C): δ 7.38-7.26 (m, 5H), 7.22-7.17 (m, 3H), 7.06-7.00 (m, 3H), 5.33 (brs, 1H), 4.84 (q, *J* = 7.3 Hz, 1H), 4.58-4.48 (m, 2H), 4.27 (brs, 1H), 3.91 (d, *J* = 6.2 Hz, 1H), 3.68 (s, 3H), 3.54 (dd, *J* = 9.2, 6.4 Hz, 1H), 3.13 (dd, *J* = 13.8, 5.7 Hz, 1H), 3.05 (dd, *J* = 13.8, 6.0 Hz, 1H), 1.43 (s, 9H). ^{13}C{^{1}H} NMR (100 MHz, $CDCl_3$, 25 °C): δ 171.4, 170.0, 155.4, 137.3, 135.7, 129.3, 128.5, 127.91, 127.86, 127.0, 80.3, 73.5, 69.8, 53.8, 53.4, 52.2, 37.8, 28.2. HPLC (Daicel CHIRALPAK IC-3, temperature: 30 °C, hexane : ^{i}PrOH = 80 : 20, detector : 215 nm, flow rate 1.0 mL/min, t_1(L,L) = 18.4 min, t_2(D,L) = 20.6 min). $[\alpha]^{22}_{D}$ = +58.6 (c = 1.01, $CHCl_3$). HRMS (ESI^{+}) m/z calc. for $C_{25}H_{32}O_6N_2Na$ 479.21526 found 479.21474.

Methyl (*tert*-Butoxycarbonyl)-L-tyrosyl-L-phenylalaninate (8g)

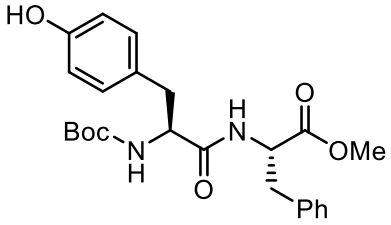

White solid, 75.4 mg, 85% yield. IR (ATR, ν/cm^{-1}): 3315 br, 3026 w, 2976 w, 2952 w, 2932 w, 1740 m, 1657 s, 1515 s, 1366 m, 1217 s, 1162 s, 1020 m, 750 s. ^{1}H NMR (400 MHz, $CDCl_3$, 25 °C): δ 7.26-7.19 (m, 3H), 7.03-6.96 (m, 4H), 6.70 (d, *J* = 8.7 Hz, 2H), 6.29 (brs, 1H), 6.05 (brs, 1H), 5.02 (brs, 1H), 4.76 (brm, 1H), 4.26 (brs, 1H), 3.65 (s, 3H), 3.10-2.98 (m, 2H), 2.93 (d, *J* = 5.7 Hz, 2H), 1.41 (s, 9H). ^{13}C{^{1}H} NMR (100 MHz, $CDCl_3$, 25 °C): δ 171.4, 171.0, 155.4, 155.1, 135.5, 130.4, 129.2, 128.6, 128.0, 127.1, 115.6, 80.4, 55.9, 53.3, 52.3, 38.0, 37.5, 28.2. HPLC (Daicel CHIRALPAK IC-3, temperature: 30 °C, hexane : ^{i}PrOH = 90 : 10, detector : 230 nm, flow rate 1.0 mL/min, t_1(L,L) = 17.7 min, t_2(D,L) = 25.8 min). $[\alpha]^{25}_{D}$ = +34.2 (c = 1.03, $CHCl_3$). HRMS (ESI^{+}) m/z calc. for $C_{24}H_{30}O_6N_2Na$ 465.19961 found 465.19880.

Methyl (*tert*-Butoxycarbonyl)-L-tryptophyl-L-phenylalaninate (8h)[28]

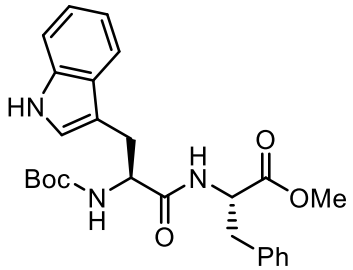

White solid, 78.5 mg, 84% yield. ^{1}H NMR (400 MHz, $CDCl_3$, 25 °C): δ 8.05 (s, 1H), 7.66 (d, *J* = 7.8 Hz, 1H), 7.36 (d, *J* = 8.0 Hz, 1H), 7.23-7.10 (m, 5H), 7.02 (s, 1H), 6.81 (dd, *J* = 6.6, 1.6 Hz, 2H), 6.19 (brd, *J* = 5.7 Hz, 1H), 5.11 (s, 1H), 4.73 (q, *J* = 6.2 Hz, 1H), 4.43 (s, 1H), 3.62 (s, 3H), 3.35-3.24 (m, 1H), 3.13 (dd, *J* = 14.7, 7.1 Hz, 1H), 2.94 (d, *J* = 6.0 Hz, 2H), 1.42 (s, 9H). ^{13}C{^{1}H} NMR (100 MHz, $CDCl_3$, 25 °C): δ 171.3, 171.2, 155.3, 136.2, 135.6, 129.1, 128.4, 127.5, 127.0, 123.3, 122.3, 119.8, 118.9, 111.2, 110.5, 80.1, 55.1, 53.2, 52.2, 37.9, 28.2. HPLC (Daicel CHIRALPAK IA-3, temperature: 30 °C, hexane : ^{i}PrOH = 90 : 10, detector : 230 nm, flow rate 1.0 mL/min, t_1(L,L) = 24.6 min, t_2(D,L) = 29.0 min). $[\alpha]^{23}_{D}$ = +18.9 (c = 0.94, $CHCl_3$).

Methyl (2-((*tert*-Butoxycarbonyl)amino)-2-methylpropanoyl)-L-phenylalaninate (8i)[29]

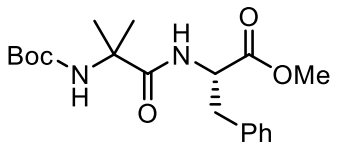

Reaction time was extended to 12 hours. White solid, 60.4 mg, 83% yield. ^{1}H NMR (400 MHz, $CDCl_3$, 25 °C): δ 7.29-7.20 (m, 3H), 7.14-7.08 (m, 2H), 6.85 (brs, 1H), 4.85 (brs, 1H), 4.85 (dt, *J* = 7.8, 6.0 Hz, 1H), 3.69 (s, 3H), 3.17-3.06 (m, 2H), 1.44 (s, 3H), 1.42 (s, 12H). ^{13}C{^{1}H} NMR (100 MHz, $CDCl_3$, 25 °C): δ 174.2, 171.9, 154.5, 136.0, 129.3, 128.5, 127.0, 80.1, 56.7, 53.3, 52.2, 38.1, 28.2, 25.6, 25.4. HPLC (Daicel CHIRALPAK IC-3, temperature: 30 °C, hexane : ^{i}PrOH = 90 : 10, detector : 215 nm, flow rate 1.0 mL/min, t_1(L) = 18.5 min, t_2(D) = 29.6 min). $[\alpha]^{23}_{D}$ = +37.5 (c = 1.00, $CHCl_3$) (for an ee of >99%).

***tert*-Butyl (*S*)-3-((1-Methoxy-1-oxo-3-phenylpropan-2-yl)carbamoyl)azetidine-1-carboxylate (8j)**

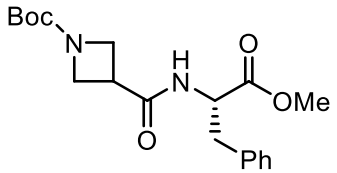

Reaction time was extended to 4 hours. **8j** was isolated by silica-gel column chromatography (hexane/EtOAc = 4/1 to 2/3), since **8j** was soluble in hexane. Colorless oil, 65.4 mg, 90% yield. IR (ATR, ν/cm^{-1}): 3299 w, 3063 w, 3030 w, 2975 w, 2953 w, 2888 w, 1743 m, 1699 s, 1655 s, 1539 m, 1409 s, 1365 s, 1210 s, 1163 s, 1137 s, 700m. ^{1}H NMR (400 MHz, $CDCl_3$, 25 °C): δ 7.31-7.21 (m, 3H), 7.06 (dd, *J* = 8.0, 1.6 Hz, 2H), 5.94 (d, *J* = 7.8 Hz, 1H), 4.90 (dt, *J* = 7.8, 6.0 Hz, 1H), 4.09-4.03 (m, 1H), 4.02-3.95 (m, 3H), 3.74 (s, 3H), 3.21-3.04 (m, 3H), 1.42 (s, 9H). ^{13}C{^{1}H} NMR (100 MHz, $CDCl_3$, 25 °C): δ 171.9, 171.1, 156.1, 135.6, 129.2, 128.6, 127.3, 79.7, 53.1, 52.5, 51.5, 37.8, 33.2, 28.3. HPLC (Daicel CHIRALPAK IB N-3, temperature: 30 °C, hexane : ^{i}PrOH = 90 : 10, detector : 215 nm, flow rate 1.0 mL/min, t_1(R) = 16.6 min, t_2(S) = 19.1 min). $[\alpha]^{28}_{D}$ = +98.2 (c = 1.00, $CHCl_3$) (for an ee of >99%). HRMS (ESI^{+}) m/z calc. for $C_{19}H_{26}O_5N_2Na$ 385.17339 found 385.17267.

Methyl (((9*H*-Fluoren-9-yl)methoxy)carbonyl)-L-phenylalanyl-L-phenylalaninate (8k)[24]

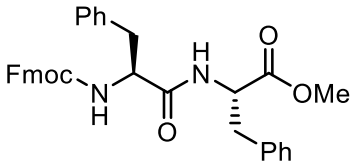

White solid, 106.1 mg, 97% yield. ^{1}H NMR (400 MHz, $CDCl_3$, 25 °C): δ 7.76 (d, *J* = 7.6 Hz, 2H), 7.52 (t, *J* = 6.9 Hz, 2H), 7.40 (t, *J* = 7.3 Hz, 2H), 7.34-7.21 (m, 5H), 7.21-7.13 (m, 5H), 6.95 (d, *J* = 5.3 Hz, 2H), 6.16 (brs, 1H), 5.24 (brs, 1H), 4.77 (dt, *J* = 7.3, 6.2 Hz, 1H), 4.45-4.36 (m, 2H), 4.33-4.25 (m, 1H), 4.18 (t, *J* = 7.1 Hz, 1H), 3.66 (s, 3H), 3.10-2.95 (m, 4H). ^{13}C{^{1}H} NMR (100 MHz, $CDCl_3$, 25 °C): δ 171.2, 170.2, 155.8, 143.7, 141.3, 136.1, 135.5, 129.4, 129.1, 128.7, 128.5, 127.7, 127.14, 127.08, 125.1, 125.0, 120.0, 67.1, 55.9, 53.3, 52.3, 47.1, 38.3, 37.9. HPLC (Daicel CHIRALPAK IB N-3, temperature: 30 °C, hexane : ^{i}PrOH = 90 : 10, detector : 215 nm, flow rate 1.0 mL/min, t_1(L,L) = 20.0 min, t_2(D,L) = 29.8 min). $[\alpha]^{15}_{D}$ = +19.2 (c = 1.02, $CHCl_3$).

Ethyl (3*R*,4*R*,5*S*)-4-Acetamido-5-((*S*)-2-((*tert*-butoxycarbonyl)amino)-3-phenylpropanamido)-3-(pentan-3-yloxy)cyclohex-1-ene-1-carboxylate (8l)

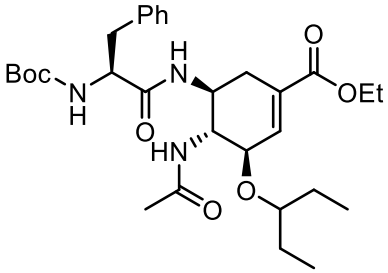

White solid, 105.8 mg, 95% yield. IR (ATR, ν/cm^{-1}): 3305 m, 3070 w, 2968 w, 2926 w, 2874 w, 1719 m, 1685 m, 1650 s, 1529 s, 1370 m, 1251 s, 1166 m, 1049 m, 940 w, 699 m. ^{1}H NMR (400 MHz, $CDCl_3$, 25 °C): δ 7.32-7.26 (m, 2H), 7.22 (tt, *J* = 7.3, 2.5 Hz, 1H), 7.19-7.15 (m, 2H), 7.00 (brd, *J* = 6.9 Hz, 1H), 6.79 (s, 1H), 5.59 (d, *J* = 7.1 Hz, 1H), 4.82 (d, *J* = 8.3 Hz, 1H), 4.40-4.30 (m, 1H), 4.21 (q, *J* = 7.1 Hz, 2H), 4.12-3.97 (m, 3H), 3.34 (quint., *J* = 5.7 Hz, 1H), 3.09-3.00 (m, 2H), 2.73 (dd, *J* = 17.9, 4.6 Hz, 1H), 2.30-2.18 (m, 1H), 1.91 (s, 3H), 1.54-1.44 (m, 4H), 1.39 (s, 9H), 1.30 (t, *J* = 7.1 Hz, 3H), 0.88 (t, *J* = 7.3 Hz, 3H), 0.87 (t, *J* = 7.6 Hz, 3H). ^{13}C{^{1}H} NMR (100 MHz, $CDCl_3$, 25 °C): δ 172.0, 171.3, 165.8, 155.2, 137.1, 136.4, 129.4, 129.3, 128.6, 126.9, 82.1, 80.0, 75.3, 60.9, 55.4, 53.3, 48.6, 38.5, 30.4, 28.3, 26.2, 25.7, 23.2, 14.2, 9.5, 9.2. HPLC (Daicel CHIRALPAK IB N-3, temperature: 30 °C, hexane : ^{i}PrOH = 95 : 5, detector : 215 nm, flow rate 0.5

mL/min, t_1(for D-Phe) = 18.0 min, t_2(for L-Phe) = 22.3 min). $[\alpha]^{28}_D$ = -64.99 (c = 0.81, $CHCl_3$). HRMS (ESI^+) m/z calc. for $C_{30}H_{45}O_7N_3Na$ 582.31497 found 582.31434.

***tert*-Butyl (*S*)-(1-(4-(2-Chlorodibenzo[*b*,*f*][1,4]oxazepin-11-yl)piperazin-1-yl)-1-oxo-3-phenylpropan-2-yl)carbamate (8m)**

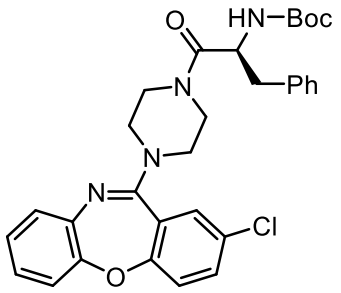

8m was isolated by silica-gel column chromatography (hexane/EtOAc = 6/1 to 4/1), since **8m** was partially soluble in hexane. White solid, 111.8 mg, >99% yield. IR (ATR, ν/cm^{-1}): 3418 br, 3300 br, 2976 w, 2926 w, 2856 w, 1705 m, 1642 m, 1602 m, 1230 s, 1164 s, 1009 s, 751 m, 700 m. ^{1}H NMR (400 MHz, $CDCl_3$, 55 °C): δ 7.39 (dd, *J* = 8.7, 2.7 Hz, 1H), 7.32-7.20 (m, 6H), 7.17 (d, *J* = 8.7 Hz, 1H), 7.13-7.05 (m, 3H), 7.02-6.97 (m, 1H), 5.35 (d, *J* = 4.6 Hz, 1H), 4.85 (dd, *J* = 14.0, 7.2 Hz, 1H), 3.72-3.55 (brm, 2H), 3.55-3.42 (brm, 2H), 3.40-3.26 (brm, 2H), 3.20-3.10 (brm, 1H), 3.04-2.94 (m, 2H), 2.94-2.82 (m, 1H), 1.44 (s, 9H). ^{13}C{^{1}H} NMR (100 MHz, $CDCl_3$, 55 °C): δ 170.6, 159.5, 158.4, 155.1, 151.8, 139.9, 136.5, 132.7, 130.5, 129.6, 128.8, 128.6, 127.2, 127.1, 125.8, 124.91, 124.86, 122.8, 120.1, 79.9, 51.2, 47.1, 45.2, 41.7, 40.4, 28.4. HPLC (Daicel CHIRALPAK IB N-3, temperature: 30 °C, hexane : ^{i}PrOH = 90 : 10, detector : 215 nm, flow rate 1.0 mL/min, t_1(*R*) = 9.8 min, t_2(*S*) = 16.1 min). $[\alpha]^{25}_D$ = +13.95 (c = 0.73, $CHCl_3$) (for an ee of >99%). HRMS (ESI^+) m/z calc. for $C_{31}H_{34}O_4N_4Cl$ 561.22631 found 561.22539.

Benzyl (*tert*-Butoxycarbonyl)-L-valyl-L-valinate (8n)[30]

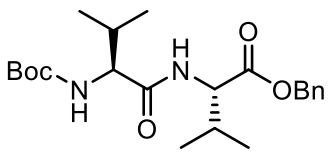

Reaction time was extended to 12 hours. **8n** was isolated by silica-gel column chromatography (hexane/EtOAc = 19/1 to 17/3). Colorless oil, 70.0 mg, 86% yield. ^{1}H NMR (400 MHz, $CDCl_3$, 25 °C): δ 7.40-7.29 (m, 5H), 6.33 (brd, *J* = 7.6 Hz, 1H), 5.20 (d, *J* = 12.1 Hz, 1H), 5.13 (d, *J* = 12.1 Hz, 1H), 5.03 (brd, *J* = 7.3 Hz, 1H), 4.60 (dd, *J* = 8.9, 4.8 Hz, 1H), 3.90 (dd, *J* = 8.7, 6.4 Hz, 1H), 2.27-2.04 (m, 2H), 1.44 (s, 9H), 0.97-

0.84 (m, 12H). $^{13}C\{^{1}H\}$ NMR (100 MHz, $CDCl_3$, 25 °C): δ 171.6, 171.5, 155.8, 135.3, 128.6, 128.5, 128.4, 79.9, 67.0, 60.2, 57.0, 31.3, 30.6, 28.3, 19.3, 18.9, 17.9, 17.6. HPLC (Daicel CHIRALPAK IA-3, temperature: 30 °C, hexane : ^{i}PrOH = 90 : 10, detector : 215 nm, flow rate 1.0 mL/min, t_1(L,L) = 7.9 min, t_2(D,L) = 25.1 min). $[\alpha]^{17}_{D}$ = -21.8 (c = 1.01, $CHCl_3$).

Procedure for Synthesizing 4c at 10 mmol Scale

In an argon-filled glove box, Boc-L-Phe-OH (2.65 g, 10 mmol), gold(I) complex **3a** (26.6 mg, 0.04 mmol, 0.4 mol%), $Zn(acac)_2$ (10.5 mg, 0.04 mmol, 0.4 mol%), and $AgPF_6$ (10.1 mg, 0.04 mmol, 0.4 mol%) were placed in a screw-cap vial containing a magnetic stirring bar. After addition of methyl 2-octynoate (1.82 mL, 11 mmol, 1.1 equiv), the reaction vial was sealed with a screw-cap and removed from the glove box. The mixture was stirred at 80 °C in an oil-bath for 16 hours, as shown in a right picture. The crude product was purified by silica-gel column chromatography (hexane/EtOAc=98/2 to 80/20). Residual solvents were removed under reduced pressure at 70 °C, and **4c** was afforded in 98% yield (4.132 g, 9.85 mmol, >99% ee).

2.4.3. Computational Studies

General Procedure

All geometry optimizations and single-point energy calculations were performed by Gaussian 16 package.[31] The geometry optimizations of all structures were conducted at the ωB97X-D functional in conjunction with the 6-311G(d,p) basis set with the solvation model (SMD: EtOAc) to evaluate solution phase electronic energies. Frequency analyses were performed at the same level of theory for geometry optimizations, in which the thermal free energy corrections were provided. All the transition states have the single imaginary frequency, and all the optimized structures as minima have no imaginary frequency. The transition states were traced with intrinsic reaction coordinate (IRC) analyses by using Global Reaction Route Mapping (GRRM) program[32] to confirm the connection of the reaction pathway. For the purpose of discussion, relative Gibbs free

energies (ΔG_{sol}) were calculated from $\Delta G_{sol} = \Sigma G_{sol}$ for products – ΣG_{sol} for reactants. 3D models of optimized structures were described by CYLview20.[33]

Summary of Energies

Structure Name	solvation electronic energies [Hartree]	thermal free energy corrections [Hartree]	solution phase Gibbs free energies [Hartree]
SM	-974.833543	0.259696	-974.573847
TS-amine	-1298.556871	0.362749	-1298.194122
INT	-1298.570502	0.358435	-1298.212067
TS'-amine	-1298.568902	0.354234	-1298.214668
Pro-amine	-877.577800	0.237869	-877.339931
TS-water	-1051.231909	0.284433	-1050.947476
Pro-water	-630.271448	0.167831	-630.103617
Gly-OMe	-323.730986	0.077216	-323.653770
H_2O	-76.429704	0.003912	-76.425792
A	-421.019490	0.096498	-420.922992
B	-421.019069	0.092645	-420.926425
TS''-amine	-1298.552839	0.363733	-1298.189107
TS'''-amine	-1374.989321	0.383724	-1374.605597

Energy Diagram

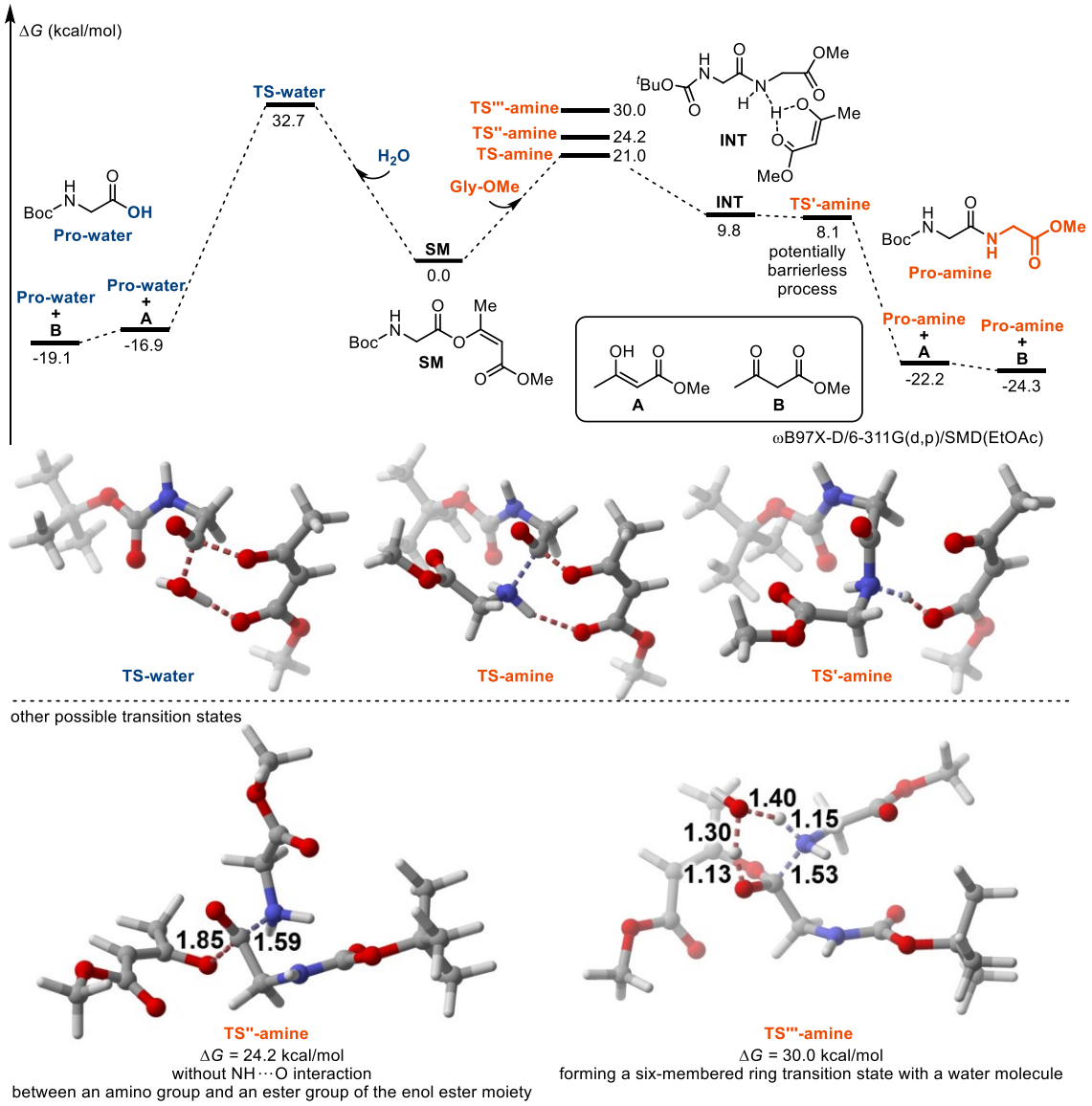

Figure 2.4. An energy diagram for amide-bond formation steps with an α-methoxycarbonyl enol ester. Relative free energies were given in kcal/mol.

2.4.4. HPLC Charts

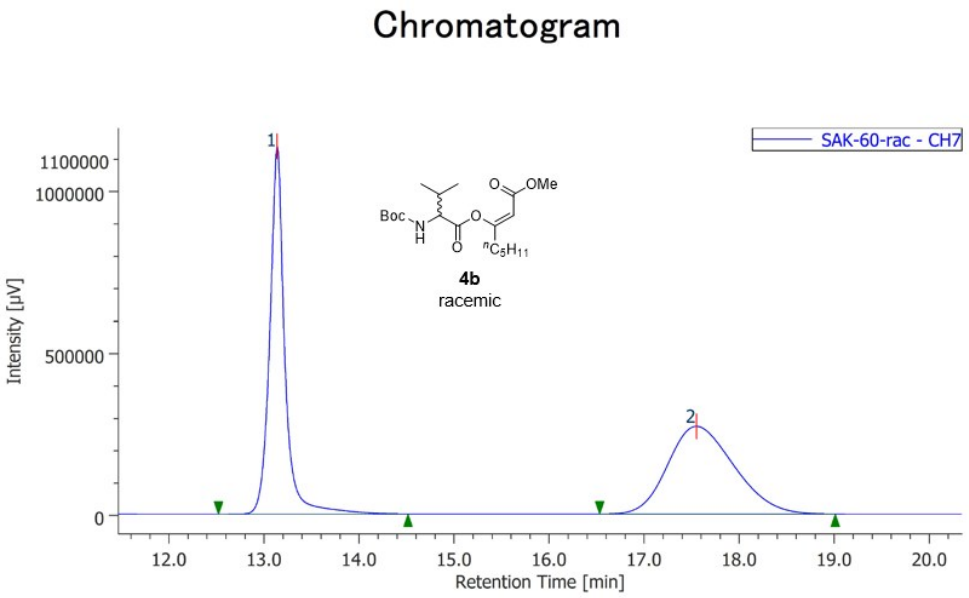

#	Peak Name	CH	tR [min]	Area [μV·sec]	Height [μV]	Area%	Height%	Quantity	NTP	Resolution	Symmetry Factor	Warning
1	Unknown	7	13.137	12552405	1134850	48.742	80.699	N/A	44024	5.734	1.109	
2	Unknown	7	17.547	13200275	271418	51.258	19.301	N/A	2952	N/A	1.220	

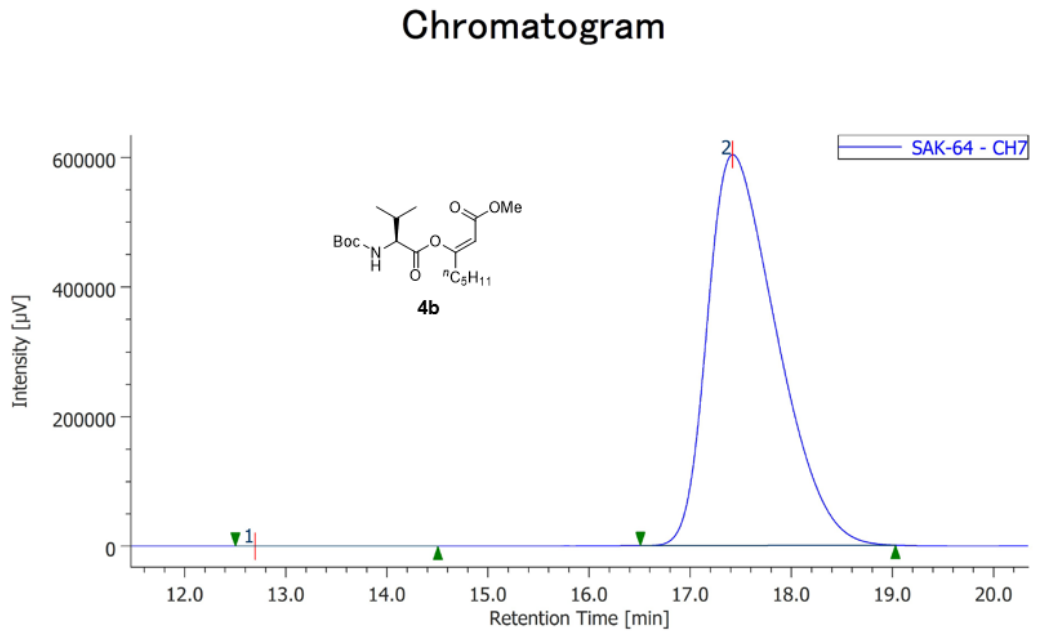

#	Peak Name	CH	tR [min]	Area [μV·sec]	Height [μV]	Area%	Height%	Quantity	NTP	Resolution	Symmetry Factor	Warning
1	Unknown	7	12.697	501	35	0.002	0.006	N/A	313	2.288	5.129	
2	Unknown	7	17.417	28739382	602735	99.998	99.994	N/A	3023	N/A	1.510	

Chromatogram

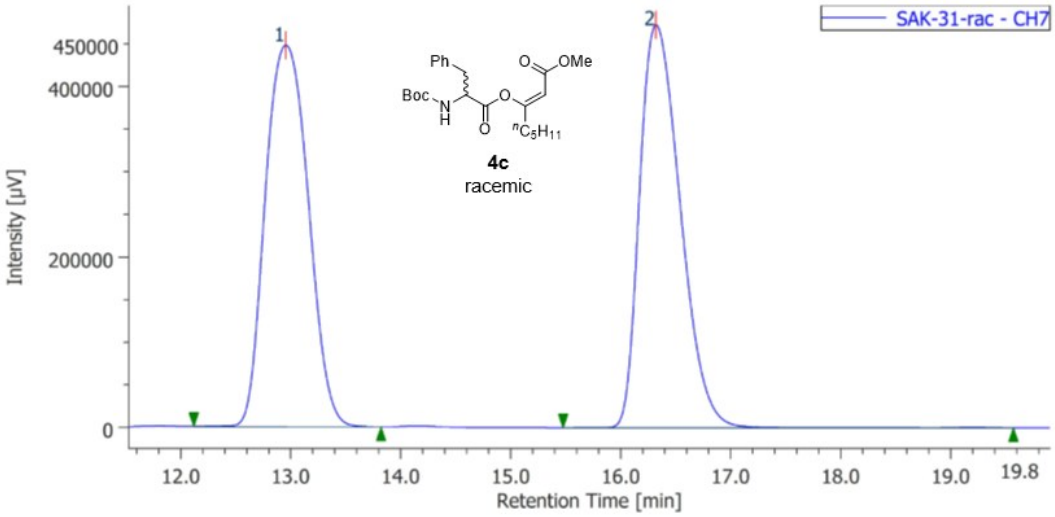

#	Peak Name	CH	tR [min]	Area [μV·sec]	Height [μV]	Area%	Height%	Quantity	NTP	Resolution	Symmetry Factor	Warning
1	Unknown	7	12.953	12210906	447995	50.053	48.639	N/A	4727	4.680	1.122	
2	Unknown	7	16.320	12185188	473060	49.947	51.361	N/A	8979	N/A	1.386	

Chromatogram

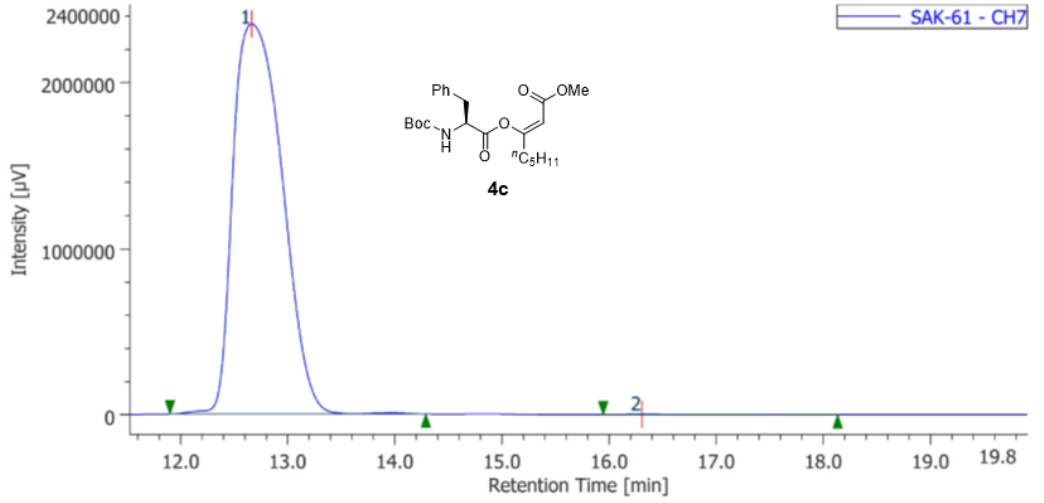

#	Peak Name	CH	tR [min]	Area [μV·sec]	Height [μV]	Area%	Height%	Quantity	NTP	Resolution	Symmetry Factor	Warning
1	Unknown	7	12.663	75154593	2347231	99.863	99.851	N/A	3260	4.756	1.417	
2	Unknown	7	16.307	103034	3492	0.137	0.149	N/A	10106	N/A	2.862	

Chromatogram

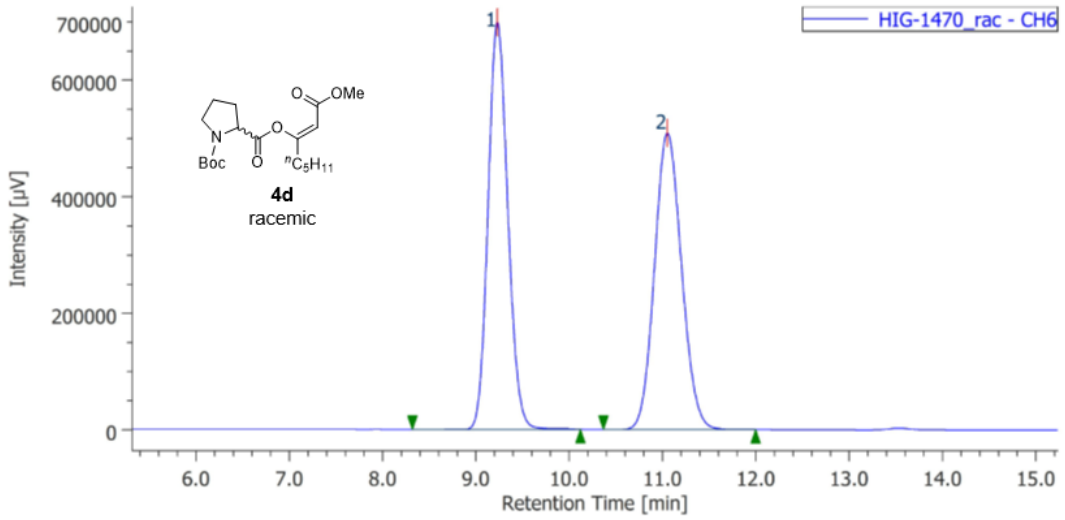

#	Peak Name	CH	tR [min]	Area [μV·sec]	Height [μV]	Area%	Height%	Quantity	NTP	Resolution	Symmetry Factor	Warning
1	Unknown	6	9.227	10279496	698576	50.038	57.867	N/A	9123	3.977	1.126	
2	Unknown	6	11.050	10263745	508626	49.962	42.133	N/A	6876	N/A	1.095	

Chromatogram

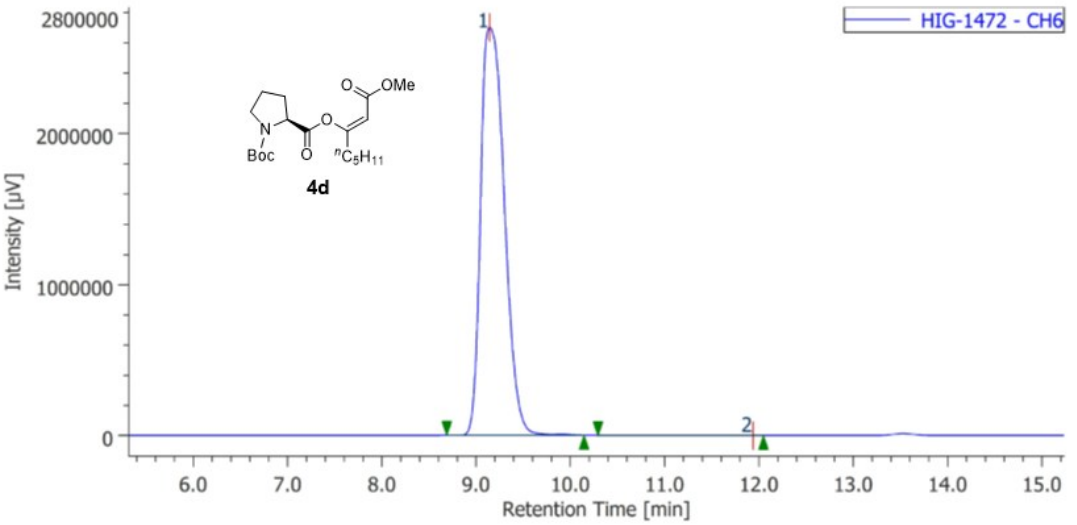

#	Peak Name	CH	tR [min]	Area [μV·sec]	Height [μV]	Area%	Height%	Quantity	NTP	Resolution	Symmetry Factor	Warning
1	Unknown	6	9.143	47244284	2697453	99.942	99.997	N/A	6153	1.687	1.370	
2	Unknown	6	11.937	27237	75	0.058	0.003	N/A	280	N/A	0.531	

Chromatogram

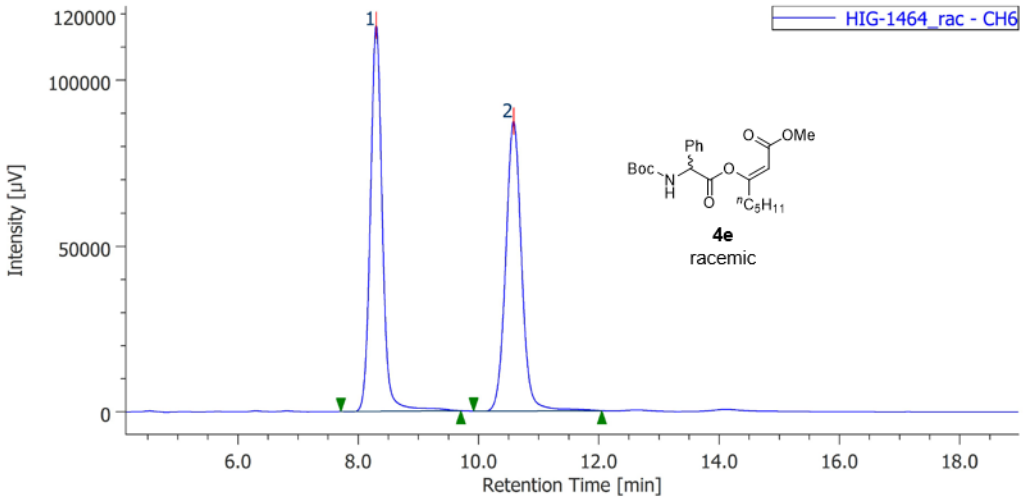

#	Peak Name	CH	tR [min]	Area [μV·sec]	Height [μV]	Area%	Height%	Quantity	NTP	Resolution	Symmetry Factor	Warning
1	Unknown	6	8.297	1612916	116286	50.170	57.111	N/A	9180	5.640	1.074	
2	Unknown	6	10.580	1602006	87327	49.830	42.889	N/A	8264	N/A	1.048	

Chromatogram

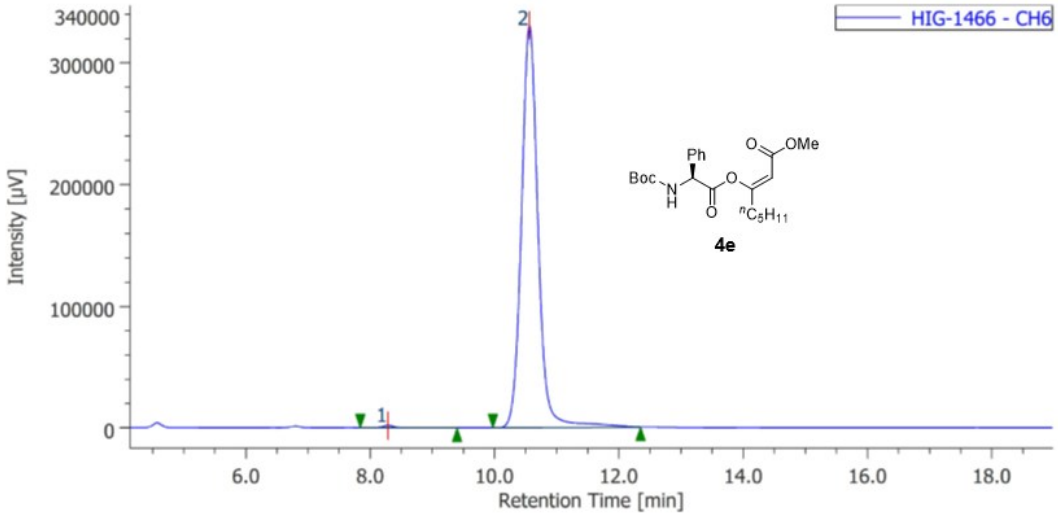

#	Peak Name	CH	tR [min]	Area [μV·sec]	Height [μV]	Area%	Height%	Quantity	NTP	Resolution	Symmetry Factor	Warning
1	Unknown	6	8.287	27645	1966	0.449	0.591	N/A	9571	5.686	0.964	
2	Unknown	6	10.560	6128944	330445	99.551	99.409	N/A	8324	N/A	1.076	

Chromatogram

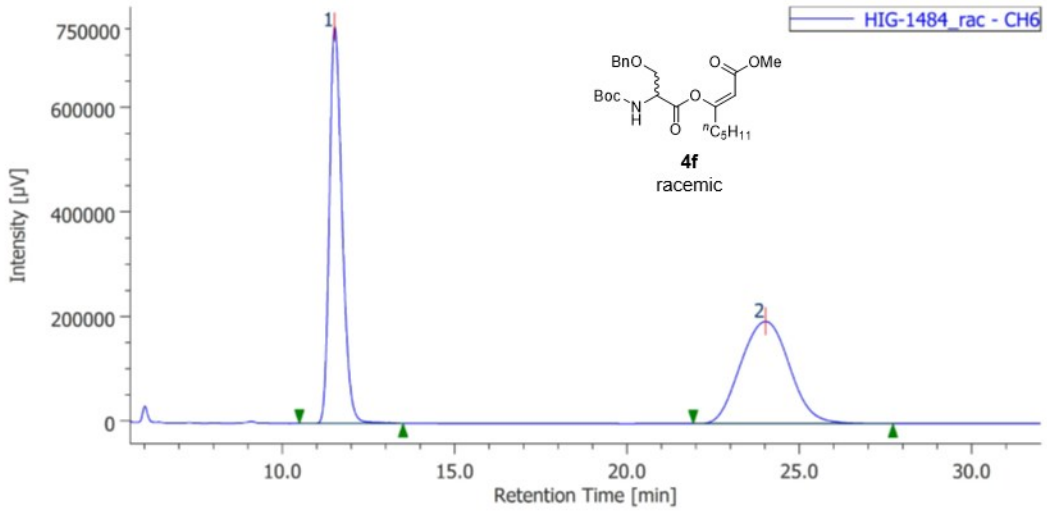

#	Peak Name	CH	tR [min]	Area [μV·sec]	Height [μV]	Area%	Height%	Quantity	NTP	Resolution	Symmetry Factor	Warning
1	Unknown	6	11.517	19492737	759450	50.157	79.475	N/A	4769	7.502	1.294	
2	Unknown	6	24.013	19370513	196128	49.843	20.525	N/A	1291	N/A	1.064	

Chromatogram

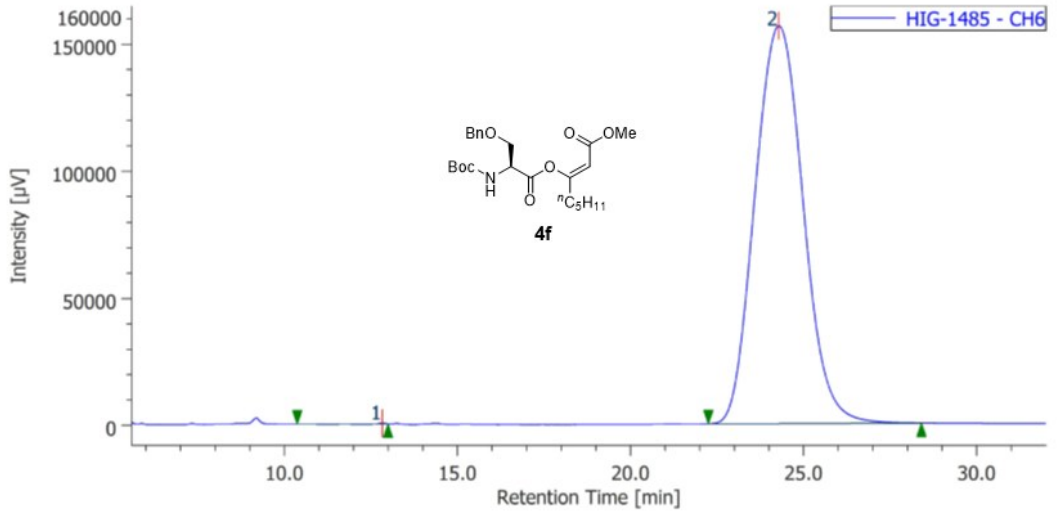

#	Peak Name	CH	tR [min]	Area [μV·sec]	Height [μV]	Area%	Height%	Quantity	NTP	Resolution	Symmetry Factor	Warning
1	Unknown	6	12.823	2419	218	0.016	0.139	N/A	25082	7.864	1.006	
2	Unknown	6	24.277	15150785	156451	99.984	99.861	N/A	1398	N/A	1.104	

Chromatogram

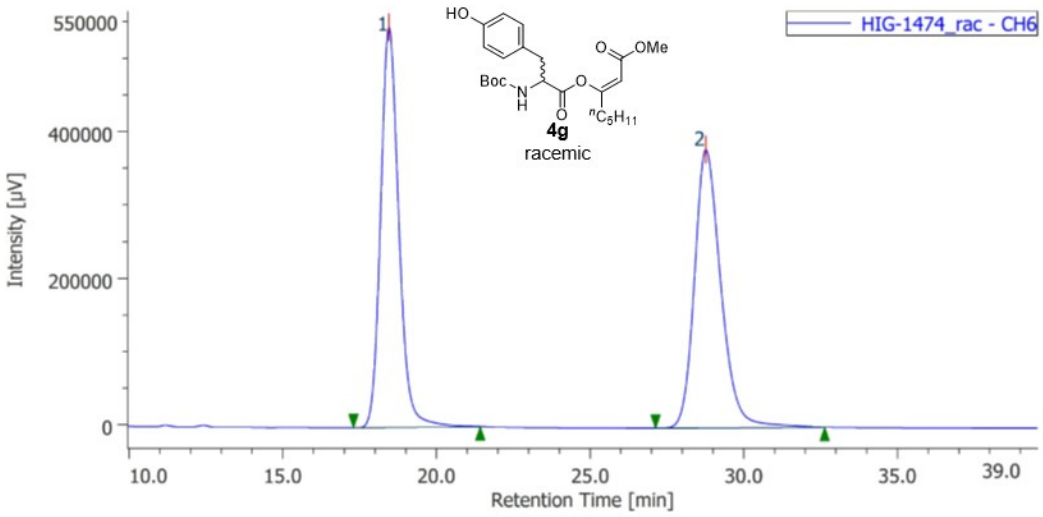

#	Peak Name	CH	tR [min]	Area [μV·sec]	Height [μV]	Area%	Height%	Quantity	NTP	Resolution	Symmetry Factor	Warning
1	Unknown	6	18.453	22499652	546055	49.705	58.995	N/A	4936	8.038	1.161	
2	Unknown	6	28.760	22766564	379536	50.295	41.005	N/A	5722	N/A	1.240	

Chromatogram

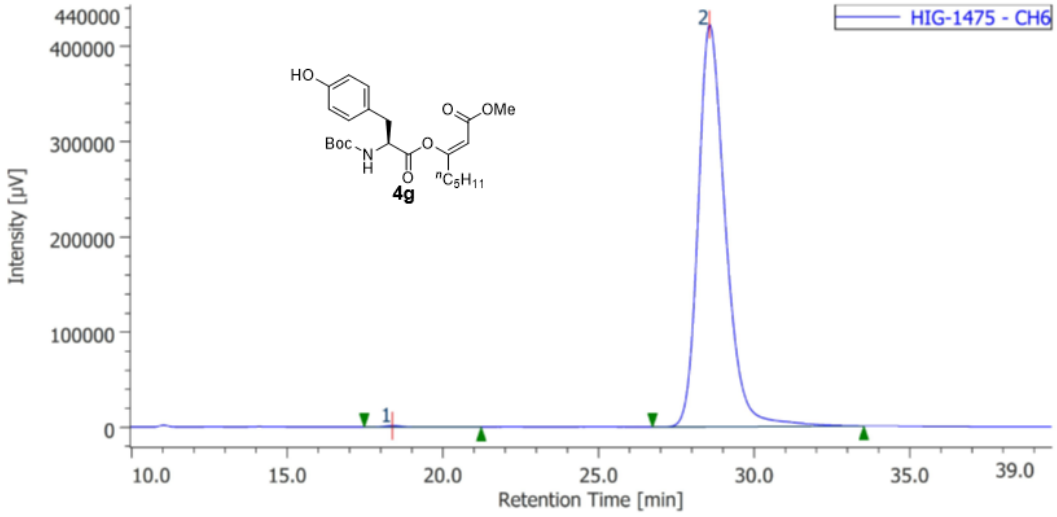

#	Peak Name	CH	tR [min]	Area [μV·sec]	Height [μV]	Area%	Height%	Quantity	NTP	Resolution	Symmetry Factor	Warning
1	Unknown	6	18.380	60840	1570	0.236	0.371	N/A	4909	7.905	1.025	
2	Unknown	6	28.567	25698495	421884	99.764	99.629	N/A	5541	N/A	1.274	

Chromatogram

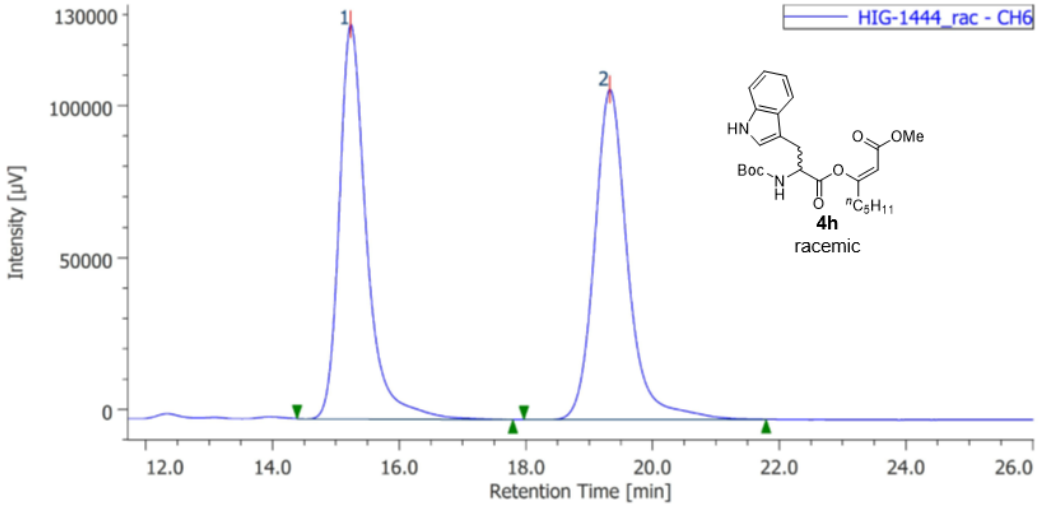

#	Peak Name	CH	tR [min]	Area [μV·sec]	Height [μV]	Area%	Height%	Quantity	NTP	Resolution	Symmetry Factor	Warning
1	Unknown	6	15.233	3869393	129814	49.327	54.448	N/A	7142	5.067	1.390	
2	Unknown	6	19.323	3975019	108603	50.673	45.552	N/A	7416	N/A	1.206	

Chromatogram

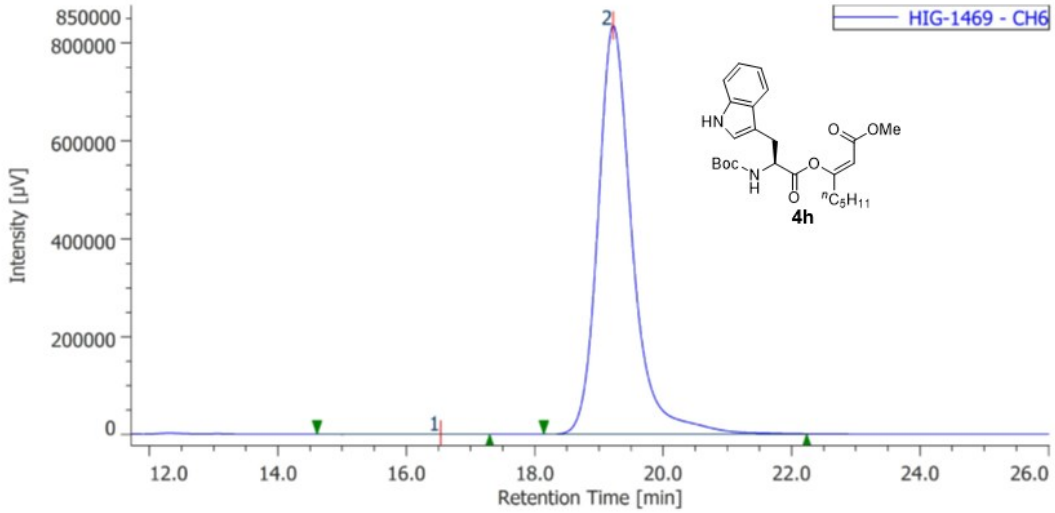

#	Peak Name	CH	tR [min]	Area [μV·sec]	Height [μV]	Area%	Height%	Quantity	NTP	Resolution	Symmetry Factor	Warning
1	Unknown	6	16.530	13970	319	0.045	0.038	N/A	2943	2.539	0.839	
2	Unknown	6	19.220	31028671	834689	99.955	99.962	N/A	7206	N/A	1.268	

Chromatogram

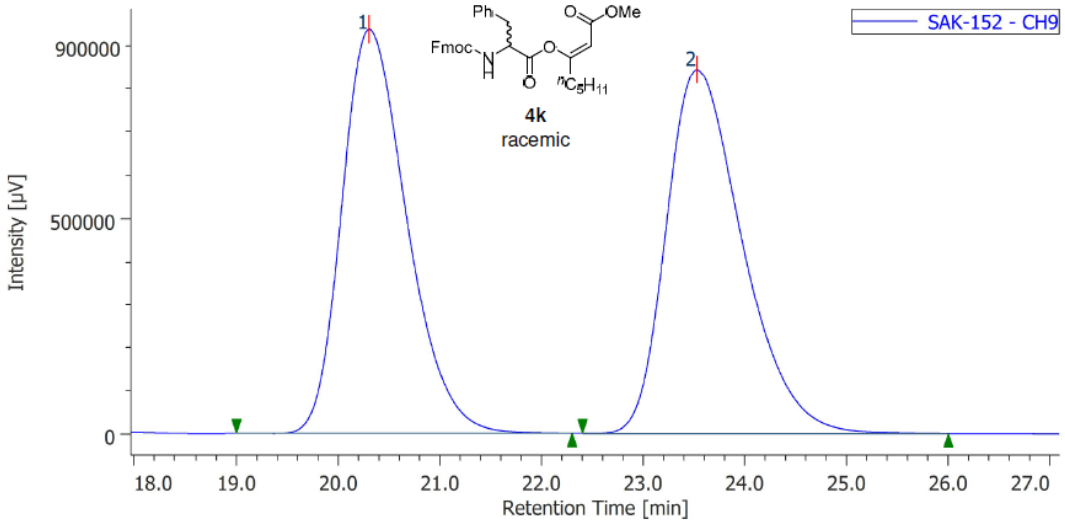

#	Peak Name	CH	tR [min]	Area [μV·sec]	Height [μV]	Area%	Height%	Quantity	NTP	Resolution	Symmetry Factor	Warning
1	Unknown	9	20.303	41620431	936619	48.688	52.653	N/A	4871	2.562	1.301	
2	Unknown	9	23.530	43863655	842220	51.312	47.347	N/A	4779	N/A	1.374	

Chromatogram

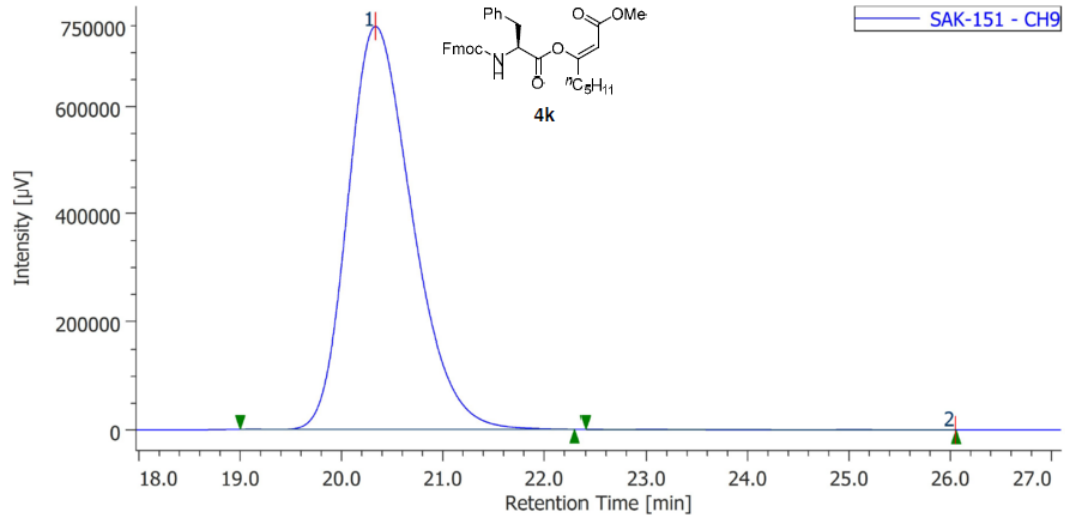

#	Peak Name	CH	tR [min]	Area [μV·sec]	Height [μV]	Area%	Height%	Quantity	NTP	Resolution	Symmetry Factor	Warning
1	Unknown	9	20.333	32948716	747271	99.991	100.000	N/A	4980	N/A	1.282	
2	Unknown	9	26.050	3030	1	0.009	0.000	N/A	N/A	N/A	N/A	

Chromatogram

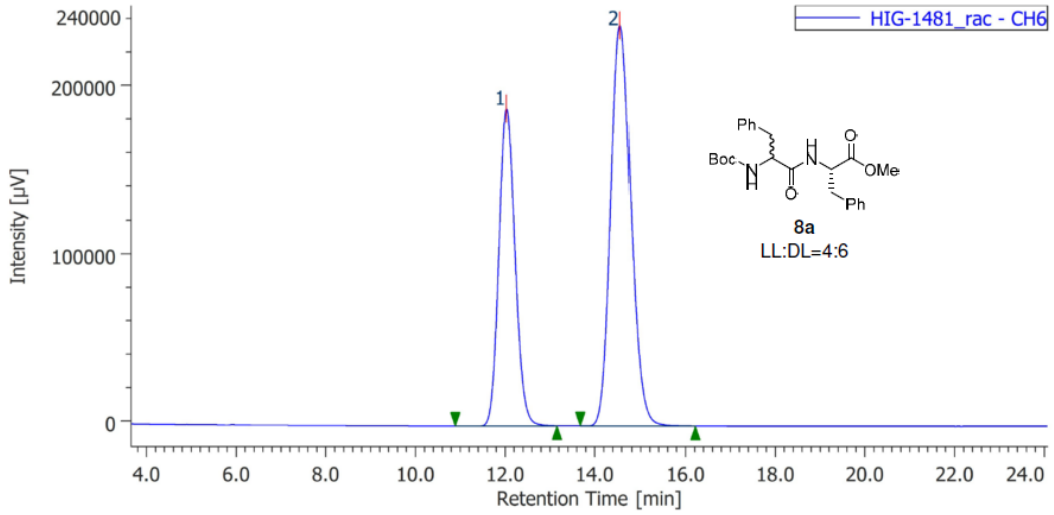

#	Peak Name	CH	tR [min]	Area [μV·sec]	Height [μV]	Area%	Height%	Quantity	NTP	Resolution	Symmetry Factor	Warning
1	Unknown	6	12.027	4762137	188986	39.541	44.196	N/A	5267	3.457	1.126	
2	Unknown	6	14.553	7281503	238621	60.459	55.804	N/A	5255	N/A	1.136	

Chromatogram

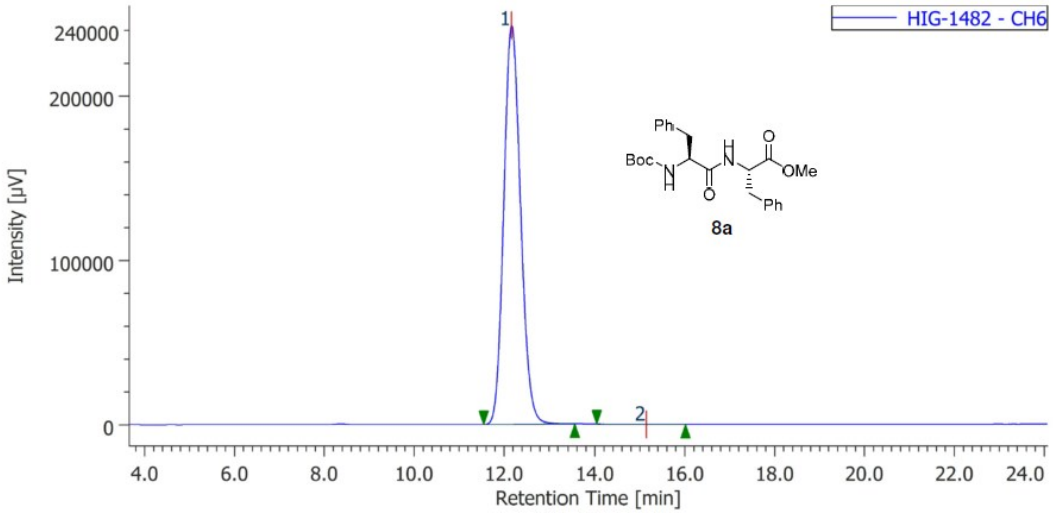

#	Peak Name	CH	tR [min]	Area [μV·sec]	Height [μV]	Area%	Height%	Quantity	NTP	Resolution	Symmetry Factor	Warning
1	Unknown	6	12.167	6317271	242533	99.940	99.972	N/A	5046	2.083	1.137	
2	Unknown	6	15.143	3770	67	0.060	0.028	N/A	772	N/A	0.739	

Chromatogram

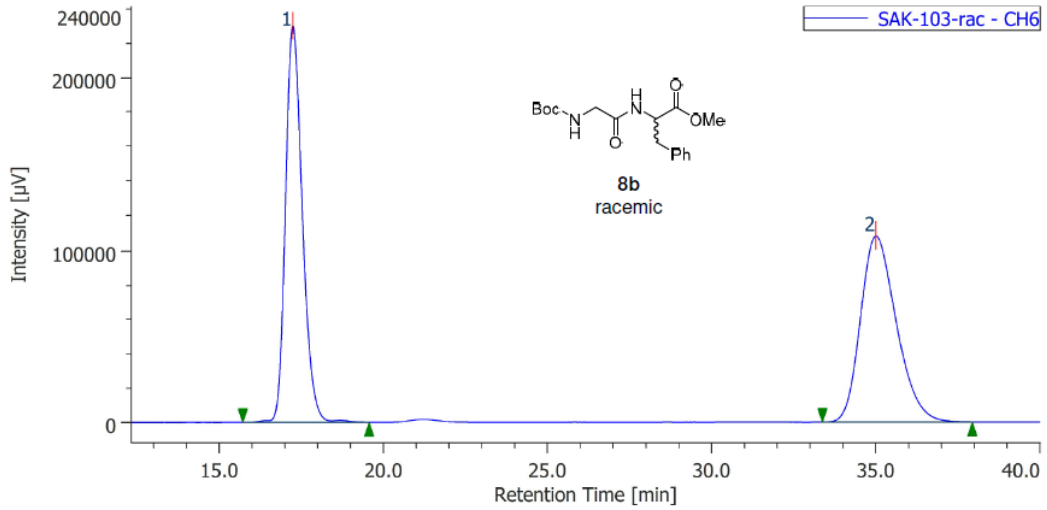

#	Peak Name	CH	tR [min]	Area [μV·sec]	Height [μV]	Area%	Height%	Quantity	NTP	Resolution	Symmetry Factor	Warning
1	Unknown	6	17.243	8247433	229879	50.021	67.952	N/A	5519	12.210	1.247	
2	Unknown	6	35.003	8240624	108416	49.979	32.048	N/A	4959	N/A	1.265	

Chromatogram

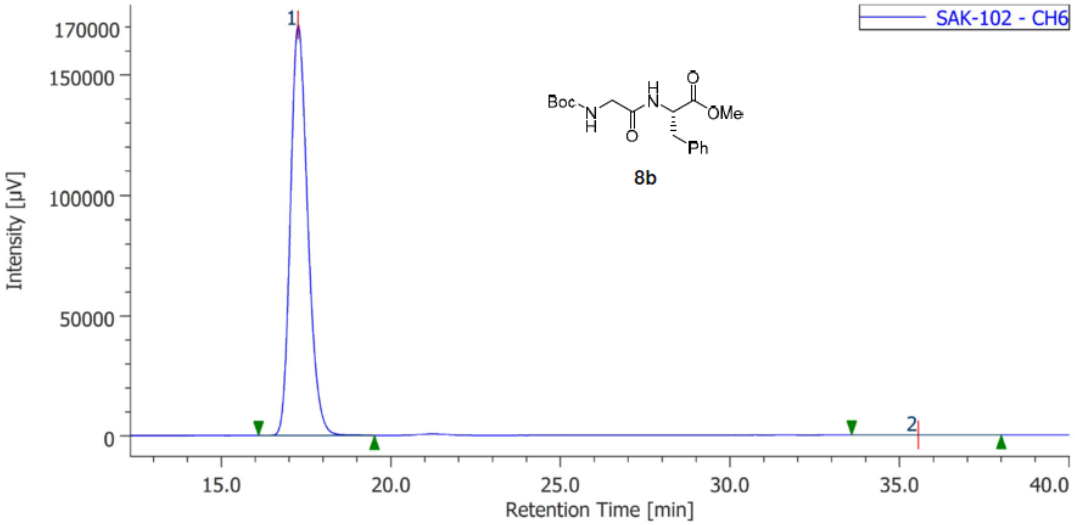

#	Peak Name	CH	tR [min]	Area [μV·sec]	Height [μV]	Area%	Height%	Quantity	NTP	Resolution	Symmetry Factor	Warning
1	Unknown	6	17.263	6057825	170518	99.932	99.960	N/A	5579	11.428	1.232	
2	Unknown	6	35.547	4105	68	0.068	0.040	N/A	3876	N/A	1.113	

Chromatogram

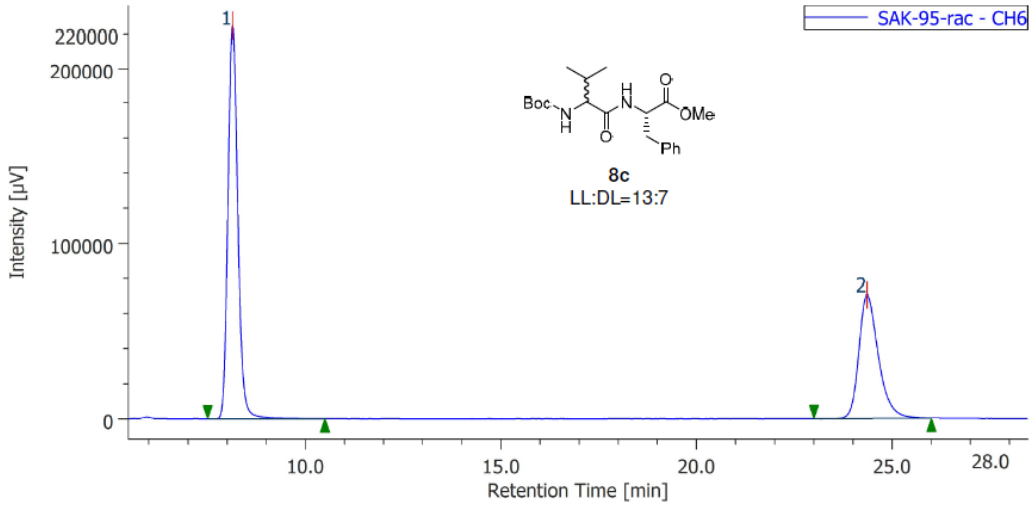

#	Peak Name	CH	tR [min]	Area [μV·sec]	Height [μV]	Area%	Height%	Quantity	NTP	Resolution	Symmetry Factor	Warning
1	Unknown	6	8.140	3959194	224309	61.875	76.181	N/A	5108	24.288	1.149	
2	Unknown	6	24.357	2439483	70134	38.125	23.819	N/A	12163	N/A	1.323	

Chromatogram

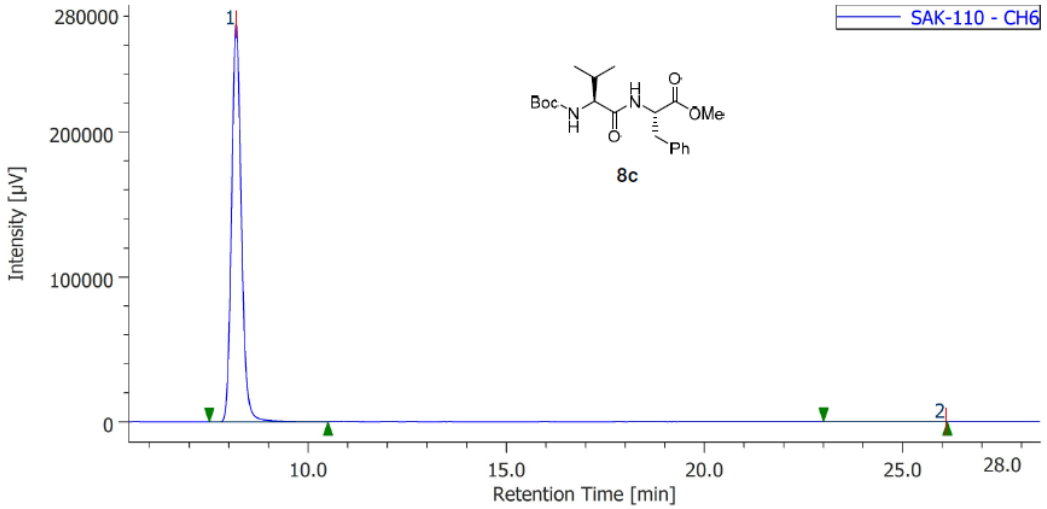

#	Peak Name	CH	tR [min]	Area [μV·sec]	Height [μV]	Area%	Height%	Quantity	NTP	Resolution	Symmetry Factor	Warning
1	Unknown	6	8.183	4728861	274150	99.958	99.998	N/A	5479	6.270	1.148	
2	Unknown	6	26.093	1972	7	0.042	0.002	N/A	390	N/A	0.504	

Chromatogram

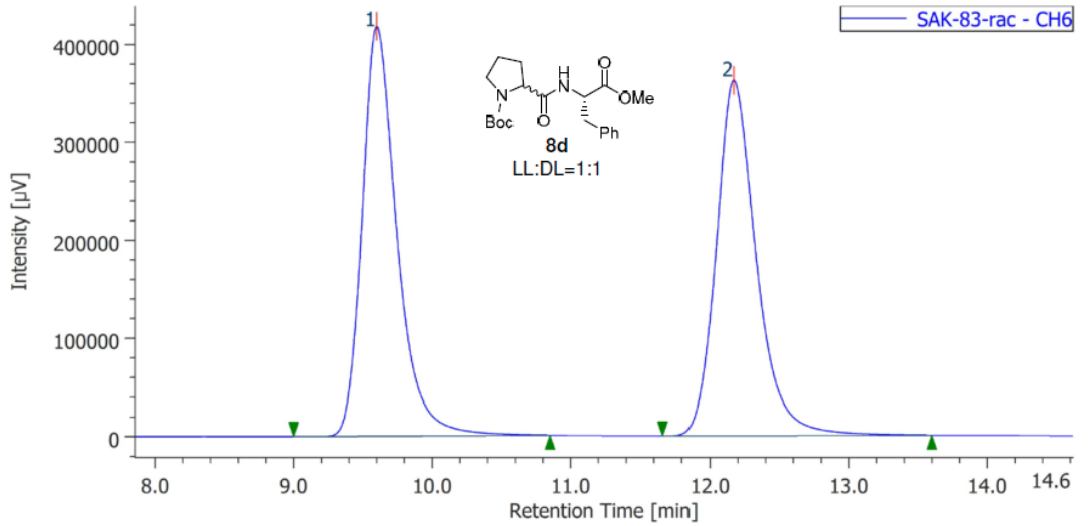

#	Peak Name	CH	tR [min]	Area [μV·sec]	Height [μV]	Area%	Height%	Quantity	NTP	Resolution	Symmetry Factor	Warning
1	Unknown	6	9.600	7283063	417566	50.072	53.549	N/A	7873	5.532	1.355	
2	Unknown	6	12.170	7261977	362209	49.928	46.451	N/A	9522	N/A	1.260	

Chromatogram

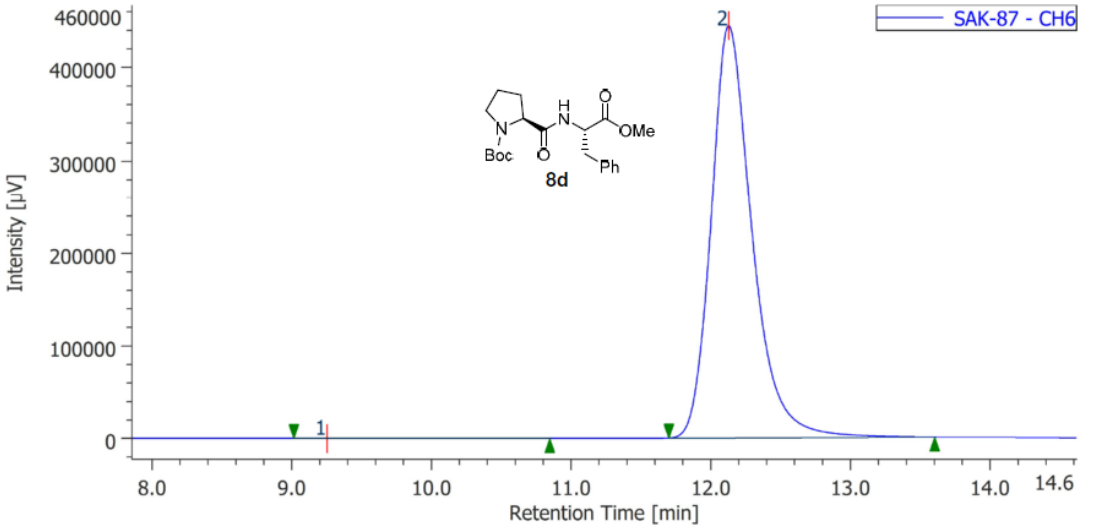

#	Peak Name	CH	tR [min]	Area [μV·sec]	Height [μV]	Area%	Height%	Quantity	NTP	Resolution	Symmetry Factor	Warning
1	Unknown	6	9.253	1984	52	0.022	0.012	N/A	264	2.067	3.846	
2	Unknown	6	12.127	9070830	444148	99.978	99.988	N/A	9079	N/A	1.308	

Chromatogram

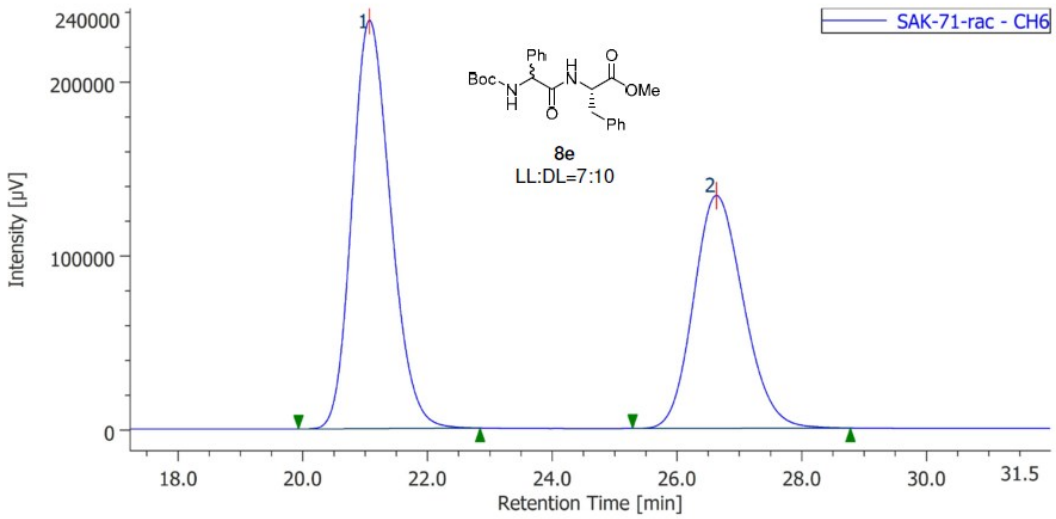

#	Peak Name	CH	tR [min]	Area [μV·sec]	Height [μV]	Area%	Height%	Quantity	NTP	Resolution	Symmetry Factor	Warning
1	Unknown	6	21.067	10073392	234433	57.437	63.716	N/A	5570	4.292	1.189	
2	Unknown	6	26.630	7464746	133499	42.563	36.284	N/A	5248	N/A	1.157	

Chromatogram

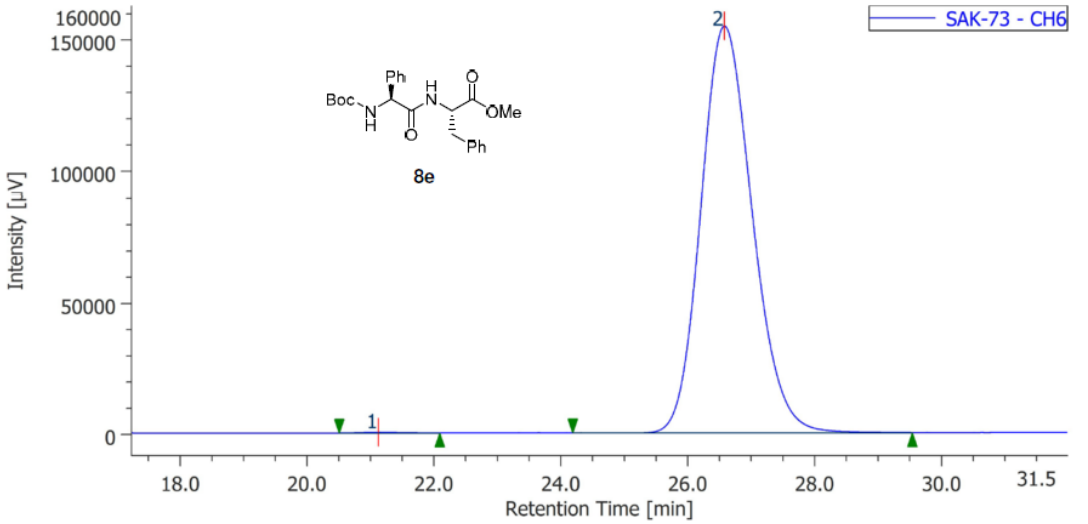

#	Peak Name	CH	tR [min]	Area [μV·sec]	Height [μV]	Area%	Height%	Quantity	NTP	Resolution	Symmetry Factor	Warning
1	Unknown	6	21.123	12821	308	0.147	0.198	N/A	5527	4.181	1.205	
2	Unknown	6	26.573	8705813	154638	99.853	99.802	N/A	5173	N/A	1.169	

Chromatogram

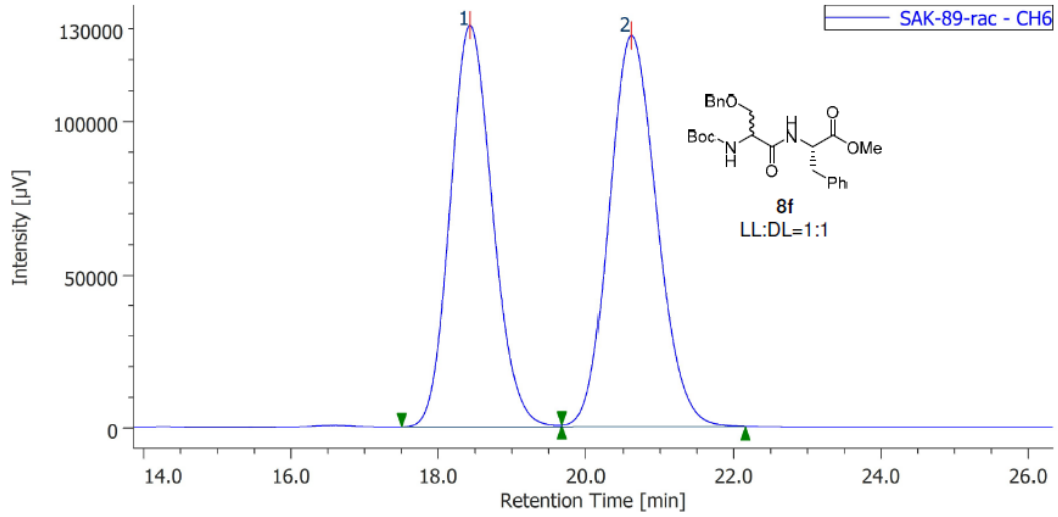

#	Peak Name	CH	tR [min]	Area [μV·sec]	Height [μV]	Area%	Height%	Quantity	NTP	Resolution	Symmetry Factor	Warning
1	Unknown	6	18.430	5236784	130719	47.786	50.654	N/A	4870	1.947	1.132	
2	Unknown	6	20.607	5722030	127345	52.214	49.346	N/A	4833	N/A	1.133	

Chromatogram

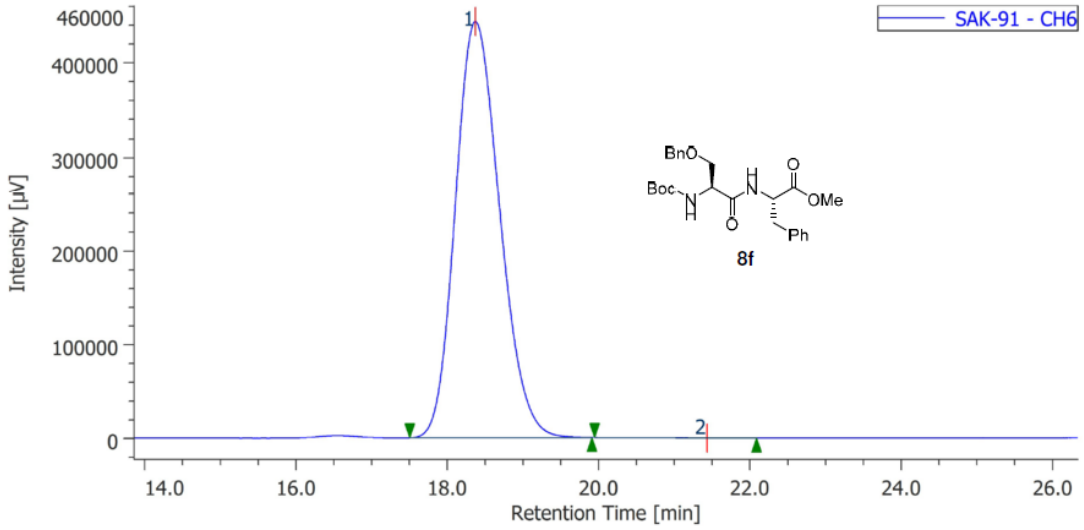

#	Peak Name	CH	tR [min]	Area [μV·sec]	Height [μV]	Area%	Height%	Quantity	NTP	Resolution	Symmetry Factor	Warning
1	Unknown	6	18.370	18052015	442916	99.930	99.971	N/A	4630	1.587	1.184	
2	Unknown	6	21.430	12634	130	0.070	0.029	N/A	946	N/A	0.707	

Chromatogram

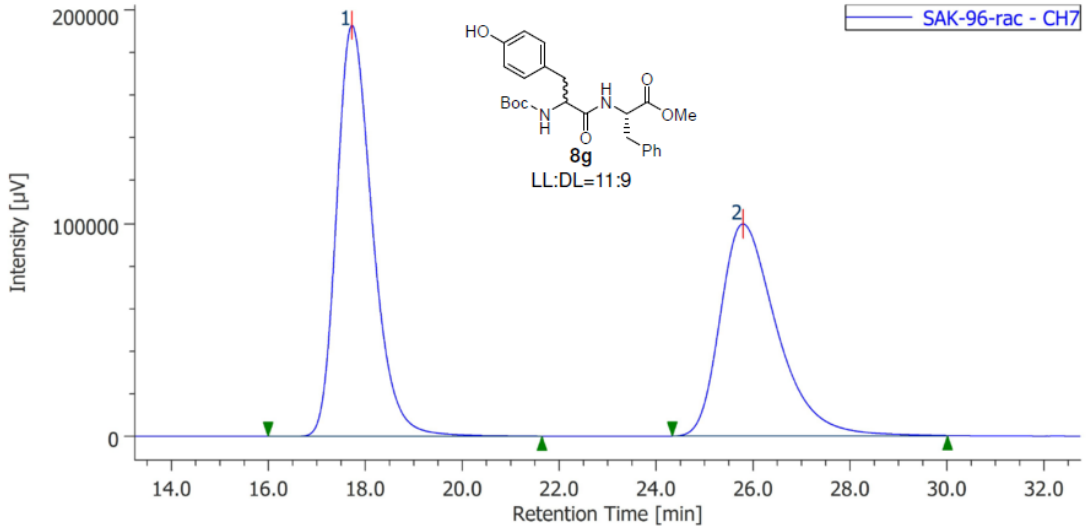

#	Peak Name	CH	tR [min]	Area [μV·sec]	Height [μV]	Area%	Height%	Quantity	NTP	Resolution	Symmetry Factor	Warning
1	Unknown	7	17.723	9899158	192747	54.883	65.885	N/A	2875	4.760	1.295	
2	Unknown	7	25.790	8137619	99802	45.117	34.115	N/A	2469	N/A	1.448	

Chromatogram

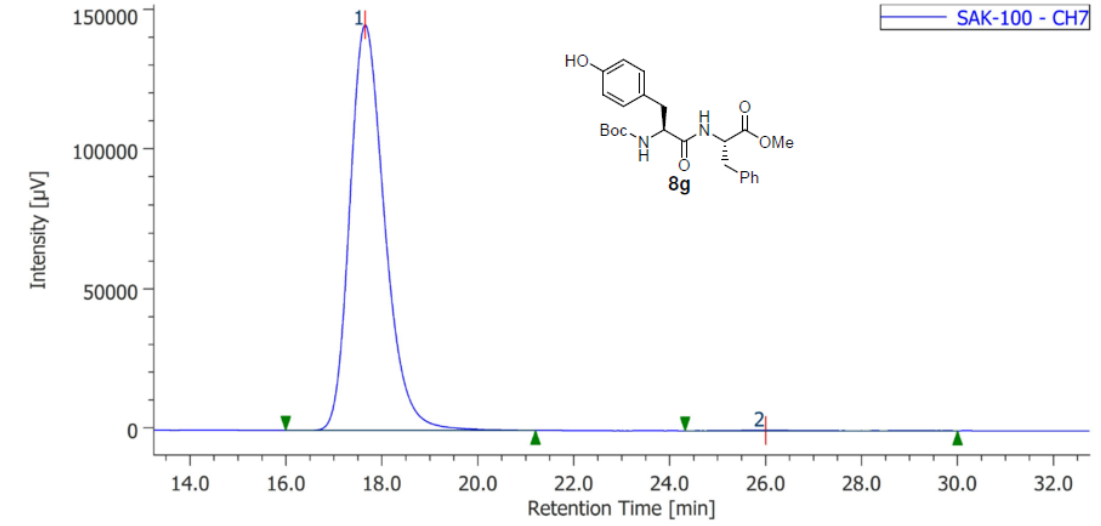

#	Peak Name	CH	tR [min]	Area [μV·sec]	Height [μV]	Area%	Height%	Quantity	NTP	Resolution	Symmetry Factor	Warning
1	Unknown	7	17.650	7343157	145233	99.748	99.866	N/A	2941	4.620	1.263	
2	Unknown	7	25.997	18575	195	0.252	0.134	N/A	2008	N/A	1.727	

Chromatogram

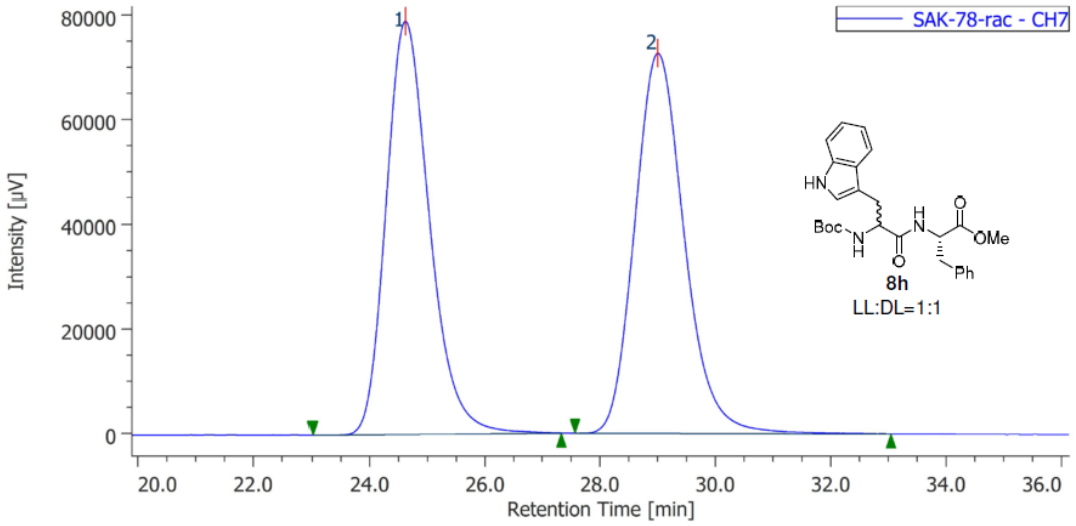

#	Peak Name	CH	tR [min]	Area [μV·sec]	Height [μV]	Area%	Height%	Quantity	NTP	Resolution	Symmetry Factor	Warning
1	Unknown	7	24.617	4135064	78972	48.811	52.070	N/A	5303	3.038	1.254	
2	Unknown	7	29.000	4336553	72693	51.189	47.930	N/A	5665	N/A	1.189	

Chromatogram

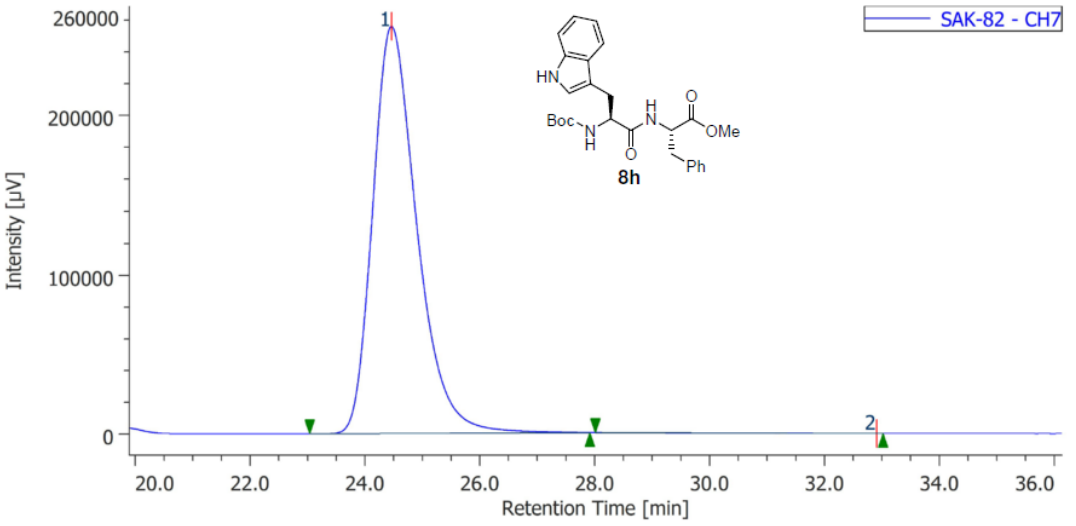

#	Peak Name	CH	tR [min]	Area [μV·sec]	Height [μV]	Area%	Height%	Quantity	NTP	Resolution	Symmetry Factor	Warning
1	Unknown	7	24.460	13655150	255450	99.999	99.993	N/A	5125	11.209	1.345	
2	Unknown	7	32.903	86	18	0.001	0.007	N/A	836764	N/A	0.959	

Chromatogram

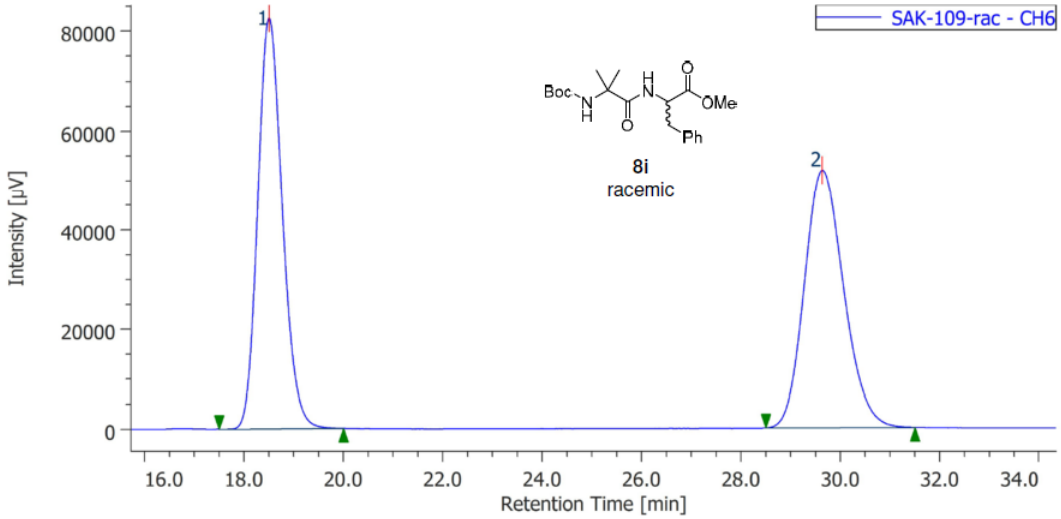

#	Peak Name	CH	tR [min]	Area [μV·sec]	Height [μV]	Area%	Height%	Quantity	NTP	Resolution	Symmetry Factor	Warning
1	Unknown	6	18.503	2833725	82486	49.948	61.427	N/A	6788	9.533	1.178	
2	Unknown	6	29.633	2839609	51797	50.052	38.573	N/A	6748	N/A	1.174	

Chromatogram

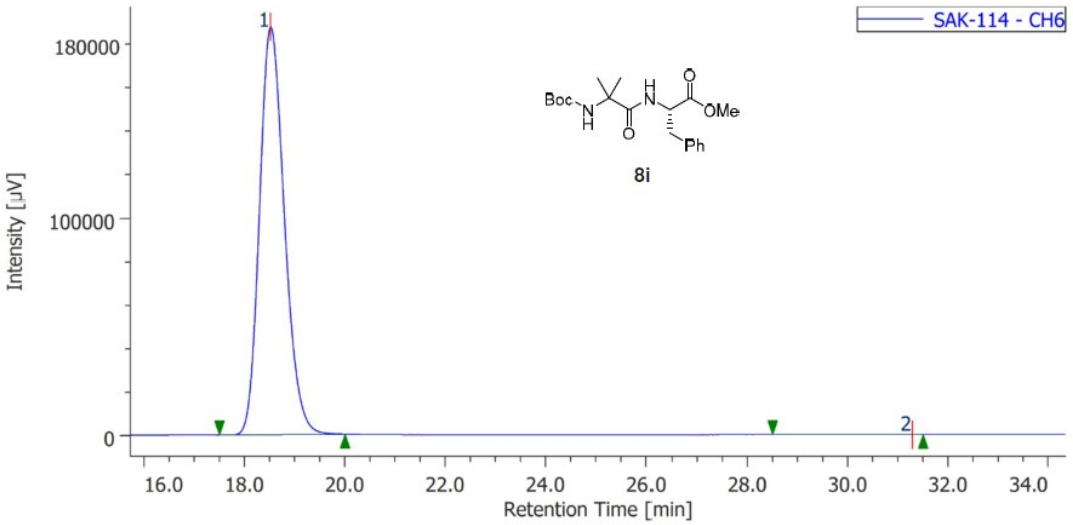

#	Peak Name	CH	tR [min]	Area [μV·sec]	Height [μV]	Area%	Height%	Quantity	NTP	Resolution	Symmetry Factor	Warning
1	Unknown	6	18.520	6443717	187282	99.958	99.985	N/A	6754	4.502	1.212	
2	Unknown	6	31.283	2692	28	0.042	0.015	N/A	684	N/A	0.539	

Chromatogram

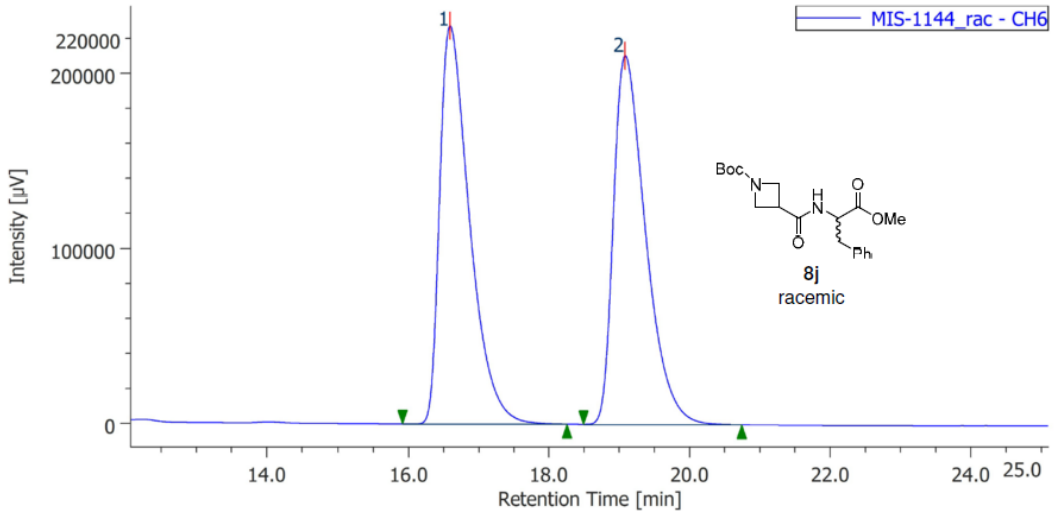

#	Peak Name	CH	tR [min]	Area [μV·sec]	Height [μV]	Area%	Height%	Quantity	NTP	Resolution	Symmetry Factor	Warning
1	Unknown	6	16.587	6727739	227461	50.076	51.916	N/A	7628	3.163	1.752	
2	Unknown	6	19.083	6707392	210676	49.924	48.084	N/A	8601	N/A	1.614	

Chromatogram

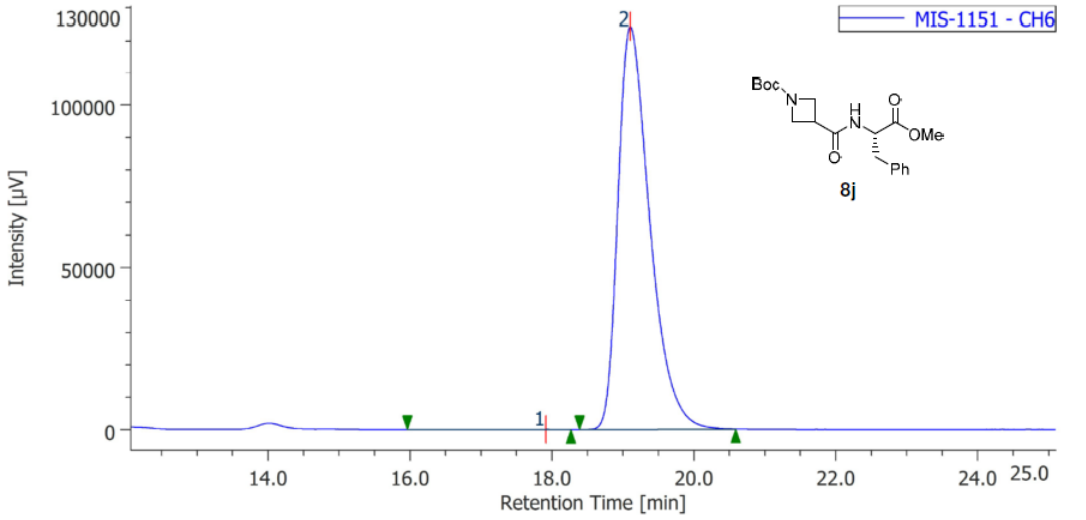

#	Peak Name	CH	tR [min]	Area [μV·sec]	Height [μV]	Area%	Height%	Quantity	NTP	Resolution	Symmetry Factor	Warning
1	Unknown	6	17.913	1802	40	0.047	0.032	N/A	650	0.661	0.580	
2	Unknown	6	19.103	3872359	124210	99.953	99.968	N/A	9082	N/A	1.500	

Chromatogram

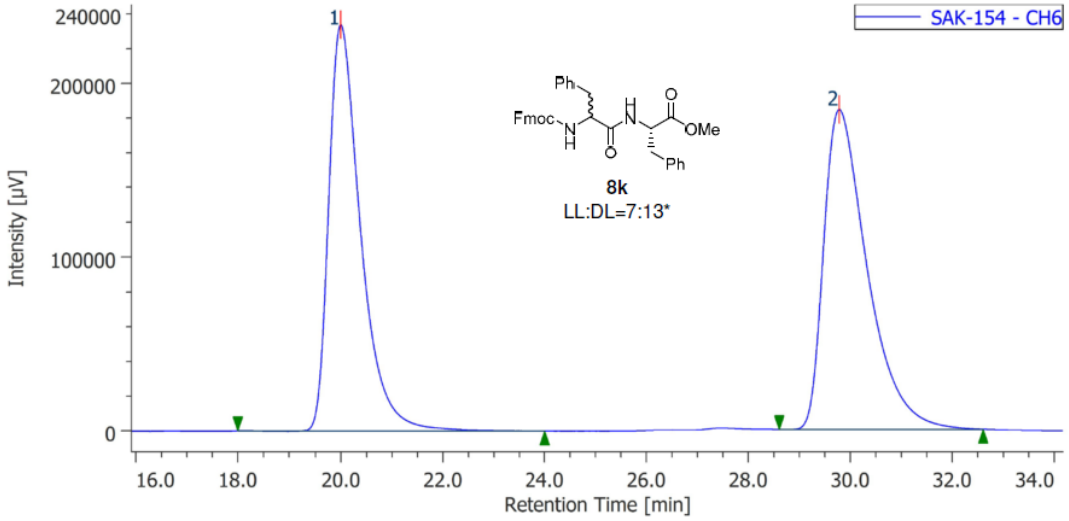

#	Peak Name	CH	tR [min]	Area [μV·sec]	Height [μV]	Area%	Height%	Quantity	NTP	Resolution	Symmetry Factor	Warning
1	Unknown	6	19.993	10170197	233721	48.211	55.932	N/A	5378	7.545	1.602	
2	Unknown	6	29.777	10925090	184144	51.789	44.068	N/A	6222	N/A	1.735	

* Since the HPLC sample was prepared from a filtered IPA suspension due to poor soluble **8k**,
the diastereomeric ratio of the sample for HPLC measurement might differ from that of the sample for NMR measurement.

Chromatogram

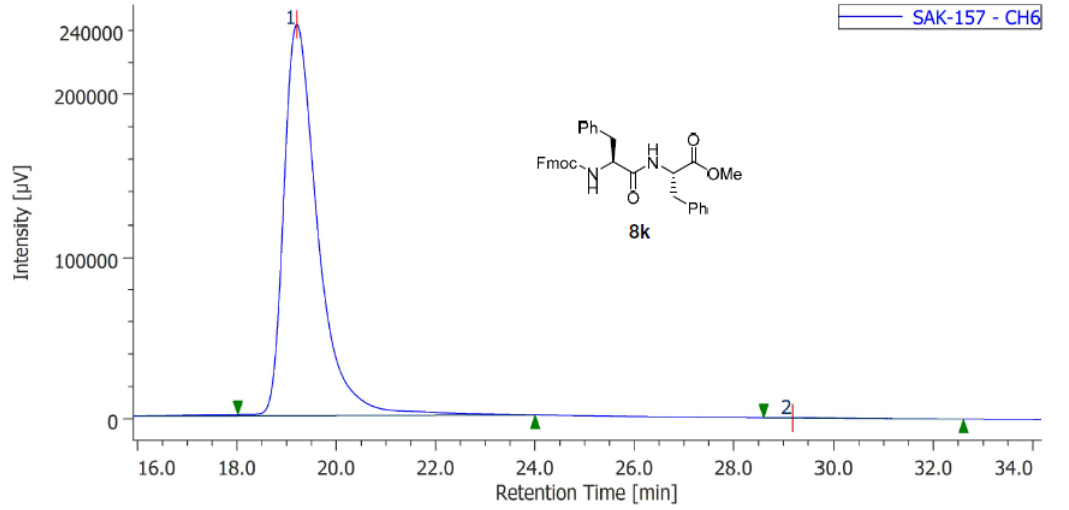

#	Peak Name	CH	tR [min]	Area [μV·sec]	Height [μV]	Area%	Height%	Quantity	NTP	Resolution	Symmetry Factor	Warning
1	Unknown	6	19.203	11507476	241660	99.930	99.944	N/A	4362	6.534	1.635	
2	Unknown	6	29.183	8005	135	0.070	0.056	N/A	3775	N/A	3.457	

Chromatogram

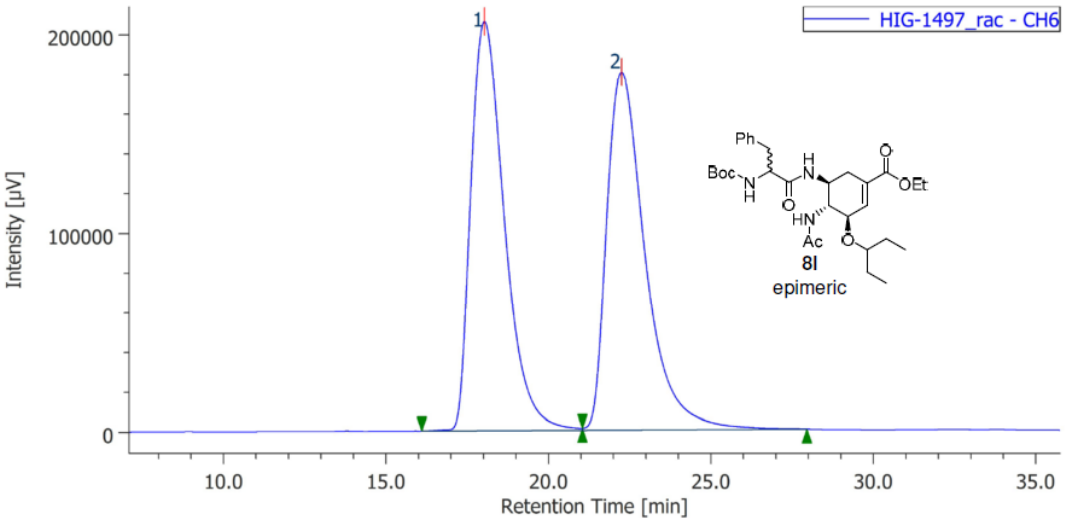

#	Peak Name	CH	tR [min]	Area [μV·sec]	Height [μV]	Area%	Height%	Quantity	NTP	Resolution	Symmetry Factor	Warning
1	Unknown	6	18.027	14770418	205718	49.926	53.354	N/A	1485	2.146	1.512	
2	Unknown	6	22.250	14814472	179854	50.074	46.646	N/A	1839	N/A	1.656	

Chromatogram

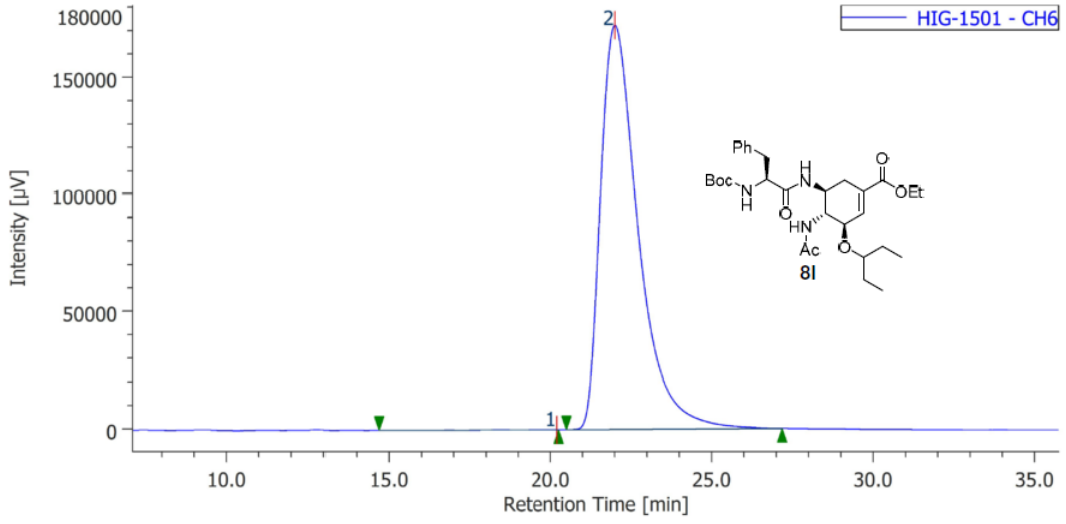

#	Peak Name	CH	tR [min]	Area [μV·sec]	Height [μV]	Area%	Height%	Quantity	NTP	Resolution	Symmetry Factor	Warning
1	Unknown	6	20.200	3417	31	0.024	0.018	N/A	76	0.319	0.505	
2	Unknown	6	22.003	14018449	172317	99.976	99.982	N/A	1850	N/A	1.689	

Chromatogram

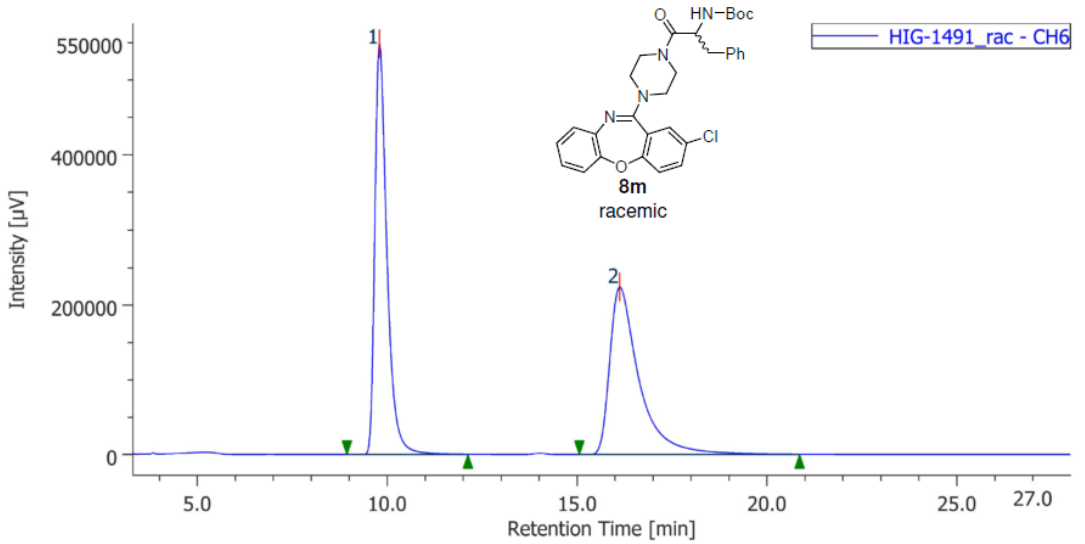

#	Peak Name	CH	tR [min]	Area [μV·sec]	Height [μV]	Area%	Height%	Quantity	NTP	Resolution	Symmetry Factor	Warning
1	Unknown	6	9.793	12182544	547978	50.210	70.946	N/A	5001	6.970	1.562	
2	Unknown	6	16.120	12080551	224408	49.790	29.054	N/A	2593	N/A	1.972	

Chromatogram

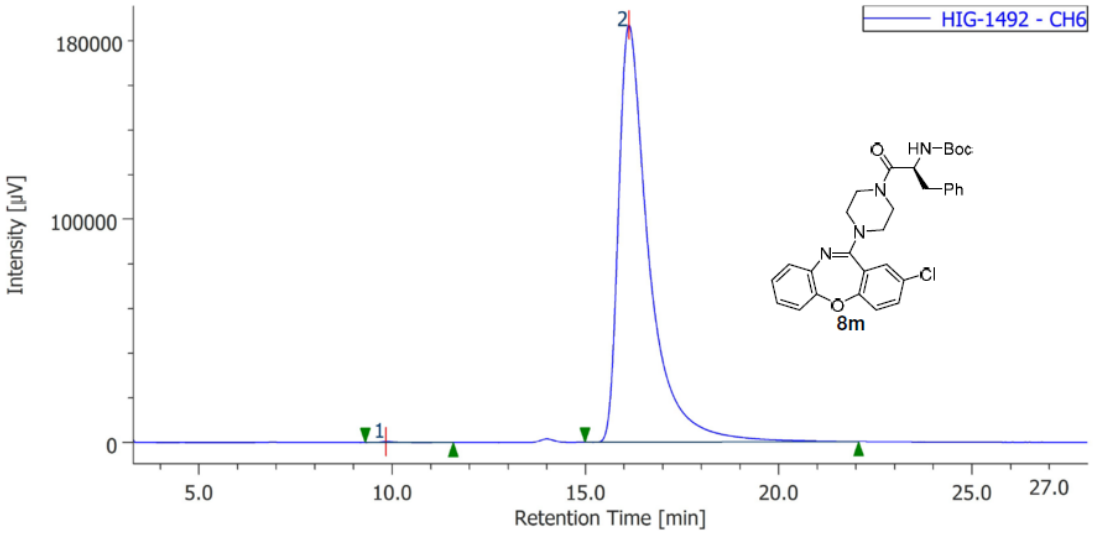

#	Peak Name	CH	tR [min]	Area [μV·sec]	Height [μV]	Area%	Height%	Quantity	NTP	Resolution	Symmetry Factor	Warning
1	Unknown	6	9.840	9865	470	0.096	0.251	N/A	5441	6.930	1.373	
2	Unknown	6	16.123	10260070	186837	99.904	99.749	N/A	2520	N/A	1.980	

Chromatogram

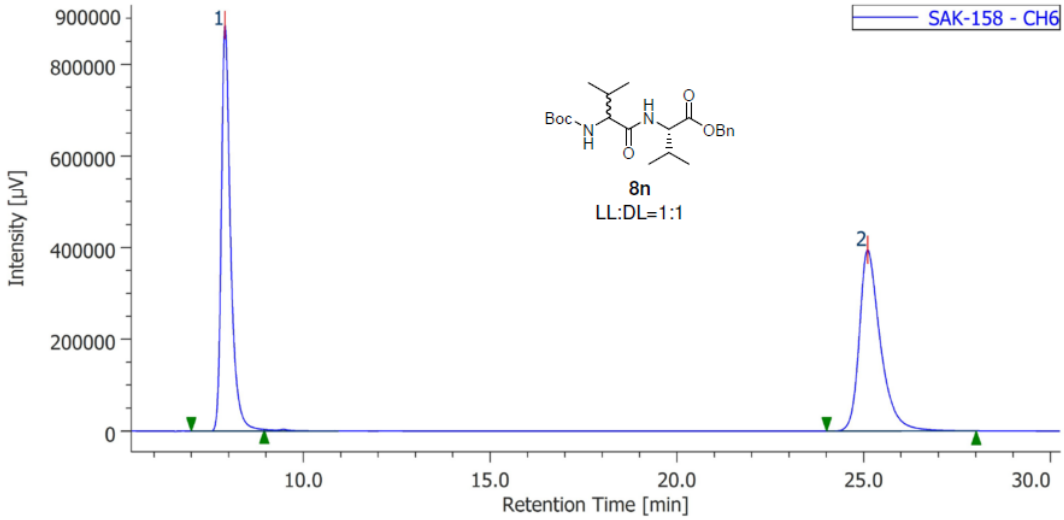

#	Peak Name	CH	tR [min]	Area [μV·sec]	Height [μV]	Area%	Height%	Quantity	NTP	Resolution	Symmetry Factor	Warning
1	Unknown	6	7.903	15308040	884449	49.712	69.146	N/A	5657	24.950	1.466	
2	Unknown	6	25.100	15485188	394659	50.288	30.854	N/A	10897	N/A	1.417	

Chromatogram

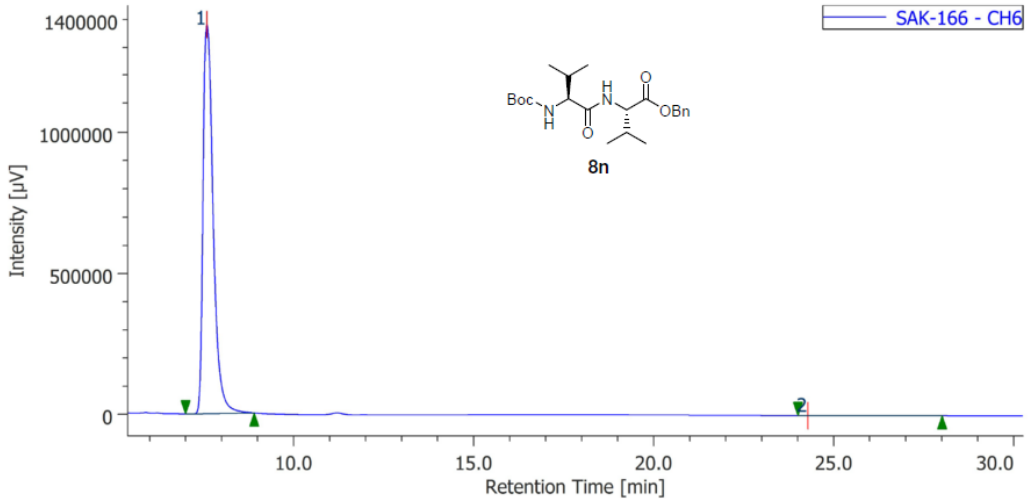

#	Peak Name	CH	tR [min]	Area [μV·sec]	Height [μV]	Area%	Height%	Quantity	NTP	Resolution	Symmetry Factor	Warning
1	Unknown	6	7.593	27063246	1378601	99.960	99.997	N/A	3740	4.960	1.584	
2	Unknown	6	24.280	10844	48	0.040	0.003	N/A	241	N/A	7.223	

2.5 References

[1] a) K. Sharma, K. K. Sharma, A. Sharma, R. Jain, *Drug Discov. Today* **2023**, *28*, 103464; b) L. Wang, N. Wang, W. Zhang, X. Cheng, Z. Yan, G. Shao, X. Wang, R. Wang, C. Fu, *Signal Transduct. Target. Ther.* **2022**, *7*, 48; c) M. Muttenthaler, G. F. King, D. J. Adams, P. F. Alewood, *Nat. Rev. Drug Discov.* **2021**, *20*, 309–325; d) A. C.-L. Lee, J. L. Harris, K. K. Khanna, J.-H. Hong, Int. J. Mol. Sci. 2019, 20, 2383; e) P. Vlieghe, V. Lisowski, J. Martinez, M. Khrestchatisky, *Drug Discov. Today* **2010**, *15*, 40–56.

[2] a) Y. Ruan, M. Sohail, J. Zhao, F. Hu, Y. Li, P. Wang, L. Zhang, *ACS Biomater. Sci. Eng.* **2022**, *8*, 4738–4750; b) S. Mondal, S. Das, A. K. Nandi, *Soft Matter* **2020**, *16*, 1404–1454; c) J. Li, R. Xing, S. Bai, X. Yan, *Soft Matter* **2019**, *15*, 1704–1715; d) R. de la Rica, H. Matsui, Chem. Soc. Rev. 2010, 39, 3499–3509; e) B. J. Pepe-Mooney, R. Fairman, *Curr. Opin. Struct. Biol.* **2009**, *19*, 483–494.

[3] a) J. Yang, H. Huang, J. Zhao, *Org. Chem. Front.* **2023**, *10*, 1817–1846; b) K. Hollanders, B. U. W. Maes, S. Ballet, *Synthesis* **2019**, *51*, 2261–2277; c) A. El-Faham, F. Albericio, *Chem. Rev.* **2011**, *111*, 6557–6602; d) E. Valeur, M. Bradley, *Chem. Soc. Rev.* **2009**, *38*, 606–631; e) C. A. G. N. Montalbetti, V. Falque, *Tetrahedron* **2005**, *61*, 10827–10852; f) S.-Y. Han, Y.-A. Kim, *Tetrahedron* **2004**, *60*, 2447–2467; g) Z. J. Kamiński, *Int. J. Peptide Protein Res.* **1994**, *43*, 312–319.

[4] Z. Wang, X. Wang, P. Wang, J. Zhao, *J. Am. Chem. Soc.* **2021**, *143*, 10374–10381.

[5] a) R. B. Woodward, R. A. Olofson, *J. Am. Chem. Soc.* **1961**, *83*, 1007–1009; b) R. B. Woodward, R. A. Olofson, H. Mayer, *J. Am. Chem. Soc.* **1961**, *83*, 1010–1012; c) R. B. Woodward, R. A. Olofson, H. Mayer, *Tetrahedron* **1966**, *22*, 321–346; d) R. B. Woodward, D. J. Woodman, *J. Am. Chem. Soc.* **1968**, *90*, 1371–1372; e) D. J. Woodman, A. I. Davidson, *J. Org. Chem*. **1970**, *35*, 83–87.

[6] a) H.-J. Gais, *Angew. Chem.* **1978**, *90*, 625–626; Related push-pull-acetylenes were also utilized for peptide synthesis; b) H. P. Fahrni, U. Lienhard, M. Neuenschwander, *Org. Synth.* **1985**, *63*, 175; c) U. Lienhard, H.-P. Fahrni, M. Neuenschwander, *Helv. Chim. Acta.* **1978**, *61*, 1609–1621; d) M. Neuenschwander, H.-P. Fahrni, U. Lienhard, *Helv. Chim. Acta.* **1978**, *61*, 2437–2451.

[7] a) B. Iorga, J.-M. Campagne, *Synlett* **2004**, 1826–1828; Related amide-bond formation through activated α-carbonyl enol ester intermediates was also reported; b) X. Xu, H. Feng, L. Huang, X. Liu, *J. Org. Chem.* **2018**, *83*, 7962–7969.

[8] a) J. Francos, V. Cadierno, *Catalysts* **2017**, *7*, 328; b) V. Cadierno, *Catalysts* **2020**, *10*, 1206; c) C. H. Leung, M. Baron, A. Biffis, *Catalysts* **2020**, *10*, 1210.

[9] a) V. K. Rawat, K. Higashida, M. Sawamura, *ACS Catal.* **2022**, *12*, 8325–8330; b) M. Sato, V. K. Rawat, K. Higashida, M. Sawamura, *Chem. Eur. J.* **2023**, *29*, e202301917.

[10] Examples of catalytic hydrocarboxylation of carbonyl-substituted alkynes; a) R. E. Ireland, D. M. Obrecht, *Helv. Chim. Acta.* **1986**, *69*, 1273–1286; b) X. Lu, G. Zhu, S. Ma, *Tetrahedron Lett.* **1992**, *33*, 7205–7206; c) N. Menashe, Y. Shvo, *J. Org. Chem.* **1993**, *58*, 7434–7439; d) T. Wakabayashi, Y. Ishii, T. Murata, Y. Mizobe, M. Hidai, *Tetrahedron Lett.* **1995**, *36*, 5585–5588; e) M.-J. Fan, G.-Q. Li, Y.-M. Liang, *Tetrahedron* **2006**, *62*, 6782–6791; f) B. C. Chary, S. Kim, *J. Org. Chem.* **2010**, *75*, 7928–7931; g) S. Dupuy, D. Gasperini, S. P. Nolan, *ACS Catal.* **2015**, *5*, 6918–6921; h) J.-F. Chen, C. Li, *Org. Lett.* **2018**, *20*, 6719–6724.

[11] Simple enol esters prepared by ruthenium- or gold-catalyzed hydrocarboxylation of alkynes were also utilized for amide-bond formation, a) Z. Kabouche, C. Bruneau, P. H. Dixneuf, *Tetrahedron Lett.* **1991**, *32*, 5359–5362; b) Y. Wang, Z. Wang, Y. Li, G. Wu, Z. Cao, L. Zhang, *Nat. Commun.* **2014**, *5*, 3470; c) T. Krause, S. Baader, B. Erb, L. J. Gooβen, *Nat. Commun.* **2016**, *7*, 11732.

[12] Methyl 2-octynoate (CAS: 111-12-6; 5,600 JPY/25 mL) was purchased from Tokyo Chemical Industry Co., Ltd. (TCI) and used as received.

[13] Hydrocarboxylation was also tried with alkynyl ketones and an alkynyl amide, but the corresponding α-carbonyl enol esters were not obtained. See Experimental Section.

[14] A. M. Api, D. Belsito, S. Biserta, D. Botelho, M. Bruze, G. A. Burton Jr., J. Buschmann, M. A. Cancellieri, M. L. Dagli, M. Date, W. Dekant, C. Deodhar, A. D. Fryer, S. Gadhia, L. Jones, K. Joshi, A. Lapczynski, M. Lavelle, D. C. Liebler, M. Na, D. O'Brien, A. Patel, T. M. Penning, G. Ritacco, F. Rodriguez-Ropero, J. Romine, N. Sadekar, D. Salvito, T. W. Schultz, F. Siddiqi, I. G. Sipes, G. Sullivan, Y. Thakkar, Y. Tokura, S. Tsang, *Food Chem. Toxicol.* **2019**, *134*, 110825.

[15] Suitability of solvent-free conditions was also described in the Nolan's report (ref 10g) on the acid-base di-NHC-gold(I) bimetallic cooperative catalysts for alkyne hydrocarboxylation.

[16] Silver-catalyzed hydrocarboxylation of alkynes was reported; N. Kikui, T. Hinoue, Y. Usuki, T. Satoh, *Chem. Lett.* **2018**, *47*, 141–143.

[17] Gold-catalyzed nucleophilic addition of benzoic acid toward methyl 2-octynoate (1) was reported with $(Ph_3P)AuCl$ (5 mol%) and AgOAc (5 mol%) in water; P. J. González-Liste, S. E. García-Garrido, V. Cadierno, *Org. Biomol. Chem.* **2017**, *15*, 1670–1679.

[18] a) D. Prat, A. Wells, J. Hayler, H. Sneddon, C. R. McElroy, S. Abou-Shehada, P. J. Dunn, *Green Chem.* **2016**, *18*, 288–296; b) D. Prat, J. Hayler, A. Wells, *Green Chem.* **2014**, *16*, 4546–4551.

[19] C. U. Kim, W. Lew, M. A. Williams, H. Liu, L. Zhang, S. Swaminathan, N. Bischofberger, M. S. Chen, D. B. Mendel, C. Y. Tai, W. G. Laver, R. C. Stevens, *J. Am. Chem. Soc.* **1997**, *119*, 681–690.

[20] T. A. Ban, M. Fujimori, W. M. Petrie, M. Ragheb, W. H. Wilson, *Int. Pharmacopsychiatry* **1982**, *17*, 18–27.

[21] Computational details are given in Experimental Section. Structures and relative free energies for other possible transition states in amide-bond formation step were also described in Figure 2.4.

[22] Vong, K. K. H.; Maeda, S.; Tanaka, K. *Chem. Eur. J.* **2016**, *22*, 18865–18872.

[23] Suárez-Picado, E.; Quiñoá, E.; Riguera, R.; Freire, F. *Angew. Chem., Int. Ed.* **2020**, *59*, 4537–4543.

[24] Morisset, E.; Chardon, A.; Rouden, J.; Blanchet, J. *Eur. J. Org. Chem.* **2020**, *2020*, 388–392.

[25] Wu, W.; Zhang, Z.; Liebeskind, L. S. *J. Am. Chem. Soc.* **2011**, *133*, 14256–14259.

[26] Su, J.; Mo, J.-N.; Chen, X.; Umanzor, A.; Zhang, Z.; Houk, K. N.; Zhao, J. *Angew. Chem., Int. Ed.* **2022**, *61*, e202112668.

[27] Hardee, D. J.; Kovalchuke, L.; Lambert, T. H. *J. Am. Chem. Soc.* **2010**, *132*, 5002–5003.

[28] Marciniak, M.; Mróz, P.; Napolitano, V.; Kalel, V. C.; Fino, R.; Pykacz, E.; Schliebs, W.; Plettenburg, O.; Erdmann, R.; Sattler, M.; Popowicz, G. M.; Dawidowski, M. *Eur. J. Med. Chem.* **2023**, *258*, 115587.

[29] Crich, D.; Sana, K.; Guo, S. *Org. Lett.* **2007**, *9*, 4423–4426.

[30] Thaqi, A.; McCluskey, A.; Scott, J. L. *Tetrahedron Lett.* **2008**, *49*, 6962–6964.

[31] Gaussian 16, Revision C.01, M. J. Frisch, G. W. Trucks, H. B. Schlegel, G. E. Scuseria, M. A. Robb, J. R. Cheeseman, G. Scalmani, V. Barone, G. A. Petersson, H. Nakatsuji, X. Li, M. Caricato, A. V. Marenich, J. Bloino, B. G. Janesko, R. Gomperts, B. Mennucci, H. P. Hratchian, J. V. Ortiz, A. F. Izmaylov, J. L. Sonnenberg, D. Williams-Young, F. Ding, F. Lipparini, F. Egidi, J. Goings, B. Peng, A. Petrone, T. Henderson, D. Ranasinghe, V. G. Zakrzewski, J. Gao, N. Rega, G. Zheng, W. Liang, M. Hada, M. Ehara, K. Toyota, R. Fukuda, J. Hasegawa, M. Ishida, T. Nakajima, Y. Honda, O. Kitao, H. Nakai, T. Vreven, K. Throssell, J. A. Montgomery, Jr., J. E. Peralta, F. Ogliaro, M. J. Bearpark, J. J. Heyd, E. N. Brothers, K. N. Kudin, V. N. Staroverov, T. A. Keith, R. Kobayashi, J. Normand, K. Raghavachari, A. P. Rendell,

J. C. Burant, S. S. Iyengar, J. Tomasi, M. Cossi, J. M. Millam, M. Klene, C. Adamo, R. Cammi, J. W. Ochterski, R. L. Martin, K. Morokuma, O. Farkas, J. B. Foresman, and D. J. Fox, Gaussian, Inc., Wallingford CT, 2019.

[32] Global Reaction Route Mapping (GRRM) Program Version 20, Produced by Satoshi Maeda, Yu Harabuchi, Yosuke Sumiya, Makito Takagi, Kimichi Suzuki, Kanami Sugiyama, Yuriko Ono, Miho Hatanaka, Yuto Osada, Tetsuya Taketsugu, Keiji Morokuma, Koichi Ohno.

[33] CYLview20; C. Y. Legault, Université de Sherbrooke, **2020**. (http://www.cylview.org)

Chapter 2

Gold-Zinc Cooperative Catalysis for Seven-*exo-dig* Hydrocarboxylation of Internal Alkynes

3.1 Introduction

Hydrocarboxylative *exo* cyclization of alkyne-tethered carboxylic acids is a direct method for preparing synthetically important *exo*-alkylidene lactones.[1] Various late transition metals, especially gold, provide effective catalysts owing their strong π-acidity to activate alkynes.[2] While cyclizations leading to five- and six-membered ring *exo*-alkylidene lactones have been well-developed,[3] the formation of lactones with ring sizes larger than six remains challenging.[4] While there have been several seven-membered-ring-forming cyclizations of alkyne-tethered carboxylic acids,[5, 6-10, 11, 12] their scopes were mostly limited to those with terminal alkynes, which produce *exo*-methylidene ε-lactones. Kundu[7] and Porcel[6] individually reported 7-*exo-dig* hydrocarboxylation of internal alkynes with copper(I) catalysts and silver(I)/gold(I) catalysts, respectively. In these reactions, the only competent substrates were alkyne-tethered benzoic acid derivatives, which produced benzofused lactones. Nolan and co-workers reported that a dinuclear hydroxy-bridged gold(I) complex served as a catalyst for seven-*exo-dig* hydrocarboxylation of hept-6-ynoic acid derivatives, which are more conformationally flexible than the benzoic acid derivatives, but the scope of the internal alkynes was limited to only 7-bromohept-6-ynoic acid.[5c] Thus, the synthesis of lactones with ring sizes larger than six through hydrocarboxylation of nonactivated internal alkynes with flexible linker chains remains a formidable challenge (Figure 3.1a), demanding the design of a novel catalytic system.

Recently, Higashida and Sawamura reported the development of gold-zinc cooperative catalysts with an imidazo[1,5-*a*]pyridinylidene ligand bearing a bipyridine coordination site to bind a zinc salt at the C5-position, and their application to the intermolecular nucleophilic addition of carboxylic acids toward nonactivated internal alkynes (Figure 3.1b).[13] In this system, a proximity effect of gold and zinc sites was essential for their high catalytic performance, in which the carboxylic acid was activated through deprotonation by the basic zinc site for attacking the alkyne activated by the cationic gold(I) site. Based on this result, the author envisioned that the gold-zinc cooperative system might realize the unmet intramolecular hydrocarboxylation of internal alkynes, directing the internal alkyne moiety and the carboxylic acid moiety within a molecule in mutual proximity (Figure 3.1c). In addition, the author expected that introduction of a bulky *N*-substituent (**R**) would produce a concave catalytic pocket favorable for inducing a bent conformation of the flexible substrate to facilitate the desired hydrocarboxylative cyclization.[14]

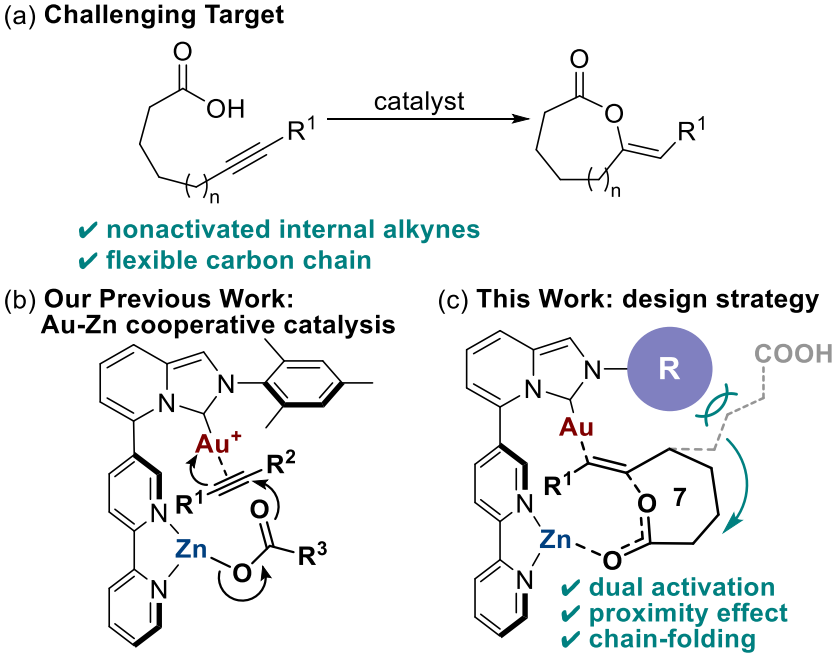

Figure 3.1. *Exo-dig* hydrocarboxylation of internal alkynes.

Here, the author report that the gold-zinc cooperative catalysts prepared based on this concept show remarkable activity for 7-*exo-dig* hydrocarboxylative cyclizations of linear internal alkynes affording ε-*exo*-alkylidene ε-lactones.

3.2 Results and Discussion

The author commenced the catalyst development by examining various groups as *N*-substituents (**R**) for the imidazo[1,5-*a*]pyridinylidene ligand of gold complex **1** (Table 3.1). When 7-phenylhept-6-ynoic acid (**2a**, 0.1 mmol) was subjected to the conditions using gold complex **1a**, $Zn(acac)_2$, and sodium tetrakis[3,5-bis(trifluoromethyl)phenyl]borate ($NaBAr^F$) in 1,2-dichloroethane (DCE) (0.1 M) at 80 °C for 16 h, the desired seven-membered ring lactone **3a** was obtained in 20 % yield. Along with **3a**, byproducts giving multiple $C(sp^2)$–H ^{1}H NMR signals were observed in the crude mixture. These byproducts were identified as oligomeric mixtures of **2a** generated through intermolecular hydrocarboxylations.[15] The selectivity for the 7-*exo-dig* reaction over total hydrocarboxylation defined as $\%_{\mathbf{3a}}$ was calculated to be 69 %. As expected, the use of **1b** with the bulky 2,6-diisopropylphenyl group markedly improved the yield (72 %) of the ε-lactone (**3a**) as the product of simple intramolecular hydrocarboxylation with a higher selectivity (77 $\%_{\mathbf{3a}}$) than that of **1a** (69 $\%_{\mathbf{3a}}$). Gold

catalyst **1c** with the bulkier 2,4,6-tricyclohexyl group showed catalytic activity similar to that of **1b**, affording **3a** in 71 % yield with 78 %$_{\mathbf{3a}}$ selectivity. The amount of byproducts was significantly reduced by using **1d** with an even bulkier aromatic substituent, 2,6-dibenzhydryl-4-methylphenyl group, to give the desired product **3a** in 74 % yield (88 %$_{\mathbf{3a}}$). However, **1e** bearing bis(3,5-dimethylphenyl)methyl groups at the *ortho*-positions of the aromatic substituent on the NHC ligand led to decreased yield of **3a** with an increased proportion of the byproducts (78 %$_{\mathbf{3a}}$). Additionally, a 3,5-di-*tert*-butylphenyl group as the *N*-substituent **R** of **1f** was not effective for the seven-membered ring cyclization, giving **3a** in 33 % yield with poor product selectivity (55 %$_{\mathbf{3a}}$). Effects of *N*-alkyl substituents for gold complex **1** were also examined. When **1g** with an *N*-cyclohexyl group was utilized for the 7-*exo-dig* hydrocarboxylation, the yield of **3a** was significantly decreased (7 %) (entry 7). A large quantity of byproducts was formed with 1 h bearing a 1-adamantyl group as a bulky substituent (33 %$_{\mathbf{3a}}$), indicating that bulky *N*-alkyl substituents are unsuitable for facilitating the 7-*exo-dig* cyclization. Hence, **1d** bearing a 2,6-diphenylmethyl-4-methylphenyl group was selected for further study. The molecular structure of **1d** was confirmed by single crystal XRD analysis (Figure 3.2).[21]

Table 3.1. Screening of gold catalysts.[a]

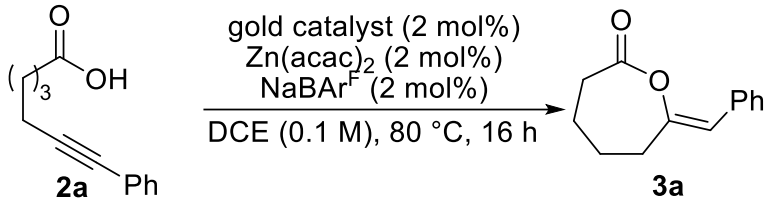

2a **3a**

entry	gold catalyst	yield of **3a** [%][b]	byproducts [%][b]	selectivity [%$_{3a}$][c]
1	**1a**	20	9	69
2	**1b**	72	22	77
3	**1c**	71	20	78
4	**1d**	74	10	88
5	**1e**	42	12	78
6	**1f**	33	27	55
7	**1g**	7	6	54
8	**1h**	31	63	33

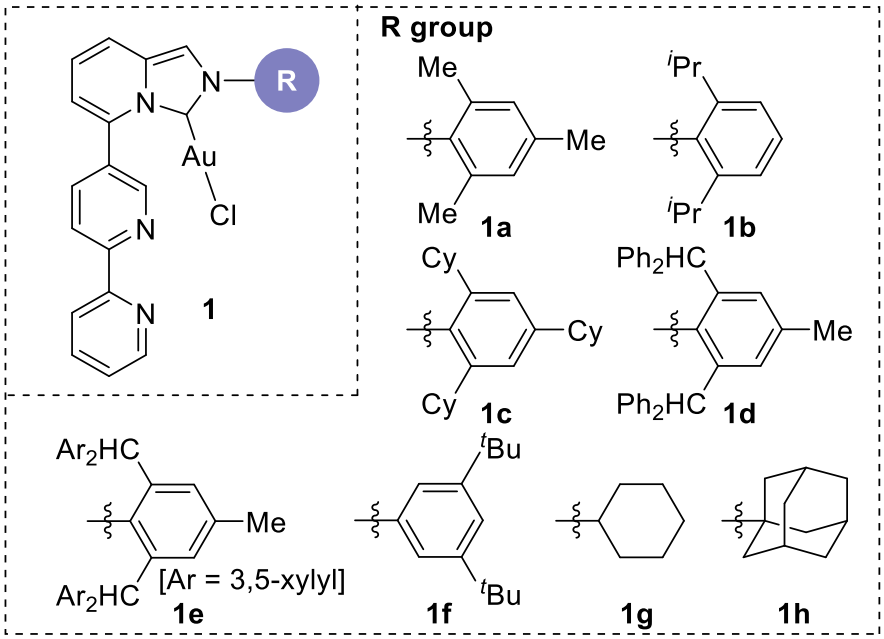

[a] Gold catalyst **1** (2 mol%), $Zn(acac)_2$ (2 mol%), $NaBAr^F$ (2 mol%), and **2a** (0.10 mmol) in DCE (1.0 mL, 0.1 M). [b] Determined by ^1H NMR analysis using phenanthrene as an internal standard. [c] Percentage of **3a** (%$_{3a}$) was calculated by dividing the yield of **3a** by the sum of yields of **3a** and byproducts and then multiplying the result by 100.

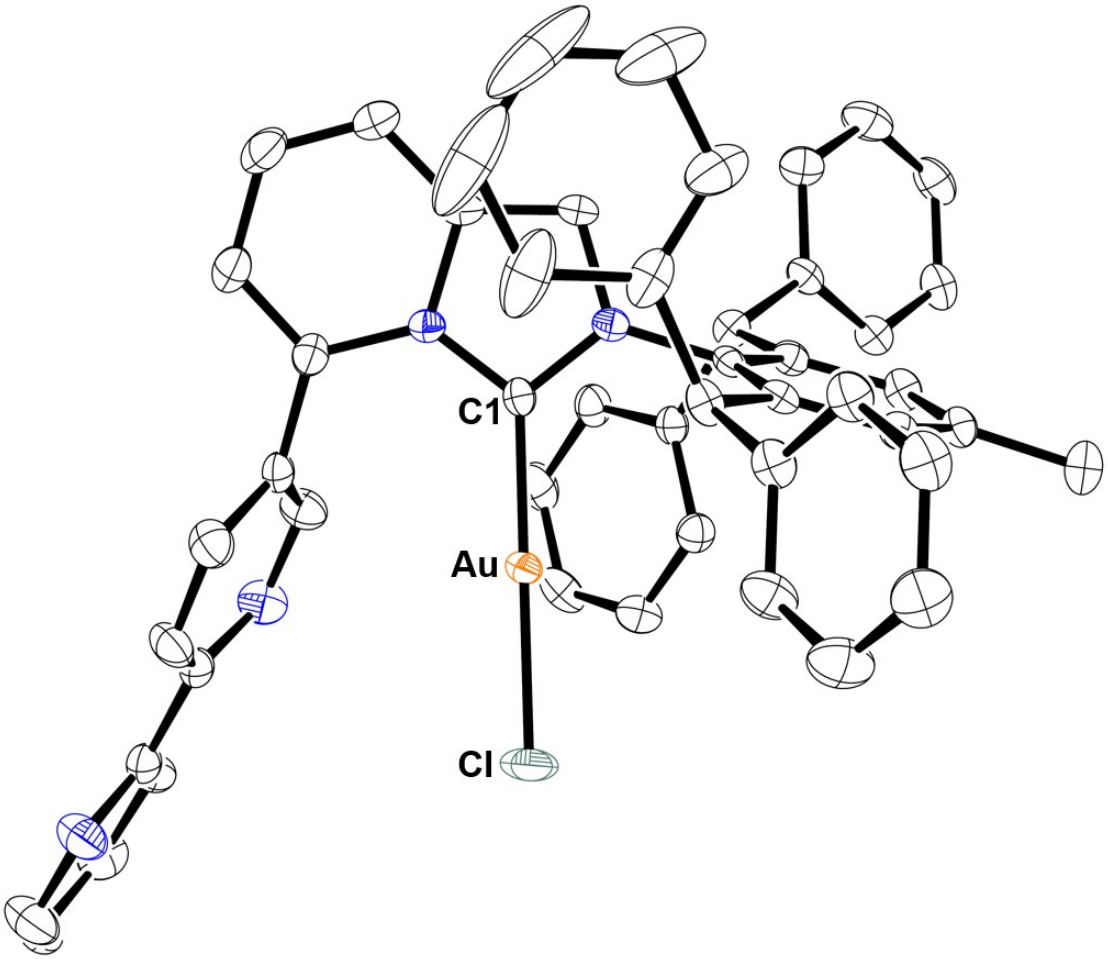

Figure 3.2. ORTEP drawing of **1d** showing 50% probability thermal ellipsoids. All hydrogen atoms and solvent molecules were omitted for clarity.

The effects of counter anions on the zinc salts were then investigated (Table 3.2). When zinc salts including $C_6F_5^-$ (p*K*a of C_6F_5H=23)[16] and 2,2,6,6-tetramethyl-3,5-heptanedionate (tmhd) (p*K*a of tmhdH=11.8),[17] which are more basic than acetylacetonate (p*K*a of acacH=8.9),[17] were utilized for the cyclization with **1d**, yields of **3a** and selectivities ($\%_{\mathbf{3a}}$) were comparable to those with $Zn(acac)_2$ (entries 1–3). $Zn(hfac)_2 \cdot 2H_2O$ including less basic hexafluoroacetylacetonate (hfac) (p*K*a of hfacH=4.4)[18] significantly increased the catalytic efficacy of **1d** to afford **3a** in 92 % yield with a low proportion of byproducts (92 $\%_{\mathbf{3a}}$) (entry 4). In contrast, neutral zinc salts such as $ZnCl_2$ (p*K*a of HCl=−7)[19] and $Zn(OTf)_2$ (p*K*a of TfOH=−12)[19] led to decreased yields of **3a** (entries 5 and 6). Gold complex **1d** showed almost no catalytic activity in the absence of zinc salt (entry 7). Similarly, NHC-gold(I) complex **1i** bearing a non-coordinative biphenyl substituent at the C5 position instead of a bipyridine moiety gave

only a trace amount of **3a** (entry 8). Addition of 2,2′-bipyridine to the **1i** system as an external ligand failed to recover the catalytic activity (entry 9), indicating that the proximity of the gold and zinc sites is crucial for the catalytic performance. Thus, $Zn(hfac)_2 \cdot 2H_2O$ was selected as the optimized zinc salt. Since the p*K*a values for the conjugated acids of the counter anions for $Zn(C_6F_5)_2$, $Zn(tmhd)_2$, and $Zn(acac)_2$ are much higher than that of the carboxylic acid (ex: p*K*a of valeric acid=4.9),[20] zinc salts might serve as basic sites after conversion into zinc carboxylates through deprotonation of substrate **2a**, resulting in almost equal yields and selectivities. In contrast, hfacH is comparable to the carboxylic acid in acidity. Thus, a hfac molecule may remain bound to the zinc center and participate in the gold-zinc cooperative catalysis (see Experimental Section for titration experiments). Additionally, the poor catalytic activities of $ZnCl_2$ and $Zn(OTf)_2$ may be attributed to the basicities of the chloride and triflate anions being too weak to deprotonate the carboxylic acid.

Table 3.2. Screening of counter anions for zinc salts.[a]

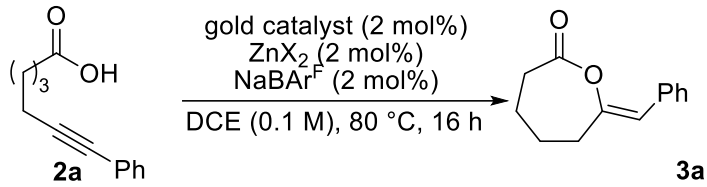

2a **3a**

entry	gold catalyst	ZnX_2	yield of **3a** [%][b]	byproducts [%][b]	selectivity [$\%_{\mathbf{3a}}$][c]
1	**1d**	$Zn(C_6F_5)_2$	71	13	85
2	**1d**	$Zn(tmhd)_2$	70	13	84
3	**1d**	$Zn(acac)_2$	74	10	88
4	**1d**	$Zn(hfac)_2{\cdot}2H_2O$	92	8	92
5	**1d**	$ZnCl_2$	5	2	71
6	**1d**	$Zn(OTf)_2$	18	4	82
7	**1d**	none	1	<1	N/A
8	**1i**	$Zn(hfac)_2{\cdot}2H_2O$	<1	1	N/A
9[d]	**1i**	$Zn(hfac)_2{\cdot}2H_2O$	<1	4	N/A
10[d]	**1i**	none	<1	<1	N/A
11[e]	**1d**	$Zn(acac)_2$	63	9	88
12[f]	**1d**	$Zn(hfac)_2{\cdot}2H_2O$	95	5	95

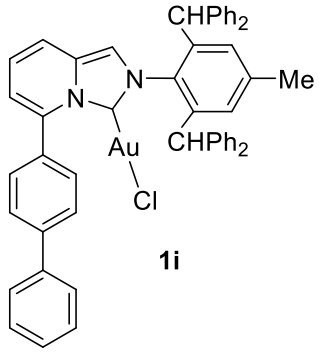

1i

[a] Gold catalyst **1** (2 mol%), zinc salt (2 mol%), $NaBAr^F$ (2 mol%), and **2a** (0.10 mmol) in DCE (1.0 mL, 0.1 M). [b] Determined by ^1H NMR analysis using phenanthrene as an internal standard. [c] Percentage of **3a** ($\%_{\mathbf{3a}}$) was calculated by dividing the yield of **3a** by the sum of yields of **3a** and byproducts and then multiplying the result by 100. [d] 2,2′-Bipyridine (2 mol%) was added. [e] H_2O (30 mol%) was added. [f] 2.0 mL of DCE (0.05 M) was used. $NaBAr^F$=sodium tetrakis[3,5-bis(trifluoromethyl)phenyl]borate, hfac=hexafluoroacetylacetonate, tmhd=2,2,6,6-tetramethyl-3,5-heptanedionate.

The cyclization with **1i** and an external 2,2′-bipyridine in the absence of zinc salts gave almost no reaction (Table 3.2, entry 10). This result indicated that bipyridine could not promote the hydrocarboxylation as a free base deprotonating carboxylic acids. The

addition of 30 mol% of H_2O to the reaction system with $Zn(acac)_2$ resulted in a slightly lower yield of **3 a** (Table 3.2, entries 3 vs 11), indicating that the effect of water molecules in $Zn(hfac)_2 \cdot 2H_2O$ is less important than the counter anion effect. Finally, diluted conditions (0.05 M) improved the selectivity (95 %$_{\mathbf{3a}}$) of the hydrocarboxylation to give **3a** in 95% yield (entry 12). Hence, the optimized catalytic conditions were identified to be the use of **1d**, $Zn(hfac)_2 \cdot 2H_2O$, and $NaBAr^F$ in DCE (0.05 M) at 80 °C for 16 h as in entry 12.

With the optimized conditions in hand, the substrate scope was investigated at the 0.4 mmol scale, as shown in Scheme 3.1. Analytically pure **3a** was obtained in 93% yield through silica gel column chromatography. Alkyne-tethered carboxylic acids with *para*-bromo and *para*-nitro phenyl groups were compatible substrates, giving **3b** and **3c** in 96% and 90% yields, respectively. A *para*-methoxyphenyl substituted internal alkyne as an electron-rich substrate was also compatible in the cyclization to give the desired product **3d** in high yield (91%), although a higher reaction temperature (100 °C) was required for obtaining the maximum yield. The cyclization of 7-(benzo[*d*][1,3]dioxol-5-yl)hept-6-ynoic acid (**2e**) gave the corresponding product **3e** in 93% yield. Whereas low yields were found in the cyclization of 3,5-dichlorophenyl and benzothiophen-3-yl substituted alkynoic acids, the use of **1c** as the gold catalyst promoted these reactions to afford **3f** and **3g** in 87% and 76% yields, respectively. The cyclization of an estrone-substituted substrate was also catalyzed by gold catalyst **1c** to give the corresponding ε-lactone **3h** in 80% yield. The structure of **3h** was unambiguously determined by SC-XRD analysis.[21] Catalytic activity toward alkyl-substituted internal alkynes was also investigated. When 6-octadecynoic acid, a natural product named tariric acid,[22] was subjected to the catalytic conditions, ε-lactone **3i** was obtained in 54% yield along with a mixture of dimeric lactones (20% as a total). A methoxymethyl-substituted alkyne was compatible, giving **3j** in 80% yield. A terminal alkyne was also applicable for the 7-*exo*-*dig* cyclization to afford **3k** in 92% yield. In addition, the hydrocarboxylation was scalable, and the cyclization of **2a** at the 500 mg (2.47 mmol) scale gave **3a** in 93% yield. We also attempted eight-membered ring formation with 8-phenyloct-7-ynoic acid under the optimized conditions, but in vain.

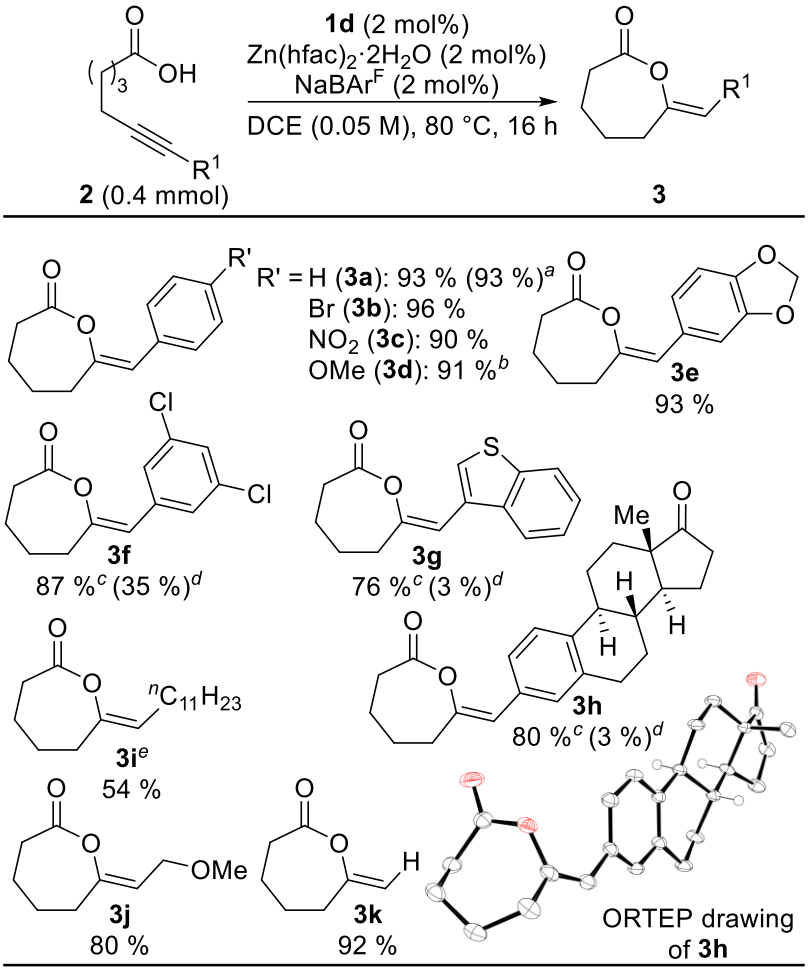

Scheme 3.1. Substrate scope. [a] Yield at the 500 mg (2.47 mmol) scale reaction. [b] Reaction was conducted at 100 °C. [c] **1c** was used instead of **1d**. [d] ^{1}H NMR yield at the 0.1 mmol scale using **1d** as the catalyst. [e] Mixture of 14-, 15-, and 16-membered lactones was also obtained in 20% yield.

Based on the above results, DFT calculations were performed at the M06/SDD,6-311+G(d,p)/SMD(DCE)//M06/SDD,6-31G(d) level of theory with the Gaussian 16 package (Figure 3.3a).[23] Gold-zinc complexes were calculated as monocationic species without the non-coordinated outer-sphere BAr^F anion. The computational study was initiated from a gold(I)-$Zn(hfac)_2$ complex (**Int-1**), and **Int-2** was generated through coordination of the alkyne moiety of **2a** to the cationic gold(I) metal of **Int-1**. From **Int-2**, deprotonation of the carboxylic acid by the hfac anion on the zinc metal gave zinc carboxylate intermediate **Int-3** and hfacH as a 5.0 kcal/mol endergonic process. This energetically unfavorable nature for the deprotonation is in accord with the experimental observations from ^{1}H NMR titration. Nucleophilic *anti*-addition of the carboxylate to the

alkyne moiety in a 7-*exo-dig* mode proceeds via **TS$_{3\text{-}4}$** to form a seven-membered ring lactone (**Int-4**). This step has a 16.9 kcal/mol Gibbs free energy barrier, and the actual energy barrier from **Int-2** is 21.9 kcal/mol. The 3D-molecular structure of **TS$_{3\text{-}4}$** is shown in Figure 3.3b. A phenyl ring (**Ph1**) at the dibenzhydryl group constructs a concave catalytic pocket around the gold atom, which may induce chain-folding of substrate **2a**. After coordination of another molecule of carboxylic acid **2a** to the zinc metal of **Int-4** to produce **Int-5**, protonation of the Au−C bond occurs through **TS$_{5\text{-}6}$** with a small energy barrier (2.3 kcal/mol) as an exergonic process to give **Int-6**, which contains **3a** bound to the cationic gold atom.

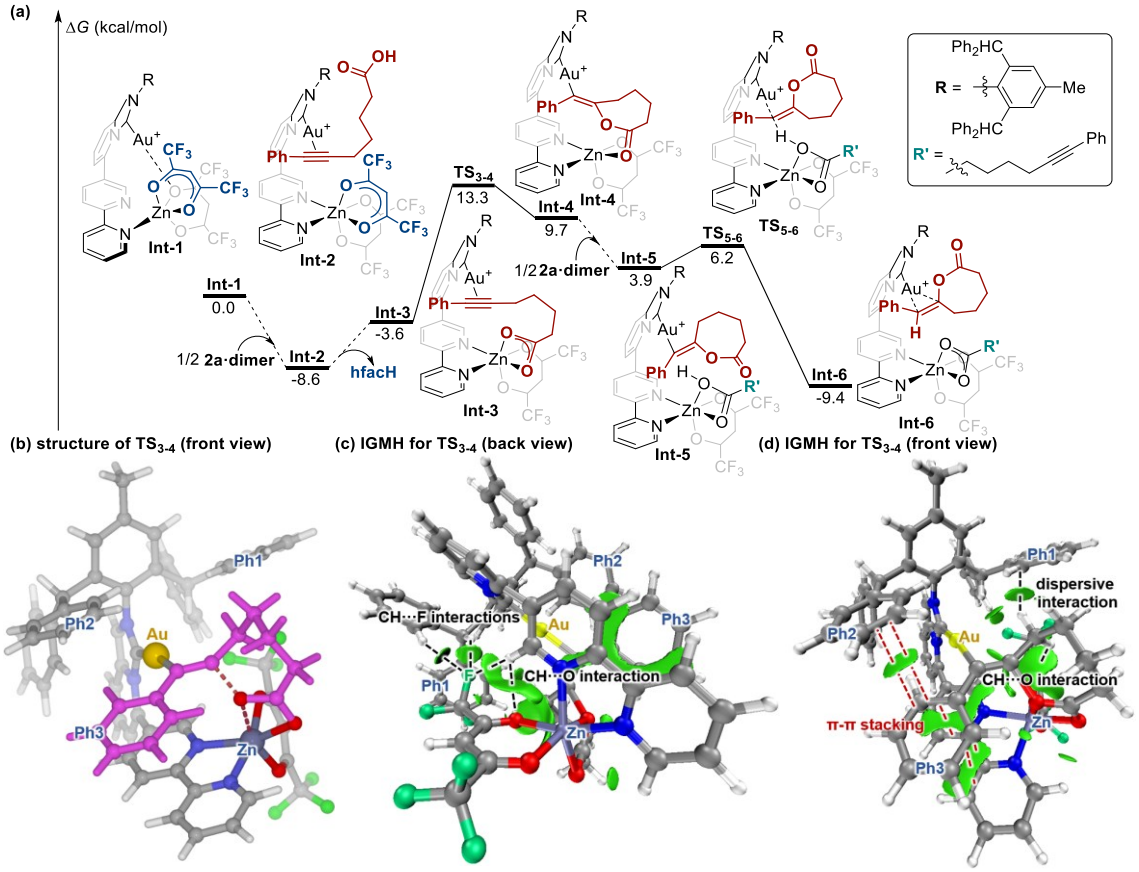

Figure 3.3. (a) Energy diagram for seven-membered cyclization. The relative energies were corrected for Gibbs free energy and reported in kcal/mol. (b) 3D-structure of **TS$_{3\text{-}4}$**. (c), (d) IGMH for **TS$_{3\text{-}4}$** mapped with colored isosurfaces of the δg^{inter}=0.006 a.u. The color scale of mapped function sign(λ_2)ρ is −0.05 < sign(λ_2)ρ < 0.05.

To gain further mechanistic insights, noncovalent interactions for **TS$_{3\text{-}4}$** were investigated by the independent gradient model based on the Hirshfeld partition (IGMH) method[24] using the Multiwfn program.[25] As a feature of **TS$_{3\text{-}4}$**, a fluorine atom of the

hfac ligand at the zinc metal undergoes multiple C(sp^2)–H···F and C(sp^3)–H···F interactions with the dibenzhydryl and bipyridine moieties (Figure 3.3c). These interactions may contribute to the formation of a well-defined catalytic environment suitable for reducing undesired intermolecular side-reactions. Folding of **2a** might be induced through interactions of the flexible carbon chain of **2a** with the phenyl ring (**Ph1**) of the dibenzhydryl group and hfac oxyanion at the zinc metal (Figure 3.3d) to facilitate seven-membered ring formation. The substrate **2a** was captured by the catalytic molecule through two π-π stacking interactions among a phenyl ring (**Ph2**) of the dibenzhydryl group, a phenyl ring (**Ph3**) of **2a**, and the bipyridine moiety, which might contribute to the substrate molecule approaching the gold-zinc cooperative catalytic site.

3.3 Conclusions

The author developed gold-zinc cooperative catalytic systems for 7-*exo*-*dig* hydrocarboxylations of nonactivated internal alkynes containing conformationally flexible linker chains to produce ε-*exo*-alkylidene ε-lactones. The cooperative catalysts were designed based on three strategies: 1) dual activation of the alkyne with a cationic gold atom and of the carboxylic acid with a basic zinc salt, 2) proximity effect of the gold and zinc catalytic sites to promote nucleophilic attack of the carboxylic acid toward the alkyne, and 3) a folding effect for the flexible carbon-linker of the substrate with a bulky *N*-substituent of the NHC ligand to facilitate cyclization. Consequently, the gold complex **1d** with a 2,6-dibenzhydryl-4-methylphenyl group as an *N*-substituent served as an effective catalyst for seven-membered ring formation, in which the use of $Zn(hfac)_2 \cdot 2H_2O$ as the basic zinc site led to high catalytic performance of gold complex **1d**. Computational studies suggested that a phenyl ring of the dibenzhydryl group of **1d** participated in producing a concave catalytic pocket around the gold atom to induce a folded conformation of the flexible substrate.

3.4 Experimental Section

3.4.1 General Remarks

All air and moisture-sensitive reactions were operated using the standard Schlenk techniques and glove box under nitrogen gas atmosphere. THF and DCM were dried and deoxygenated by using Grubbs column (Glass Counter Solvent Dispensing System,

Nikko Hansen & Co, Ltd.). Anhydrous 1,2-dichloroethane (DCE) was purchased from Sigma-Aldrich Co. LLC and Kanto Chemical Co., Inc.. Dry CH_3CN was purchased from Kanto Chemical Co., Inc.. Sodium tetrakis[3,5-bis(trifluoromethyl)phenyl]borate ($NaBAr^F$), $Zn(hfac)_2 \cdot 2H_2O$, $Zn(OTf)_2$, $Zn(C_6F_5)_2$, and $ZnCl_2$ were purchased from Sigma-Aldrich Co. LLC.. $Zn(acac)_2$ was purchased from Tokyo Chemical Industry Co., Ltd.. $Zn(tmhd)_2$ was purchased from FUJIFILM Wako Pure Chemical Corporation. 6-Heptynoic acid was purchased from BLD Pharmatech Ltd.. 1H NMR (400 MHz), $^{13}C\{^1H\}$ NMR (100 MHz), and ^{19}F NMR (376 MHz) spectra were measured on JEOL ECZ-400S spectrometer. All ^1H NMR chemical shifts were reported in ppm (δ) relative to the chemical shifts of residual solvent resonances ($CDCl_3$ at δ 7.26, CD_2Cl_2 at δ 5.32, and DMSO-d_6 at δ 2.49). All $^{13}C\{^1H\}$ NMR chemical shifts were reported in ppm (δ) relative to carbon resonances of $CDCl_3$ at δ 77.0, CD_2Cl_2 at δ 53.8, and DMSO-d_6 at δ 39.5. High-resolution mass spectra were obtained with Thermo Fisher Scientific Exactive at the Instrumental Analysis Division, Equipment Management Center, Creative Research Institution, Hokkaido University. IR spectra were obtained on JASCO FT-IR-4600 spectrometer. Melting points were obtained with OptiMelt (MPA100) of Stanford Research Systems. Flash column chromatography was performed using silica gel (Wakogel FC-40, 0.020-0.040 nm >70%) and activated basic alumina (Wako, about 75 μm). Gold catalyzed nucleophilic addition (0.1 mmol scale) was conducted using EYELA RCH-1000 of TOKYO RIKAKIKAI CO, LTD as a heating reactor with a screw-cap vial (NN-13, φ = 13 mm) of Maruemu Corporation. Gold catalyzed nucleophilic addition (0.4 mmol scale) was conducted using oil-bath as a heating reactor with a screw-cap vial (NX-50, φ = 35 mm) of Maruemu Corporation.

3.4.2 Synthesis of Gold Complexes

Synthesis of [2,2':5',2''-Terpyridine]-6''-carbaldehyde

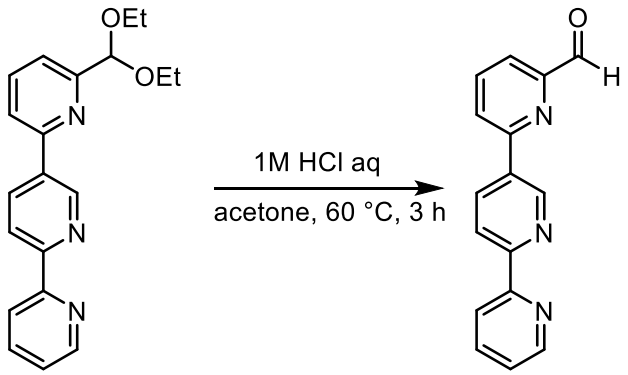

6''-(Diethoxymethyl)-2,2':5',2''-terpyridinen[13] (792 mg, 2.36 mmol, 1 equiv) was

dissolved in acetone (4.7 mL) and 1M HCl aq. (2.4 mL) under nitrogen atmosphere. The resulting solution was stirred at 60 ºC for 3 hours. The reaction mixture was neutralized with saturated $NaHCO_3$ aqueous solution, and the aqueous layer was extracted with DCM. The combined organic layer was dried over Na_2SO_4 and filtrated, and all volatiles were evaporated. The crude mixture was purified by silica-gel flash column chromatography (DCM/MeOH=99/1 to 98/2) to afford the desired product (572 mg, 2.19 mmol, 93% yield).

White solid. mp: 167-170 ºC. IR (ATR, ν/cm^{-1}): 3063 w, 3010 w, 2841 w, 1706 s, 1591 m, 1449 m, 1350 w, 1309 w, 1214 w, 1164 w, 1019 w, 989 w, 787 s. ^{1}H NMR (400 MHz, $CDCl_3$, 25 ºC): δ 10.20 (s, 1H), 9.38 (s, 1H), 8 .73 (dt, J = 4.8, 0.9 Hz, 1H), 8.59-8.56 (m, 2H), 8.49 (dd, J = 8.0, 0.7 Hz, 1H), 8.08-7.96 (m, 3H), 7.86 (td, J = 7.6, 1.4 Hz, 1H), 7.36 (dd, J = 7.3, 4.8 Hz, 1H). ^{13}C{^{1}H} NMR (100 MHz, $CDCl_3$, 25 °C): δ 193.6, 156.8, 155.5, 155.2, 153.0, 149.3, 147.7, 138.1, 137.0, 135.3, 133.4, 124.4, 124.1, 121.4, 121.1, 120.4. HRMS (ESI$^+$) m/z calc. for $C_{16}H_{11}ON_3Na$ 284.0794 found 284.0788.

Synthesis of 5-([2,2'-Bipyridin]-5-yl)-2-(2,6-diisopropylphenyl)imidazo[1,5-*a*]pyridin-2-ium Chloride

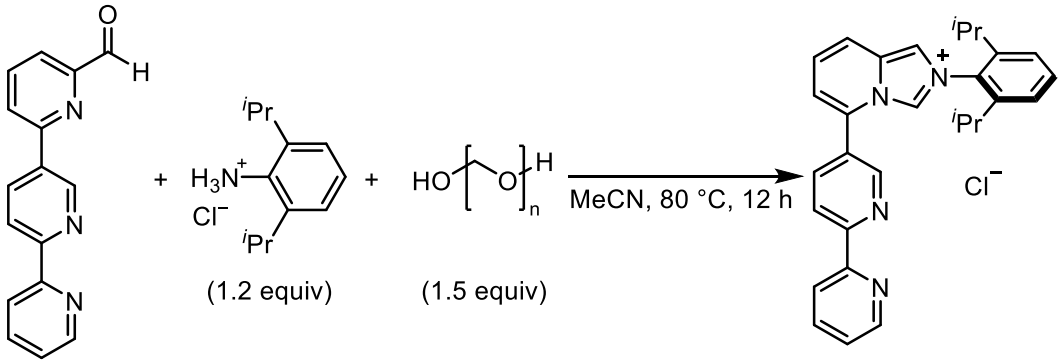

[2,2':5',2"-Terpyridine]-6"-carbaldehyde (131 mg, 0.50 mmol, 1 equiv), 2,6-diisopropylbenzenaminium chloride (128 mg, 0.60 mmol, 1.2 equiv), and paraformaldehyde (22.5 mg, 0.75 mmol, 1.5 equiv) were suspended in acetonitrile (2.5 mL) in a screw-cap vial. After stirring the mixture at 80 ºC for 12 hours, all volatile compounds were removed under reduced pressure. The crude mixture was purified by basic alumina column chromatography (DCM/MeOH=99/1) and silica-gel column chromatography (DCM/MeOH=99/1 to 95/5) to afford the desired product (195 mg, 0.42 mmol, 83% yield).

White solid. mp: 130 ºC (decomp.). IR (ATR, ν/cm^{-1}): 2960 m, 2867 w, 1650 w, 1587 m, 1539 w, 1457 s, 1362 m, 1303 m, 1242 w, 1170 m, 1112 w, 1061 w, 1023 w, 799 s, 751 s, 728 s, 677 m, 619 m, 567 m. ^{1}H NMR (400 MHz, $CDCl_3$, 25 °C): δ 9.05 (d, J =

1.8 Hz, 1H), 8.98 (s, 1H), 8.95 (s, 1H), 8.78 (d, *J* = 9.6 Hz, 1H), 8.75-8.67 (m, 2H), 8.46 (d, *J* = 7.8 Hz, 1H), 8.34 (dd, *J* = 8.2, 2.3 Hz, 1H), 7.89 (t, *J* = 7.8 Hz, 1H), 7.60-7.50 (m, 2H), 7.41 (dd, *J* = 6.4, 6.0 Hz, 1H), 7.35-7.29 (m, 3H), 2.24 (sept., *J* = 6.4 Hz, 2H), 1.23 (d, *J* = 6.9 Hz, 6H), 1.15 (d, *J* = 6.9 Hz, 6H). $^{13}C\{^{1}H\}$ NMR (100 MHz, $CDCl_3$, 25 ºC): δ 158.3, 154.2, 149.2, 148.4, 145.0, 137.6, 137.3, 132.4, 132.2, 131.8, 130.5, 127.0, 126.0, 124.8, 124.7, 122.6, 122.2, 121.9, 121.2, 120.8, 119.6, 28.7, 24.6, 24.4. HRMS (ESI^+) calc. for $C_{29}H_{29}N_4$ 433.2387 found 433.2387.

Synthesis of (5-([2,2'-Bipyridin]-5-yl)-2-(2,6-diisopropylphenyl)imidazo[1,5-*a*]pyridin-3(2*H*)-ylidene)gold(I) Chloride (1b)

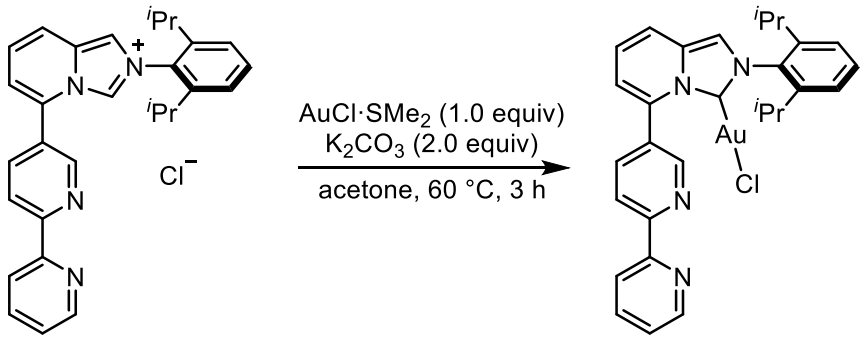

In a nitrogen filled glove box, 5-([2,2'-bipyridin]-5-yl)-2-(2,6-diisopropylphenyl)imidazo[1,5-*a*]pyridin-2-ium chloride (75.0 mg, 0.16 mmol, 1 equiv), $AuCl{\cdot}SMe_2$ (47.2 mg, 0.16 mmol, 1 equiv), dry K_2CO_3 (44.2 mg, 0.32 mmol, 2.0 equiv), and dry acetone (3.0 mL) were filled in a screw vial containing a magnetic stirring bar. The reaction mixture was stirred at 60 ºC for 3 hours under dark conditions. The mixture was then filtered through celite and subsequently eluted with DCM. The filtrate was evaporated and purified by silica-gel flash column chromatography (DCM/EtOAc=95/5 to 85/15) to afford the desired product (86.4 mg, 0.13 mmol, 81% yield).

White solid. mp: 150 ºC (decomp.). IR (ATR, ν/cm^{-1}): 3055 w, 2962 s, 2926 w, 2867 w, 1652 w, 1588 m, 1573 w, 1550 w, 1458 s, 1434 m, 1384 m, 1365 m, 1314 m,1283 w, 1175 m, 1092 w, 1059 w, 1025 w, 992 w, 953 w, 852 w, 789 m, 750 m, 687 w. ^1H NMR (400 MHz, CD_2Cl_2, 25 °C): δ 8.86 (dd, *J* = 2.3, 0.9 Hz, 1H), 8.69 (ddd, *J* = 4.8, 1.8, 0.9 Hz, 1H), 8.58 (dd, *J* = 8.2, 0.7 Hz, 1H), 8.47 (dt, *J* = 8.0, 0.9 Hz, 1H), 8.00 (dd, *J* = 8.2, 2.3 Hz, 1H) , 7.85 (td, *J* = 7.6, 1.8 Hz, 1H), 7.58 (dd, *J* = 9.2, 1.1 Hz, 1H), 7.54 (t, *J* = 7.8 Hz, 1H), 7.46 (s, 1H), 7.35 (ddd, *J* = 7.6, 4.8, 1.1 Hz, 1 H), 7.30 (d, *J* = 8.0 Hz, 2H), 7.13 (dd, *J* = 9.4, 6.6 Hz, 1H), 6.74 (dd, *J* = 6.6, 1.1 Hz, 1H), 2.30-2.18 (m, 2H), 1.24 (d, *J* =7.1 Hz, 6H), 1.13 (d, *J* = 6.9 Hz, 6H). $^{13}C\{^{1}H\}$ NMR (100 MHz, CD_2Cl_2, 25 ºC): δ 165.8, 157.6, 155.9, 149.64, 149.61, 145.7, 138.7, 137.3, 136.7, 135.9, 132.1, 131.03. 130.97,

124.5, 124.4, 123.7, 121.8, 121.2, 118.4, 118.1, 114.7, 28.8, 24.6, 24.3. HRMS (ESI^+) m/z calc. for $C_{29}H_{28}AuClN_4Na$ 687.1560 found 687.1561.

Synthesis of 5-([2,2'-Bipyridin]-5-yl)-2-(2,4,6-tricyclohexylphenyl)imidazo[1,5-*a*]pyridin-2-ium Chloride

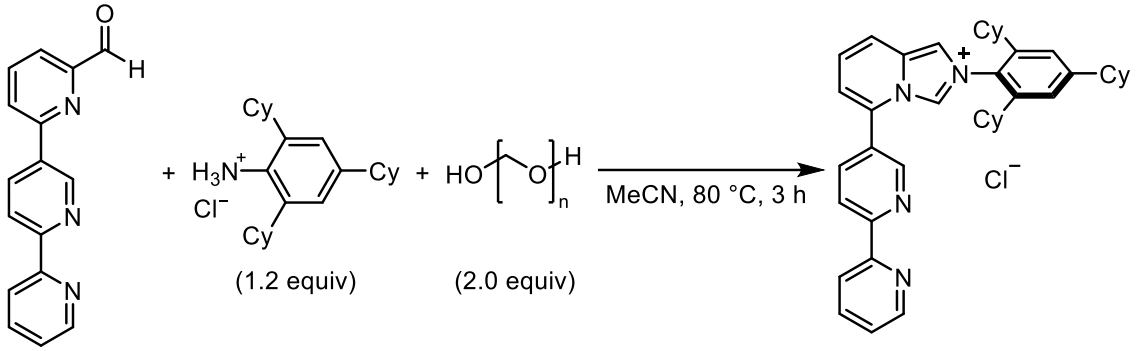

[2,2':5',2"-Terpyridine]-6"-carbaldehyde (311 mg, 1.19 mmol, 1 equiv), 2,4,6-tricyclohexylbenzenaminium chloride[26] (538 mg, 1.43 mmol, 1.2 equiv), and paraformaldehyde (71.5 mg, 2.38 mmol, 2.0 equiv) were suspended in acetonitrile (6.0 mL) in a screw-cap vial. After stirring the mixture at 80 ºC for 3 hours, all volatile compounds were removed under reduced pressure. The crude mixture was purified by basic alumina column chromatography (DCM/MeOH=99/1 to 95/5) and silica-gel column chromatography (DCM/MeOH=99/1 to 80/20). The resulting solid compound was triturated with EtOAc to afford the desired product (550 mg, 0.87 mmol, 73% yield).

White solid. mp: 170 ºC (decomp.). IR (ATR, ν/cm^{-1}): 2925 m, 2850 m, 1651 w, 1589 w, 1541 w, 1448 m, 1371 w, 1307 w, 1238 w, 1174 w, 1149 w, 1121 w, 1025 w, 995 w, 923 m, 863 w, 797 w, 797 w, 638 m, 569 w, 536 w. ^1H NMR (400 MHz, $CDCl_3$, 25 ºC): δ 9.05 (d, *J* = 1.4 Hz, 1H), 8.96-8.90 (m, 2H), 8.72 (d, *J* = 4.6 Hz, 1H), 8.70-8.64 (m, 2H), 8.46 (d, *J* = 8.0 Hz, 1H), 8.20 (dd, *J* = 8.3, 2.1 Hz, 1H), 7.87 (td, *J* = 7.6, 1.6 Hz, 1H), 7.59 (dd, *J* = 9.2, 6.9 Hz, 1H), 7.41 (dd, *J* = 7.6, 4.8 Hz, 1H), 7.34 (d, *J* = 6.8 Hz, 1H), 7.11 (s, 2H), 2.61-2.48 (m, 1H), 1.95-1.03 (m, 32H).$^{13}C\{^1H\}$ NMR (100 MHz, $CDCl_3$, 25 °C): δ 158.6, 154.3, 152.0, 149.4, 148.2, 143.6, 137.3, 136.8, 132.4, 131.5, 128.2, 126.9, 126.1, 124.8, 123.8, 122.4, 121.9, 121.7, 121.50, 121.45, 121.0, 119.74, 119.70, 44.8, 39.5, 35.3, 34.4, 34.2, 26.7, 26.5, 26.3, 25.9, 25.6. HRMS (ESI^+) calc. for $C_{41}H_{47}N_4$ 595.3795 found 595.3793.

Synthesis of (5-([2,2'-Bipyridin]-5-yl)-2-(2,4,6-tricyclohexylphenyl)imidazo[1,5-*a*]pyridin-3(2*H*)-ylidene)gold(I) Chloride (1c)

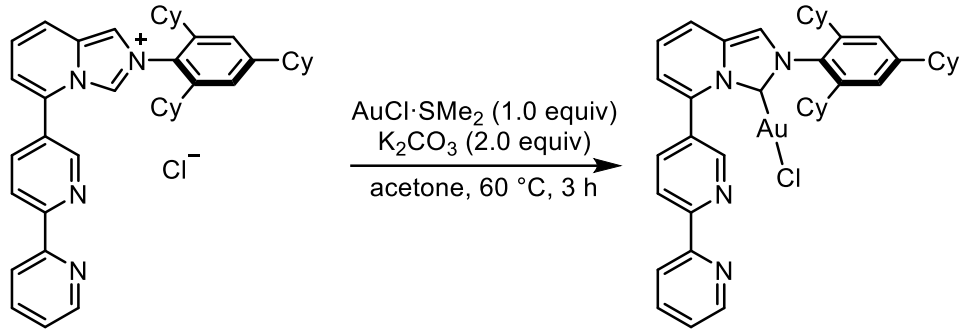

In a nitrogen-filled glove box, 5-([2,2'-bipyridin]-5-yl)-2-(2,4,6-tricyclohexylphenyl)imidazo[1,5-*a*]pyridin-2-ium chloride (94.7 mg, 0.15 mmol, 1 equiv), $AuCl{\cdot}SMe_2$ (44.4 mg, 0.15 mmol, 1 equiv), dry K_2CO_3 (41.6 mg, 0.30 mmol, 2.0 equiv), and dry acetone (4.0 mL) were added into a screw-cap vial containing a magnetic stirring bar. The reaction mixture was stirred at 60 ºC for 3 hours under dark conditions. The mixture was then filtered through celite and subsequently eluted with DCM. The filtrate was evaporated and purified by silica-gel column chromatography (DCM/EtOAc=98/2 to 96/4) to afford the desired product (101 mg, 0.12 mmol, 81% yield).

White solid. mp: 145 ºC (decomp.). IR (ATR, ν/cm^{-1}): 3052 w, 2925 s, 2849 m, 1651 w, 1588 w, 1541 w, 1458 m, 1448 m, 1382 w, 1315 w, 1194 w, 1175 w, 1151 w, 1092 w, 1064 w, 1025 w, 993 w, 953 w, 864 w, 788 m, 749 m, 710 m, 689 w, 672 w, 652 w, 624 w. ^{1}H NMR (400 MHz, CD_2Cl_2, 25 ºC): δ 8.85 (dd, *J* = 2.3, 0.9 Hz, 1H), 8.69 (ddd, *J* = 4.6, 1.8, 0.9 Hz, 1H), 8.58 (d, *J* = 8.2 Hz, 1H), 8.49 (dt, *J* = 8.2, 0.9 Hz, 1H), 7.98 (dd, *J* = 7.8, 1.8 Hz, 1H), 7.85 (td, *J* = 7.8, 1.8 Hz, 1H), 7.57 (dd, *J* = 9.2, 0.9 Hz, 1H), 7.40 (s, 1H), 7.35 (ddd, *J* = 7.8, 5.0, 1.4 Hz, 1H), 7.12 (dd, *J* = 9.2, 6.4 Hz, 1H), 7.09 (s, 2H), 6.74 (dd, *J* = 6.9, 1.4 Hz, 1H), 2.63-2.51 (m, 1H), 2.11-1.82 (m, 6H), 1.81-1.55 (m, 10H), 1.49-1.33 (m, 8H), 1.32 -1.16 (m, 4H), 1.15-1.00 (m, 4H). $^{13}C\{^1H\}$ NMR (100 MHz, CD_2Cl_2, 25 ºC): 165.5, 157.2, 155.6, 150.1, 149.3, 149.2, 143.9, 138.4, 137.0, 136.4, 133.5, 131.6, 130.8, 124.1, 123.31, 123.28, 121.5, 120.9, 118.2, 117.8, 114.6, 44.7, 39.3, 34.9, 34.4, 27.0, 26.8, 26.2, 26.0. HRMS (ESI^+) calc. for $C_{41}H_{46}N_4AuClNa$ 849.2969 found 849.2956.

Synthesis of 5-([1,1'-Biphenyl]-4-yl)-2-(2,6-dibenzhydryl-4-methylphenyl)imidazo[1,5-*a*]pyridin-2-ium Chloride

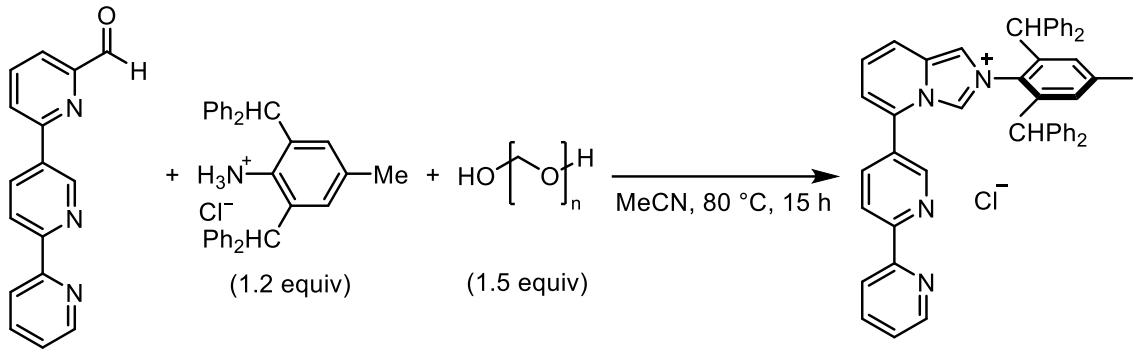

[2,2':5',2''-Terpyridine]-6''-carbaldehyde (261 mg, 1.0 mmol, 1 equiv), 2,6-dibenzhydryl-4-methylbenzenaminium chloride[27] (571 mg, 1.2 mmol, 1.2 equiv), and paraformaldehyde (45.0 mg, 1.5 mmol, 1.5 equiv) were suspended in acetonitrile (5.0 mL) in a screw-cap vial. After stirring the mixture at 80 ºC for 15 hours, all volatile compounds were removed under reduced pressure. The crude mixture was purified by silica-gel column chromatography (DCM/MeOH=99/1 to 90/10). The resulting solid compound was triturated with EtOAc to afford the desired product (493 mg, 0.67 mmol, 67% yield).

White solid. mp: 155 ºC (decomp.). IR (ATR, ν/cm^{-1}): 3345 w, 3049 w, 3025 w, 1541 w, 1589 m, 1541 w, 1494 m, 1454 m, 1378 w, 1355 w, 1307 w, 1244 w, 1029 w, 952 w, 916 w, 857 w, 796 m, 771 m, 749 s, 634 s, 578 m. ^{1}H NMR (400 MHz, DMSO-d_6, 25 ºC): δ 9.18 (d, J = 0.9 Hz, 1H), 8.83 (d, J = 1.8 Hz, 1H), 8.79 (d, J = 4.1 Hz, 1H), 8.52 (d, J = 4. 1 Hz, 1H), 8.50 (d, J = 4.1 Hz, 1H), 8.06 (td, J = 7.8, 1.8 Hz, 1H), 7.84 (dd, J = 8.2, 2.3 Hz, 1H), 7.81-7.75 (m, 2H), 7.57 (ddd, J = 7.8, 5.0, 0.9 Hz, 1H), 7.48-7.37 (m, 2H), 7.30-7.11 (m, 12H), 7.02-6.91 (m, 8H), 6.78 (s, 2H), 5.26 (s, 2H), 2.20 (s, 3H). ^{13}C{^{1}H} NMR (100 MHz, DMSO-d_6, 25 ºC): δ 156.4, 154.1, 149.6, 149.1, 141.55, 141.47, 140.9, 140.4, 137.8, 137.1, 132.0, 131.0, 130.3, 129.2, 129.0, 128.8, 128.5, 128.4, 127.1, 126.83, 126.78, 126.4, 125.4, 125.0, 120.9, 120.3, 119.3, 118.3, 116.7, 50.7, 21.4. HRMS (ESI^{+}) calc. for $C_{50}H_{39}N_4$ 695.3169 found 695.3163.

Synthesis of (5-([2,2'-Bipyridin]-5-yl)-2-(2,6-dibenzhydryl-4-methylphenyl)imidazo[1,5-*a*]pyridin-3(2*H*)-ylidene)gold(I) Chloride (1d)

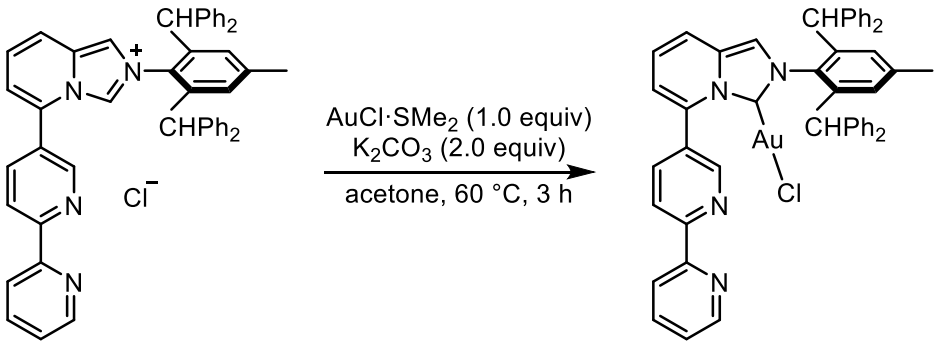

In a nitrogen-filled glove box, 5-([2,2'-bipyridin]-5-yl)-2-(2,6-dibenzhydryl-4-methylphenyl)imidazo[1,5-*a*]pyridin-2-ium chloride (73.1 mg, 0.10 mmol, 1 equiv), $AuCl{\cdot}SMe_2$ (29.6 mg, 0.10 mmol, 1 equiv), dry K_2CO_3 (27.8 mg, 0.20 mmol, 2.0 equiv), and dry acetone (2.7 mL) were added into a screw-cap vial containing a magnetic stirring bar. The reaction mixture was stirred at 60 ºC for 3 hours under dark conditions. The mixture was then filtered through celite and subsequently eluted with DCM. The filtrate was evaporated and purified by silica-gel column chromatography (DCM/EtOAc=98/2 to 96/4) to afford the desired product (70.6 mg, 0.076 mmol, 76% yield).

White solid. mp: 230 ºC (decomp.). IR (ATR, ν/cm^{-1}): 3056 w, 3024 w, 2921 w, 1731 w, 1651 w, 1587 w, 1548 w, 1493 m, 1450 m, 1315 w, 1289 w, 1242 w, 1199 w, 1174 w, 1146 w, 1092 w, 1078 w, 1029 w, 992 w, 914 w, 883 w, 850 w, 783 w, 747 s, 621 m, 606 s, 588 m, 549 w, 472 w. ^{1}H NMR (400 MHz, CD_2Cl_2, 25 ºC): δ 8.77 (s, 1H), 8.73 (d, J = 5.0 Hz, 1H), 8.52 (d, J = 7.8 Hz, 2H), 7.88 (t, J = 7.8 Hz, 1H), 7.81 (d, J = 8.2 Hz, 1H), 7.38 (dd, J = 6.0, 4.6 Hz, 1H), 7.28-7.16 (m, 12H), 7.11-6.97 (m, 5H), 6.94 (dd, J = 8.7, 6.4 Hz, 1H), 6.91-6.81 (m, 4H), 6.77 (s, 2H), 6.63 (d, J = 6.4 Hz, 1H), 6.15 (s, 1H), 5.38 (s, 1H), 5.26 (s, 1H), 2.22 (s, 3H). ^{13}C{^{1}H} NMR (100 MHz, CD_2Cl_2, 25 ºC): δ 165.5, 157.5, 156.0, 149.64, 149.57, 142.6, 142.4, 141.5, 140.3, 138.9, 137.3, 136.3, 136.0, 130.9, 130.7, 130.4, 129.8, 129.6, 128.9, 128.8, 127.03, 126.98, 124.4, 122.9, 121.8, 121.0, 118.3, 117.9, 115.5, 52.0, 21.9. HRMS (ESI^+) calc. for $C_{50}H_{38}N_4AuClNa$ 949.2343 found 949.2332. The crystal suitable for SC-XRD analysis was grown from THF and ether solution.

Synthesis of 5-([2,2'-Bipyridin]-5-yl)-2-(2,6-bis(bis(3,5-dimethylphenyl)methyl)-4-methylphenyl)imidazo[1,5-*a*]pyridin-2-ium Chloride

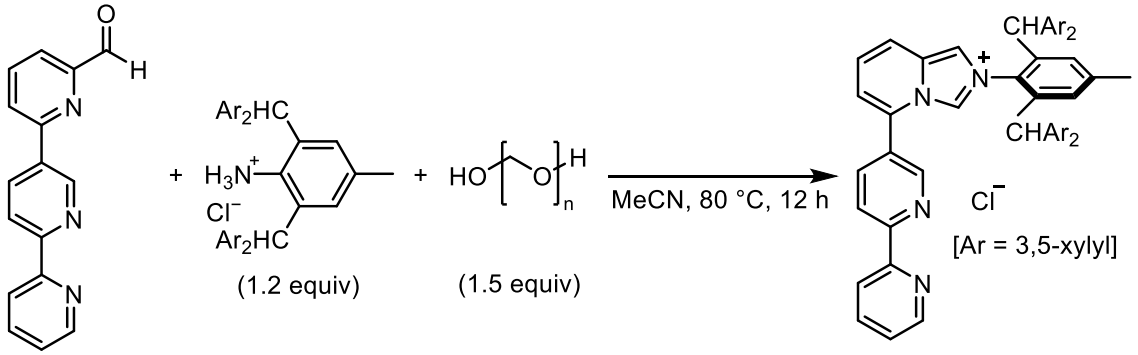

[2,2':5',2''-Terpyridine]-6''-carbaldehyde (262 mg, 1.0 mmol, 1 equiv), 2,6-bis(bis(3,5-dimethylphenyl)methyl)-4-methylbenzenaminium chloride[28] (707 mg, 1.2 mmol, 1.2 equiv), and paraformaldehyde (45.3 mg, 1.5 mmol, 1.5 equiv) were suspended in acetonitrile (5.0 mL) in a screw-cap vial. After stirring the mixture at 80 ºC for 12 hours, all volatile compounds were removed under reduced pressure. The crude mixture was purified by silica-gel column chromatography (DCM/MeOH=99/1 to 90/10) to afford the desired product (605 mg, 0.72 mmol, 72% yield).

White solid. mp: 170 ºC (decomp.). IR (ATR, ν/cm^{-1}): 3322 w, 3008 w, 2915 m, 1651 w, 1595 s, 1542 w, 1457 s, 1376 m, 1308 m, 1245 w, 1199 w, 1173 w, 1146 w, 1092 w, 1065 w, 1037 m, 994 w, 953 w, 850 s, 797 m, 747 s, 712 s, 697 m, 662 s, 619 m, 581 m, 545 m. ^{1}H NMR (400 MHz, $CDCl_3$, 25 ºC): δ 9.78 (d, *J* = 1.4 Hz, 1H), 9.09 (d, *J* = 9.4 Hz, 1H), 8.80 (dt, *J* = 4.8, 0.9 Hz, 1H), 8.55 (d, *J* = 8.0 Hz, 1H), 8.39 (d, *J* = 8.3 Hz, 1H), 8.11 (d, *J* = 2.1 Hz, 1H), 7.94 (td, *J* = 7.6, 1.6 Hz, 1H), 7.45 (dd, *J* = 7.6, 4.8 Hz, 1H), 7.34 (dd, *J* = 9.2, 6.9 Hz, 1H), 6.98 (d, *J* = 6.9 Hz, 1H), 6.85 (s, 2H), 6.75 (dd, *J* = 8.3, 2.3 Hz, 1H), 6.72 (s, 2H), 6.64 (s, 4H), 6.59-6.54 (m, 3H), 6.28 (s, 4H), 5.01 (s, 2H), 2.26 (s, 3H), 2.22 (s, 12H), 1.99 (s, 12H). ^{13}C{^{1}H} NMR (100 MHz, $CDCl_3$, 25 ºC): δ 157.8, 154.2, 149.5, 148.0, 143.1, 141.4, 140.7, 140.5, 138.2, 138.0, 137.4, 134.8, 131.4, 130.6, 130.4, 128.73, 128.70, 127.5, 126.3, 125.9, 124.8, 124.3, 122.2, 121.4, 120.5, 118.9, 51.6, 22.0, 21.2, 21.0. HRMS (ESI^{+}) calc. for $C_{58}H_{55}N_4$ 807.4421 found 807.4406.

Synthesis of (5-([2,2'-Bipyridin]-5-yl)-2-(2,6-bis(bis(3,5-dimethylphenyl)methyl)-4-methylphenyl)imidazo[1,5-*a*]pyridin-3(2*H*)-ylidene)gold(I) Chloride (1e)

In a nitrogen-filled glove box, 5-([2,2'-bipyridin]-5-yl)-2-(2,6-bis(bis(3,5-dimethylphenyl)methyl)-4-methylphenyl)imidazo[1,5-*a*]pyridin-2-ium chloride (84.6 mg, 0.10 mmol, 1 equiv), AuCl·SMe_2 (29.5 mg, 0.10 mmol, 1 equiv), dry K_2CO_3 (27.6 mg, 0.20 mmol, 2.0 equiv), and dry acetone (2.7 mL) were added into a screw-cap vial containing a magnetic stirring bar. The reaction mixture was stirred at 60 ºC for 3 hours under dark conditions. The mixture was then filtered through celite and subsequently eluted with DCM. The filtrate was evaporated and purified by silica-gel column chromatography (DCM/EtOAc=98/2 to 96/4) to afford the desired product (72.1 mg, 0.069 mmol, 69% yield).

White solid. mp: 260 ºC (decomp.). IR (ATR, ν/cm^{-1}): 3009 w, 2915 w, 2862 w, 1653 w, 1597 s, 1541 w, 1435 m, 1376 m, 1315 w, 1290 w, 1175 w, 1146 w, 1092 w, 1038 w, 953 m, 783 m, 749 m, 675 m, 655 w. ^{1}H NMR (400 MHz, CD_2Cl_2, 25 ºC): δ 8.73 (dt, *J* = 4.8, 0.7 Hz, 1H), 8.70 (d, *J* = 2.3 Hz, 1H), 8.54-8.48 (m, 2H), 7.88 (td, *J* = 7.6, 1.8 Hz, 1H), 7.77 (dd, *J* = 8.3, 2.3 Hz, 1H), 7.37 (ddd, *J* = 7.6, 4.8, 0.9 Hz, 1H), 7.11 (d, *J* = 9.2 Hz, 1H), 6.92 (dd, *J* = 9.2, 6.6 Hz, 1H), 6.87 (s, 2H), 6.81 (s, 2H), 6.75 (s, 2H), 6.65 (brs, 4H), 6.58 (dd, *J* = 6.6, 0.9 Hz, 1H), 6.45 (s, 4H), 6.17 (s, 1H), 5.39 (s, 1H), 5.19 (s, 1H), 2.24 (s, 3H), 2.20 (s, 12H), 2.17 (s, 12H). ^{13}C{^{1}H} NMR (100 MHz, CD_2Cl_2, 25 ºC): δ 165.7, 157.4, 156.1, 149.6, 149.5, 142.6, 142.1, 141.6, 139.8, 138.7, 138.3, 138.2, 137.3, 136.3, 135.9, 130.8, 130.7, 130.1, 128.6, 128.4, 127.5, 124.4, 122.5, 121.8, 120.9, 118.2, 117.5, 115.5, 52.3, 22.0, 21.4, 21.3. HRMS (ESI^+) calc. for $C_{58}H_{54}N_4AuClNa$ 1061.3595 found 1061.3580.

Synthesis of 5-([2,2'-Bipyridin]-5-yl)-2-(3,5-di-*tert*-butylphenyl)imidazo[1,5-*a*]pyridin-2-ium Chloride

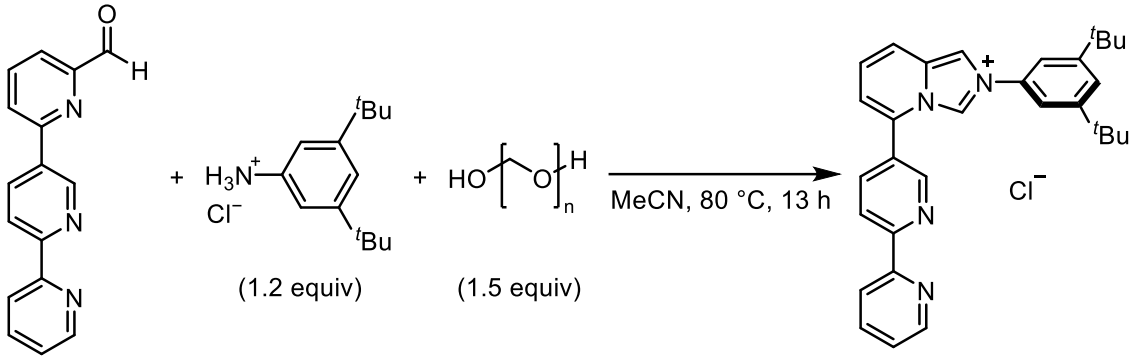

[2,2':5',2''-Terpyridine]-6''-carbaldehyde (387 mg, 1.48 mmol, 1 equiv), 3,5-di-*tert*-butylanilinium chloride (435 mg, 1.80 mmol, 1.2 equiv), and paraformaldehyde (67.6 mg, 2.25 mmol, 1.5 equiv) were suspended in acetonitrile (5.0 mL) in a screw-cap vial. After stirring the mixture at 80 ºC for 13 hours, all volatile compounds were removed under reduced pressure. The crude mixture was purified by basic alumina column chromatography (acetone/MeOH=96/4 to 80/20). The resulting solid compound was further purified by silica-gel column chromatography (acetone/MeOH = 96/4 to 80/20) and triturated with EtOAc to afford the desired product (432 mg, 0.87 mmol, 59% yield).

White solid. mp: 160 ºC (decomp.). IR (ATR, ν/cm^{-1}): 3368 w, 3022 w, 2953 m, 2866 w, 1652 w, 1589 m, 1573 w, 1542 w, 1508 w, 1456 s, 1434 m, 1396 w, 1362 m, 1327 w, 1285 w, 1247 m, 1205 w, 1175 w, 1141 w, 1102 m, 1064 w, 1025 w, 992 w, 960 w, 929 w, 901 w, 876 m, 839 w, 795 s, 771 w, 747 s, 705 m, 681 w, 650 s, 638 m, 604 m, 552 m, 519 m. ^{1}H NMR (400 MHz, DMSO-d_6, 25 ºC): δ 10.23 (d, J = 0.9 Hz, 1H), 9.16 (d, J = 1.8 Hz, 1H), 8.97 (d, J = 1.4 Hz, 1H), 8.76 (d, J = 4.1 Hz, 1H), 8.62 (d, J = 8.7 Hz, 1H), 8.52 (dd, J = 8.2, 2.3 Hz, 1H), 8.48 (d, J = 8.2 Hz, 1H), 8.05-7.99 (m, 2H), 7.67-7.64 (m, 3H), 7.55-7.46 (m, 2H), 7.41 (dd, J = 6.9, 0.9 Hz, 1H), 1.34 (s, 18H). ^{13}C{^{1}H} NMR (100 MHz, DMSO-d_6, 25 ºC): δ 156.7, 154.3, 152.7, 149.6, 149.1, 137.7, 137.6, 134.9, 132.5, 130.7, 127.8, 125.5, 125.4, 124.8, 124.1, 120.9, 120.7, 119.4, 118.3, 118.2, 114.1, 35.0, 31.0. HRMS (ESI^{+}) calc. for $C_{31}H_{33}N_4$ 461.2700 found 461.2690.

Synthesis of (5-([2,2'-Bipyridin]-5-yl)-2-(3,5-di-*tert*-butylphenyl)imidazo[1,5-*a*]pyridin-3(2*H*)-ylidene)gold(I) Chloride (1f)

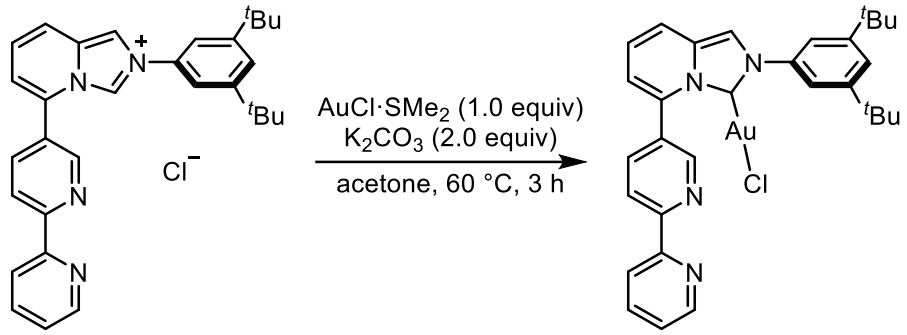

In a nitrogen filled glove box, 5-([2,2'-bipyridin]-5-yl)-2-(3,5-di-*tert*-butylphenyl)imidazo[1,5-*a*]pyridin-2-ium chloride (74.6 mg, 0.15 mmol, 1 equiv), $AuCl{\cdot}SMe_2$ (44.2 mg, 0.15 mmol, 1 equiv), dry K_2CO_3 (41.5 mg, 0.30 mmol, 2.0 equiv), and dry acetone (4.0 mL) were filled in a screw vial containing a magnetic stirring bar. The reaction mixture was stirred at 60 ºC for 3 hours under dark conditions. The mixture was then filtered through celite and subsequently eluted with DCM. The filtrate was evaporated and purified by silica-gel flash column chromatography (DCM/EtOAc = 9/1 to 8/2) to afford the desired product (86.9 mg, 0.125 mmol, 84% yield).

White solid. mp: 150 ºC (decomp.). IR (ATR, ν/cm^{-1}): 2949 w, 2864 w, 1654 w, 1589 m, 1550 w, 1456 m, 1361 m, 1320 w, 1295 w, 1271 w, 1245 m, 1201 w, 1173 w, 1119 w, 1092 w, 1051 w, 1038 w, 1024 w, 887 w, 869 w, 856 w, 789 s, 746 s, 709 m, 674 w, 650 w, 614 w, 520 w. ^{1}H NMR (400 MHz, CD_2Cl_2, 25 ºC): δ 8.84 (s, 1H), 8.70 (d, J = 4.6 Hz, 1H), 8.59 (d, J = 8.2 Hz, 1H), 8.50 (d, J = 7.8 Hz, 1H), 7.99 (dt, J = 8.2, 1.8 Hz, 1H), 7.86 (t, J = 7.8 Hz, 1H), 7.75 (s, 1H), 7.60-7.55 (m, 4H), 7.36 (dd, J = 6.0, 5.0 Hz, 1H), 7.08 (dd, J = 9.6, 7.3 Hz, 1H), 6.69 (d, J = 6.9 Hz, 1H), 1.362 (s, 9H), 1.360 (s, 9H). ^{13}C{^{1}H} NMR (100 MHz, CD_2Cl_2, 25 ºC): δ 163.3, 157.5, 156.0, 152.9, 149.7, 149.6, 140.2, 138.7, 137.3, 136.6, 132.4, 131.1, 124.4, 123.8, 123.5, 121.8, 121.2, 120.3, 118.2, 118.1, 113.2, 35.5, 31.4. HRMS (ESI^+) m/z calc. for $C_{31}H_{32}AuClN_4Na$ 715.1873 found 715.1852.

5-([2,2'-Bipyridin]-5-yl)-2-cyclohexylimidazo[1,5-*a*]pyridin-2-ium Chloride

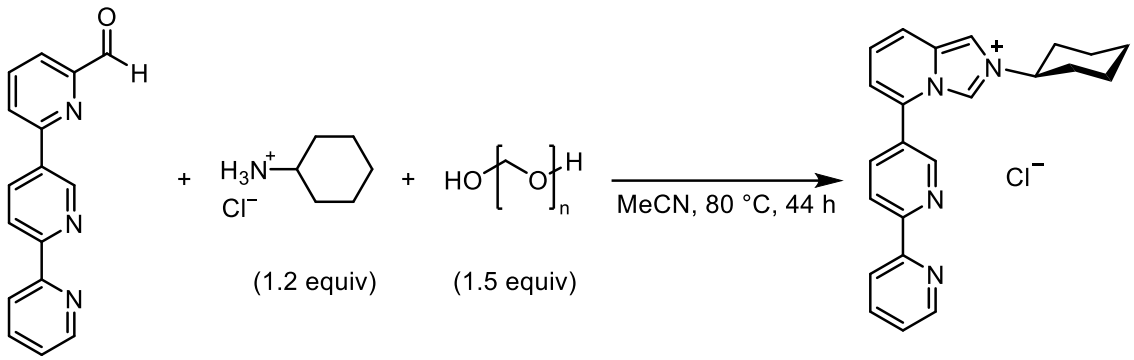

[2,2':5',2''-Terpyridine]-6''-carbaldehyde (261 mg, 1.00 mmol, 1 equiv), cyclohexanaminium chloride (163 mg, 1.20 mmol, 1.2 equiv), and paraformaldehyde (46.1 mg, 1.54 mmol, 1.5 equiv) were suspended in acetonitrile (4.0 mL) in a screw-cap vial. After stirring the mixture at 80 ºC for 44 hours, all volatile compounds were removed under reduced pressure. The crude mixture was purified by basic alumina column chromatography (DCM/MeOH = 94/6 to 80/20). The resulting solid compound was further purified by silica-gel column chromatography (DCM/MeOH = 94/6 to 75/25) to afford the desired product (358 mg, 0.916 mmol, 92% yield).

Light brown solid. mp: 100 ºC (decomp.). IR (ATR, ν/cm^{-1}): 3363 m, 3048 m, 2931 m, 2856 m, 1651 m, 1587 m, 1540 m, 1504 w, 1456 s, 1435 m, 1378 w, 1324 m, 1273 w, 1245 m, 1153 s, 1122 m, 1092 w, 1023 m, 991 m, 952 w, 897 w, 797 s, 749 s, 679 m, 655 s. ^{1}H NMR (400 MHz, $CDCl_3$, 25 ºC): δ 10.47 (s, 1H), 8.88 (s, 1H), 8.70-8.54 (m, 3H), 8.41-8.32 (m, 2H), 7.86 (d, *J* = 9.6 Hz, 1H), 7.82 (t, *J* = 7.8 Hz, 1H), 7.34 (dd, *J* = 6.0, 5.0 Hz, 1H), 7.27 (dd, *J* = 9.2, 6.9 Hz, 1H), 7.04 (d, *J* = 6.9 Hz, 1H), 5.31 (tt, *J* = 11.9, 3.7 Hz, 1H), 2.41-2.31 (m, 2H), 1.97-1.69 (m, 5H), 1.67-1.52 (m, 2H), 1.28 (qt, *J* = 13.3, 3.7 Hz, 1H). ^{13}C{^{1}H} NMR (100 MHz, $CDCl_3$, 25 ºC): δ 157.6, 154.3, 148.9, 148.8, 137.4 (2C), 133.0, 131.0, 126.7, 124.8, 124.7, 124.5, 122.0, 121.7, 118.45, 118.40, 112.0, 61.0, 33.9, 24.9, 24.7. HRMS (ESI^{+}) calc. for $C_{23}H_{23}N_4$ 355.1917 found 355.1909.

(5-([2,2'-Bipyridin]-5-yl)-2-cyclohexylimidazo[1,5-*a*]pyridin-3(2*H*)-ylidene)gold(I) Chloride (1g)

In nitrogen filled glove box, 5-([2,2'-bipyridin]-5-yl)-2-cyclohexylimidazo[1,5-*a*]pyridin-2-ium chloride (78.2 mg, 0.20 mmol, 1 equiv), $AuCl{\cdot}SMe_2$ (58.7 mg, 0.20 mmol, 1 equiv), dry K_2CO_3 (55.5 mg, 0.40 mmol, 2.0 equiv), and dry acetone (4.0 mL) were filled in a screw vial containing a magnetic stirring bar. The reaction mixture was stirred at 60 ºC for 3 hours under dark conditions. The mixture was then filtered through celite and subsequently eluted with DCM. The filtrate was evaporated and purified by silica-gel flash column chromatography (DCM/EtOAc = 95/5 to 90/10) to afford the desired product (78.4 mg, 0.134 mmol, 67% yield).

White solid. mp: 140 ºC (decomp.). IR (ATR, ν/cm^{-1}): 3108 w, 3050 w, 2932 s, 2855 m, 1652 m, 1588 m, 1573 w, 1549 w, 1457 s, 1434 m, 1380 m, 1360 w, 1326 w, 1269 w, 1243 w, 1175 m, 1092 w, 1065 w, 1025 w, 994 w, 955 w, 895 w, 855 w, 789 s, 751 s, 710 w, 670 w, 651 w. ^{1}H NMR (400 MHz, CD_2Cl_2, 25 ºC): δ 8.77 (d, *J* =1.8 Hz, 1H), 8.71 (ddd, *J* = 5.0, 1.8, 0.9 Hz, 1H), 8.58 (d, *J* = 8.2 Hz, 1H), 8.50 (d, *J* = 7.8 Hz, 1H), 7.93 (dd, *J* =8.2, 2.3 Hz, 1H), 7.86 (td, *J* = 7.8, 1.8 Hz, 1H), 7.50 (s, 1H), 7.47 (dd, *J* = 9.2, 0.9 Hz, 1H), 7.36 (ddd, *J* = 7.8, 5.0, 1.4 Hz, 1H), 7.00 (dd, *J* = 9.2, 6.4 Hz, 1H), 6.61 (dd, *J* = 6.6, 1.1 Hz, 1H), 4.88 (tt, *J* = 12.4, 3.7 Hz, 1H), 2.24-2.14 (m, 2H), 1.95- 1.87 (m, 2H), 1.81-1.68 (m, 3H), 1.54-1.43 (m, 2H), 1.33-1.20 (m, 1H). $^{13}C\{^1H\}$ NMR (100 MHz, CD_2Cl_2, 25 ºC): δ 162.5, 157.5, 156.0, 149.64, 149.62, 138.6, 137.3, 136.2, 132.4, 131.1, 124.4, 122.9, 121.8, 121.3, 118.3, 117.6, 108.9, 63.8, 34.6, 25.8, 25.5. HRMS (ESI^+) m/z calc. for $C_{23}H_{22}AuClN_4Na$ 609.1091 found 609.1073.

Synthesis of 5-([2,2'-Bipyridin]-5-yl)-2-((3s,5s,7s)-adamantan-1-yl)imidazo[1,5-*a*]pyridin-2-ium Chloride

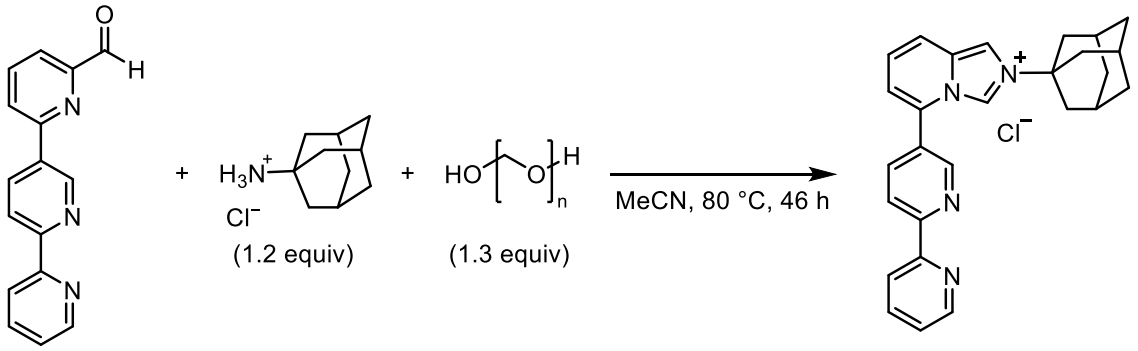

[2,2':5',2''-Terpyridine]-6''-carbaldehyde (261 mg, 1.00 mmol, 1 equiv), 1-adamantanamine hydrochloride (225 mg, 1.20 mmol, 1.2 equiv), and paraformaldehyde (40.0 mg, 1.33 mmol, 1.3 equiv) were suspended in acetonitrile (5.0 mL) in a screw-cap vial. After stirring the mixture at 80 ºC for 46 hours, all volatile compounds were removed under reduced pressure. The crude mixture was purified by basic alumina column chromatography (DCM/MeOH=99/1 to 90/10). The resulting solid compound was triturated with EtOAc to afford the desired product (408 mg, 0.92 mmol, 92% yield).

White solid. mp: 151 ºC (decomp.). IR (ATR, ν/cm^{-1}): 3418 w, 3347 w, 3194 w, 3091 w, 2914 w, 2854 w, 1651 w, 1587 w, 1543 w, 1461 m, 1437 w, 1376 w, 1342 w, 1308 w, 1236 w, 1194 w, 1146 m, 1120 w, 1108 w, 1075 w, 1040 w, 1016 w, 995 w, 869 w, 805 s, 742 m, 698 w, 657 m, 636 m, 600 m, 560 m, 523 m. ^{1}H NMR (400 MHz, $CDCl_3$, 25 ºC): δ 9.10 (d, *J* = 1.8 Hz, 1H), 8.94 (d, *J* = 1.4 Hz, 2H), 8.76-8.69 (m, 3H), 8.45 (d, *J* = 7.8 Hz, 1H), 8.07 (d, *J* = 9.2 Hz, 1H), 7.88 (td, *J* = 7.8, 1.8 Hz, 1H), 7.39 (dd, *J* = 6.9, 5.0 Hz, 1H), 7.30 (dd, *J* = 9.2, 6.9 Hz, 1H), 7.06 (dd, *J* = 5.5, 1.4 Hz, 1H), 2.43-2.39 (m, 6H), 2.36-2.29 (m, 3H), 1.87-1.73 (m, 6H). ^{13}C{^{1}H} NMR (100 MHz, $CDCl_3$, 25 °C): δ 158.2, 154.6, 149.3, 148.7, 137.9, 137.4, 132.8, 131.4, 127.0, 124.7, 124.6, 122.2, 121.8, 120.8, 119.4, 118.9, 113.2, 62.8, 42.8, 35.2, 29.6. HRMS (ESI$^+$) calc. for $C_{27}H_{27}N_4$ 407.2230 found 407.2224.

Synthesis of (5-([2,2'-bipyridin]-5-yl)-2-((3s,5s,7s)-adamantan-1-yl)-2,3-dihydroimidazo[1,5-*a*]pyridin-3-yl)gold(I) Chloride (1h)

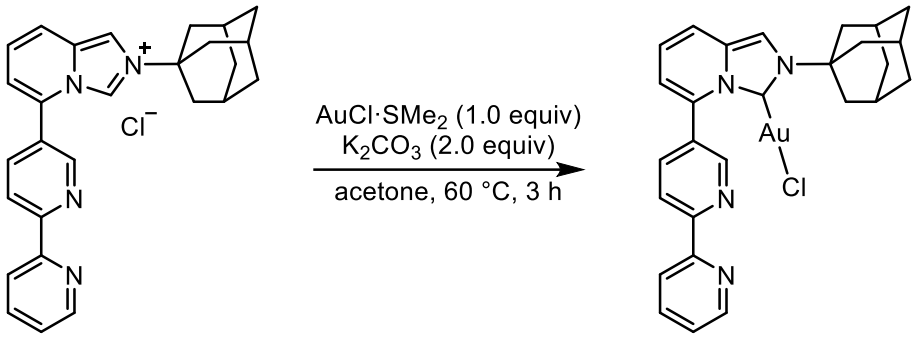

In a nitrogen-filled glove box, 5-([2,2'-bipyridin]-5-yl)-2-((3s,5s,7s)-adamantan-1-yl)imidazo[1,5-*a*]pyridin-2-ium chloride (66.4 mg, 0.15 mmol, 1 equiv), $AuCl{\cdot}SMe_2$ (44.2 mg, 0.15 mmol, 1 equiv), dry K_2CO_3 (41.6 mg, 0.30 mmol, 2.0 equiv), and dry acetone (4.0 mL) were added into a screw-cap vial containing a magnetic stirring bar. The reaction mixture was stirred at 60 ºC for 3 hours under dark conditions. The mixture was then filtered through celite and subsequently eluted with DCM. The filtrate was evaporated and purified by silica-gel column chromatography (DCM/EtOAc=9/1 to 8/2) to afford the desired product (82.7 mg, 0.13 mmol, 86% yield).

Pale yellow solid. mp: 169 ºC (decomp.). IR (ATR, ν/cm^{-1}): 3165 w, 3049 w, 3006 w, 2907 s, 2850 m, 1652 w, 1587 m, 1573 w, 1549 w, 1457 s, 1434 m, 1379 m, 1358 m, 1343 m, 1305 m, 1283 w, 1252 w, 1157 m, 1082 m, 1026 w, 992 w, 954 m, 854 w, 787 s, 749 s, 709 s, 672 m, 651 w. ^{1}H NMR (400 MHz, CD_2Cl_2, 25 ºC): δ 8.74 (s, 1H), 8.73-8.68 (m, 1H), 8.57 (dt, *J* = 8.0, 1.4 Hz, 1H), 8.50 (dd, *J* =8.0, 1.1 Hz, 1H), 7.91-7.83 (m, 2H), 7.66 (d, *J* = 1.6 Hz, 1H), 7.49 (dd, *J* = 9.2, 0.9 Hz, 1H), 7.39-7.32 (m, 1H), 6.98 (t, *J* = 8.0 Hz, 1H), 6.62 (dd, *J* = 5.2, 1.1 Hz, 1H), 2.64 (s, 6H), 2.28 (s, 3H), 1.77 (s, 6H). ^{13}C{^{1}H} NMR (100 MHz, CD_2Cl_2, 25 ºC): δ 161.7, 157.3, 156.1, 149.6, 138.5, 137.2, 136.4, 131.7, 130.5, 124.3, 122.4, 121.7, 121.2, 118.5, 118.0, 109.7, 61.4, 44.4, 36.1, 30.5. HRMS (ESI^+) calc. for $C_{27}H_{26}N_4AuClNa$ 661.1404 found 661.1397.

Synthesis of 2-([1,1'-Biphenyl]-4-yl)-6-(diethoxymethyl)pyridine

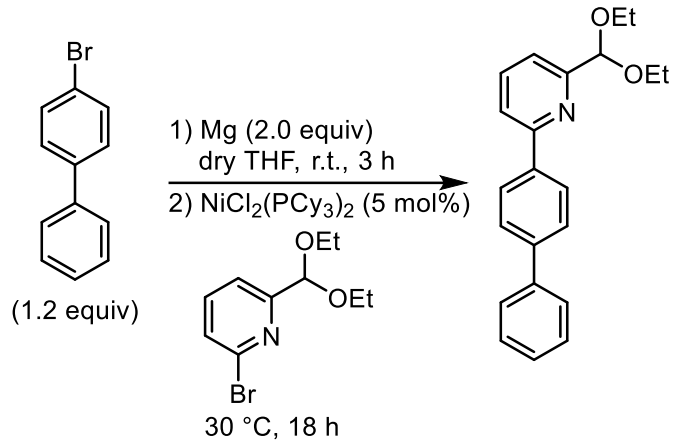

Dry THF (30 mL) was added to a Schlenk flask containing a magnetic stirring bar and magnesium turnings (487 mg, 20 mmol, 2.0 equiv) under nitrogen atmosphere. After addition of 4-bromo-1,1'-biphenyl (2.80 g, 12 mmol, 1.2equiv), the mixture was stirred at room temperature for 3 hours. The resulting organo-magnesium solution was added dropwise to the solution of 2-bromo-6-(diethoxymethyl)pyridine (2.61 g, 10 mmol, 1.0 equiv) and $Ni(PCy_3)_2Cl_2$ (345 mg, 0.5 mmol, 5 mol%) in dry THF (30 mL), and the dark-brown mixture was stirred for 18 hours at 30 ºC. After quenching with saturated NH_4Cl aqueous solution, the aqueous layer was extracted with DCM, and the combined organic layer was dried over Na_2SO_4, filtrated, and evaporated. The crude mixture was purified by silica-gel column chromatography (hexane/EtOAc=100/0 to 80/20) to afford the desired product (3.13 g, 9.4 mmol, 94% yield).

White solid. mp: 67-70 ºC. IR (ATR, ν/cm^{-1}): 2977 w, 2870 w, 1575 m, 1488 w, 1447 m, 1371 w, 1328 m, 1106 m, 1059 s, 1023 s, 913 m, 898 w, 855 m, 807 s, 763 s, 741 m, 726 m, 714 m, 691 s, 649 m, 602 w. ^{1}H NMR (400 MHz, $CDCl_3$, 25 ºC): δ 8.12 (d, *J* = 8.7 Hz, 2H), 7.81 (t, *J* = 7.8 Hz, 1H), 7.75-7.68 (m, 3H), 7.66 (d, *J* = 7.3 Hz, 2H), 7.57 (d, *J* = 7.3 Hz, 1H), 7.47 (t, *J* = 7.6 Hz, 2H), 7.37 (t, *J* = 7.3 Hz, 1H), 5.57 (s, 1H), 3.85-3.75 (m, 2H), 3.73-3.63 (m, 2H), 1.29 (t, *J* = 6.9 Hz, 6H). ^{13}C{^{1}H} NMR (100 MHz, $CDCl_3$, 25 ºC): δ 158.4, 155.9, 141.8, 140.6, 137.9, 137.6, 128.8, 127.5, 127.4, 127.1, 120.1, 119.3, 103.2, 62.6, 15.3. HRMS (ESI$^+$) m/z calc. for $C_{22}H_{23}O_2NNa$ 356.1621 found 356.1615.

Synthesis of 5-([1,1'-Biphenyl]-4-yl)-2-(2,6-dibenzhydryl-4-methylphenyl)imidazo[1,5-*a*]pyridin-2-ium Chloride

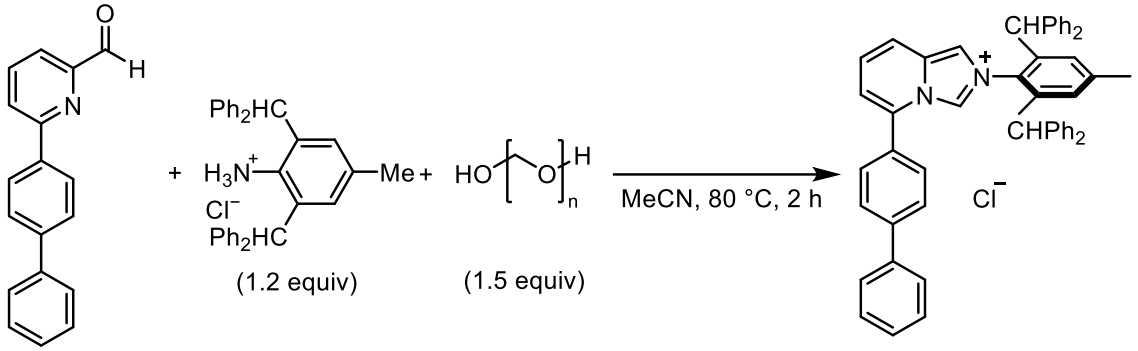

2-([1,1'-Biphenyl]-4-yl)-6-(diethoxymethyl)pyridine (333 mg, 1.0 mmol, 1 equiv), 2,6-dibenzhydryl-4-methylbenzenaminium chloride (571 mg, 1.20 mmol, 1.2 equiv), and paraformaldehyde (45.0 mg, 1.50 mmol, 1.5 equiv) were suspended in ethanol (5.0 mL) in a screw-cap vial. After stirring the mixture at 80 ºC for 2 hours, all volatile compounds were removed under reduced pressure. The crude mixture was purified by basic alumina column chromatography (DCM/MeOH=99/1). The resulting solid compound was further purified by silica-gel column chromatography (DCM/MeOH = 99/1 to 90/10) to afford the desired product (689 mg, 0.94 mmol, 94% yield).

White solid. mp: 140 ºC (decomp.). IR (ATR, ν/cm^{-1}): 3297 w, 3163 w, 3025 w, 2925 w, 1651 w, 1597 w, 1549 w, 1493 m, 1447 m, 1354 w, 1305 w, 1280 w, 1263 w, 1200 w, 1170 w, 1144 w, 1078 w, 1031 w, 1006 w, 915 w, 851 w, 793 w, 766 s, 728 s, 619 s, 605 s, 579 m. ^{1}H NMR (400 MHz, $CDCl_3$, 25 ºC): δ 9.83 (d, *J* = 1.8 Hz, 1H), 8.80 (d, *J* = 9.6 Hz, 1H), 7.65-7.60 (m, 2H), 7.59-7.45 (m, 5H), 7.33 (dd, *J* = 9.2, 6.9 Hz, 1H), 7.30-7.24 (m, 4H), 7.24-7.18 (m, 2H), 7.09-6.98 (m, 8H), 6.97-6.90 (m, 3H), 6.76-6.70 (m, 6H), 6.66 (d, *J* = 8.7 Hz, 2H), 6.58 (d, *J* = 1.4 Hz, 1H), 5.20 (s, 2H), 2.23 (s, 3H). ^{13}C{^{1}H} NMR (100 MHz, $CDCl_3$, 25 ºC): δ 143.6, 142.8, 141.6, 140.9, 140.6, 139.4, 133.9, 131.6, 130.8, 130.5, 129.8, 129.2, 129.0, 128.6, 128.5, 128.3, 128.2, 127.9, 127.1, 127.0, 126.9, 125.0, 124.0, 120.7, 118.9, 118.6, 51.6, 21.9. HRMS (ESI^{+}) m/z calc. for $C_{52}H_{41}N_2$ 693.3264 found 693.3255.

Synthesis of (5-([1,1'-Biphenyl]-4-yl)-2-(2,6-dibenzhydryl-4-methylphenyl)imidazo[1,5-*a*]pyridin-3(2*H*)-ylidene)gold(I) Chloride (1i)

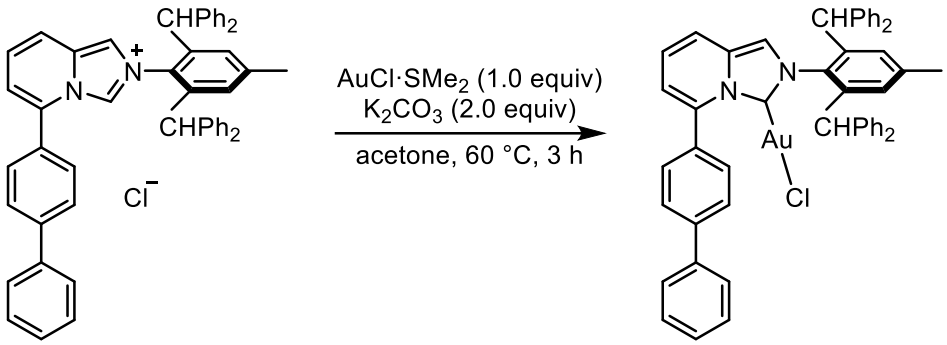

In a nitrogen filled glove box, 5-([1,1'-biphenyl]-4-yl)-2-(2,6-dibenzhydryl-4-methylphenyl)imidazo[1,5-*a*]pyridin-2-ium chloride (248 mg, 0.34mmol, 1 equiv), AuCl·SMe_2 (100 mg, 0.34 mmol, 1 equiv), dry K_2CO_3 (93.9 mg, 0.68 mmol, 2.0 equiv), and dry acetone (9.0 mL) were added into a screw vial containing a magnetic stirring bar. The reaction mixture was stirred at 60 ºC for 3 hours under dark conditions. The mixture was then filtered through celite and subsequently eluted with DCM. The filtrate was evaporated and purified by silica-gel column chromatography (DCM) to afford the desired product (260 mg, 0.28 mmol, 83% yield).

White solid. mp: 230 ºC (decomp.). IR (ATR, ν/cm^{-1}): 3159 w, 3056 w, 3026 w, 2962 w, 2909 w, 1651 w, 1597 w, 1542 w, 1491 m, 1473 w, 1445 m, 1364 w, 1316 w, 1289 w, 1262 w, 1197 w, 951 m, 764 s. ^{1}H NMR (400 MHz, CD_2Cl_2, 25 °C): δ 7.74-7.65 (m, 4H), 7.52-7.45 (m, 4H), 7.40 (tt, *J* = 6.4, 1.4 Hz, 1H), 7.28-7.17 (m, 12H), 7.08-7.04 (m, 4H), 7.03 (dd, *J* = 9.2, 0.9 Hz, 1H), 6.92 (dd, *J* = 9.2, 6.4 Hz, 1H), 6.88-6.83 (m, 4H), 6.78 (s, 2H), 6.59 (dd, *J* = 6.4, 0.9 Hz, 1H), 6.13 (s, 1H), 5.32 (s, 2H, overlapped with a residual DCM signal), 2.23 (s, 3H). ^{13}C{^{1}H} NMR (100 MHz, CD_2Cl_2, 25 ºC): δ 165.8, 143.6, 142.7, 142.6, 141.5, 141.3, 140.2, 139.4, 136.3, 133.4, 131.1, 130.6, 130.3, 129.8, 129.6, 129.1, 128.83, 128.77, 128.2, 127.99, 127.95, 127.0, 126.9, 123.1, 117.5, 116.7, 115.1, 51.9, 21.9. HRMS (ESI$^+$) m/z calc. for $C_{52}H_{40}AuClN_2Na$ 947.2438 found 947.2423. The crystal suitable for SC-XRD analysis was grown from DCM and ether solution.

3.4.3 Synthesis of Starting Materials for Cyclization

General Procedure for Sonogashira-Coupling

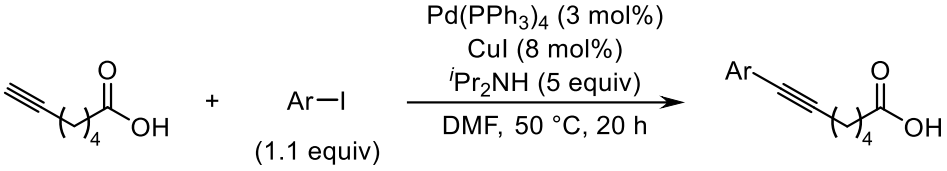

Diisopropylamine (3.5 mL, 25.0 mmol, 5.0 equiv) in DMF (10.0 mL) was degassed in the Schlenk tube under nitrogen atmosphere, and aryliodide (5.5 mmol, 1.1 equiv), $Pd(PPh_3)_4$ (173 mg, 0.15 mmol, 3 mol%), and CuI (76.2 mg, 0.4 mmol, 8 mol%) were added to the solution. After addition of hept-6-ynoic acid (666 μL, 5.0 mmol, 1.0 equiv), the resulting mixture was stirred for 20 hours at 50 ºC. EDTA·2Na·$2H_2O$ (931 mg, 2.5 mmol, 0.5 equiv) was added to the solution and the resulting mixture was stirred for 1 hour. The mixture was acidified with 1M HCl aqueous solution, and the aqueous layer was extracted with EtOAc. The combined organic layer was washed with brine, dried over Na_2SO_4, and filtrated. All volatiles were removed under the reduced pressure. The crude mixture was purified by silica-gel column chromatography to afford the desired product. As the further purification, alkyne-tethered carboxylic acids were recrystallized before using gold-zinc catalytic reactions.

7-(4-Bromophenyl)hept-6-ynoic Acid (2b)

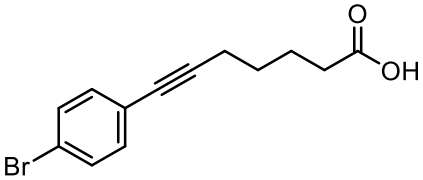

White solid (1.39 g, 4.96 mmol, 99% yield). mp: 89-91 ºC. IR (ATR, ν/cm^{-1}): 2947 m, 2869 m, 2656 br, 2240 w, 1690 s, 1583 w, 1482 m, 1460 m, 1434 m, 1410 s, 1351 m, 1316 s, 1266 m, 1250 m, 1203 s, 1096 w, 1070 m, 1028 w, 1006 m, 906 s, 837 s, 819 s, 735 s, 706 w, 680 m, 635 w, 573 m, 523 s. ^{1}H NMR (400 MHz, $CDCl_3$, 25 ºC): δ 10.37 (brs, 1H), 7.43-7.38 (m, 2H), 7.26-7.22 (m, 2H), 2.43 (t, J = 6.9 Hz, 4H), 1.86-1.77 (m, 2H), 1.71-1.62 (m, 2H). ^{13}C{^{1}H} NMR (100 MHz, $CDCl_3$, 25 ºC): δ 178.8, 133.0, 131.4, 122.8, 121.7, 90.7, 80.1, 33.3, 27.9, 23.9, 19.1. HRMS (ESI^-) m/z calc. for $C_{13}H_{12}BrO_2$ 279.0026 found 279.0028.

7-(4-Nitrophenyl)hept-6-ynoic Acid (2c)

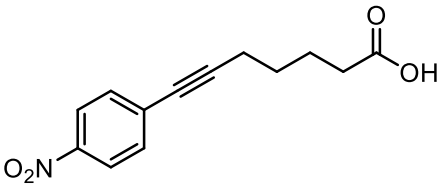

Orange solid (1.17 g, 4.72 mmol, 94 % yield). mp: 102-104 ºC. IR (ATR, ν/cm^{-1}): 2959 w, 1696 s, 1591 m, 1517 s, 1493 w, 1464 m, 1425 m, 1408 w, 1344 s, 1318 m, 1285 m, 1266 m, 1251 m, 1205 m, 1173 m, 1112 m, 1076 w, 1052 w, 1012 w, 968 w, 931 m, 853 s, 830 m, 782 w, 750 s, 727 m, 692 m, 635 w, 582 m, 552 m, 516 m. ^{1}H NMR (400 MHz, $CDCl_3$, 25 ºC): δ 10.90 (brs, 1H), 8.18-8.12 (m, 2H), 7.54-7.48 (m, 2H), 2.49 (t, *J* = 6.9 Hz, 2H), 2.44 (t, *J* = 7.3 Hz, 2H), 1.87-1.77 (m, 2H), 1.75-1.64 (m, 2H). ^{13}C{^{1}H} NMR (100 MHz, $CDCl_3$, 25 ºC): δ 179.0, 146.7, 132.3, 130.9, 123.5, 95.6, 79.8, 33.4, 27.7, 23.9, 19.3. HRMS (ESI$^-$) m/z calc. for $C_{13}H_{12}NO_4$ 246.0772 found 246.0769.

7-(4-Methoxyphenyl)hept-6-ynoic Acid (2d)

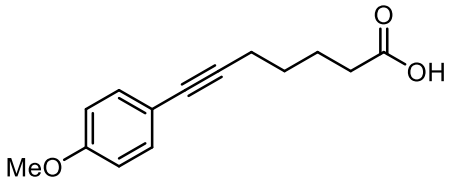

White solid (921 mg, 3.97 mmol, 79% yield). mp: 83-85 °C. IR (ATR, ν/ cm^{-1}): 3003 w, 2974 w, 2948 m, 2871 w, 2838 w, 2359 w, 2048 w, 1904 w, 1696 s, 1603 m, 1566w, 1507 s, 1456 m, 1433 m, 1407 m, 1353 w, 1320 m, 1288 m, 1246 s, 1200 s, 1176 s, 1107 m, 1074 w, 1035 m, 1024 m, 924 s, 835 s, 798 m, 735 m, 665 m, 638 m, 544 m, 514 m. ^{1}H NMR (400 MHz, $CDCl_3$, 25 ºC): δ 11.18 (brs, 1H), 7.35-7.29 (m, 2H), 6.84-6.78 (m, 2H), 3.80 (s, 3H), 2.43 (t, *J* = 6.8 Hz, 4H), 1.87-1.76 (m, 2H), 1.71-1.61 (m, 2H). ^{13}C{^{1}H} NMR (100 MHz, $CDCl_3$, 25 ºC): δ 179.4, 159.0, 132.8, 116.0, 113.8, 87.8, 80.7, 55.2, 33.5, 28.1, 23.9, 19.1. HRMS (ESI$^+$) m/z calc. for $C_{14}H_{16}O_3Na$ 255.0992 found 255.0984.

7-(Benzo[*d*][1,3]dioxol-5-yl)hept-6-ynoic Acid (2e)

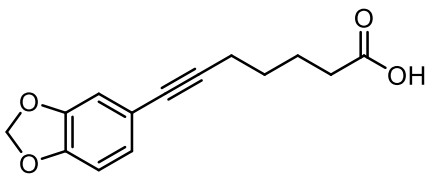

2e was prepared from 4-bromo-1,2-methylenedioxybenzene instead of aryl iodide at 80 ºC. White solid (912 mg, 3.70 mmol, 74% yield). mp: 83-85 °C. IR (ATR, ν/cm^{-1}): 2948 m, 2896 m, 1696 s, 1603 w, 1491 s, 1460 m, 1442 m, 1319 m, 1250 s, 1206 s, 1141 w,

1125 w, 1103 m, 1036 s, 936 m, 885 m, 865 m, 821 m, 727 w, 679 w, 615 w, 524 w. ^{1}H NMR (400 MHz, $CDCl_3$, 25 ºC): δ 9.94 (brs, 1H), 6.91 (dd, *J* = 8.2, 1.8 Hz, 1H), 6.84 (d, *J* = 1.4 Hz, 1H), 6.72 (d, *J* = 8.2 Hz, 1H), 5.95 (s, 2H), 2.46-2.39 (m, 4H), 1.86-1.77 (m, 2H), 1.71-1.61 (m, 2H). ^{13}C{^{1}H} NMR (100 MHz, DMSO-d_6, 25 ºC): δ 174.3, 147.2, 147.1, 125.6, 116.4, 111.0, 108.5, 101.3, 88.4, 80.5, 33.1, 27.7, 23.8, 18.3. HRMS (ESI^-) m/z calc. for $C_{14}H_{13}O_4$ 245.0819 found 245.0820.

7-(3,5-Dichlorophenyl)hept-6-ynoic Acid (2f)

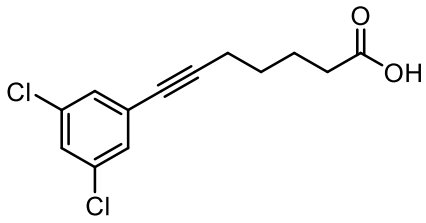

White solid (1.257 g, 4.64 mmol, 93% yield). mp: 64-66 ºC. IR (ATR, ν/cm^{-1}): 3083 w, 2941 m, 2907 m, 2871 m, 2229 w, 1690 s, 1584 m, 1556 s, 1460 m, 1425 m, 1405 s, 1309 m, 1266 m, 1246 m, 1201 s, 1114 m, 1092 m, 1072 m, 1046 w, 992 m, 943 m, 880 m, 854 s, 804 s, 726 m, 670 s, 578 w, 564 w, 535 m. ^{1}H NMR (400 MHz, DMSO-d_6, 25 ºC): δ 12.02 (s, 1H), 7.59 (t, *J* = 1.8 Hz, 1H), 7.44 (d, *J* = 1.8 Hz, 2H), 2.44 (t, *J* = 6.9 Hz, 2H), 2.25 (t, *J* = 7.3 Hz, 2H), 1.68-1.59 (m, 2H), 1.58-1.50 (m, 2H). ^{13}C{^{1}H} NMR (100 MHz, DMSO-d_6, 25 ºC): δ 174.3, 134.2, 129.7, 127.9, 126.4, 93.8, 78.1, 33.1, 27.3, 23.7, 18.4. HRMS (ESI^-) m/z calc. for $C_{13}H_{11}O_2Cl_2$ 269.0142 found 269.0142.

7-(Benzo[*b*]thiophen-3-yl)hept-6-ynoic Acid (2g)

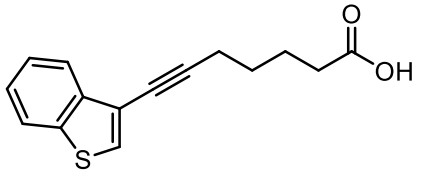

2g was prepared from 3-bromobenzo[*b*]thiophene instead of aryl iodide. White solid (1.00 g, 3.88 mmol, 78% yield). mp: 69-71 ºC. IR (ATR, ν/cm^{-1}): 3091 w, 3031 w, 2940 m, 2868 w, 1797 w, 1688 s, 1505 w, 1462 w, 1428 s, 1409 m, 1339 w, 1308 m, 1253 s, 1200 s, 1139 w, 1119 w, 1061 w, 1013 w, 933 m, 835 m, 801 m, 787 m, 755 s, 730 s, 710 m, 676 m, 582 w. ^{1}H NMR (400 MHz, $CDCl_3$, 25 ºC): δ 7.92 (dd, *J* = 7.6, 1.1 Hz, 1H), 7.83 (dd, *J* = 7.6, 1.1 Hz, 1H), 7.51 (s, 1H), 7.42 (ddd, *J* = 8.2, 7.3, 1.4 Hz, 1H), 7.37 (td, *J* = 7.6, 1.1 Hz, 1H), 2.55 (t, *J* = 6.9 Hz, 2H), 2.47 (t, *J* = 6.9 Hz, 2H), 1.94-1.84 (m, 2H), 1.79-1.69 (m, 2H). ^{13}C{^{1}H} NMR (100 MHz, $CDCl_3$, 25 ºC): δ 179.2, 139.4, 138.7, 128.8, 124.9, 124.5, 123.0, 122.5, 118.8, 91.9, 74.7, 33.4, 28.1, 23.9, 19.3. HRMS (ESI^-) m/z

calc. for $C_{15}H_{13}O_2S$ 257.0642 found 257.0641.

Estrone-substituted Alkyne-tethered Carboxylic Acid (2h)

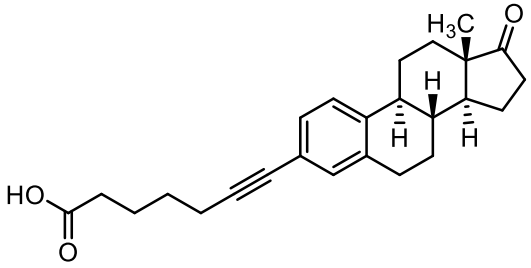

2h was prepared from estrone triflate instead of aryl iodide at 80 ºC. White solid (1.25 g, 3.3 mmol, 66% yield). mp: 185-187 ºC. IR (ATR, ν/cm^{-1}): 2933 m, 2874 m, 2655 w, 2360 w, 2341 w, 1732 s, 1709 s, 1495 m, 1463 m, 1423 m, 1403 m, 1373 w, 1314 m, 1258 m, 1200 s, 1084 m, 1053 w, 1006 m, 943 m, 893 m, 849 w, 822 m, 779 m, 726 m, 710 w, 681 m, 619 w, 578 w. ^{1}H NMR (400 MHz, $CDCl_3$, 25 ºC): δ 10.04 (brs, 1H), 7.22-7.12 (m, 3H), 2.87 (dd, *J* = 8.7, 4.1 Hz, 2H), 2.56-2.36 (m, 6H), 2.29 (td, *J* = 10.3, 4.3 Hz, 1H), 2.20-1.91 (m, 4H), 1.87-1.77 (m, 2H), 1.71-1.37 (m, 8H), 0.91 (s, 3H). ^{13}C{^{1}H} NMR (100 MHz, $CDCl_3$, 25 ºC): δ 220.9, 178.8, 139.5, 136.4, 132.0, 128.9, 125.2, 121.2, 88.7, 81.0, 50.5, 48.0, 44.4, 38.0, 35.8, 33.4, 31.5, 29.1, 28.1, 26.4, 25.6, 23.9, 21.6, 19.1, 13.8. HRMS (ESI$^-$) m/z calc. for $C_{25}H_{29}O_3$ 377.2122 found 377.2128.

Synthesis of Tariric Acid (2i)

Synthesis of Octadec-6-yn-1-ol

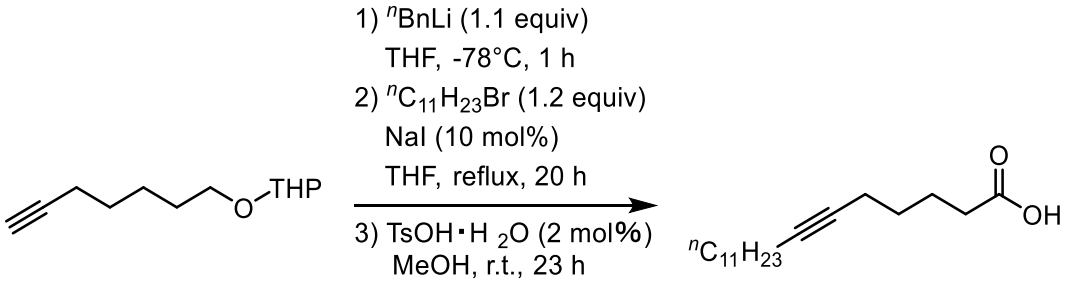

*n*BuLi (1.59 M in hexane) (3.46 mL, 5.5 mmol, 1.1 equiv) was added dropwise to 2-(hept-6-yn-1-yloxy)tetrahydro-2*H*-pyran (982 mg, 5 mmol) in dry THF (10.0 mL) at -78 ºC under nitrogen atmosphere. After stirring the mixture at -78 ºC for 1 hour, 1-bromoundecane (1.33 mL, 6.0 mmol, 1.2 equiv) and sodium iodide (75.5 mg, 0.5 mmol, 10 mol%) were added to the mixture at 0 ºC. The resulting mixture was heated under reflux conditions for 20 hours, and the mixture was quenched with saturated NH_4Cl

aqueous solution. The aqueous layer was extracted with EtOAc, and the combined organic layer was washed with brine, dried over Na_2SO_4, and filtrated. Volatiles were removed under reduced pressure, and a residue was purified by silica-gel column chromatography (hexane:EtOAc=8:2). The product and *p*-toluenesulfonic acid monohydrate (19.0 mg, 0.1 mmol, 2 mol%) were dissolved in MeOH (10.0 mL), and the mixture was stirred at room temperature for 23 hours. The resulting solution was quenched with saturated $NaHCO_3$ aqueous solution, and the aqueous layer was extracted with DCM. The combined organic layer was washed with brine, dried over Na_2SO_4, and filtrated, and volatiles were removed under reduced pressure. A residue was purified by silica-gel column chromatography (hexane:EtOAc=16:4 to 13:7) to afford the product as colorless solid (755 mg, 2.83 mmol, 57% yield). Its spectral data was in accord with the reported data.[29]

Synthesis of Tariric Acid (2i)

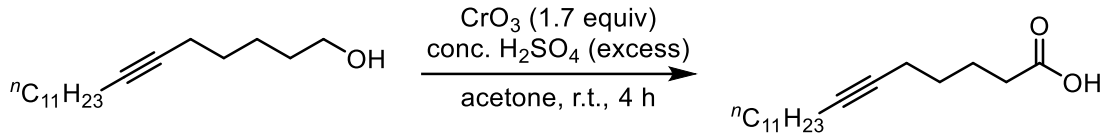

Jones reagent was prepared through mixing CrO_3 (481 mg, 4.8 mmol, 1.7 equiv) and conc. H_2SO_4 (0.4 mL) in deionized water (8.0 mL) at 0 ºC. Octadec-6-yn-1-ol (755 mg, 2.8 mmol, 1 equiv) was dissolved in acetone (18.0 mL). To the solution, Jones reagent was added dropwise at 0 ºC. The resulting mixture was warmed to room temperature and stirred for 4 hours. The reaction mixture was quenched with isopropyl alcohol. After addition of water, aqueous layer was extracted with DCM, and the combined organic layer was washed with brine, dried over Na_2SO_4, and filtrated. The crude mixture was purified by silica-gel column chromatography (hexane:EtOAc=8:2) to afford the desired product as a white solid (501 mg, 1.79 mmol, 63% yield). The spectral data of **2i** was in accord with reported data.[29]

Synthesis of 8-Methoxyoct-6-ynoic Acid (2j)

Synthesis of 8-Methoxyoct-6-yn-1-ol

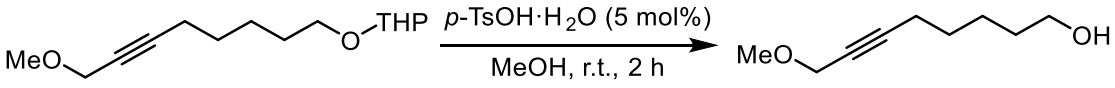

p-Toluenesulfonic acid monohydrate (95.1 mg, 0.5 mmol, 5 mol%) was added to the solution of 2-((8-methoxyoct-6-yn-1-yl)oxy)tetrahydro-2*H*-pyran (2.40 g, 10 mmol, 1.0 equiv), which was prepared through a reported method[30] for the related compound, in MeOH (20.0 mL), and the resulting colorless solution was stirred for 2 hours at room

temperature. The reaction mixture was quenched with saturated aqueous solution of $NaHCO_3$. The water layer was extracted with DCM, and the combined organic layer was washed with brine, dried over Na_2SO_4, and filtrated. All volatile compounds were evaporated, and the crude mixture was purified by silica-gel column chromatography (hexane:EtOAc=3:1) to afford the desired product (1.10 g, 7.1 mmol, 71% yield).

Colorless oil. IR (ATR, ν/$^{-1}$): 3389 br, 2934 m, 2860 m, 1450 w, 1358 m, 1332 w, 1280 w, 1187 m, 1150 w, 1131 w, 1092 s, 1046 m, 1002 m, 947 m, 904 m, 730 s, 647 m, 567 m. ^{1}H NMR (400 MHz, $CDCl_3$, 25 ºC): δ 4.07 (t, *J* = 2.1 Hz, 2H), 3.65 (t, *J* = 6.4 Hz, 2H), 3.36 (s, 3H), 2.25 (tt, *J* = 7.1, 2.1 Hz, 2H), 1.63-1.52 (m, 4H), 1.51-1.43 (m, 2H). ^{13}C{^{1}H} NMR (100 MHz, $CDCl_3$, 25 ºC): δ 86.8, 75.9, 62.8, 60.2, 57.4, 32.2, 28.3, 25.0, 18.7. HRMS (ESI$^+$) m/z calc. for $C_9H_{16}O_2Na$ 179.1043 found 179.1042.

Synthesis of 8-Methoxyoct-6-ynoic Acid (2j)

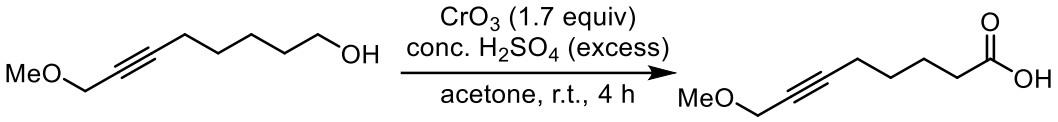

Jones reagent was prepared through mixing CrO_3 (850 mg, 8.5 mmol, 1.7 equiv) and conc. H_2SO_4 (0.7 mL) in deionized water (14.0 mL) at 0 ºC. 8-Methoxyoct-6-yn-1-ol (782.0 mg, 5.0 mmol, 1 equiv) was dissolved in acetone (32 mL). To this solution, Jones reagent was added dropwise at 0 ºC. The resulting mixture was stirred for 4 hours at room temperature. The reaction mixture was quenched with isopropyl alcohol. After addition of water, aqueous layer was extracted with DCM, and the combined organic layer was washed with brine, dried over Na_2SO_4, and filtrated. All volatile compounds were evapolated, and the crude mixture was purified by silica-gel column chromatography (hexane:EtOAc=9:1 to 6:4) to afford the desired product (446 mg, 2.6 mmol, 52% yield).

Colorless oil. IR (ATR, ν/cm^{-1}): 2936 m, 1707 s, 1451 w, 1414 w, 1379 w, 1359 w, 1334 w, 1284 w, 1233 w, 1187 m, 1149 w, 1131 w, 1094 s, 1003 w, 945 w, 904 m, 737 w. ^{1}H NMR (400 MHz, $CDCl_3$, 25 ºC): δ 11.2 (brs, 1H), 4.07 (t, *J* = 2.3 Hz, 2H), 3.37 (s, 3H), 2.38 (t, *J* = 7.6 Hz, 2H), 2.27 (tt, *J* = 6.9, 2.3 Hz, 2H), 1.80-1.71 (m, 2H), 1.63-1.53 (m, 2H). ^{13}C{^{1}H} NMR (100 MHz, $CDCl_3$, 25 ºC): δ 179.2, 86.3, 76.2, 60.2, 57.4, 33.4, 27.9, 23.8, 18.4. HRMS (ESI$^-$) m/z calc. for $C_9H_{13}O_3$ 169.0870 found 169.0870.

3.4.4. Characterization Data for Hydrocarboxylation Products

(*Z*)-7-Benzylideneoxepan-2-one (3a)

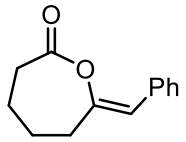

White solid (75.5 mg, 0.373 mmol, 93% yield). mp: 46-48 ºC. IR (ATR, ν/cm^{-1}): 2935 w, 2863 w, 1745 s, 1656 m, 1492 w, 1445 m, 1434 m, 1345 m, 1326 w, 1274 m, 1244 w, 1209 m, 1156 s, 1120 s, 1062 m, 1008 s, 946 w, 925 m, 896 w, 862 m, 808 w, 756 s, 695 s, 660 m, 620 m, 554 m, 526 m. ^{1}H NMR (400 MHz, $CDCl_3$, 25 ºC): δ 7.53-7.48 (m, 2H), 7.35-7.29 (m, 2H), 7.23 (tt, *J* = 6.4, 1.4 Hz, 1H), 5.90 (s, 1H), 2.62-2.58 (m, 2H), 2.51-2.46 (m, 2H), 1.92-1.78 (m, 4H). ^{13}C{^{1}H} NMR (100 MHz, $CDCl_3$, 25 ºC): δ 172.2, 150.0, 133.8, 128.7, 128.4, 127.3, 116.1, 34.2, 34.1, 29.3, 22.7. HRMS (EI^{+}) m/z calc. for $C_{13}H_{14}O_2$ 202.0994 found 202.0992.

(*Z*)-7-(4-Bromobenzylidene)oxepan-2-one (3b)

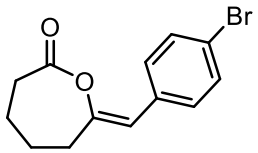

White solid (108.6 mg, 0.386 mmol, 96% yield). mp: 73-74 °C. IR (ATR, ν/cm^{-1}): 2949 w, 2860 w, 1745 s, 1659 m, 1584 w, 1485 m, 1440 m, 1399 w, 1338 m, 1320 w, 1273 m, 1243 w, 1217 m, 1158 s, 1121 s, 1070 m, 1003 s, 891 w, 863 s, 808 s, 770 w, 703 w, 682 m, 645 m, 625 w, 555 m. ^{1}H NMR (400 MHz, $CDCl_3$, 25 ºC): δ 7.44 (dd, *J* = 8.3, 0.8 Hz, 2H), 7.37 (dd, *J* = 8.3, 0.9 Hz, 2H), 5.84 (s, 1H), 2.61-2.55 (m, 2H), 2.50-2.45 (m, 2H), 1.92-1.80 (m, 4H). ^{13}C{^{1}H} NMR (100 MHz, $CDCl_3$, 25 ºC): δ 171.9, 150.8, 132.7, 131.7, 130.3, 121.3, 115.1, 34.4, 34.3, 29.3. 22.8. HRMS (ESI^{+}) m/z calc. for $C_{13}H_{13}BrNaO_2$ 302.9991 found 302.9992. The crystal suitable for SC-XRD analysis was grown from hexamethyldisiloxane solution.

(*Z*)-7-(4-Nitrobenzylidene)oxepan-2-one (3c)

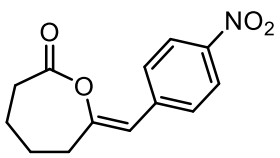

White solid (89.5 mg, 0.362 mmol, 90% yield). mp: 87-90 ºC. IR (ATR, ν/cm^{-1}): 2943 w,

2930 w, 1750 s, 1657 m, 1595 m, 1505 s, 1455 w, 1441 m, 1391 w, 1333 s, 1273 m, 1242 w, 1212 m, 1182 w, 1157 s, 1144 m, 1116 s, 1106 s, 1061 m, 1007 s, 948 m, 929 m, 902 m, 875 s, 842 s, 821 m, 805 m, 778 w, 750 m, 693 m, 650 m, 627 m, 558 m. ^{1}H NMR (400 MHz, $CDCl_3$, 25 ºC): δ 8.17 (d, *J* = 9.2 Hz, 2H), 7.66 (d, *J* = 8.7 Hz, 2H), 5.97 (s, 1H), 2.63-2.58 (m, 2H), 2.57-2.53 (m, 2H), 1.96-1.84 (m, 4H). ^{13}C{^{1}H} NMR (100 MHz, $CDCl_3$, 25 ºC): δ 171.0, 153.8, 146.4, 140.4, 129.3, 123.8, 114.2, 34.6, 34.4, 29.1, 22.7. HRMS (ESI^+) m/z calc. for $C_{13}H_{13}O_4NNa$ 270.0737 found 270.0733. The crystal suitable for SC-XRD analysis was grown from DCE and pentane solution.

(*Z*)-7-(4-Methoxybenzylidene)oxepan-2-one (3d)

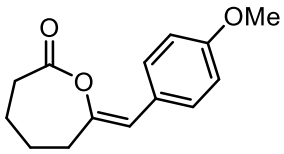

Reaction was conducted at 100 ºC. White solid (84.9 mg, 0.366 mmol, 91% yield). mp: 66-68 °C. IR (ATR, ν/cm^{-1}): 3060 w, 1748 w, 1609 w, 1592 w, 1507 w, 1397 m, 1319 s, 1256 w, 1211 w, 1169 s, 1127 s, 1061 s, 1015 m, 1000 m, 990 m, 907 m, 832 m, 802 m, 773 s, 730 s, 709 s, 667 s, 646 m, 630 m. ^{1}H NMR (400 MHz, $CDCl_3$, 25 ºC): δ 7.45 (d, *J* = 9.2 Hz, 2H), 6.86 (d, *J* = 6.9 Hz, 2H), 5.83 (s, 1H), 3.80 (s, 3H), 2.61-2.57 (m, 2H), 2.48-2.44 (m, 2H), 1.91-1.79 (m, 4H). ^{13}C{^{1}H} NMR (100 MHz, $CDCl_3$, 25 ºC): δ 172.7, 158.8, 148.3, 130.1, 126.6, 115.7, 113.9, 55.2, 34.2, 29.6, 22.8. HRMS (ESI^+) m/z calc. for $C_{14}H_{16}O_3Na$ 255.0992 found 255.0986.

(*Z*)-7-(Benzo[*d*][1,3]dioxol-5-ylmethylene)oxepan-2-one (3e)

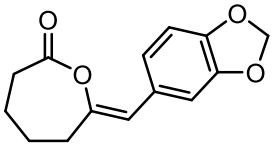

White solid (91.5 mg, 0.371 mmol, 93% yield). mp: 78-80 ºC. IR (ATR, ν/cm^{-1}): 2938 w, 1749 s, 1664 m, 1503 m, 1488 s, 1444 m, 1344 m, 1326 w, 1258 s, 1241 m, 1213 m, 1158 s, 1120 s, 1038 s, 1008 m, 876 m, 809 w, 784 w, 722 w, 685 w, 659 w. ^{1}H NMR (400 MHz, $CDCl_3$, 25 ºC): δ 7.12 (d, *J* = 1.8 Hz, 1H), 6.91 (dd, *J* = 7.8, 1.4 Hz, 1H), 6.76 (d, *J* = 8.2 Hz, 1H), 5.94 (s, 2H), 5.80 (s, 1H), 2.62-2.56 (m, 2H), 2.48-2.42 (m, 2H), 1.90-1.79 (m, 4H). ^{13}C{^{1}H} NMR (100 MHz, $CDCl_3$, 25 ºC): δ 172.3, 148.6, 147.8, 146.8, 128.1, 123.0, 115.8, 108.8, 108.3, 101.1, 34.3, 34.2, 29.5, 22.8. HRMS (ESI^+) m/z calc. for $C_{14}H_{14}O_4Na$ 269.0784 found 269.0780. The crystal suitable for SC-XRD analysis was

grown from hexane solution.

(*Z*)-7-(3,5-Dichlorobenzylidene)oxepan-2-one (3f)

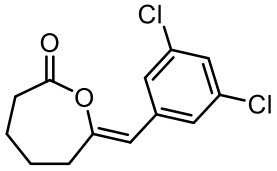

1c was used as a gold catalyst. White solid (93.9 mg, 0.346 mmol, 87% yield). mp: 49-51 ºC. IR (ATR, ν/cm^{-1}): 2940 w, 2863 w, 1755 s, 1661 m, 1583 m, 1557 m, 1436 m, 1415 m, 1346 m, 1326 w, 1274 w, 1241 w, 1209 m, 1160 s, 1118 s, 1063 w, 1009 s, 957 w, 919 w, 885 m, 856 m, 799 m, 673 m, 556 w. ^{1}H NMR (400 MHz, $CDCl_3$, 25 ºC): δ 7.38 (d, *J* = 1.8 Hz, 2H), 7.22 (t, *J* = 1.8 Hz, 1H), 5.77 (s, 1H), 2.62-2.56 (m, 2H), 2.51-2.46 (m, 2H), 1.93-1.83 (m, 4H). ^{13}C{^{1}H} NMR (100 MHz, $CDCl_3$, 25 ºC): δ 171.2, 152.5, 136.6, 135.0, 127.3, 126.9, 113.7, 34.5, 34.4, 29.2, 22.8. HRMS (ESI^{+}) m/z calc. for $C_{13}H_{12}O_2Cl_2Na$ 293.0107 found 293.0104.

(*Z*)-7-(Benzo[*b*]thiophen-3-ylmethylene)oxepan-2-one (3g)

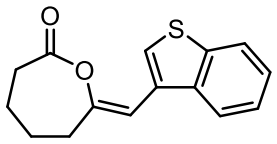

1c was used as a gold catalyst. White solid (78.6 mg, 0.304 mmol, 76% yield). mp: 85-87 ºC. IR (ATR, ν/cm^{-1}): 3010 w, 2916 w, 2862 w, 1749 w, 1652 w, 1597 m, 1458 m, 1375 w, 1147 w, 1124 w, 1038 w, 908 s, 849 s, 783 m, 646 m. ^{1}H NMR (400 MHz, $CDCl_3$, 25 ºC): δ 7.89-7.85 (m, 2H), 7.82 (d, *J* = 8.2 Hz, 1H), 7.45-7.34 (m, 2H), 6.29 (s, 1H), 2.64-2.56 (m, 4H), 1.97-1.83 (m, 4H). ^{13}C{^{1}H} NMR (100 MHz, $CDCl_3$, 25 ºC): δ 172.2, 151.1, 139.3, 138.2, 127.9, 125.9, 124.5, 124.1, 122.8, 121.0, 107.6, 34.2, 34.0, 29.6, 22.7. HRMS (ESI^{+}) m/z calc. for $C_{15}H_{14}O_2NaS$ 281.0607 found 281.0603. The crystal suitable for SC-XRD analysis was grown from hexamethyldisiloxane solution.

Estrone Substituted 7-*exo-dig* Enol Lactone (3h)

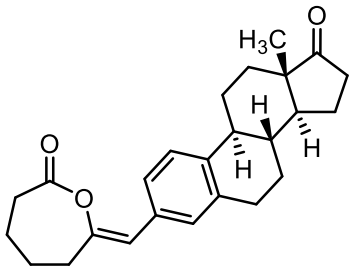

1c was used as a gold catalyst. White solid (121.8 mg, 0.322 mmol, 80% yield). mp: 163-165 ºC. IR (ATR, ν/cm^{-1}): 2929 m, 2860 w, 1736 s, 1664 w, 1498 w, 1453 w, 1435 w, 1373 w, 1345 m, 1273 w, 1244 w, 1213 m, 1158 s, 1121 s, 1084 w, 1054 w, 1008 s, 909 m, 861 w, 822 w, 730 s, 684 w, 669 w, 648 w. ^{1}H NMR (400 MHz, $CDCl_3$, 25 ºC): δ 7.30 (dd, *J* = 8.2, 1.4 Hz, 1H), 7.25-7.23 (m, 2H), 5.85 (s, 1H), 2.90 (dd, *J* = 8.9, 3.9 Hz, 2H), 2.60-2.56 (m, 2H), 2.55-2.37 (m, 4H), 2.29 (td, *J* = 10.5, 4.1 Hz, 1H), 2.20-1.93 (m, 4H), 1.91-1.80 (m, 4H), 1.69-1.37 (m, 6H), 0.90 (s, 3H). ^{13}C{^{1}H} NMR (100 MHz, $CDCl_3$, 25 ºC): δ 220.8, 172.4, 149.7, 139.2, 136.6, 131.4, 129.3, 126.3, 125.5, 116.0, 50.5, 48.0, 44.4, 38.1, 35.8, 34.3, 34.2, 31.6, 29.5, 29.4, 26.5, 25.6, 22.8, 21.6, 13.8. HRMS (ESI^{+}) m/z calc. for $C_{25}H_{30}O_3Na$ 401.2087 found 401.2084. The crystal suitable for SC-XRD analysis was grown from DCE and pentane solution.

(*Z*)-7-Dodecylideneoxepan-2-one (3i)

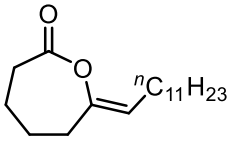

3i was isolated by Recycling Preparative GPC after silica-gel column chromatography. White solid (60.6 mg, 0.216 mmol, 54% yield). IR (ATR, ν/cm^{-1}): 2922 s, 2853 m, 1752 s, 1683 m, 1456 w, 1345 w, 1327 w, 1276 w, 1215 m, 1151 m, 1128 s, 1065 w, 1009 m, 939 w, 868 w, 831 w, 722 w, 681 w, 635 w. ^{1}H NMR (400 MHz, $CDCl_3$, 25 ºC): δ 4.99 (t, *J* = 7.8 Hz, 1H), 2.58-2.52 (m, 2H), 2.32-2.26 (m, 2H), 2.05 (q, *J* = 7.3 Hz, 2H), 1.82-1.71 (m, 4H), 1.38-1.19 (m, 18H), 0.88 (t, *J* = 6.6 Hz, 3H). ^{13}C{^{1}H} NMR (100 MHz, $CDCl_3$, 25 ºC): δ 173.4, 149.4, 117.8, 34.0, 32.9, 31.9, 29.7, 29.61, 29.59, 29.4, 29.33, 29.29, 29.1, 25.2, 22.9, 22.7, 14.1. HRMS (ESI^{+}) m/z calc. for $C_{18}H_{32}O_2Na$ 303.2295 found 303.2290.

Mixture of Dimerized Lactones

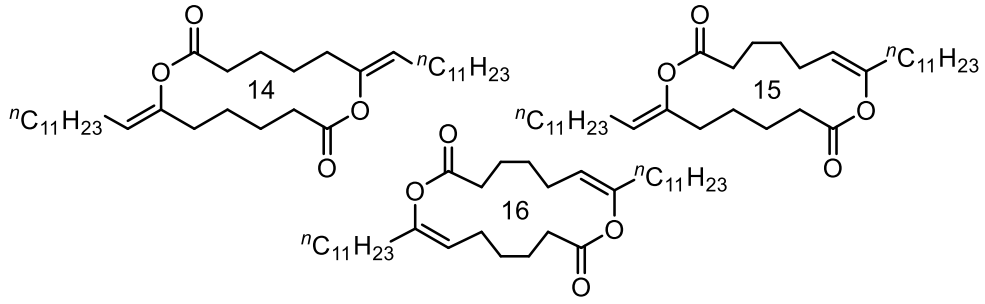

A mixture of dimerized lactones was isolated by Recycling Preparative GPC after silica-gel column chromatography. White solid (22.5 mg, 0.040 mmol, 20% yield). IR (ATR, ν/cm^{-1}): 2915 s, 2849 s, 1738 s, 1698 w, 1471 m, 1425 w, 1339 w, 1277 w, 1226 s, 1188 m, 1163 m, 1132 s, 1079 m, 1054 m, 1032 m, 1012 m, 933 w, 914 w, 858 w, 825 w, 795 w, 715 m, 655 w, 617 w, 604 w as an isomer mixture. ^{1}H NMR (400 MHz, $CDCl_3$, 25 ºC): δ 5.08-4.97 (m, 2H), 2.48-2.40 (m, 4H), 2.29-2.23 (m, 2H), 2.24-2.10 (m, 2H), 1.97-1.83 (m, 4H), 1.78-1.65 (m, 4H), 1.58-1.34 (m, 4H), 1.34-1.29 (m, 36H), 0.88 (t, *J* = 6.9 Hz, 6H) as an isomer mixture. ^{13}C{^{1}H} NMR (100 MHz, $CDCl_3$, 25 ºC): δ 171.5, 171.4, 171.3, 171.1, 149.6, 149.4, 147.7, 147.4, 117.4, 116.9, 115.3, 115.2, 33.9, 33.7, 33.6, 33.4, 33.3, 33.2, 31.9, 29.7, 29.62, 29.58, 29.55, 29.4, 29.3, 29.2, 29.0, 28.4, 28.2, 26.7, 26.6, 26.1, 25.30, 25.26, 25.0, 24.6, 24.5, 24.3, 22.7, 14.1 as an isomer mixture. HRMS (ESI$^+$) m/z calc. for $C_{36}H_{64}O_4Na$ 583.4697 found 583.4689.

(*Z*)-7-(2-Methoxyethylidene)oxepan-2-one (3j)

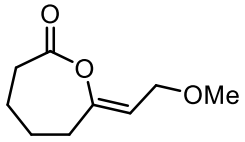

Colorless oil (54.4 mg, 0.320 mmol, 80% yield). IR (ATR, ν/cm^{-1}): 2932 w, 2864 w, 2822 w, 1752 s, 1683 m, 1438 w, 1385 w, 1346 w, 1326 w, 1276 w, 1217 m, 1195 m, 1167 m, 1124 s, 1086 m, 1050 w, 1016 s, 986 w, 959 w, 913 w, 882 w, 864 w, 819 w, 565 w. ^{1}H NMR (400 MHz, $CDCl_3$, 25 ºC): δ 5.21 (t, *J* = 6.6 Hz, 1H), 3.98 (d, *J* = 6.9 Hz, 2H), 3.31 (s, 3H), 2.63-2.53 (m, 2H), 2.38-2.29 (m, 2H), 1.87-1.75 (m, 4H). ^{13}C{^{1}H} NMR (100 MHz, $CDCl_3$, 25 ºC): δ 172.4, 152.3, 114.1, 66.1, 58.2, 34.0, 33.0, 29.2, 22.8. HRMS (ESI$^+$) m/z calc. for $C_9H_{14}O_3Na$ 193.0835 found 193.0835.

7-Methyleneoxepan-2-one (3k)[5c]

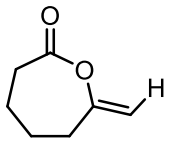

Silica-gel column chromatography for purifying **3k** resulted in significant loss of **3k**. Thus, the product was purified through pentane washing, which is reported procedure,[5c] instead of silica-gel column chromatography. A small amount of 1,2-dichloroethane was remained in the sample, since **3k** is also evaporated under reduced pressure for a long time due to its volatility. Colorless oil (47.2 mg including 2% of DCE, ca. 92% yield). ^{1}H NMR (400 MHz, $CDCl_3$, 25 ºC): δ 4.83 (s, 1H), 4.69 (s, 1H), 2.65- 2.58 (m, 2H), 2.40 2.34 (m, 2H), 1.84-1.78 (m, 4H). $^{13}C\{^{1}H\}$ NMR (100 MHz, CDCl3, 25 °C): δ 172.6, 157.7, 102.3, 33.7, 32.7, 29.1, 22.9.

3.4.5. Additional Data

3.4.5.1. Reaction Condition Screening

Experimental Procedure of Reaction Condition Screening

In a nitrogen-filled glove box, Au catalyst (2 mol%, 0.002 mmol) and anion source (2 mol%, 0.002 mmol) were placed in a screw vial containing a magnetic stirring bar. After addition of dry solvent (1.0 mL), the reaction mixture was stirred for 10 minutes. The resulting mixture was filtered through a glass-fiber pad packed into a pipette, and the filtrate was added to zinc salt (2 mol%, 0.002 mmol) and 7-phenylhept-6-ynoic acid (20.2 mg, 0.10 mmol) in a screw vial containing a magnetic stirring bar. The reaction vial was sealed with a screw-cap and taken out from the glove box. The reaction mixture was stirred at 80 ºC for 16 hours by using EYELA RCH-1000 of TOKYO RIKAKIKAI CO, LTD as an aluminum block heating reactor. After removing volatile compounds under the reduced pressure, yield was determined by ^{1}H NMR analysis using phenanthrene as an internal standard.

Experimental Procedure of Substrate Scope

In a nitrogen-filled glove box, Au catalyst (2 mol%, 0.008 mmol) and $NaBAr^{F}$ (2 mol%, 0.008 mmol) were placed in a screw vial containing a magnetic stirring bar. After addition of dry DCE (2.0 mL), the reaction mixture was stirred for 10 minutes. The resulting mixture was filtered through a glass-fiber pad packed into a pipette, and the glass-fiber pad was washed with additional dry DCE (6.0 mL) (8.0 mL in total). The filtrate was mixed with $Zn(hfac)_2 \cdot 2H_2O$ (2 mol%, 0.008 mmol) and alkyne-tethered carboxylic acids (0.40 mmol) in a screw vial containing a magnetic stirring bar. The reaction vial was sealed with a screw-cap and taken out from the glove box. The reaction mixture was stirred at 80 ºC for 16 hours. After removing volatile compounds under the reduced pressure, the crude mixture was purified by silica-gel column chromatography.

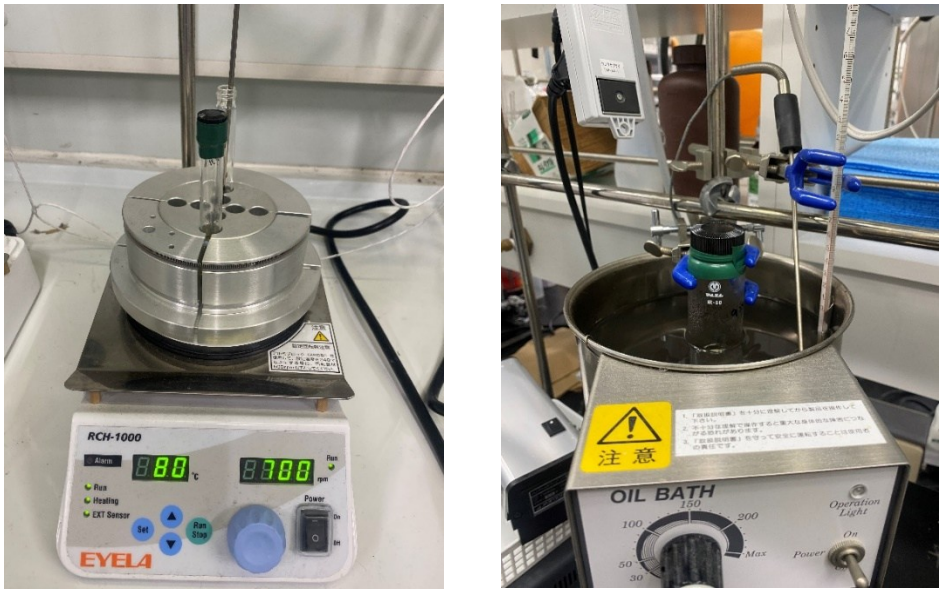

Figure 3.4. Photographic image of the catalytic reaction at 0.10 mmol scale (left) and at 0.40 mmol scale (right).

Procedure for Large Scale Experiment with 7-Phenylhept-6-ynoic Acid

In an argon-filled glove box, Au complex **1d** (45.8 mg, 2 mol%, 0.049 mmol) and $NaBAr^F$ (43.4 mg, 2 mol%, 0.049 mmol) were placed in a screw vial containing a magnetic stirring bar. After addition of dry DCE (10.0 mL), the reaction mixture was stirred for 10 minutes. The resulting mixture was filtered through a glass-fiber pad packed into a pipette, and the glass-fiber pad was washed with additional dry DCE (10.0 mL). The filtrate was mixed with $Zn(hfac)_2{\cdot}2H_2O$ (25.3mg, 2 mol%, 0.049 mmol) and 7-phenylhept-6-ynoic acid (500 mg, 2.47 mmol) in dry DCE (30.0 mL) (50 mL in total) in a 100 mL Schlenk flask containing a magnetic stirring bar. The flask was sealed with a grass cap with silicon grease and taken out from the glove box. The reaction mixture was stirred at 80 ºC for 16 hours. After removing volatiles under the reduced pressure, the crude was purified by silica-gel column chromatography to give (*Z*)-7-benzylideneoxepan-2-one (466.2 mg, 2.31 mmol) in 93% yield.

3.4.5.2. Screening of Ligands

Table 3.3. Screening of Substituents on NHC Ligands

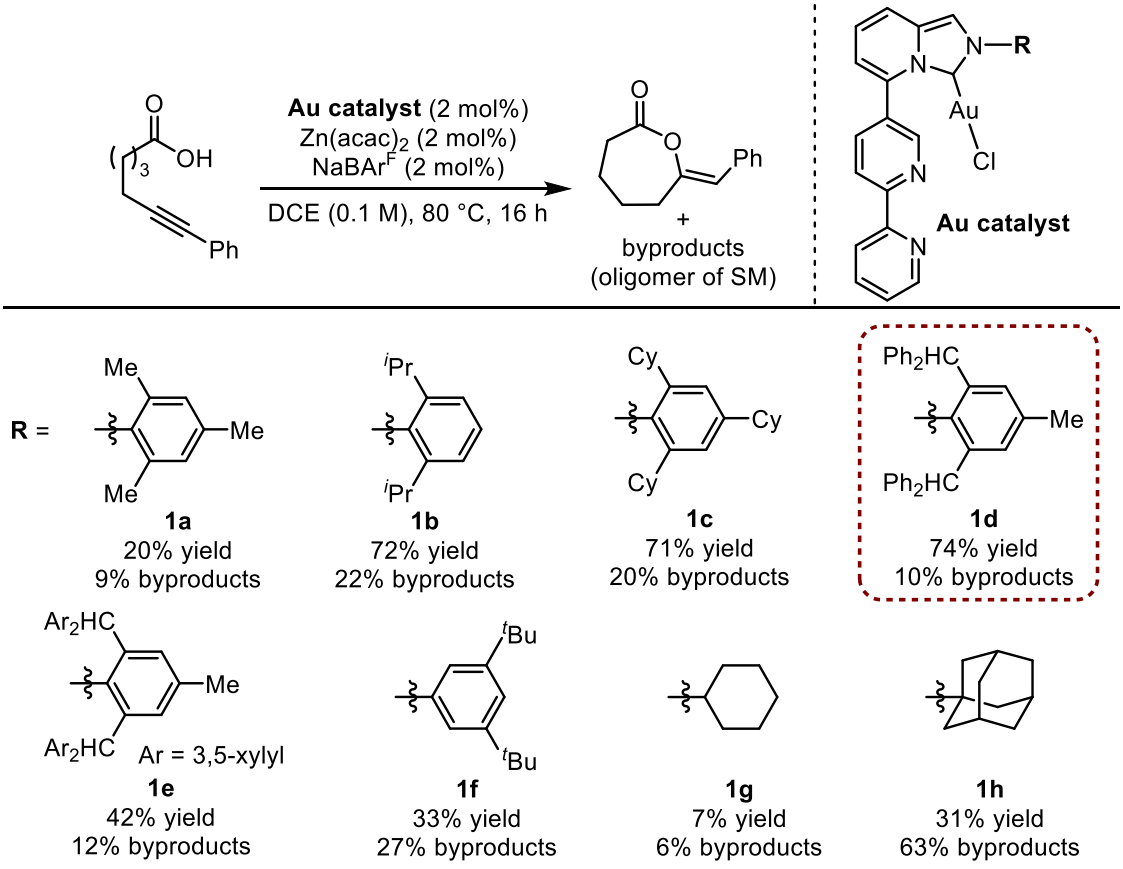

Yield was determined by ^{1}H NMR analysis using phenanthrene as an internal standard.

3.4.5.3. Discussion about Byproducts of the Cyclization

NMR analysis

^{1}H NMR charts of crude mixture showed various kinds of C(sp^2)–H signals at the 5.7-6.1 ppm region, as shown in Figure 3.5. The author assumed that these signals were arisen from intermolecular nucleophilic addition of carboxylic acid toward alkynes to form oligomers of alkyne-tethered carboxylic acid. Hence, for discussing the amount of byproduct, we used integrated spectral areas of C(sp^2)–H signals excepted with a signal of the desired product at 5.90 ppm.

ESI-MS analysis

The author analyzed the crude mixture by ESI-MS analysis for gaining insights into byproducts, as shown in Figure 3.6. The cyclization with **1h** gave large amount of

byproduct (Figure 3.5), and ESI-MS analysis of the crude mixture indicated that the mixture included oligomers of alkyne-tethered carboxylic acid, which were detected as positive molecular cations at m/z 427.19, 629.28, 831.38, and 1033.48 and negative molecular anions at m/z 605.29, 807.39, 1009.49, 1211.59, 1413.69, and 1616.79 (Figure 3.6(a)). Additionally, **1a** also gave the plausible oligomeric byproduct, which was detected as negative molecular anions at m/z 403.19, 605.29, and 807.39 (Figure 3.6(b)). Although the positive molecular cation at m/z 427.19 and the negative molecular anion at m/z 403.19 were also detected on the ESI-MS chart for isolated compound **3a** and starting material **2a** (Figure 3.6(c) and (d)), the other signals of plausible oligomeric compounds were not detected from the authentic samples. Hence, intermolecular nucleophilic addition possibly occurred as an undesired side-reaction during the cyclization to form the oligomerized byproducts.

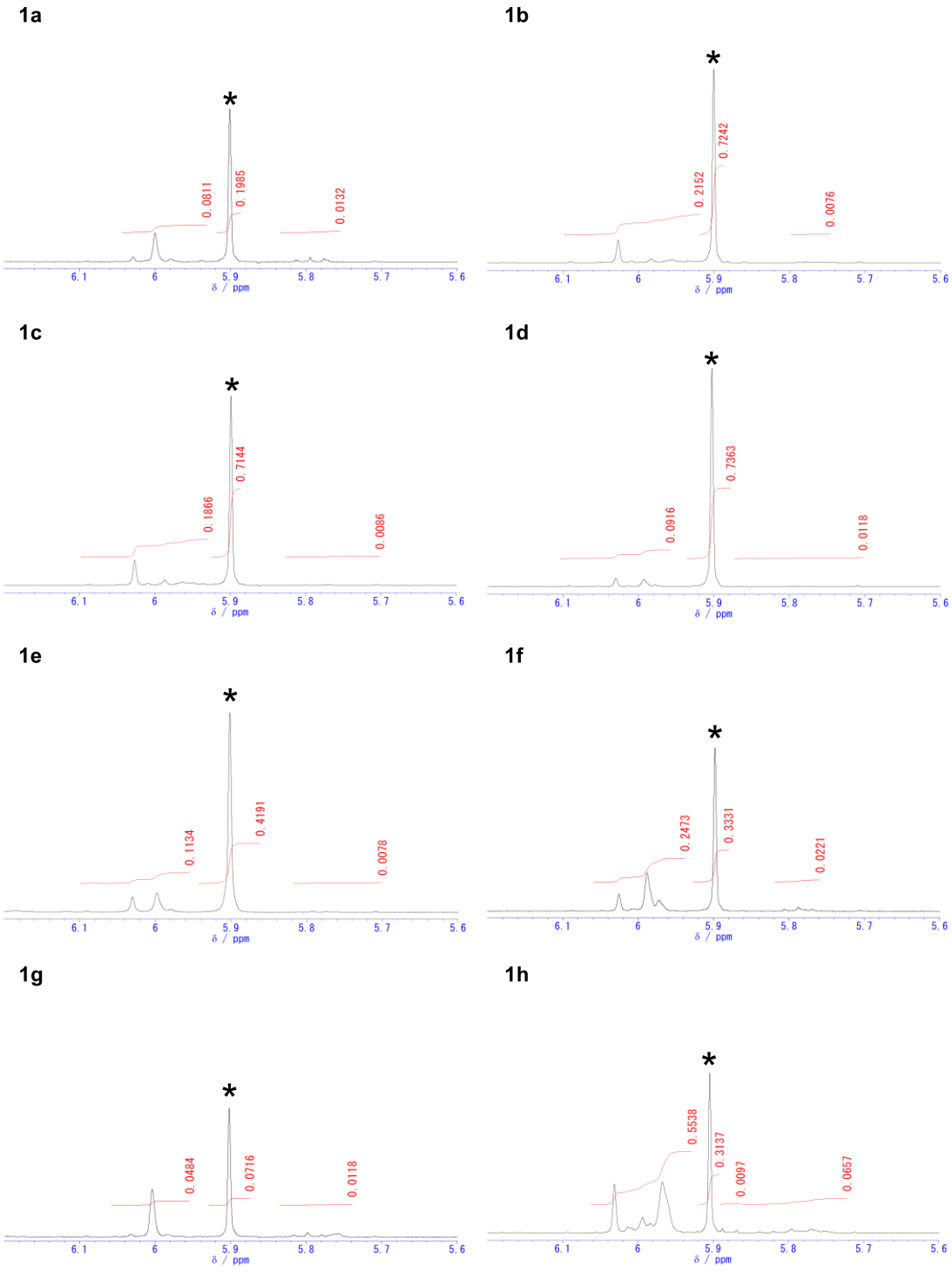

Figure 3.5. ^{1}H NMR charts for crude mixture of cyclization shown in Table 3.3. **1a**-**1h** indicates catalysts which used for the cyclization. Asterisk symbol indicates the signal of the seven-membered lactone **3a**.

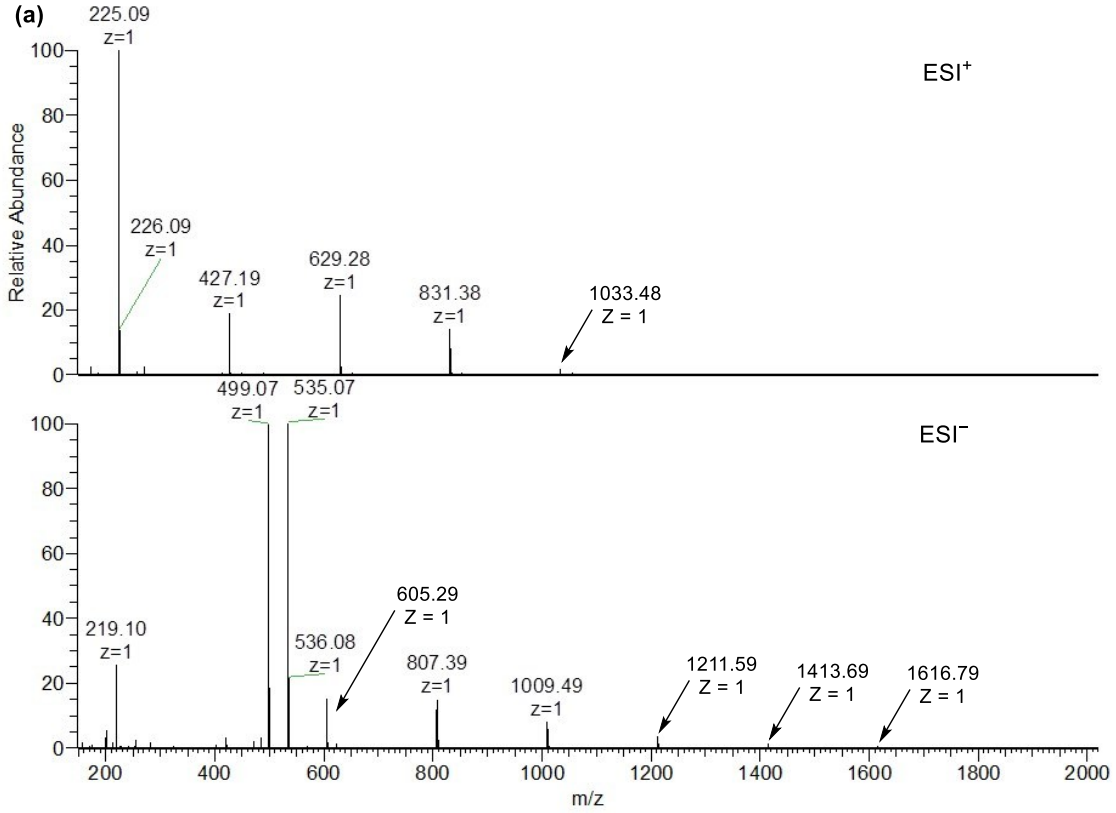
(a)
225.09
z=1
ESI+
Relative Abundance
226.09
z=1
427.19
z=1
629.28
z=1
831.38
z=1
1033.48
Z = 1
499.07
z=1
535.07
z=1
ESI−
605.29
Z = 1
219.10
z=1
536.08
z=1
807.39
z=1
1009.49
z=1
1211.59
Z = 1
1413.69
Z = 1
1616.79
Z = 1
m/z

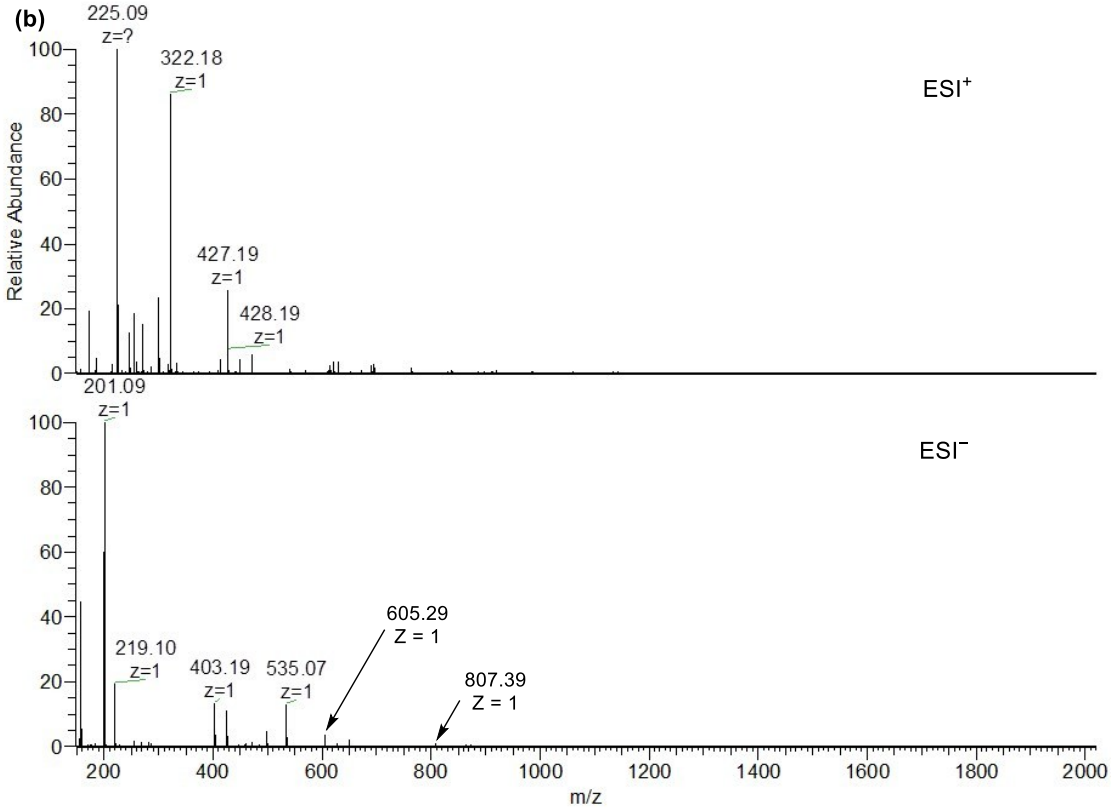
(b)
225.09
z=?
ESI+
Relative Abundance
322.18
z=1
427.19
z=1
428.19
z=1
201.09
z=1
ESI−
605.29
Z = 1
219.10
z=1
403.19
z=1
535.07
z=1
807.39
Z = 1
m/z

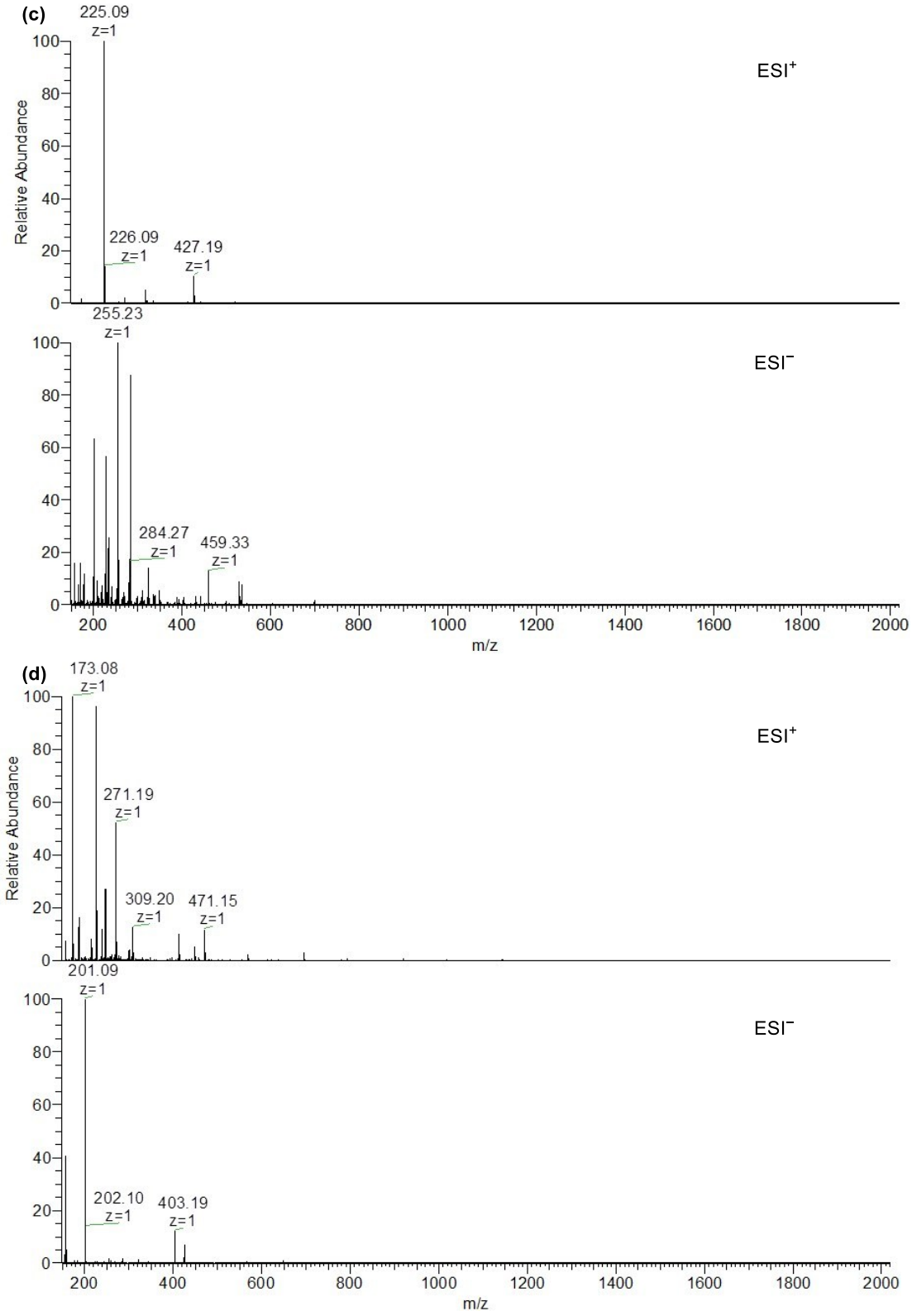

Figure 3.6 (a) ESI-MS chart for crude mixture of **1h** (R=adamantyl) on Table S1, (b) ESI-MS chart for crude mixture of **1a** (R=Mes) on Table 3.3, (c) ESI-MS chart for isolated 7-

membered lactone **3a**, (d) ESI-MS chart for alkyne-tethered carboxylic acid **2a**.

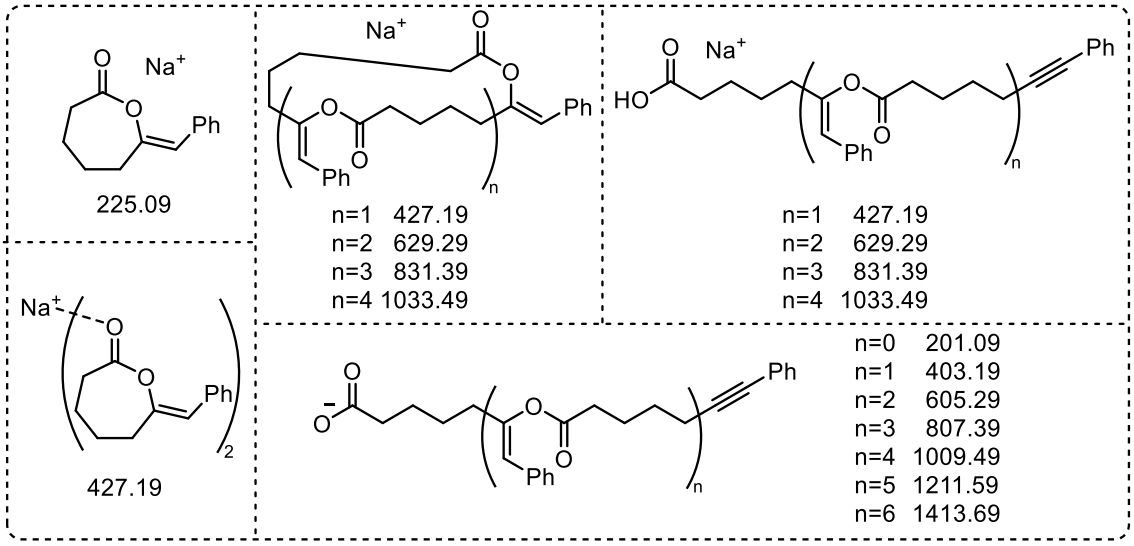

Figure 3.7. Calculated m/z values.

Comparison of ^{1}H NMR Charts

For confirming the ^{1}H NMR signals of oligomerized products, the author synthesized model products from valeric acid and 1-phenyl-1-hexyne by following our reported procedure.[13]

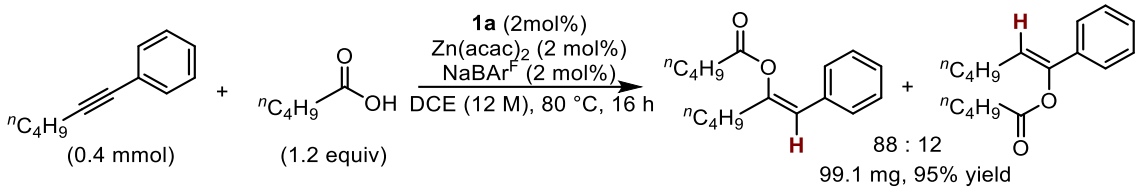

Colorless liquid. ^{1}H NMR (400 MHz, $CDCl_3$, 25 ºC): δ 7.41-7.25 (m, 4H(major)+5H(minor)), 7.19 (tt, J = 6.9, 1.4 Hz, 1H(major)), 5.97 (s, 1H(major)), 5.81 (t, J = 7.3 Hz, 1H(minor)), 2.56 (t, J = 7.3 Hz, 2H(minor)), 2.44 (t, J = 7.3 Hz, 2H(major)), 2.38 (t, J = 8.2 Hz, 2H(major)), 2.11 (q, J = 7.3 Hz, 2H(minor)), 1.79-1.69 (m, 2H(minor)), 1.69-1.60 (m, 2H(major)), 1.57-1.48 (m, 2H(major)+2H(minor)), 1.46-1.30 (m, 4H(major)+4H(minor)), 0.98-0.86 (m, 6H(major)+6H(minor)). ^{13}C{^{1}H} NMR (100 MHz, $CDCl_3$, 25 ºC): δ 171.3, 150.1, 134.6, 128.2, 126.8, 124.4, 115.7, 34.2, 34.0, 28.9, 26.9, 22.2, 22.1, 13.9, 13.7 for the major isomer; 171.5, 146.0, 135.3, 128.6, 127.9, 124.4, 118.2, 33.8, 31.1, 27.1, 25.9, 22.4, 22.3 for the minor isomer, several signals were overlapped with those of the major isomer.

The resulting ^{1}H NMR was shown in Figure 3.8. The model products showed ^{1}H NMR signals of C(sp^2)–H at 5.97 ppm as singlet and 5.81 ppm as triplet, and these chemical shifts were close to those of byproduct signals detected from the crude mixture of the cyclization catalyzed by gold complex **1a** and $Zn(acac)_2$ systems. Hence, these results also suggested that oligomers of starting material **2a** are plausible byproducts on the gold-zinc catalyzed cyclization.

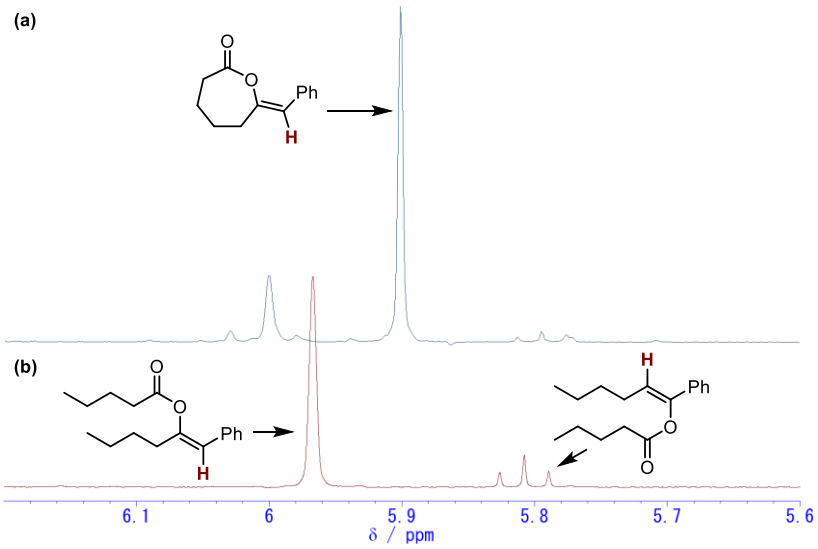

Figure 3.8. ^{1}H NMR charts for (a) crude mixture of cyclization with **1a** (R=Mes) on Table 3.3 and (b) isolated products of (*Z*)-1-phenylhex-1-en-2-yl pentanoate and (*Z*)-1-phenylhex-1-en-1-yl pentanoate.

3.4.5.4. Screening of Reaction Conditions

Screening of Zinc Salts

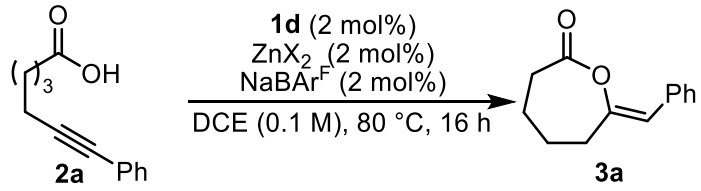

2a 3a

entry	ZnX_2	pKa of HX	yield [%]	byproducts [%]
1	$Zn(C_6F_5)_2$	23	71	13
2	$Zn(tmhd)_2$	12	70	13
3	$Zn(acac)_2$	8.9	74	10
4	$Zn(hfac)_2 \cdot 2H_2O$	4.4	92	8
5	$ZnCl_2$	-7.0	5	2
6	$Zn(OTf)_2$	-12	18	4
7	none	N/A	1	<1

Yield was determined by ^1H NMR analysis using phenanthrene as an internal standard.

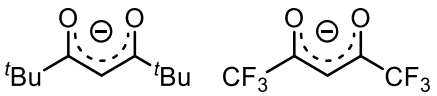

tmhd hfac

Screening of Counter Anions

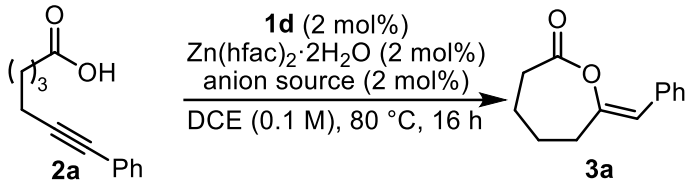

entry	anion source	yield [%]	byproducts [%]
1	$NaBAr^F$	92	8
2	$AgBF_4$	90	10
3	$AgPF_6$	87	9
4	$AgSbF_6$	81	9
5	AgOTf	30	2
6	$AgNTf_2$	17	2
7	none	n.d.	n.d.

Yield was determined by ^1H NMR analysis using phenanthrene as an internal standard. n.d. = not detected.

Screening of Solvents

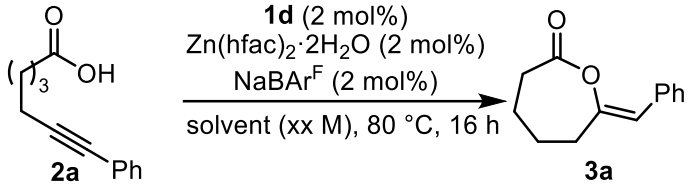

entry	solvent	xx [M]	yield [%]	byproducts [%]
1	DCE	0.1	92	8
2	DCE	0.05	95	5
3	DCE	0.2	81	10
4	$PhCF_3$	0.1	84	15
5	toluene	0.1	81	11
6[a]	1,4-dioxane	0.1	<1	<1
7	THF	0.1	n.d.	n.d.
8	CH_3CN	0.1	<1	<1

Yield was determined by ^1H NMR analysis using phenanthrene as an internal standard. n.d. = not detected. [a]The gold complex showed poor solubility after 10 minutes pre-activation.

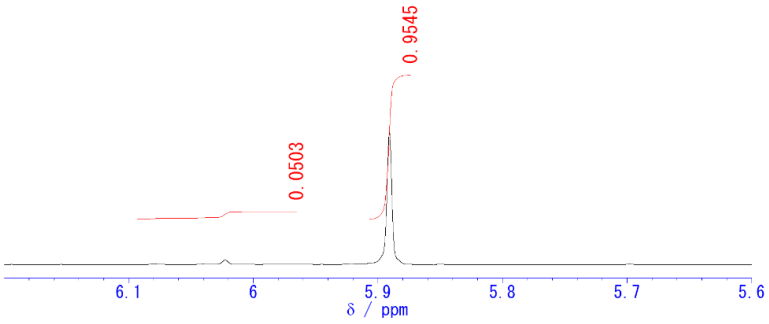

Figure 3.9. ^1H NMR charts for crude mixture of cyclization with **1d** and $Zn(hfac)_2·2H_2O$ in DCE (0.05 M), as shown in entry 2 on the above Table.

Screening of the Catalyst Loading

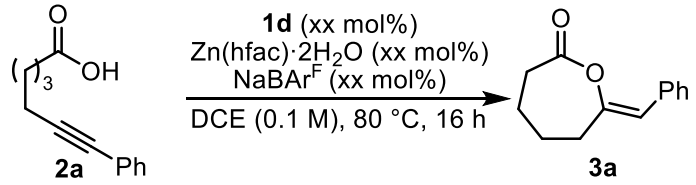

entry	xx [mol%]	yield [%]	byproducts [%]
1	2	92	8
2[a]	2	3	1
3	1	61	5
4	0.5	20	2

Yield was determined by ^{1}H NMR analysis using phenanthrene as an internal standard. [a]At 50 °C.

Cyclization of 2a with Gold(I) Complex 1i

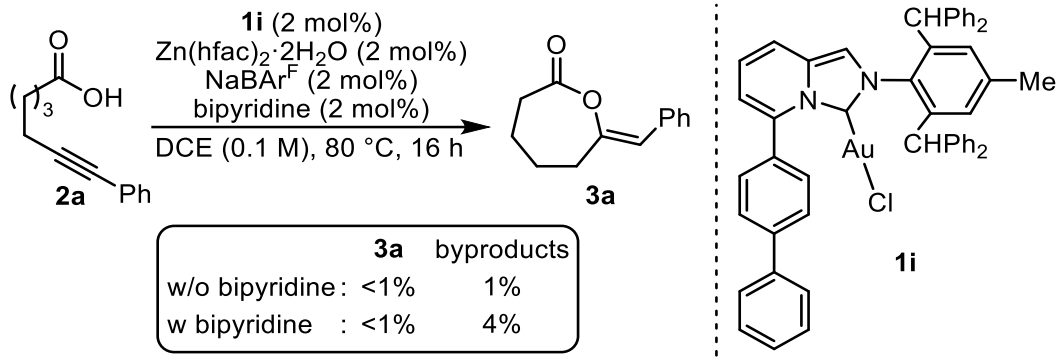

	3a	byproducts
w/o bipyridine :	<1%	1%
w bipyridine :	<1%	4%

Yield was determined by ^{1}H NMR analysis using phenanthrene as an internal standard.

3.4.5.5. NMR Spectra Based Titration

For elucidating the effects of counter anions on zinc salts, NMR spectra based titrations were conducted by using zinc salts, valeric acid, and 4,4'-di-tert-butyl-2,2'-bipyridyl ligand (dtbbpy) in $CDCl_3$ as halogenated solvent at 25 ºC.

NMR Spectra Based Titration with $Zn(hfac)_2$

$CDCl_3$ was passed throuh basic-alumina before using for avoiding contamination with HCl. $Zn(hfac)_2 \cdot 2H_2O$ (5.16 mg, 0.01 mmol) and $CDCl_3$ (0.60 mL) were added to the J-Young NMR tube. A sealed capillary tube including C_6F_6 in $CDCl_3$ was introduced into the NMR tube for the reference on ^{19}F NMR analysis. The resulting precipitation was recorded on ^1H and ^{19}F NMR analysis. After addition of dtbbpy (2.68 mg, 1.0 equiv) in $CDCl_3$ (0.10 mL), the mixture became a homogeneous solution. Addition of valeric acid was repeated to add the 50 equivalents of valeric acid in total, which was monitored by ^1H and ^{19}F NMR analysis. These results are shown in Figure 3.10-3.12. All the peaks were assigned from the reference point of a residual solvent signal for $CHCl_3$ (7.26 ppm) for ^1H NMR analysis and C_6F_6 (-164.9 ppm) for ^{19}F NMR analysis, respectatively.

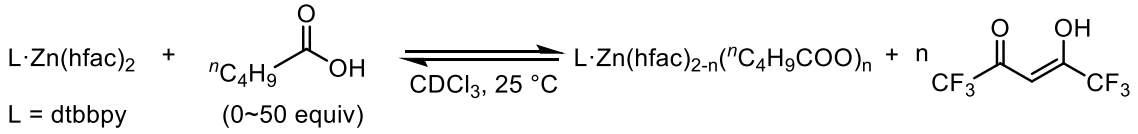

A C(sp^2)–H signal and a CF_3 signal for hexafluoroacetylacetonate of $L \cdot Zn(hfac)_2$ were observed at 5.96 ppm and -79.7 ppm in ^1H and ^{19}F NMR analysis, and a C(sp^2)–H signal and a CF_3 signal for authentic hexafluoroacetylacetone were observed at 6.39 ppm and -79.2 ppm, respectively. After addition of 1-50 equivalents of valeric acid, the corresponding C(sp^2)–H signal and CF_3 signal of hexafluoroacetylacetonate were virtually unchanged on the ^1H and ^{19}F NMR analysis. These results indicated that ligand exchange from hexafluoroacetylacetonate to carboxylate is unfavorable in the $CDCl_3$ solution. Hence, hexafluoroacetylacetonate might be incorporated as a ligand of zinc site during the cyclization with gold-zinc cooperative catalysts.

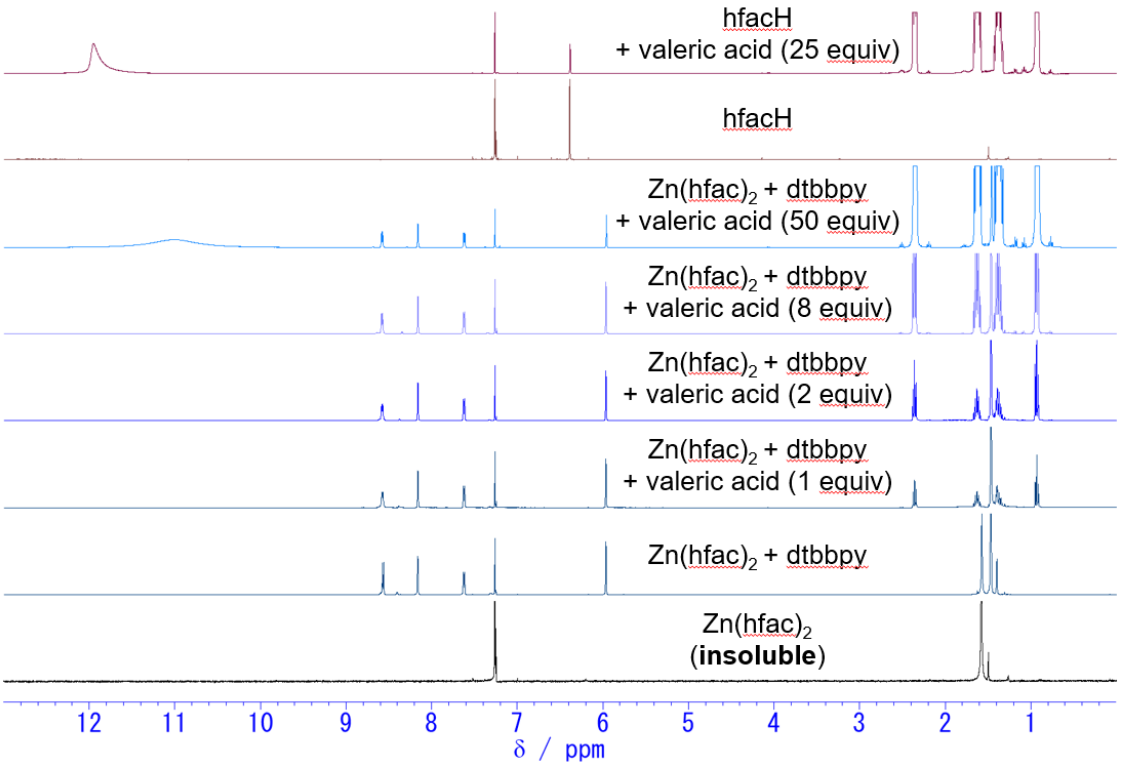

Figure 3.10. ^{1}H NMR charts for the titration with $Zn(hfac)_2$.

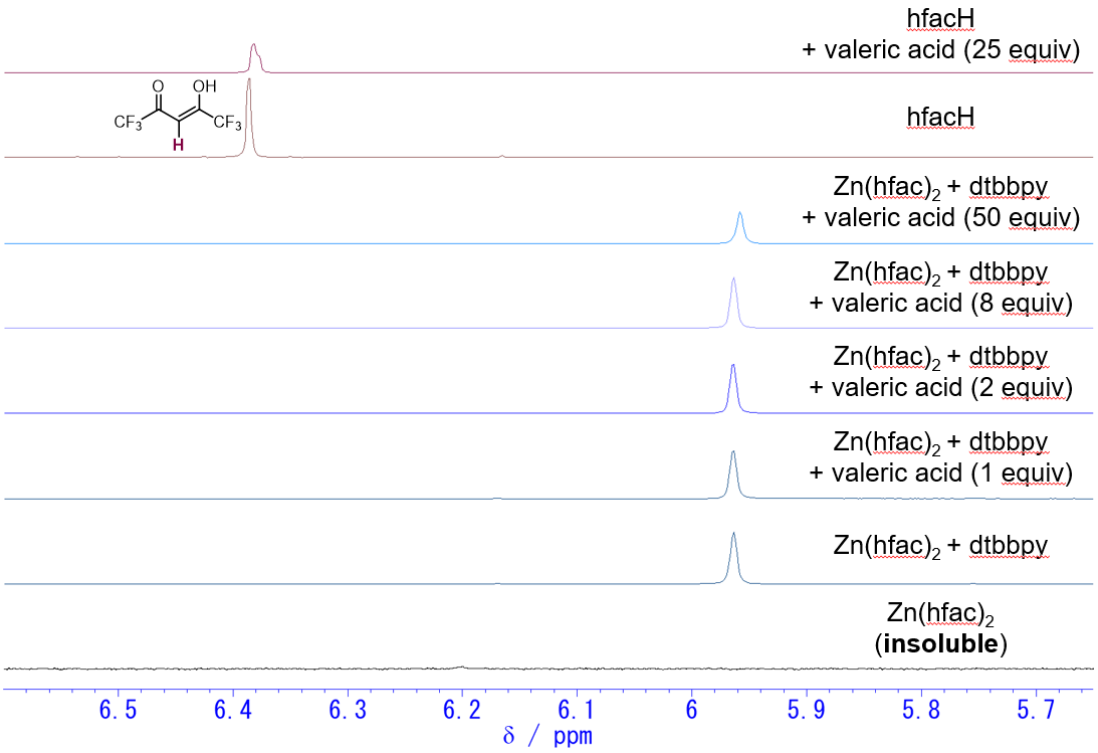

Figure 3.11. ^{1}H NMR charts for the titration with $Zn(hfac)_2$.

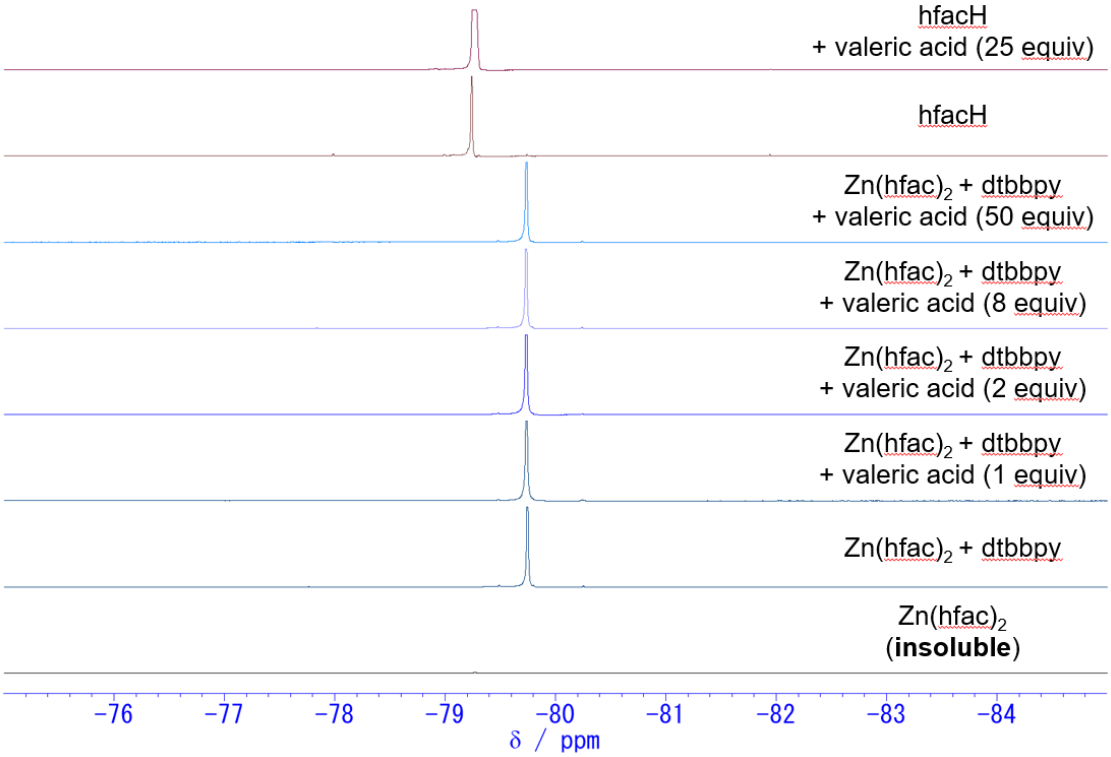

Figure 3.12. ^{19}F NMR charts for the titration with Zn(hfac)$_2$.

NMR Spectra Based Titration with $Zn(acac)_2$

$CDCl_3$ was passed throuh basic-alumina before using for avoiding contamination with HCl. $Zn(acac)_2$ (2.64 mg, 0.01 mmol) and $CDCl_3$ (0.60 mL) were added to the J-Young NMR tube. The resulting solution was recorded on ^1H NMR analysis. After addition of dtbbpy (2.68 mg, 1.0 equiv) in $CDCl_3$ (0.10 mL), the solution was monitored by ^1H NMR analysis. Addition of valeric acid was repeated to add the 50 equivalents of valeric acid in total, which was monitored by ^1H NMR analysis. These results are shown in Figure 3.13-3.14. All the peaks were assigned from the reference point of a residual solvent signal for $CHCl_3$ (7.26 ppm).

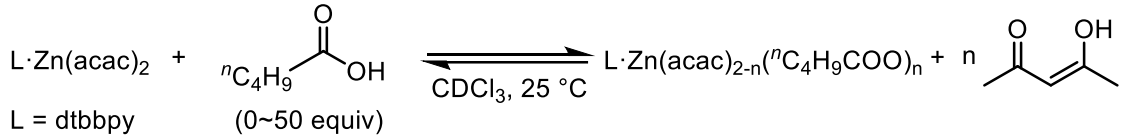

A C(sp^2)–H signal for acetylacetonate on L·$Zn(acac)_2$ was observed at 5.24 ppm on ^1H NMR analysis, and a C(sp^2)–H signal (for enol-form) and C(sp^3)–H signal (for keto-form) of authentic acetylacetone were observed at 5.50 ppm and 3.59 ppm, respectively. After addition of 1 equivalent of valeric acid, acetylacetone was detected in ^1H NMR analysis, and the corresponding C(sp^2)–H signal of acetylacetonate was decreased and shifted. At this time, dtbbpy zinc complex different from L·$Zn(acac)_2$ was detected at 8.88, 8.05, and 7.52 ppm, indicating that zinc carboxylate complex might be formed. After addition of 50 equivalents of valeric acid, acetylacetonate was fully converted to acetylacetone. These results indicated that acetylacetonate ligand quickly exchange to carboxylate ligand in the $CDCl_3$ solution. Hence, zinc carboxylate is plausibly worked as the basic site during the cyclization with gold-zinc cooperative catalysts.

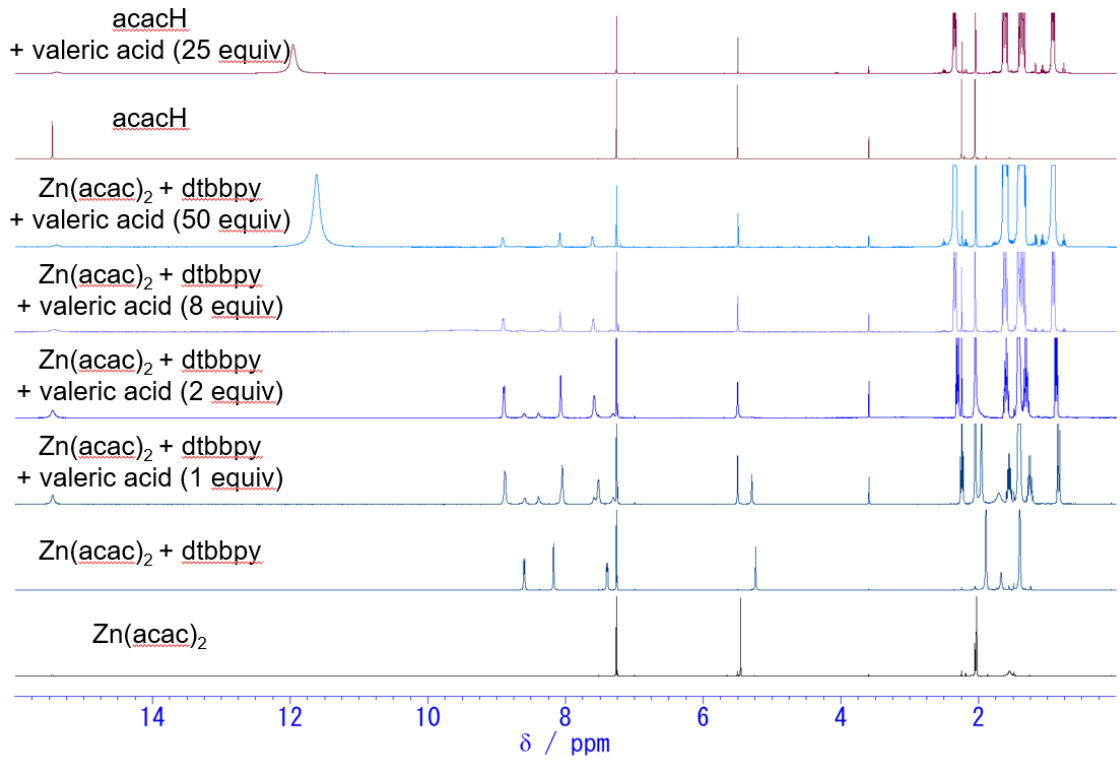

Figure 3.13. ^{1}H NMR charts for the titration with $Zn(acac)_2$.

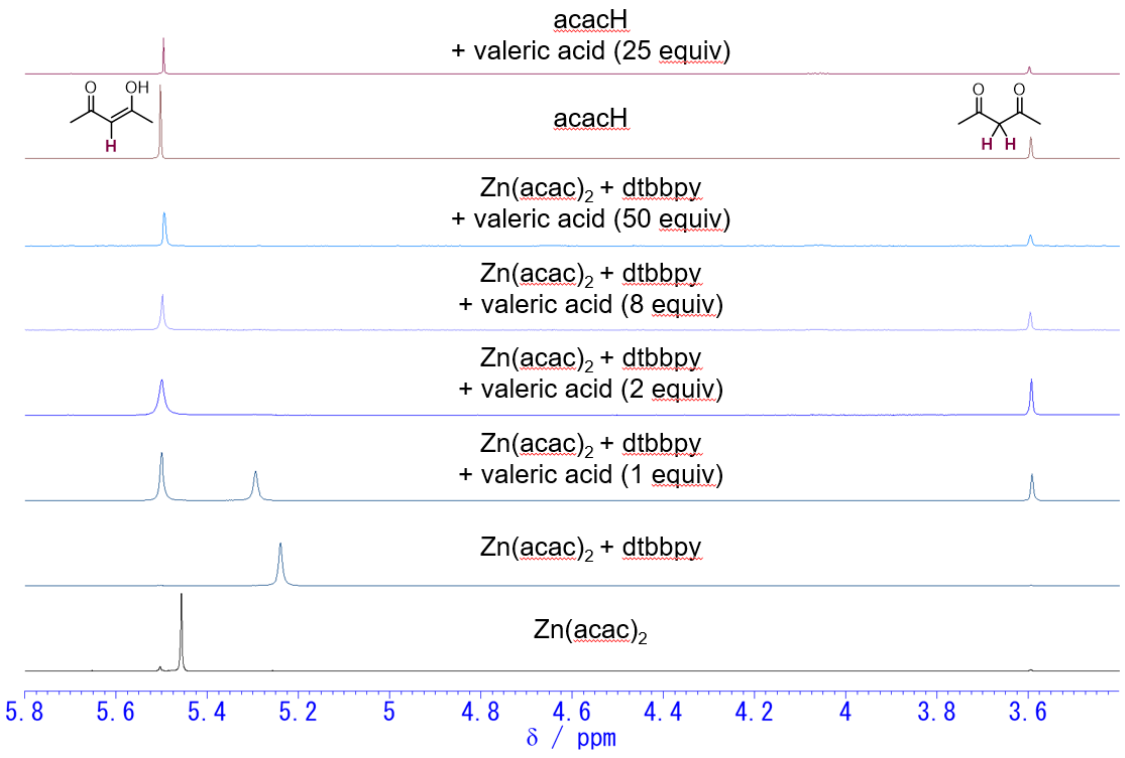

Figure 3.14. ^{1}H NMR charts for the titration with $Zn(acac)_2$.

3.4.5.6. XRD Analysis

General Procedure

A suitable crystal was mounted with liquid paraffin on a MiTeGen MicroMounts and transferred to the goniometer in a nitrogen stream at 133(2) K. Measurement was made on a RIGAKU XtaLAB Synergy-DW system with 1.2 kW PhotonJet-DW microfocus rotating anode using graphite monochromated Mo-K_a radiation (λ = 0.71073 Å) and HyPix-6000HE detector. Cell parameters were determined and refined, and raw frame data were integrated using CrysAlis^{Pro} (Agilent Technologies, 2010). The structures were solved by direct methods with SHELXT[31] and refined by full-matrix least-squares techniques against F^2 with SHELXL-2018/3[32] by using Olex2 software package.[33] The non-hydrogen atoms were anisotropically refined, and hydrogen atoms were placed using AFIX instructions. Crystal data and structure refinement parameters are in Table 3.4. The ORTEP-3 program was used to draw the molecule structures.[34]

ORTEP Drawing

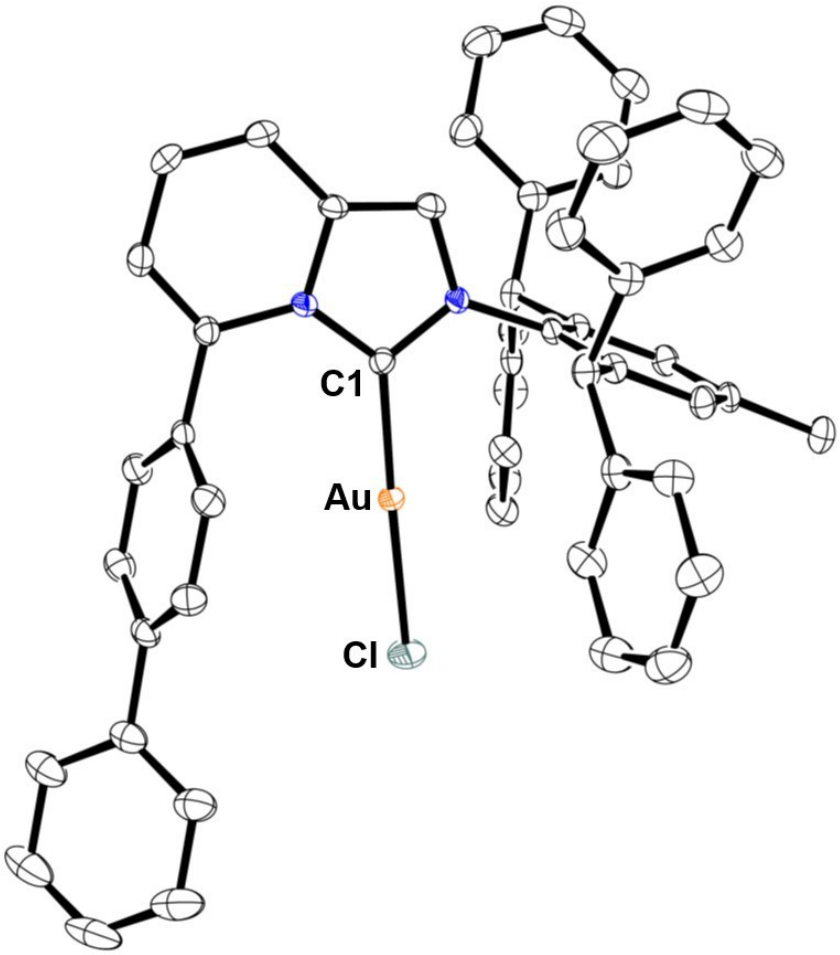

Figure 3.15. ORTEP drawing of **1i** showing 50% probability thermal ellipsoids. All hydrogen atoms and solvent molecules were omitted for clarity.

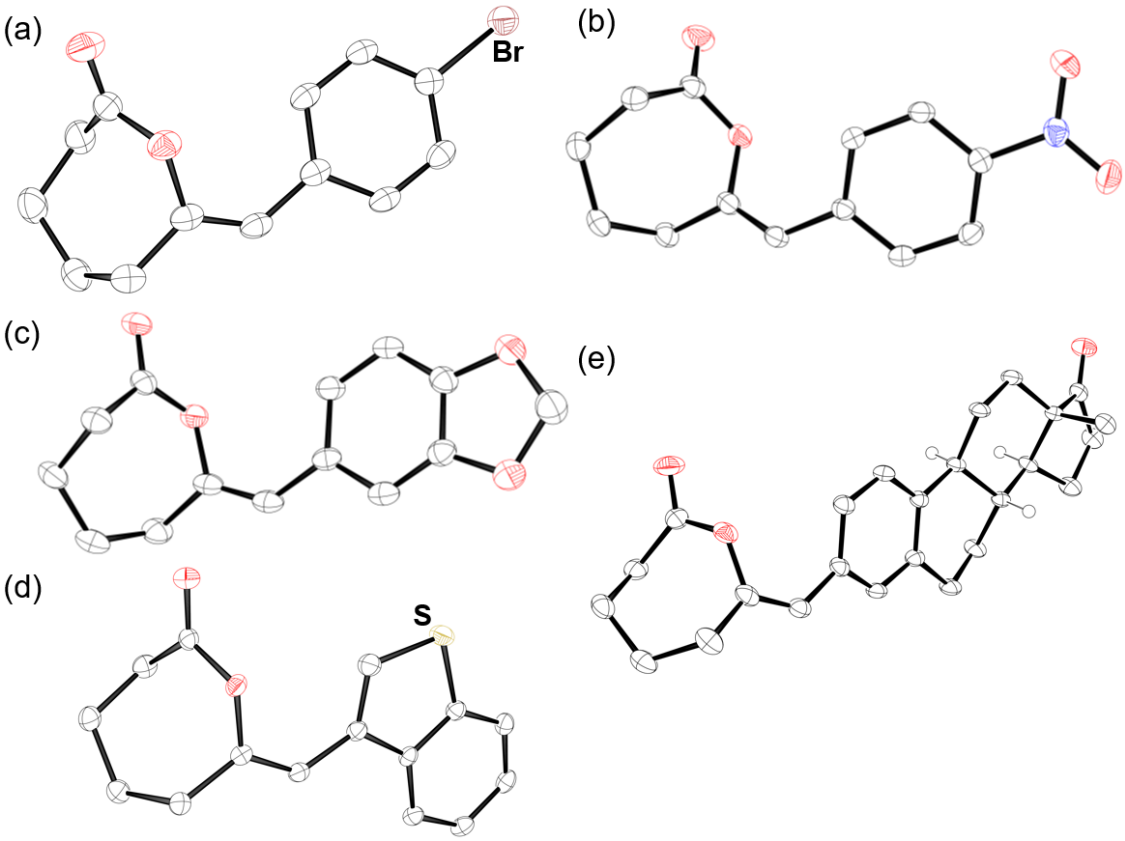

Figure 3.16. ORTEP drawing of (a) **3b**, (b) **3c**, (c) **3e**, (d) **3g**, and (e) **3h** showing 50% probability thermal ellipsoids. Selected hydrogen atoms were omitted for clarity.

Table 3.4. Crystal Data and Structure Refinement Parameters.

	1d	**1i**	**3b**	**3c**
empirical formula	$C_{58}H_{54}AuClN_4O_2$	$C_{54}H_{44}AuCl_5N_2$	$C_{13}H_{13}BrO_2$	$C_{13}H_{13}NO_4$
CCDC number	2267315	2267316	2267317	2267318
formula weight	1071.47	1095.13	281.14	247.24
crystal system	triclinic	monoclinic	monoclinic	monoclinic
space group	*P*-1 (#2)	$P2_1/c$ (#14)	$P2_1/c$ (#14)	$P2_1/c$ (#14)
a, Å	10.0433(2)	17.3848(6)	11.6328(3)	8.1517(4)
b, Å	14.9410(2)	11.16090(10)	12.4431(3)	11.4677(5)
c, Å	16.0517(2)	32.6433(12)	8.2405(2)	12.8249(5)
α, deg.	89.7100(10)	-	-	-
β, deg.	78.7720(10)	132.811(6)	99.629(3)	99.367(4)
γ, deg.	87.3820(10)	-	-	-
V, Å^3	2360.08(6)	4646.5(4)	1175.99(5)	1182.90(9)
Z	2	4	4	4
D_{calcd}, g/cm^{-3}	1.508	1.565	1.588	1.388
radiation, mm^{-1}	Mo-*K*α: 0.71073	Mo-*K*α: 0.71073	Mo-*K*α: 0.71073	Mo-*K*α: 0.71073
T, K	133(2)	133(2)	133(2)	133(2)
crystal size, mm	0.18 × 0.18 × 0.04	0.20 × 0.20 × 0.04	0.15 × 0.10 × 0.03	0.13 × 0.13 × 0.02
θ range for data collection (deg.)	4.138 to 58.658	4.362 to 62.152	4.83 to 61.92	5.064 to 61.834
no. of reflections measured	46648	86763	21866	16487
unique data (R_{int})	11133 (0.0505)	12693 (0.0392)	3110 (0.0369)	3126 (0.0310)
data/restraints/parameters	11133 / 0 / 596	12693/ 0 / 560	3110 / 0 / 145	3126 / 0 / 163
*R*1 ($I > 2.0\sigma(I)$)	0.0286	0.0251	0.0278	0.0373
*wR*2 ($I > 2.0\sigma(I)$)	0.0654	0.0505	0.0504	0.0900
*R*1 (all data)	0.0362	0.0353	0.0421	0.0508
*wR*2 (all data)	0.0675	0.0528	0.0533	0.0947
GOF on F^2	1.054	1.051	1.034	1.046

a) $R1 = (\Sigma||Fo|-|Fc||)/(\Sigma|Fo|)$ b) $wR2 = [\{\Sigma w(Fo^2-Fc^2)^2\}]/(\Sigma w(Fo^4)\}]^{1/2}$

	3e	**3g**	**3h**
empirical formula	$C_{14}H_{14}O_4$	$C_{15}H_{14}O_2S$	$C_{25}H_{30}O_3$
CCDC number	2267319	2267320	2267321
formula weight	246.25	258.32	378.49
crystal system	monoclinic	monoclinic	orthorhombic
space group	$P2_1$ (#4)	$P2_1/n$ (#14)	$P2_12_12$ (#18)
a, Å	6.4657(4)	10.6234(3)	26.3801(10)
b, Å	8.3424(5)	6.6515(2)	11.8259(4)
c, Å	11.1419(8)	17.8964(5)	6.4981(2)
α, deg.	-	-	-
β, deg.	96.230(7)	91.390(3)	-
γ, deg.	-	-	-
V, Å^3	597.44(7)	1264.22(6)	2027.20(12)
Z	2	4	4
D_{calcd}, g/cm^{-3}	1.369	1.357	1.240
radiation, mm^{-1}	Mo-*K*α: 0.71073	Mo-*K*α: 0.71073	Mo-*K*α: 0.71073
T, K	133(2)	133(2)	133(2)
crystal size, mm	0.20 × 0.05 × 0.02	0.20 × 0.15 × 0.06	0.20 × 0.12 × 0.02
θ range for data collection (deg.)	6.114 to 61.868	4.412 to 61.52	4.626 to 61.814
no. of reflections measured	7357	15450	23013
unique data (R_{int})	2758 (0.0396)	3363 (0.0302)	5224 (0.0727)
data/restraints/parameters	2758 / 1 / 163	3363 / 0 / 163	5224 / 0 / 254
*R*1 (*I* > 2.0σ(*I*))	0.0447	0.0321	0.0565
*wR*2 (*I* > 2.0σ(*I*))	0.1006	0.0820	0.1262
*R*1 (all data)	0.0607	0.0388	0.0711
*wR*2 (all data)	0.1060	0.0851	0.1328
GOF on F^2	1.045	1.056	1.021

a) $R1 = (\Sigma||Fo|-|Fc||)/(\Sigma|Fo|)$ b) $wR2 = [\{\Sigma w(Fo^2-Fc^2)^2\}]/(\Sigma w(Fo^4)\}]^{1/2}$

3.4.6. Computational Data

General Procedure

All geometry optimizations and single-point energy calculations were performed by Gaussian 16 package.[23] The geometry optimizations of all structures were conducted at the M06 functional in conjunction with the SDD (for Au, Zn) and 6-31G(d) (for others) basis set. Frequency analyses were performed at the same level of theory for geometry optimizations, in which the thermal free energy corrections were provided. All the transition states have the single imaginary frequency, and all the optimized structures as minima have no imaginary frequency. The transition states were traced with intrinsic reaction coordinate (IRC) analyses by using Global Reaction Route Mapping (GRRM) program (ver. 20) to confirm the connection of the reaction pathway. Further single-point energy calculations were performed at the M06 functional in conjunction with the SDD (for Au, Zn) and 6-311+G(d,p) (for others) basis set with the solvation model (SMD: dichloroethane) to evaluate solution phase electronic energies. The solution phase Gibbs free energies (G_{sol}) at 298.15 K (25 ºC) were obtained from $G_{sol} = E + G_{corr}$, wherein the solvation electronic energies (E) were given from single-point energy calculations at the M06/SDD,6-311+G(d,p)/SMD level and gas-phase thermal free energy corrections (G_{corr}) were given from frequency analyses at the M06/SDD,6-31G(d) level. For the purpose of discussion, relative Gibbs free energies (ΔG_{sol}) were calculated from $\Delta G_{sol} = \Sigma G_{sol}$ for products – ΣG_{sol} for reactants. IGMH was described with Multiwfn program[25] after preparing wfn file at the M06/SDD,6-31G(d) level of theory by Gaussian 16 package. 3D models for IGMH were described by VMD software.[35] 3D models of optimized structures were described by CYLview20. [36]

Summary of Energies

Structure Name	solvation electronic energies [Hartree]	thermal free energy corrections [Hartree]	solution phase Gibbs free energies [Hartree]
Int-1	-4390.186319	0.775285	-4389.411034
Int-2	-5044.192111	1.000858	-5043.191253
Int-3	-4103.022039	0.934325	-4102.087714
TS_{3-4}	-4102.992761	0.931962	-4102.060799
Int-4	-4103.001119	0.934528	-4102.066591
Int-5	-4757.003577	1.161116	-4755.842461
TS_{5-6}	-4756.994992	1.156202	-4755.838790
Int-6	-4757.024406	1.160754	-4755.863652
2a·dimer	-1307.952536	0.419349	-1307.533187
hfacH	-941.135145	0.039572	-941.095573

3.5 References

[1] Synthetic methods for lactones, a) A. Parenty, X. Moreau, and J.-M. Campagne, *Chem. Rev.* **2006**, *106*, 911–939; b) W. Liu, N. Winssinger. *Synthesis* **2021**, *53*, 3977–3990; c) S. K. Sartori, M. A. N. Diaz, G. Diaz-Muñoz, *Tetrahedron* **2021**, *84*, 132001; d) Z.-K. Liu, Y. Gao, X.-Q. Hu, *Catal. Sci. Technol.* **2021**, *11*, 6931–6946.

[2] a) N. T. Patil, R. D. Kavthe, V. S. Shinde, *Tetrahedron* **2012**, *68*, 8079–8146; b) J. Francos, V. Cadierno, *Catalysts* **2017**, *7,* 328; c) V. Cadierno, *Catalysts* **2020**, *10*, 1206; d) S. Bhakta, T. Ghosh, *Asian J. Org. Chem.* **2021**, *10*, 496–505.

[3] Recent examples, a) B. Lin, T. Yang, D. Zhang, Y. Zhou, L. Wu, J. Qiu, G.-Q. Chen, C.-M. Che, X. Zhang, *Angew. Chem. Int. Ed.* **2022**, 61, e202201739; b) Q.-A. Huang, T. Ikeda, K. Haruguchi, S. Kawai, E. Yamamoto, H. Murayama, T. Ishida, T. Honma, M. Tokunaga, *Appl. Catal. A: Gen.* **2022**, *643*, 118765; c) V. K. Rawat, K. Higashida, M. Sawamura, *Adv. Synth. Catal.* **2021**, *363*, 1631–1637; d) C. Ruiz-Zambrana, A. Gutiérrez-Blanco, S. Gonell, M. Poyatos, E. Peris, *Angew. Chem. Int. Ed.* **2021**, *60*, 20003–20011; e) B. Lin, X. Zhang, C.-Y. Zhou, C.-M. Che, *Org. Chem. Front.* **2021**, *8*, 1216-1222; f) S. Gonell, J. N. H. Reek, *ChemCatChem* **2019**, *11*, 1458–1464; g) M. B. Kindervater, J. F. Binder, S. R. Baird, C. M. Vogels, S. J. Geier, C. L. B. Macdonald, S. A. Westcott, *J. Organomet. Chem.* **2019**, *880*, 378–385; h) T. D. Ho, M. P. Schramm, *Eur. J. Org. Chem.* **2019**, 5678–5684.

[4] R. L. Reyes, T. Iwai, M. Sawamura, *Chem. Rev*. **2021**, *121*, 8926–8947.

[5] Gold-catalyzed cyclization, a) H. Harkat, J.-M. Weibel, P. Pale, *Tetrahedron Lett*. **2006**, *47*, 6273–6276; b) H. Harkat, A. Y. Dembelé, J.-M. Weibel, A. Blanc, P. Pale, *Tetrahedron* **2009**, *65*, 1871–1879; c) D. Gasperini, L. Maggi, S. Dupuy, R. M. P. Veenboer, D. B. Cordes, A. M. Z. Slawin, S. P. Nolan, *Adv. Synth. Catal.* **2016**, *358*, 3857–3862; d) N. V. Tzouras, A. Gobbo, N. B. Pozsoni, S. G. Chalkidis, S. Bhandary, K. V. Hecke, G. C. Vougioukalakis, S. P. Nolan, *Chem. Commun*. **2022**, *58*, 8516–8519; e) Q.-A. Huang, T. Ikeda, K. Haruguchi, S. Kawai, E. Yamamoto, H. Murayama, T. Ishida, T. Honma, M. Tokunaga, *Applied Catalysis A, General* **2022**, *643*, 118765; f) L. Deiana, E. Badali, A. A. Rafi, C.-W. Tai, J.-E. Bäckvall, A. Córdova, *ACS Catal.* **2023**, *13*, 10418–10424.

[6] Silver and gold-catalyzed cyclization, R. Nolla-Saltiel, E. Robles-Marín, S. Porcel, *Tetrahedron Lett*. **2014**, *55*, 4484–4488.

[7] Copper-catalyzed cyclization, G. Chaudhuria, N. G. Kundu, *J. Chem. Soc., Perkin Trans*. *1*, **2000**, 775–779.

[8] Mercury-catalyzed cyclization, H. Imagawa, Y. Fujikawa, A. Tsuchihiro, A.

Kinoshita, T. Yoshinaga, H. Takao, M. Nishizawa, *Synlett* **2006**, *4*, 639–641.

[9] Platinum-catalyzed cyclization, D. Ke, N. Á. Espinosa, S. Mmallet-Ladeira, J. Monot, B. Martin-Vaca, D. Bourissou, *Adv. Synth. Catal.* **2016**, *358*, 2324–2331.

[10] Palladium-catalyzed cyclization, a) T. Wakabayashi, Y. Ishii, K. Ishikawa, M. Hidai, *Angew. Chem., Int. Ed.* **1996**, *35*, 2123–2124. b) N. Nebra, J. Monot, R. Shaw, B. Martin-Vaca, D. Bourissou, *ACS Catal*. **2013**, *3*, 2930–2934; c) N. Á. Espinosa-Jalapa, D. Ke, N. Nebra, L. L. Goanvic, S. Mallet-Ladeira, J. Monot, B. Martin-Vaca, D. Bourissou, *ACS Catal*. **2014**, *4*, 3605–3611.

[11] Iridium-catalyzed cyclization, Y. Huang, X. Zhang, X.-Q. Dong, X. Zhang, *Adv. Synth. Catal.* **2020**, *362*, 782–788.

[12] Ruthenium-catalyzed cyclization, a) M. Jiménez-Tenorio, M. C. Puerta, P. Valerga, F. J. Moreno-Dorado, F. M. Guerra, G. M. Massanet, *Chem. Commun.* **2001**, 2324–2325. b) C. K. Barik, M. E. Tessensohn, R. D. Webster, W. K. Leong, *J. Organomet. Chem.* **2019**, 889, 40–44.

[13] V. K. Rawat, K. Higashida, M. Sawamura, *ACS Catal.* **2022**, *12*, 8325–8330.

[14] a) A. Ochida, H. Ito, and M. Sawamura, *J. Am. Chem. Soc.* **2006**, *128*, 16486–16487; b) T. Iwai, H. Okochi, H. Ito, M. Sawamura, *Angew. Chem., Int. Ed*. **2013**, *52*, 4239–4242; c) T. Iwai, M. Ueno, H. Okochi, and M. Sawamura, *Adv. Synth. Catal.* **2018**, *360*, 670–675.

[15] For the purpose of discussion, yield of byproducts was calculated by using integrated spectral areas of C(sp^2)–H signals observed in 5.7-6.1 ppm, excepted with a signal of the desired product at 5.90 ppm. The detailed information was described in the Experimental Section.

[16] K. P. Butin, I. P. Beletskaya, A. N. Kashin, O. A. Reutov, *J. Organomet. Chem.* **1967**, *10*, 197–210.

[17] H. E. Zaugg, A. D. Schaefer, *J. Am. Chem. Soc.* **1965**, *87*, 1857–1866.

[18] R. W. Taft Jr., E. H. Cook, *J. Am. Chem. Soc.* **1959**, *81*, 46–54.

[19] E. Raamat, K. Kaupmees, G. Ovsjannikov, A. Trummal, A. Kütt, J. Saame, L. Koppel, I. Kaljurand, L. Lipping, T. Rodima, V. Pihl, I. A. Koppel, I. Leito, *J. Phys. Org. Chem.* **2013**, *26*, 162–170.

[20] A. D. Headley, S. D. Starnes, L. Y. Wilson, G. R. Famini, *J. Org. Chem.* **1994**, *59*, 8040–8046.

[21] CCDC Deposition Numbers 2267315 (for **1d**), 2267316 (for **1i**), 2267317 (for **3b**), 2267318 (for **3c**), 2267319 (for **3e**), 2267320 (for **3g**), and 2267321 (for **3h**).

[22] X.-C. Li, M. R. Jacob, H. N. ElSohly, D. G. Nagel, T. J. Smillie, L. A. Walker, A. M. Clark, *J. Nat. Prod.* **2003**, *66*, 1132–1135.

[23] Gaussian 16, Revision C.01, G. W. T. M. J. Frisch, H. B. Schlegel, G. E. Scuseria, M. A. Robb, J. R. Cheeseman, G. Scalmani, V. Barone, G. A. Petersson, H. Nakatsuji, X. Li, M. Caricato, A. V. Marenich, J. Bloino, B. G. Janesko, R. Gomperts, B. Mennucci, H. P. Hratchian, J. V. Ortiz, A. F. Izmaylov, J. L. Sonnenberg, D. Williams-Young, F. Ding, F. Lipparini, F. Egidi, J. Goings, B. Peng, A. Petrone, T. Henderson, D. Ranasinghe, V. G. Zakrzewski, J. Gao, N. Rega, G. Zheng, W. Liang, M. Hada, M. Ehara, K. Toyota, R. Fukuda, J. Hasegawa, M. Ishida, T. Nakajima, Y. Honda, O. Kitao, H. Nakai, T. Vreven, K. Throssell, J. A. Montgomery, Jr., J. E. Peralta, F. Ogliaro, M. J. Bearpark, J. J. Heyd, E. N. Brothers, K. N. Kudin, V. N. Staroverov, T. A. Keith, R. Kobayashi, J. Normand, K. Raghavachari, A. P. Rendell, J. C. Burant, S. S. Iyengar, J. Tomasi, M. Cossi, J. M. Millam, M. Klene, C. Adamo, R. Cammi, J. W. Ochterski, R. L. Martin, K. Morokuma, O. Farkas, J. B. Foresman, D. J. Fox, Gaussian, Inc., Wallingford CT, 2019.

[24] T. Lu, Q. Chen, *J. Comput. Chem*. **2022**, *43*, 539–555.

[25] Multiwfn program ver. 3.8 was used, T. Lu, F. Chen, *J. Compute. Chem*. **2012**, *33*, 580–592.

[26] R. Savka, H. Plenio, *Eur. J. Inorg. Chem.* **2014**, 6246–6253.

[27] X. Tian, J. Lin, S. Zou, J. Lv, Q. Huang, J. Zhu, S. Huang, Q. Wang, *J. Organomet. Chem.* 2018, **861**, 125–130.

[28] T. Yamamoto, S. Yamakawa, JP2015168640 A, **2015**.

[29] J. M. Renga, A. G. Olivero, M. Bosse, US5093536 A, **1992**.

[30] L. Zhao, X. Lu, W. Xu, *J. Org. Chem.* **2005**, *70*, 4059–4063.

[31] G. M. Sheldrick, *Acta Crystallogr. Sect. A* **2015**, *71*, 3–8.

[32] G. M. Sheldrick, *Acta Crystallogr. Sect. C* **2015**, *71*, 3–8.

[33] O. V. Dolomanov, L. J. Bourhis, R. J. Gildea, J. A. K. Howard, H. Puschmann, *J. Appl. Crystallogr.* **2009**, *42*, 339–341.

[34] ORTEP3: L. J. Farrugia, *J. Appl. Crystallogr.* **1997**, *30*, 565.

[35] W. Humphrey, A. Dalke, K. Schulten, *J. Mol. Graphics* **1996**, *14*, 33.

[36] CYLview20; C. Y. Legault, Université de Sherbrooke **2020**, (http://www.cylview.org).

Publication List

[1] **Miyu Sato**, Vishal Kumar Rawat, Kosuke Higashida, Masaya Sawamura, Gold-Zinc Cooperative Catalysis for Seven-*exo*-*dig* Hydrocarboxylation of Internal Alkynes. *Chemistry: A European Journal* **2023**, *29*. e202301917.

[2] Ayaka Sakurada, **Miyu Sato**, Kosuke Higashida, Masaya Sawamura, Gold-Zinc Co-Catalyzed Alkynoate Hydrocarboxylation with *N*-Protected Amino Acids for Preparation of Storable Acylating Reagents and Racemization-Free Peptide Synthesis.
Advanced Synthesis & Catalysis **2024**, *366*, 2507–2513.

Acknowledgement

The research described in this thesis was carried out under the supervision of Prof. Dr. Masaya Sawamura at Graduate School of Chemical Sciences and Engineering, Hokkaido University from Apr. 2019 to Mar. 2025.

M. Sato thanks Prof. Dr. Masaya Sawamura for kind supervision and meaningful discussions, which revealed the insight of the reaction nature and significantly improved the quality of research.

M. Sato thanks Lecture Dr. Tomohiro Iwai (present address: Graduate School of Arts and Science, The University of Tokyo) during undergraduate graduate school research. M. Sato is deeply grateful to Assistant Professor Dr. Kousuke Higashida (present address: Graduate School of Science Division of Chemistry, Kyoto University) and Assistant Professor Dr. Yusuke Masuda for helpful discussion during the doctor course research. M. Sato appreciates to Associate professor Dr. Yohei Shimizu, Prof. Tsuyoshi Mita and Associate Professor Dr. Dennis Chuang-Yang Huang for warm encouragements.

M. Sato is much grateful to Prof. Dr. A. Stephen K. Hashmi and his laboratory members belonging in Institute of Organic Chemistry at the University of Heidelberg for their kind support during the short-term visit from May to July in 2024.

M. Sato thanks examiners of her doctoral thesis. The insightful suggestions form Prof. Hajime Ito, Prof. Keiji Tanino and Prof. Takanori Suzuki were meaningful for sophisticating this thesis.

M. Sato thanks Shoshisha Foundation (scholarship for master's degree) and Japan Society for the Promotion of Science (JSPS research fellow) for scholarship support.

M. Sato would like to express her deep appreciation to her family, Mr. Tadaaki Sato and Ms. Toshiko Sato and Mr. Yusuke Sato.

M. Sato thanks Organometallic Chemistry Laboratory alumni and present members, Dr. Yuto Yasuda, Dr. Yusuke Ueda, Mr. Akito Kitabayashi, Ms. Irtaza Qureshi and Postdoctoral Researcher Dr. Vishal Kumar Rawat (present address: Graduate School of Engineering, Osaka University) for the excellent collaborations and continuous encouragements.

Miyu Sato
Graduate School of Chemical Sciences and Engineering, Hokkaido University
Mar. 2025